ANALYSIS AND PROCEDURES FOR DESIGN OF DIAPHRAGM CHUCKS

by

Onyewuchi Nduwuishi Oguoma

B.Sc., M.Sc.

A Doctoral Thesis

Submitted in partial fulfilment of the requirements for the award of The Degree of Doctor of Philosophy of the Loughborough University of Technology

1985

ANALYSIS AND PROCEDURES FOR DESIGN OF DIAPHRAGM CHUCKS

BY

O. N. OGUOMA

In modern automated manufacturing systems, there is a need for work-holding devices that provide for precision, accuracy, reliability, flexibility and remoteness of control. One of such devices is the diaphragm chuck which utilizes the strain energy of its varying thickness diaphragm plate for gripping action. The jaw-carrying diaphragm plate is deflected by a thrust load, and the jaws are bored or ground to the nominal diameter of the workpiece. Gripping action occurs when the workpiece is inserted into the jaws and the thrust is relieved.

Designers and manufacturers of diaphragm chucks have in the past been limited to the use of empirical data for diaphragm chuck design. This design limitation has been caused by complex problems due to factors such as the varying thickness encastré diaphragm plate, the gripping couples and the stiffening effects of the jaw slides.

This work involved the establishment, by theory and experimental verification, of the design and performance parameters of a diaphragm chuck, and the provision of diaphragm chuck design methodology. The designer is therefore able to achieve the *a priori* design of the diaphragm chuck. In addition, the user is able to adapt existing diaphragm plates to achieve required gripping forces within existing constraints.

The scope of this research is the static gripping action for any number of symmetric jaws. The design method is for diaphragm plates with small thickness taper, and carry detachable jaw slides.

The concept of the equivalent constant thickness is applied to the diaphragm plate. Gripping action is divided into two major phases - the separate deflections of the diaphragm plate by a thrust load and symmetric couples. These deflections are equated to obtain the gripping force.

This research concludes that the gripping force of a diaphragm chuck is closely predicted by the equivalent constant thickness method. Design data and methodology are provided for diaphragm chuck design. Thus, a designer can now design a diaphragm chuck based on a desired and pre-specified gripping force requirement.

ACKNOWLEDGEMENTS

I would like to express my gratitude to the following people for making this work possible:

Dr.D.J.Billau, my Supervisor, for his advice, guidance and encouragement.

Dr.A.C.Pugh, of Mathematics Department, for his useful suggestions in the solution of the differential equations.

Mr.Ralph Pearson, and all his colleagues at the Centre for Industrial Studies, for their help and understanding in manufacturing the equipment and experimental tests.

Mr.S.Beets, of Mechanical Engineering Department, for his assistance in the mounting of the strain gauges.

Mrs.W.R.Flitton for the typing of the script.

And all those who gave their help in uncountable ways.

CONTENTS

LIST OF FIGURES

LIST OF TABLES

NOMENCLATURE

a	outer radius of diaphragm plate
b	inner radius of diaphragm plate
b'	width of strain ring
d	circumferential width of jaw slide
d_o	workpiece diameter capacity of a diaphragm chuck
e	distance from the neutral axis to the centroidal axis of ring
h	moment arm
h'	radial thickness of strain ring
h_1	height of lower edge of jaw gripping face from plate surface
h_i	distance from the neutral axis to the inside fibre of strain ring
h_o	distance from the neutral axis to the outside fibre of strain ring
ℓ	length of jaw gripping face
m, n	integer numbers
p	distributed load on strain ring
q	distributed load over diaphragm plate
q_1, q_2	dimensionless factors for calculating chuck capacity
r	radius
r_n	radius of curvature of the neutral axis of strain ring
r_o	reference radius
r_x	radius of the circle around which Fourier's expansion takes place
s	circumferential distance around strain ring
s_f	factor of safety
t	plate thickness

t_a thickness at outer edge of plate

t_b thickness at inner edge of plate

t_e equivalent constant thickness of plate

t_o reference thickness

x dimensionless radius

x_1 dimensionless radius at the outer radius of jaw slide

x_a dimensionless radius at outer edge of plate

x_b dimensionless radius at inner edge of plate

z axial direction of plate axis

A, A_1, A_m, A_o constants

A' area of cross-section of strain ring

B, B_1, B_m, B_o constants

C, C_1, C_2, C_3, C_m, C_o constants

C_s, C_{ss} deflection dimensionless parameters

D flexural rigidity

D_a flexural rigidity at radius a

D_e average flexural rigidity

D_o reference flexural rigidity

D_o, D_m, D_1 constants

E Modulus of Elasticity

F gripping force

F_o distributed gripping force

H_o tangential force on strain ring

I strain energy

I' area moment of inertia

K_N ratio of strains or gripping forces for N jaws to three jaws

K_r a tabulated function of x_b, x, N and d for calculating gripping force

K_s	ratio of deflection with shear effects to deflection without shear effects
M	bending moments
M_o	couples
M_o^N	couples due to N number of jaws
M_r, M_x	radial bending moment per unit length
M_t	circumferential bending moment per unit length
N	number of jaws
P	thrust load
ΔP	incremental thrust load
Q	shear stress
Q_r, Q_o	internal radial shear force per unit length
R	mean radius of strain ring
R_o, R_m, R_m'	constants
R_T	tolerance factor
S_u	ultimate strength
S_y	yield strength
U	total strain energy of strain ring
α	angle around strain ring
β	plate taper angle
ν	Poisson's ratio
ω, ω'	deflection
ω_s	deflection with annular stiffening and thrust load
ω_N	thrust load deflection for N symmetric jaws
ω_m	deflection due to moments
ω_{ms}	deflection due to moments with annular stiffening
ω_1	deflection at bored diameter
ω_{mN}	deflection due to moments for N symmetric jaws

ω_b deflection at inner hole

θ angle around plate axis

ϕ deflected plate surface slope

ϕ' angular displacement of strain ring

σ stress

2δ tolerance

δ' linear displacement of strain ring

ε half-angle between jaws

ψ half-angle subtending the distributed load on strain ring

ξ_o, ξ_i, ξ_T outer fibre, inner fibre and total strains of strain ring

ξ^N total strain due to N number of jaws on strain ring

CHAPTER ONE

INTRODUCTION

1.1 APPLICATION OF THE DIAPHRAGM CHUCK

The advance in the technology of automated manufacturing systems has necessitated the need for work - and tool - holding devices that provide for precision, accuracy, reliability, rapid operation and flexibility. At the present, two of these precision devices are in frequent use in automated manufacturing systems. One of these devices in frequent use is the hydraulically - or pneumatically - operated power chuck. This type of chuck is subject to wear and reduced accuracy in centring because of moving jaws. The hydraulically-operated chuck requires a hydraulic motor that makes the system bulky. An alternative system of such devices is the diaphragm chuck which, to an extent, possesses all the desired characteristics listed above.

The diaphragm chuck, though it has been in use for more than forty years, has not changed significantly from its original design as a precision chucking device. It consists of a set of radial jaws symmetrically and rigidly mounted on an encastré annular plate of thickness variation that increases towards the centre. This plate is mounted on a housing that forms a pneumatic piston and cylinder assembly. The chuck utilizes the elastic strain energy of the plate to achieve the gripping action. The jaws open up when the piston deflects the plate and are bored to the nominal size of the work-piece. The work-piece is gripped when the air pressure is relieved.

One of the main advantages of the diaphragm chuck over conventional chucks is its automatic centring capability. Errors due to wear of moving jaws in a conventional chuck are

eliminated. This maintains the required accuracy and precision of the system during a manufacturing process irrespective of the skill of the operator. Another advantage is the resulting reduction in chucking time as the chuck is quick-acting. The gripping action is essentially completed once the work-piece is placed in the jaws and the air pressure is relieved. These important features make the chuck applicable to batch and continuous production systems. In addition, the pneumatic operation of the diaphragm chuck lends it to remoteness of control, a necessary and desirable quality in modern automated manufacturing systems.

1.2 DESCRIPTION OF MANUFACTURERS' CHUCKS

The limited list of manufacturers of standard diaphragm chucks includes Bristol Erickson Limited and Pratt Burnerd International Limited. A modified version of the chuck, manufactured by Pratt Burnerd, for pitch-line chucking of gears has appeared in the market recently. Regardless of the manufacturers, the basic design of the standard diaphragm chuck remains the same for both external and internal chucking. The gripping force capacity of the available chucks ranges from 875 lbs. for a 5 in. diameter chuck to 12300 lbs. for a 17 in. diameter chuck.

Two sizes of Bristol Erickson Standard Diaphragm Chucks were used in the analysis. A nickel-chrome steel diaphragm plate carrying four jaws only and four holes for support buttons used as additional means of location, and an EN 38 Steel diaphragm plate capable of carrying three, four and six jaws were mounted on the 7 in. diameter chuck. A smaller three-jaw nickel-chrome steel diaphragm plate[1] with locating holes was mounted on the 5½ in. diameter chuck. Figures 1.2.1 and 1.2.2 show the chuck and the plate respectively.

1 From Chidlow's(4) Measurements. Cross-checked by this author.

Figure 1.2.3 is a sectional view of the Bristol Erickson Standard Diaphragm Chuck as first illustrated by Astrop (1). The annular and encastré diaphragm plate A carries the dove-tail slides B which are affixed to the diaphragm plate by dowels and screws through the cleet plate C. Soft jaws D slide in the dove-tails and can be adjusted by block and screw E. Buttons F pass through holes in the diaphragm plate to be used as an additional means of locating the work-piece. The diaphragm plate is mounted on the face plate adaptor G which serves as a cylinder for short-stroke piston H. Between the diaphragm plate and the face plate adaptor is an intermediate plate I which closes the cylinder and serves as a stop for the piston. Air is admitted through connection J and the movement of the piston is transmitted to the diaphragm plate through sleeve K. The soft jaws are bored out to the nominal diameter of the work-piece upon supplying a pre-determined air pressure to the piston. A further and slight increase in pressure deflects the plate to allow the work-piece to be inserted. On relieving the pressure, the work-piece is concentrically and firmly gripped by the jaws under the elastic strain energy stored in the plate.

1.3 THE OBJECTIVE OF THIS RESEARCH

The behaviour of the diaphragm plate, which is the primary element in the diaphragm chuck, has to be defined, understood and predicted in order to quantify the resulting gripping force. The varying thickness of the encastré plate, and the concentrated couples on the plate through the jaws pose complex problems that designers of diaphragm chucks aim to resolve. As a result, manufacturers and designers have been restricted to information that is wholly or partly empirical in nature. This *a posteriori design* is achieved by manufacturing and testing a given diaphragm chuck. Specifications from this prototype are then used to produce more

chucks of the same empirical force rating. At the present, the designer is not able to design a chuck to a desired and prescribed force rating within existing constraints. Moreover, users of these chucks have to be able to adapt or modify their own diaphragm plates to suit individual production system constraints such as air line pressure, number of jaws and height of gripping from the plate. This has made it necessary for research to be conducted to furnish designers and users tools that can be used to design or adapt a chuck from a gripping force requirement to the geometric and material specifications of the chuck.

Factors that can constrain a designer include available air line pressure, maximum size of chuck that can fit on a given space (machine), number of jaws and height of clamping of work-piece from the plate. The objective of this research is to establish the design and performance parameters of a diaphragm chuck within a given set of constraints. It makes possible the *a priori design* of the chuck. A designer decides on the amount of force required to grip a work-piece, and methodically designs the corresponding diaphragm chuck. A user will also be able to predict the gripping force that a diaphragm chuck at hand can deliver. It is intended that design and usage data be made as simple and handy as possible.

The design equation and data supplied here are for static gripping action and cover any number of symmetric jaws that can physically mount on the plate. This design is limited to chucks with detachable jaw slides. There is a fundamental difference between plates with detachable jaw slides, and incorporated jaw slides. Detachable jaw slides, as a boundary condition, influence the deflection of the plate while the incorporated jaw slides which are manufactured into the plate, contribute directly to the flexural rigidity of the plate through the individual moments of inertia of the jaw slides.

The boundary condition imposed by detachable jaw slides is the constant slope caused along the slide length over the plate.

Using the concept of equivalent constant thickness, the plate is analyzed in two major phases. Firstly, the deflection equation for a plate carrying any number of jaws and loaded by a uniform thrust at the inner edge is established. This deflection equation is then compared with experimental measurements. Secondly, a deflection equation is obtained for the same plate loaded by concentric couples around the inner edge. These two deflections are equated to obtain the gripping force of the chuck.

Equations for the gripping force are only valid for small variations in the thickness of the plate. A large variation introduces shear stress effects that must be taken into account and plane sections will no longer remain plane. In addition, the concept of an equivalent constant thickness can no longer be applicable if the thickness variation is large. The finite element method is most suitable for plates with large thickness variation.

In summary, the objectives of this research are stated as follows:

1. Formulation of a general prediction equation giving the deflection of the diaphragm plate with uniform thrust loads for any number of jaws.
2. Comparision of this predicted deflection equation with the deflections obtained from experiment.
3. Formulation of a general prediction equation giving the deflection of the diaphragm plate loaded by couples for any number of jaws.

4. Determination of a general prediction equation for the gripping force of a diaphragm chuck with any number of jaws. This is to be achieved by equating the deflection due to couples resulting from the gripping force to the deflection due to uniform thrust load. The significant parameters that influence gripping force are also to be determined.

5. Experimental verification of the predicted gripping force and the parameters that influence the gripping force.

6. Provision of a systematic method for the designer to design a diaphragm chuck *a priori*, and for the user to adapt existing diaphragm plates.

1.4 CONCLUSION

The research concludes that the gripping force of a diaphragm chuck can be closely predicted using an equivalent constant thickness method. It is established that parameters such as workpiece diameter, the inner and outer diameters of the diaphragm plate, number of jaws, and workpiece-jaw bore tolerance significantly influence the gripping force. Gripping force is not directly influenced by diaphragm plate thickness.

Design data and methodology are provided for designing diaphragm chucks to perform within specified constraints. Thus, a designer can design a diaphragm chuck based on a specified gripping force requirement.

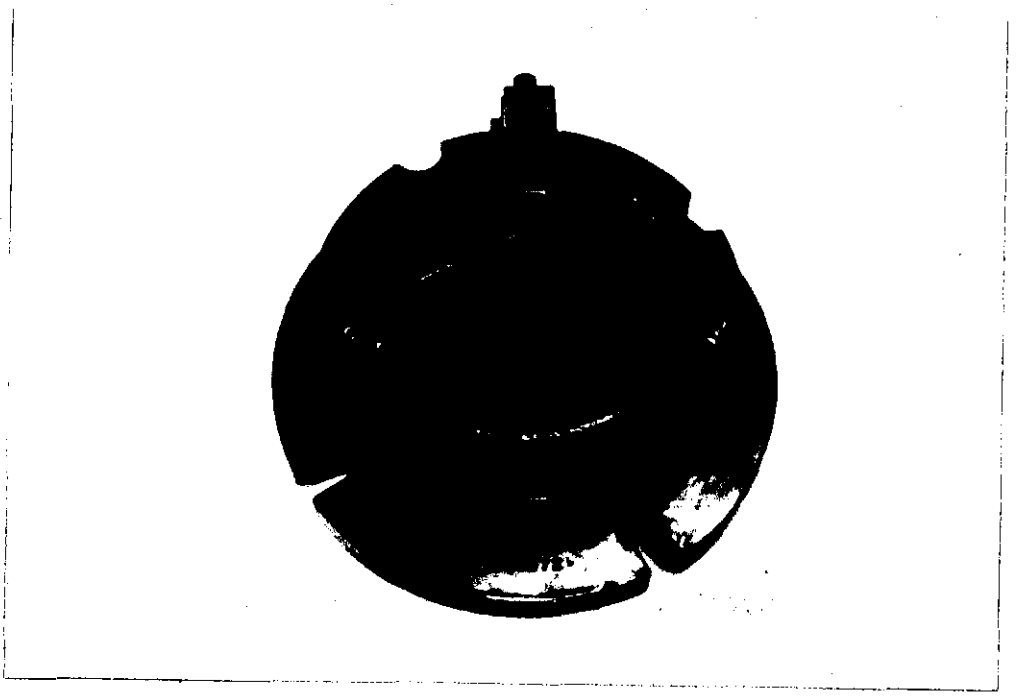

FIG.1.2.1 THE ERICKSON DIAPHRAGM CHUCK
(Plate C)

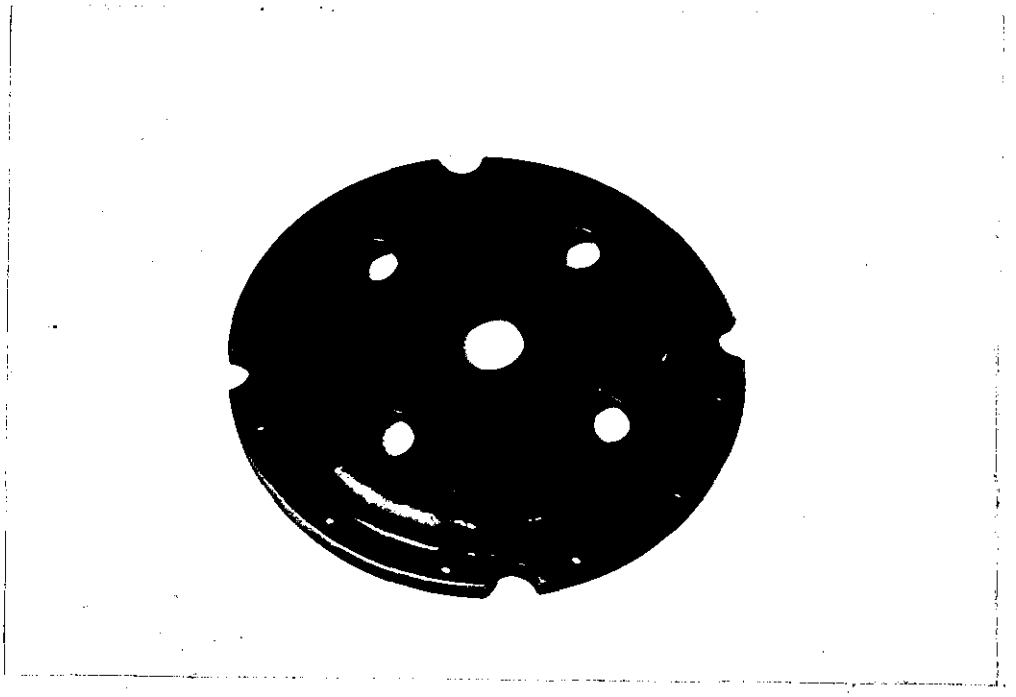

FIG.1.2.2 THE DIAPHRAGM PLATE
(Plate B)

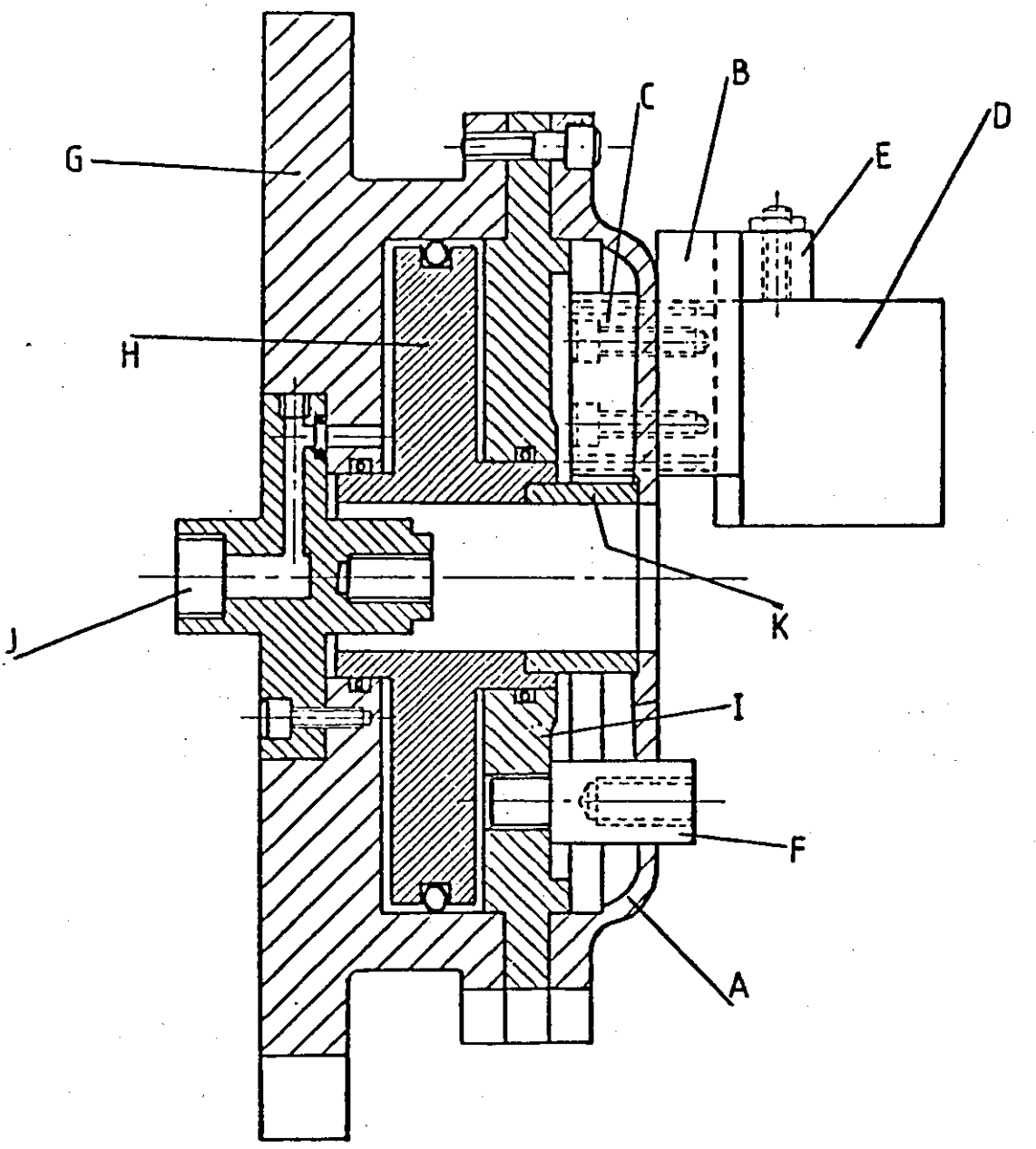

FIG.1.2.3 A SECTIONAL VIEW OF THE ERICKSON DIAPHRAGM CHUCK

CHAPTER TWO

LITERATURE REVIEW

2.1 EARLIER STUDIES OF DIAPHRAGM CHUCKS

Although diaphragm chucks are increasingly becoming essential elements in modern manufacturing systems, there is a significant lack of published materials related to the design and performance parameters of diaphragm chucks. The primary parameter of any chuck is the gripping force which should be both measurable and predictable. An early investigator of the gripping force of conventional chucks is Pahlitzsch (2) whose use of rings in chuck force measurements proved to be a simple and fairly accurate method for subsequent investigators. Strain gauges attached to 10mm wide rings were calibrated for point forces to measure the static and dynamic gripping forces in three-jaw conventional chucks.

The first systematic study of the design criteria of diaphragm chucks was done by Robertson (3), who analysed the diaphragm chuck as primarily consisting of a jaw-carrying annular plate with encastré support at the outer boundary. Each jaw is assumed to be mounted on a radial strip of plate that acted as a short cantilever beam. The beam equations for force and moment loadings were used to determine the gripping force. This approach fundamentally neglects the extra rigidity caused by the adjacent strips of plate.

This work was carried further by Chidlow (4) using Robertson's concept of equating the deflections due to uniform ring loads and uniform moments at the central hole. Grashof's flat plate theory is applied to obtain the deflections which are reduced by the stiffening effect of the jaw slides. The

stiffening factors are determined empirically for only three-jaws and a given plate.

Billau (5) conducted investigations into the effects of jaw bore and component tolerances on the gripping force for the three-jaw 5½ in. and four-jaw 7 in. chucks. For over-size components (or under-size bores), the gripping force is considered to act at the centre of the base quarter of the jaw face, while for under-size components (or over-size bores) the force acts at the centre of the top quarter of the jaw face.

Work on the dynamic characteristics of the diaphragm chuck was carried out by Prickett (6). An equation for the calculation of losses in the gripping force of a chuck due to centrifugal effects is determined. These losses vary with the mass of the jaw, position of the centroid of the jaw and the height of clamping.

2.2 ELASTIC THIN PLATE THEORIES

Further literature search covered the elastic thin plate theories which may be applicable to the diaphragm plate. Many publications are available on the application of Grashof's flat plate theory to the solution of plate problems in engineering. Foremost of authors in this area are Timoshenko and Woinowsky-Krieger (7) whose works are extensively applied to plate problems. Thin plates with small deflections are classified by the following fundamental assumptions:

1. The deflection of the middle surface of the plate is small compared to the thickness of the plate. In consequence, the slope is small and higher orders of slope are negligible.
2. There is no straining of the middle surface of the plate during bending.

3. The principal cause of deflection is the bending strain. Plane sections before bending remain plane after bending.

4. The normal stresses transverse to the middle plane of the plate are small and can be neglected.

Vinson (8) adds that for assumption (4) to hold, the following conditions must exist:

$$t/_a \ll 1 \quad \text{and} \quad t/_b \ll 1$$

where t is the thickness, a and b are the outer and inner radii respectively.

The determination of the gripping force of a diaphragm chuck is possible with the use of the total energy method i.e. by equating the energy due to the total ring load, P and the energy due to the symmetric couples, M_o. Timoshenko and Woinowsky-Krieger (7) give the total energy, I due to thrust P as

$$I = \iint \left\{ \frac{D}{2} \left[\left(\frac{\partial^2 \omega}{\partial r^2} + \frac{1}{r} \frac{\partial \omega}{\partial r} \right)^2 - \frac{2(1-\nu)}{r} \frac{\partial \omega}{\partial r} \frac{\partial^2 \omega}{\partial r^2} \right] - \omega q \right\} r dr d\theta$$

the term containing $(1-\nu)$ being zero for plates clamped along the boundary where

flexural rigidity, $D = Et^3/12(1-\nu^2)$

ν = Poisson's ratio

ω = deflection at radius, r

θ = angle around the plate axis

q = load distributed over the plate

The term in brackets is the strain energy of bending and the term ωq is the potential energy of the distributed load. The total energy of the plate due to any system of moments, M is

given by

$$I = \iint \left\{ \frac{D}{2} \left[\left(\frac{\partial^2 \omega^1}{\partial r^2} + \frac{1}{r} \frac{\partial \omega^1}{\partial r} \right) - \frac{2(1-\nu)}{r} \frac{\partial \omega^1}{\partial r} \frac{\partial^2 \omega^1}{\partial r^2} \right] - M \frac{\partial \omega^1}{\partial r} \right\} r dr d\theta$$

where ω^1 is the deflection due to moment, M and the term $\frac{\partial \omega^1}{\partial r} M$ is the potential energy of the moment. The energy method is particularly useful because any variation in flexural rigidity D or any system of loads can be included within the integral signs. Jaeger (9) and Ugural (10) also used energy methods for plate problems and state that a fairly correct form of the equation for deflection, ω must be assumed. The assumed form of deflection must satisfy the boundary conditions of the plate. This therefore, is the main disadvantage of the application of the energy method to the deflection of the diaphragm plate.

Another method of solving the gripping force problem is to obtain exact solutions for the deflections of a plate loaded by uniform ring load and symmetric couples. Exact solutions of the differential equation for symmetrical bending of laterally loaded circular and annular constant thickness plates are given by Timoshenko and Woinowsky-Krieger (8), Jaeger (9), Ugural (10), Szilard (11), Mansfield (12) and many other authors. These solutions are for different load distributions and boundary conditions. Wahl and Lobo (13) compared theoretical and experimental results for maximum stress and deflection of annular plates of constant thickness with various loads and boundary conditions. Experimental results suggest that the deflection due to shear may be considerable if the thickness of the plate is greater than one-third the difference in diameters for simply supported edges or one-sixth the difference in diameters for built-in edges. There is close agreement between theoretical and experimental results for those edge conditions, such as free or simply supported edges, that can be reproduced in practice. The

stresses for built-in edges closely agree while there is a large discrepancy in the deflection for built-in edges. This was attributed to the imperfect reproduction of actual built-in edges. In the discussion section of the same paper, S.Timoshenko[2] argues that built-in edges are simpler to realize than other edge conditions. Timoshenko and Woinowski-Krieger (7) give the solution for the deflection due to shear stresses in cases of short or thick plates.

The varying thickness of the diaphragm plate poses additional complexity to the solution for deflection. Chidlow (4) took account of the radial taper by establishing an average thickness of the plate, t_e given as:

$$t_e = \frac{\left[t_b/\text{Tan } \beta - (a-b)\right] \tan \beta + t_b}{2}$$

where a is the outer radius, β is the amount of taper and t_b is the thickness at inside radius, b. Ugural (10) and Lord and Yousef (14) used the matrix method to solve problems of the deflection of circular plates on any thickness variation and any system of loading. This method considers the plate as being composed of a finite number of concentric rings of constant thickness. As the number of rings gets large, the surface of the plate approaches that of the real plate. Each of these rings must satsify known solutions for plate bending, boundary conditions and continuity between rings. Lord and Yousef (14) used electrical strain gauges to measure strain and compared exact, matrix method and experimental results, all of which are generally in close agreement. Significant discrepancies exist for models of large thickness variation indicating the important influence of the taper. Conway (15) gives a general closed-form solution to the symmetrical bending of linearly varying thickness cantilever plates for the case of Poisson's ratio of $^1/_3$. Comparison with the solution for a corresponding constant thickness

2. Professor of Mechanical Engineering, University of Michigan, Ann Arbor, Michigan, U.S.A.

plate shows an increase in the maximum stress of up to 14% for the varying thickness plate.

Additional rigidity is given to the diaphragm plate by the jaws which act as radial stiffeners. Chidlow (4) empirically determined a stiffening factor for the deflection of a specific three-jaw chuck by finding the ratio of measured deflections with and without jaws. This extra rigidity can also be accommodated by regarding the part of the plate between jaws as a sector plate with free inner boundary, fixed outer boundary and the radial edges are such that the slope at the edges are zero but the deflection is non-zero. Mansfield (12) gives the solution to the problem of lateral bending of sector plates of constant or varying thickness. Another approach to include the extra rigidity is to take the plate and jaw as a flange and web arrangement and using elementary solutions of beam flanges and webs.

Conway (16) has looked at the problem of a clamped and uniformly loaded circular plate, reinforced by a diametral rib. The rib is symmetric with the middle plane of the plate, incorporated into the plate, and carries part of the load. He used an approximate method which replaces the continuous distribution of the shearing force between plate and rib with concentrated forces at certain points on the diametral line. The solution for eccentric point loadings with corresponding boundary conditions of rib and plate were applied to the problem. The maximum bending stress of the unstiffened plate decreased by about half. Timoshenko and Woinowsky-Krieger(7) give equivalent flexural rigidities for the bending of rectangular anisotropic plates with equidistant stiffeners that are incorporated into the plate. Simitses (17) optimized the load carrying capacity of a constant thickness plate by eccentrically stiffening the plate circumferentially and radially. The basic assumption being that if the lateral loading and geometry are axisymmetric, then the plate response

will be axisymmetric. It is already known that concentric stiffening does not affect the axisymmetry of plate response. Lekhnitskii (18) also solves the problem of the bending of plates with curvilinear anisotropy; particularly cylindrical anisotropy and gives equivalent radial and circumferential rigidities due to stiffening. A prohibitively long differential equation is given for cylindrical anisotropy.

For the reason that exact mathematical solutions of radially stiffened plates are intractable, Harvey and Duncan (19) took an empirical approach to the design of radially stiffened flat plates with a concentric inner stiffener joined to the ribs. The ribs behave as simple beams with a distributed load along the length of the rib, a supporting force at the outer free end, and a bending moment at the inner end joined to the concentric stiffener. Application of the solution for bending of sector plates with rigid and encastré radial edges gave wide discrepancies in comparison with experimental measurements. These errors were attributed to the plate and rib behaving respectively as flange and variable thickness web. An empirical equation for the central deflection of the plate with eight ribs was determined, and there appeared to be a continuous reduction in deflection with increased web depth. Blake (20) quotes the work of Harvey and Duncan (19) and states that no flexure theory has been established for calculating the deflections of plates with radial stiffeners. Concentric stiffeners are known to reduce stresses and deflections, but where deflection is the primary consideration, radial stiffeners are appropriate.

The gripping action of the diaphragm chuck causes the diaphragm plate to be loaded by symmetric couples which depend on the height of the point at which the gripping force acts on the jaw face. The classical theory of bending of thin elastic plates using the complex variable method to determine the complex potentials and deflections is a powerful tool for

solving problems of concentrated loads. There is a significant amount of literature available on this topic. Using this method, Yu (21) obtained exact closed-form solutions for a circular plate subjected to two bending couples on the outside boundary. The deflection is negative along the radial line half-way between the couples and the deflection is zero at the centre. Away from the couples, the deflection goes negative at an angular position, θ of about $\pi/3$ radians. Amon and Widera (22) applied the same method to an annular plate simply supported at both edges and loaded with an eccentric concentrated force. The deflection of the region diametrically opposite the point of load application is zero and the width of this region is a sector of about $\pi/2$ radians. Amon and Widera (23) solved the same problem for clamped inner and outer boundaries. The deflection in the region $\pi/2 < \theta < 3\pi/2$ is very small compared to that in the region $-\pi/2 < \theta < \pi/2$. For all practical purposes therefore, the plate can be treated as being fixed along $\theta = \pm \pi/2$. Comparing the results for clamped and simply supported edges, there is indication that the deflection in the deflection region for simply-supported case is twice as large as for the clamped case.

Dhaliwal (24) also used the complex variable method for two concentrated couples applied at the outer boundary of an annular plate. The deflection along the loaded radial line becomes negative at about half-way between diameters while the deflection half-way between the couples decreases from the inside to the outside and remains positive. The deflections at the point of couple application and at $\pi/2$ radians from the couple on the outer boundary increase as the size of the concentric hole increases. Bassali (25) determined the deflection for an annulus and a sector plate simply supported at the radial lines, both with free circular edges and loaded by concentrated couples and forces.

These solutions of concentrated couples using the complex variable method have all been for two couples. Extension to any multiples of two couples is possible by adequate coordinate transformation and super position. The main disadvantage of applying this method to the diaphragm plate is that a different solution must always be found each time any number of couples that is not a multiple of two are considered.

Concentrated loadings can also be expanded in the form of infinite series that is valid for all points except at the point of load application where singularities occur. In addition, convergence of the series solution may become very slow around the load point. Timoshenko and Woinowsky-Krieger (7), Jaeger (9), Szilard (11), Lekhnitskii (18), Symonds (26) and Lukasiewicz (27) used Fourier series to represent concentrated forces on plates. Lukasiewicz eliminated the problem of convergence of solutions with the expansion of the concentrated forces in Fourier Integrals and Transforms. Conway (28) gives the solution to the non-axial bending of annular plates of varying thickness under any system of couples and normal forces. The loadings are also expanded in Fourier series.

For reasons that will become clear later in the theoretical analysis of this research, the Fourier series representation of the couples is particularly appropriate in the analysis of the deflection of the diaphragm plate.

CHAPTER THREE

THEORY OF THE DIAPHRAGM PLATE

3.1 DIAPHRAGM PLATE GEOMETRY

As discussed earlier, Robertson (3) and Chidlow (4) define the diaphragm plate shown in Figure 3.1.1 as a varying thickness encastré plate. Accepting this definition, the plate geometry is given in Figure 3.1.2 and the parameters are thus defined.

Let a and b be the respective outer and inner radii of the plate. The thickness at the outer edge is t_a and t_b at the inner edge. Let t_o be a reference thickness at the centre and r_o is a reference radius geometrically defined in Figure 3.1.2. This reference radius, r_o is

$$r_o = \frac{at_b - bt_a}{t_b - t_a} \qquad \ldots\ldots\ldots 3.1.1$$

and the reference thickness, t_o is

$$t_o = \frac{r_o\, t_a}{r_o - a} \qquad \ldots\ldots\ldots 3.1.2$$

At any radius, r the thickness, t is

$$t = t_o\,(1 - {}^{r}/_{r_o}) \qquad \ldots\ldots\ldots 3.1.3$$

If $x = {}^{r}/_{r_o}$, a dimensionless radius, then

$$t = t_o\,(1 - x) \qquad \ldots\ldots\ldots 3.1.4$$

The flexural rigidity, D of a plate is defined as

$$D = \frac{Et^3}{12(1-\nu^2)} \qquad \ldots\ldots\ldots 3.1.5$$

where E is the Modulus of Elasticity of the plate material and

ν is its Poisson's ratio. For any point on the plate,

$$D = D_o (1 - x)^3 \quad \ldots\ldots\ldots 3.1.6$$

where D_o is a hypothetical flexural rigidity at r_o given by

$$D_o = \frac{E\, t_o^3}{12(1-\nu^2)} \quad \ldots\ldots\ldots 3.1.7$$

3.2 DIFFERENTIAL EQUATION OF DIAPHRAGM PLATE

Timoshenko and Woinowsky - Krieger (7) give the equilibrium equation of an element of a circular plate of Figure 3.2.1 symmetrically loaded by a transverse load, q as

$$M_r + r\frac{dM_r}{dr} - M_t + Qr = 0 \quad \ldots\ldots\ldots 3.2.1$$

where the radial bending moment per unit length, M_r acting on θz section is

$$M_r = D\left(\frac{d\phi}{dr} + \frac{\nu}{r}\phi\right), \quad \ldots\ldots\ldots 3.2.2$$

the circumferential bending moment per unit length, M_t acting on rz section is

$$M_t = D\left(\frac{\phi}{r} + \nu\frac{d\phi}{dr}\right) \quad \ldots\ldots\ldots 3.2.3$$

Q is the shear stress caused by transverse load, q, and slope $\phi = -\frac{d\omega}{dr}$ where ω is the deflection at a radius, r.

Substituting equations 3.2.2 and 3.2.3 into equation 3.2.1,

$$D\frac{d}{dr}\left(\frac{d\phi}{dr} + \frac{\phi}{r}\right) + \frac{dD}{dr}\left(\frac{d\phi}{dr} + \nu\frac{\phi}{r}\right) = -Q \quad \ldots\ldots 3.2.4$$

For the thrust load, P on the edge of the central hole,

$$Q = \frac{P}{2\pi r} \quad \ldots\ldots\ldots 3.2.5$$

Since $x = \frac{r}{r_o}$, then $\frac{d\phi}{dr} = \frac{1}{r_o}\frac{d\phi}{dx}$ and

$$\frac{d(\ )}{dr} = \frac{1}{r_o}\frac{d(\ )}{dx}$$

The equilibrium equation 3.2.4 is transformed to the new dimensionless variable, x as

$$\frac{(1-x)^3}{r_o^2}\frac{d}{dx}\left(\frac{d\phi}{dx} + \frac{\phi}{x}\right) - \frac{3(1-x)^2}{r_o^2}\left(\frac{d\phi}{dx} + \frac{\nu\phi}{x}\right) = \frac{-P}{2\pi D_o r_o x} \quad \ldots 3.2.6$$

Using $\nu = \frac{1}{3}$ and expanding

$$x^2(1-x)^3\frac{d^2\phi}{dx^2} + x(1-x)^2(1-4x)\frac{d\phi}{dx} - (1-x)^2\phi = \frac{-Pr_o x}{2\pi D_o} \quad \ldots 3.2.7$$

This is a hypergeometric differential equation and Conway (15) gives the solution as

$$\phi = \left[\frac{2x+1}{x}\right]A + \left[\frac{3x-2x^2}{(1-x)^2}\right]B - \frac{Pr_o}{12\pi D_o}\left[\frac{2x^2+x-1}{x(1-x)^2} + \frac{(2x+1)}{x}\ln(1-x) + \frac{(3x-2x^2)}{(1-x)^2}\ln x\right] \quad \ldots 3.2.8$$

The first two terms form the general solution of the differential equation which obtains when there are no external shear forces acting on the plate. The non-dimensional deflection of the plate is given by

$$-\frac{\omega}{r_o} = (2x + \ln x)A + \left[2(1-x) - \ln(1-x) + \frac{1}{1-x}\right]B + C - \frac{Pr_o}{12\pi D_o}\left[2(1+x)\ln(1-x) + \left(\frac{3x}{1-x} - 1 - \frac{2x^2}{1-x} - 4x\right)\ln x + \frac{2}{(1-x)} - \ln x \ln(1-x) + 2 - 2\left(x + \frac{x^2}{4} + \frac{x^3}{9} + \ldots\right)\right] \quad \ldots 3.2.9$$

The constants A, B, C are determined according to the boundary conditions of the plate.

3.3 BOUNDARY CONDITIONS

Boundary conditions at the outer edge of the plate are difficult to establish. The word "encastre " has been used to describe the plate support. The support is in reality an elastically restrained boundary; somewhere between fixed (encastre or clamped) and simply supported boundary. For simplicity, it is assumed to be fixed. All the boundary conditions to be used for determining the constants of equation 3.2.8 are

1. $\phi = 0$ at $x = \frac{a}{r_o} = x_a$

2. $-\frac{\omega}{r_o} = 0$ at $x = x_a$

3. $M_r = 0$ at $x = \frac{b}{r_o} = x_b$

Using these conditions, the following simultaneous equations result:

$$(2 + \frac{1}{x_a}) A + \frac{(3x_a - 2x_a^2)}{(1-x_a)^2} B - \frac{Pr_o}{12\pi D_o x_a (1-x_a)^2}\left[2x_a^2 + x_a - 1 + (1-x_a)^2 (2x_a+1) \ln(1-x_a) - (3x_a^2 - 2x_a^3) \ln x_a\right] = 0 \quad \ldots 3.3.1$$

$$(2x_a + \ln x_a) A + \left[\frac{1}{1-x_a} - \ln(1-x_a) + 2(1-x_a)\right] B - \frac{Pr_o}{12\pi D_o}\left[2(1+x_a) \ln(1-x_a) + \left(\frac{3x_a}{1-x_a} - 1 - \frac{2x_a^2}{1-x_a} - 4x_a\right) \ln x_a + \frac{2}{1-x_a} - \ln x_a \ln(1-x_a) + 2 - 2\left(x_a + \frac{x_a^2}{4} + \frac{x_a^3}{9} + \ldots\right)\right]$$

$$+ C = 0 \quad \ldots\ldots\ldots\ldots\ldots\ldots\ldots\ldots\ldots\ldots\ldots\ldots 3.3.2$$

$$-(1-x_b)^4 A + \left[x^2_b \ (6-4x_b + x^2_b)\right]B - \frac{Pr_o}{12\pi D_o}\left[1 - 5x_b + 11x^2_b - \right.$$

$$\left.(1-x_b)^4 \ \ell n(1-x_b) + x^2_b \ (6-4x_b + 4x^2_b) \ \ell n \ x_b - x^3_b\right] = 0 \ldots . 3.3.3$$

Equations 3.3.1, 3.3.2 and 3.3.3 are solved for A, B and C, and substituted into equation 3.2.9 to obtain the deflection equation of the plate.

The main disadvantage of using equation 3.2.9 is that the variation in thickness inherent in the equation is geometrically symmetrical about the plate's middle surface as shown in Figure 3.3.1,as opposed to the diaphragm plate geometry shown in Fig.3.1.2. Discrepancies exist between the deflections of these two plates because the middle surface of the diaphragm plate is not geometrically symmetrical but eccentric. Shear stress effects are high and are difficult to determine mathematically, making the diaphragm plate less stiff. The result is that the diaphragm plate geometry will give a higher deflection by approximately 40% more than the geometrically symmetrical plate. For plates with very small variation in thickness, closer values of deflection are obtainable.

Another disadvantage of using equation 3.2.9 is the laborious computation required to determine the constants A, B and C. The resulting deflection equation is cumbersome, needing the use of computer.

3.4 THE IMPORTANCE OF A LINEARLY VARYING THICKNESS

For the purposes of illustrating the importance of linear variation in thickness, computer methods were used to solve for the constants A, B and C of equations 3.3.1, 3.3.2 and 3.3.3. The resulting calculated deflection is shown in Figure 3.4.1. It can be noticed that away from the outer

edge of the plate, the slope of the deflection changes slowly if not approaching a constant. This is the primary effect of a linear variation in thickness. For it to be an exact constant the variation has to be curvilinear which will be difficult to manufacture.

When the jaw slides are mounted on the plate as in Figure 3.4.2, the relatively infinite rigidity of the slides tends to give the plate a constant slope. Since the plate has an almost constant slope, little or no stresses are induced in the plate in order to conform to the constant slope imposed by the jaw slides. This small amount of induced stresses allows for a more natural reduction in deflection due to the stiffening effect of the slides. The reduction is such that it is from one constant slope line to another constant slope line. Consequently, energy is conserved for conversion to gripping force. Thus, a higher gripping force is achieved by using a varying thickness plate.

3.5 OPTIMUM ANGLE OF THICKNESS VARIATION

The thickness variation angle of Figure 3.3.1 was varied for a plate of specified outer radius, a = 2.5578 in., inner radius, b = 0.5178 in. and minimum thickness, t_a = 0.208 in. The aim is to illustrate how the slope of the deflection curve varies with angle, β, and determine an optimum angle of thickness variation. The fact that three parameters - a, b and t_a have to be specified makes it difficult to establish one exact optimum angle which will require the consideration of all possible combinations of a, b and t_a. Figure 3.5.1 shows the deflection curve for the specified plate as β is varied. The curve begins to have portions of approximately constant slope as from about $\beta = 0.4°$. The number of these portions of constant slope approaches a minimum at about the range of $\beta = 1.6°$ to $\beta = 2.4°$. This is the optimum range of the angle of thickness variation for this particular plate.

Similar analysis can be applied to a plate with a different set of a, b and t_a. This method is so far based on the geometrically symmetric plate thickness. To accurately establish this angle for the diaphragm plate geometry, the finite element method is more appropriate.

This optimum range of the angle of thickness variation is not expected to be affected by changing t_a. A change in t_a should result in a change in the magnitude of deflection only.

Complex shear stress and warping problems arise if the angle, β continues to increase. Shear stress effects are discussed in the section on equivalent constant thickness.

3.6 EQUIVALENT CONSTANT THICKNESS PLATE

A way of circumventing the complexities introduced by the plate taper is to use an equivalent constant thickness plate concept. This is particularly useful in view of this work seeking to predict the gripping force of the chuck. It must be emphasized here that it is incorrect to use this method when calculating the stress distributions in the plate. It also gives a different deflection pattern for the plate because a constant thickness plate will always have a non-constant slope deflection. This constant thickness plate is less stiff at the central portion and much stiffer towards the outer boundary than the diaphragm plate.

In determining the equivalent constant thickness, Chidlow (4) used the average of the two extreme thicknesses. This method, while there is no indication of it being less accurate, ignores the fact that thickness is cubic in the flexural rigidity, D of the plate. An average flexural rigidity gives a better estimation of equivalent constant thickness.

The centroidal surface of the triangular section (t_b-t_a) is one-third its height from the base. To approximate an average rigidity, D_e, the flexural rigidity due to this triangular section is added to that due to the constant thickness part of the cross-section, i.e.

$$D_e = D_a + \frac{E}{12(1-\nu^2)}\left(\frac{t_b-t_a}{3}\right)^3 \quad \ldots\ldots\ldots 3.6.1$$

where $D_a = \dfrac{Et_a^3}{12(1-\nu^2)}$

If t_e is the equivalent constant thickness, then

$$D_e = \frac{Et_e^3}{12(1-\nu^2)} = \frac{Et_a^3}{12(1-\nu^2)} + \frac{E}{12(1-\nu^2)}\left(\frac{t_b-t_a}{3}\right)^3 \quad \ldots 3.6.2$$

which gives

$$t_e = \left\{ t_a^3 + \left(\frac{t_b-t_a}{3}\right)^3 \right\}^{\frac{1}{3}} \quad \ldots\ldots\ldots\ldots\ldots 3.6.3$$

With this equivalent constant thickness, the deflection of the constant thickness plate of Figure 3.6.1 is examined. The differential equation is modified for constant thickness (8) and the deflection, ω is satisfied by the form

$$\omega = A_1 + B_1 \ell nx + C_1 x^2 + C_2 x^2 \ell nx \quad \ldots\ldots\ldots 3.6.4$$

where $x = \frac{r}{a}$, r being any radius and A_1, B_1, C_1 and C_2 are integration constants. From this deflection the internal radial moment per unit length, M_r is given by

$$M_r = \frac{-D}{a^2}\left\{(\nu-1)\frac{B_1}{x^2} + 2(1+\nu)\,C_1 + \left[2(1+\nu)\ell nx + (3+\nu)\right]C_2\right\} \ldots 3.6.5$$

and the internal radial shear force per unit length, Q_r is

$$Q_r = \frac{-4DC_2}{a^3 x} \quad \ldots\ldots\ldots\ldots\ldots\ldots 3.6.6$$

In this form, the additional boundary condition,

$$Q_r = Q_o = \frac{P}{2\pi a x_b} \quad \text{at } x = x_b = {}^{b}/_{a} \quad \ldots\ldots 3.6.7$$

is used with the conditions of Section 3.3 to give the equation describing the plate deflection,

$$\omega = \frac{-a^2 P}{16\pi D}\left[(1-x^2)\ (1+2C_s) + 2(2C_s+x^2)\ \ell n x\right] \ldots 3.6.8$$

where $$C_s = x_b^2 \frac{\left[(1+\nu)\ \ell n\ x_b + 1\right]}{\left[(1-\nu) + x_b^2\ (1+\nu)\right]} \quad \ldots\ldots\ldots 3.6.9$$

This is a simpler equation to handle than the deflection equation for the varying thickness plate.

3.7 EFFECT OF JAW SLIDES

Many factors, as can be noticed from the deflection equation, influence the amount of deflection in a plate when loaded transversely. One such factor is the plate thickness, which when increased, directly results in a decrease in deflection through the flexural rigidity and vice versa. It is well established that by employing stiffeners and ribs, the overall flexural rigidity is increased and the plate deflection is reduced, thereby substantially increasing the load-carrying capacity of the plate. These ribs and stiffeners also introduce directional properties into the plate hitherto considered isotropic. Complexities, therefore, exist in the solution of such plate problems. Lekhnitskii (18) and Lukasiewicz(27) have given the differential equations of such anisotropic circular plates. An approximate contribution of the individual moments of inertia of the ribs to the overall rigidity of the plate is also given for rectangular plates only.

For the diaphragm plate with jaw slides as in Fig.3.4.2, the jaw slides increase its flexural rigidity and reduce the

amount of deflection. This reduction tends to increase with decreasing thickness. The jaw slides also impose a constant slope deflection on the plate. The differential equations for anisotropic plates strictly apply to cases where the stiffener is incorporated as part of the plate. This restriction suits the type of diaphragm plate with incorporated jaw slides. Nevertheless, the equations are laborious to handle. When the jaw slide is detachable, as is the case with the diaphragm plate under consideration, the stiffening effect is present as a boundary condition of constant slope deflection. Chidlow (4) used an empirical stiffening coefficient, which is the ratio of the deflection with jaws to the deflection without jaws. This method has to be applied experimentally each time a different plate is in consideration.

A different approach is used in this work to account for the stiffening effect of the jaw slides. It is reasoned that the maximum deflection occurs without jaw slides while the minimum occurs for plate with a hypothetical annular stiffener. The stiffening effect increases with number of jaw slides and the deflection must lie between these two extremes. Since the deflection for a plate with annular stiffening cannot be zero under load, it is deduced from observation that the deflection decreases assymptotically to a minimum for an increase in the number of symmetric jaw slides. This minimum can only be the deflection of the plate with annular stiffening. This method is used to obviate the difficulties of analyzing the directional effects of the jaw slides.

As a result, boundary condition number 3 of Section 3.3 is replaced by

$$\left.\frac{d\omega}{dx}\right|_{x_1} = \left.\frac{d\omega}{dx}\right|_{x_b} \quad \ldots\ldots\ldots 3.7.1$$

to include the constant slope effect of the slides;

$x_1 = r_1/a$, r_1 being the outer radius of the slide running from $x_b = b/a$. The reduced deflection, ω_s becomes

$$\omega_s = \frac{a^2P}{16\pi D}\left[(2C_{ss}-1)\ (1-x^2) + 2(2C_{ss}-x^2)\ \ell nx \right] \quad \ldots\ldots 3.7.2$$

$$\text{where } C_{ss} = \frac{x_b x_1\ (x_b \ell nx_b - x_1 \ell nx_1)}{(x_1-x_b)\ (1+x_b x_1)} \quad \ldots\ldots\ldots 3.7.3$$

For simplicity, the assumption is that the slide runs from b to a, ie. $x = 1$.

If ω_N is the deflection of a plate with N symmetric jaws, the deduced assymptotic relationship is of the form

$$\omega_N = \left\{ \omega_s + (\omega-\omega_s) e^{\left[-Nd/\pi(a+b)\right]} \right\} \left(\frac{1-x_b}{1-x}\right) \quad \ldots\ldots\ldots 3.7.4$$

where d is the circumferential width of the jaw slide. Substituting for ω and ω_s, the deflection of the diaphragm plate for N symmetric jaws is given by

$$\omega_N = \frac{a^2P}{16\pi D} \left\{ (2C_{ss}-1)\ (1-x^2) \left[1-e^{\left(\frac{-Nd}{\pi(a+b)}\right)} \right] + 2\left[1-e^{\left(\frac{-Nd}{\pi(a+b)}\right)} \right] (2C_{ss}-x^2)\ \ell n \right.$$

$$\left. +(x^2-1)\ (1+2C_s)\ e^{\left(\frac{-Nd}{\pi(a+b)}\right)} - 2e^{\left(\frac{-Nd}{\pi(a+b)}\right)} (2C_s+x^2)\ \ell nx \right\} \left(\frac{1-x_b}{1-x}\right) \quad \ldots 3.7.5$$

Figure 3.7.1 shows the pattern of ω and ω_s. ω_N fits between the two lines. It can be observed from Figure 3.7.1 that ω_s, though a curve, can be assumed to be a straight line while ω is not. To proportion ω_N between ω and ω_s means that ω_N is not a straight line. This is a major deviation from the constant slope deflection of the diaphragm plate due to the jaw slide and the plate taper.

3.8 ESTIMATION OF THE OUTER DIAMETER OF PLATE

The taper in the diaphragm plate thickness is a uniqueness that gives the plate a deflection curve that is close to a straight line as the central hole of the plate is approached. It also creates a difficulty in locating the point about which the plate flexes in bending. This flexure point locates the effective outer diameter of the plate. Chidlow (4) located this flexure point empirically by measuring the deflection along a radius, plotting the curve, and extrapolating it backwards to establish the point of zero deflection. A point of zero deflection is difficult to measure ordinarily. This method, though very sound, requires that it be done for every plate and taper size.

A simple method of estimating the effective outer diameter of the plate is to extend the tangents at the ends of the radiused support shown in Figure 3.8.1 to meet at point P. Without this stress-relieving radius at this support, the plate will flex at point P. For large plates, locating point P', the inner end of the radius, is sufficient to estimate the outer radius, a.

In practice, a is measured by using, say, a jig borer, to clock the taper of the plate. The distance at which the clock indicates a change in slope is read off the scale of the borer as a.

3.9 SHEAR STRESS EFFECT

The theory of plate deflection used so far holds for small $t/_a$ ratio where shear stress effects are negligible (7). The effects of shear for large $t/_a$ ratios are significant and should be considered. At $t/_a = 0.2$ for example, the error introduced by neglecting shear is 21% for a simply supported annular plate. To eliminate this error, the shear

stress effect has to be included in the evaluation of the plate deflection. Wahl and Lobo (13) give the condition that if $\frac{t}{a-b} > 0.167$ for annular plate with fixed edges, shear may be taken into account.

Deflection, ω^1 due to shear (7) is given as

$$\omega^1 = \frac{-Pt^2}{8\pi(1-\nu)D} \ln (1/x) \quad \ldots\ldots\ldots\ldots .3.9.1$$

where t is the equivalent thickness of the plate. This effect is added to equations 3.6.8 and 3.7.2. The ratio, K_s of the deflection with shear effect included to the deflection without shear is

$$K_s = 1 + \frac{2}{(1-\nu)} (t/a)^2 \frac{\ln (1/x)}{(1-x^2)(1+2C_s)+2(2C_s+x^2)\ln x} \quad \ldots .3.9.2$$

$K_s = 1$ when shear stress effects are neglected and the second term of equation 3.9.2 is the error in the calculated deflection. K_s for the maximum plate deflection is plotted as t/a is varied in Figure 3.9.1 for $x_b = b/a = 0.1$ and 0.3. If a maximum error of 10% is assumed, the effects of shear should be considered when

$$t/a > \begin{cases} 0.13 \text{ for } b/a = 0.10 \text{ and } 0.50 \\ 0.15 \text{ for } b/a = 0.20 \text{ and } 0.40 \\ 0.16 \text{ for } b/a = 0.30 \end{cases} \quad \ldots .3.9.3$$

For purposes of research, it is suggested that the shear stress effects should be considered if

$$\frac{t_b}{a} > 0.12 \quad \ldots\ldots\ldots\ldots\ldots\ldots .3.9.4$$

for the diaphragm plate since the inner thickness, t_b is the largest.

Figure 3.9.2 shows that K_s is a minimum around $b/a = 0.30$ and increases to infinity as the inner radius, b approaches zero. Any increase in deflection due to thrust loading without a similar increase in deflection due to the gripping couples, increases the gripping force of a diaphragm plate. Shear stress consideration has this effect on deflection if other parameters remain constant. To exploit this shear stress contribution, the following condition is obtained from Figure 3.9.2:

$$\frac{b}{a} \leq 0.2 \quad \text{or} \quad b/a \geq 0.4 \qquad \ldots\ldots\ldots\ldots 3.9.5$$

For the diaphragm plate,

$$b/a \leq 0.2 \qquad \ldots\ldots\ldots\ldots 3.9.6$$

This is based on shear stress considerations only and does not take into account such things as higher stresses as b gets small and other physical requirements of the chuck. It will be shown later in Chapter 5 that gripping force increases as b/a ratio decreases.

Most diaphragm plates are made of high strength steel which allows the plates to be thin, thereby making the effects of shear negligible. Theoretical solutions in this work exclude shear effects.

3.10 MAXIMUM STRESS AND MINIMUM THICKNESS OF PLATE

The maximum bending moment on the plate, M_r occurs at the outer boundary, a where $t = t_a$.

For simplicity, t_a is taken as the limiting thickness, and the maximum stress, σ is

$$\sigma = \frac{6M_r}{t_a^2} \qquad \ldots\ldots\ldots\ldots 3.10.1$$

From equation 3.6.5 M_r at x=1 is

$$M_r\Big|_{max} = \frac{P(1-2C_s)}{4\pi} \quad \ldots\ldots\ldots\ldots 3.10.2$$

where P is the maximum allowable thrust. Therefore,

$$\sigma = \frac{3}{2} \frac{P(1-2C_s)}{\pi t_a^2} \quad \ldots\ldots\ldots\ldots 3.10.3$$

With a safety factor, s_f and a plate material yield strength, S_y, the minimum outer thickness, t_a is defined by:

$$t_a \geq \left[\frac{s_f P(1-2C_s)}{\pi S_y}\right]^{\frac{1}{2}} \quad \ldots\ldots\ldots\ldots 3.10.4$$

This minimum thickness does not take into account the in-plane stress due to the gripping force.

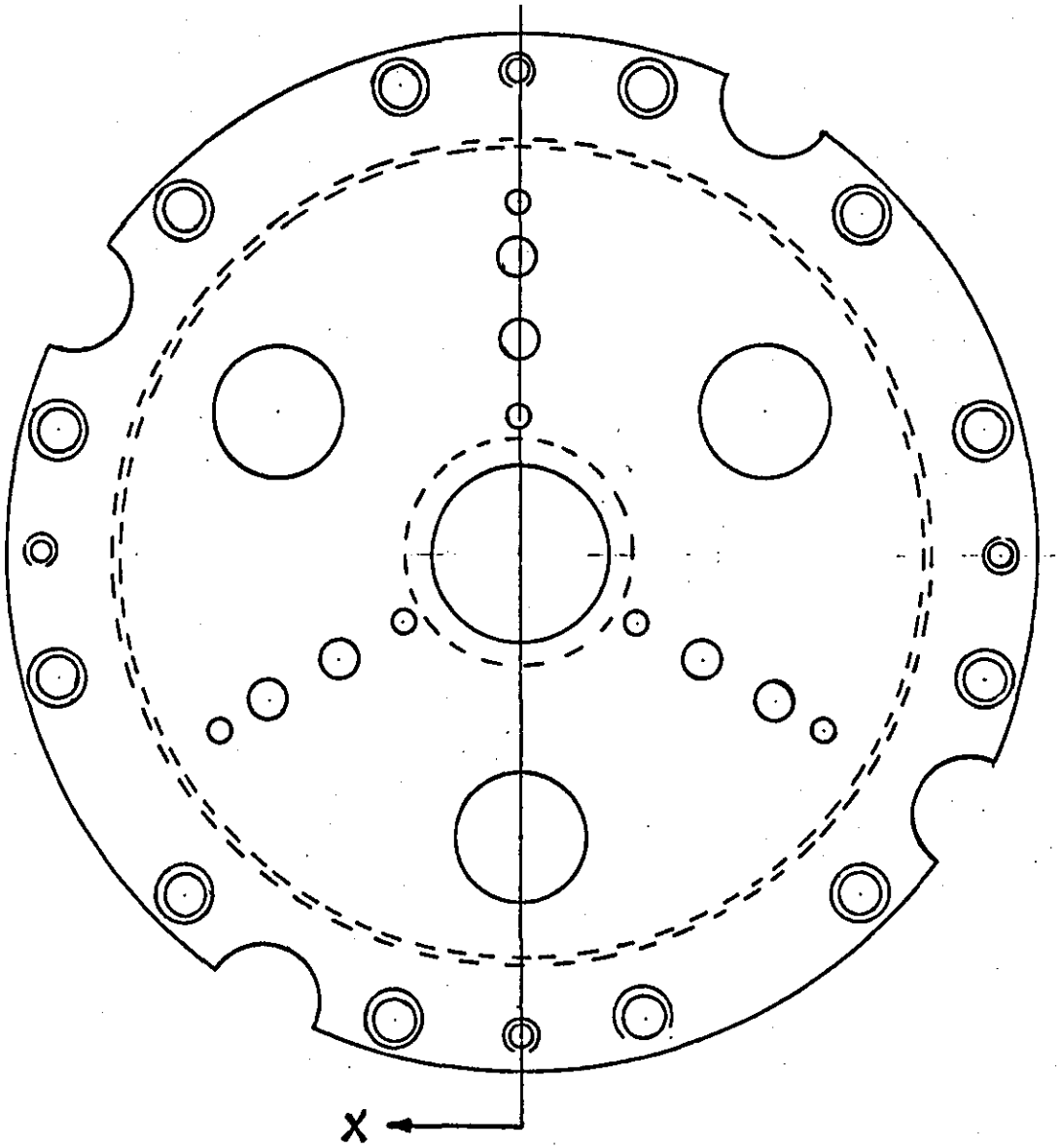

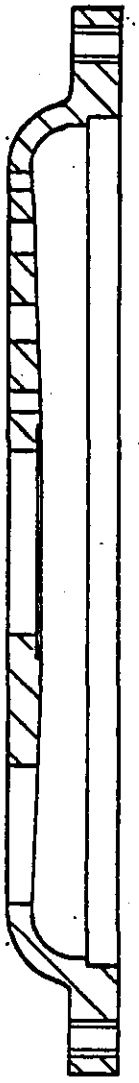

SECTION X—X

FIG.3.1.1 DIAPHRAGM PLATE

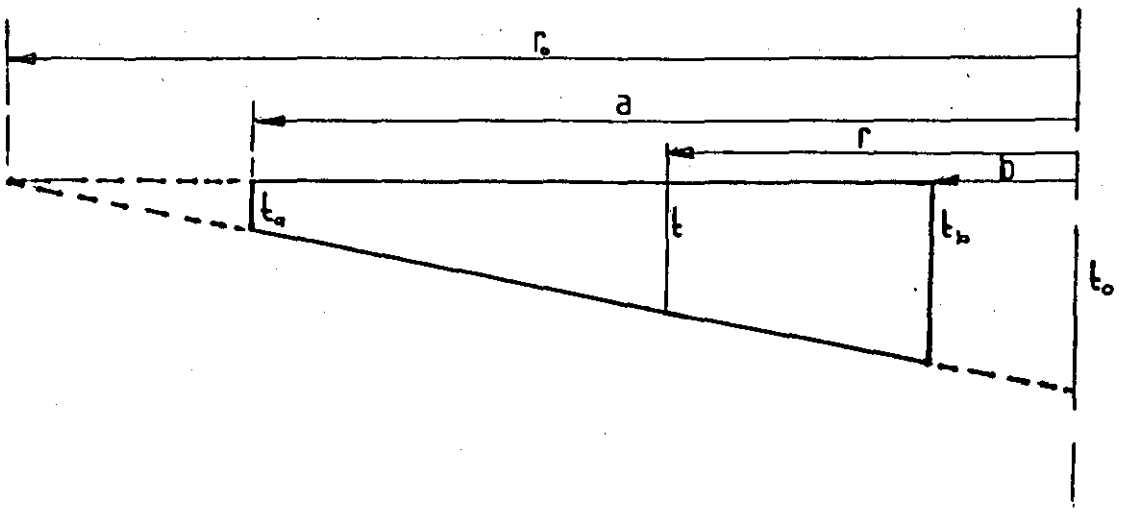

FIG. 3.1.2 A CROSS—SECTION OF PLATE THICKNESS

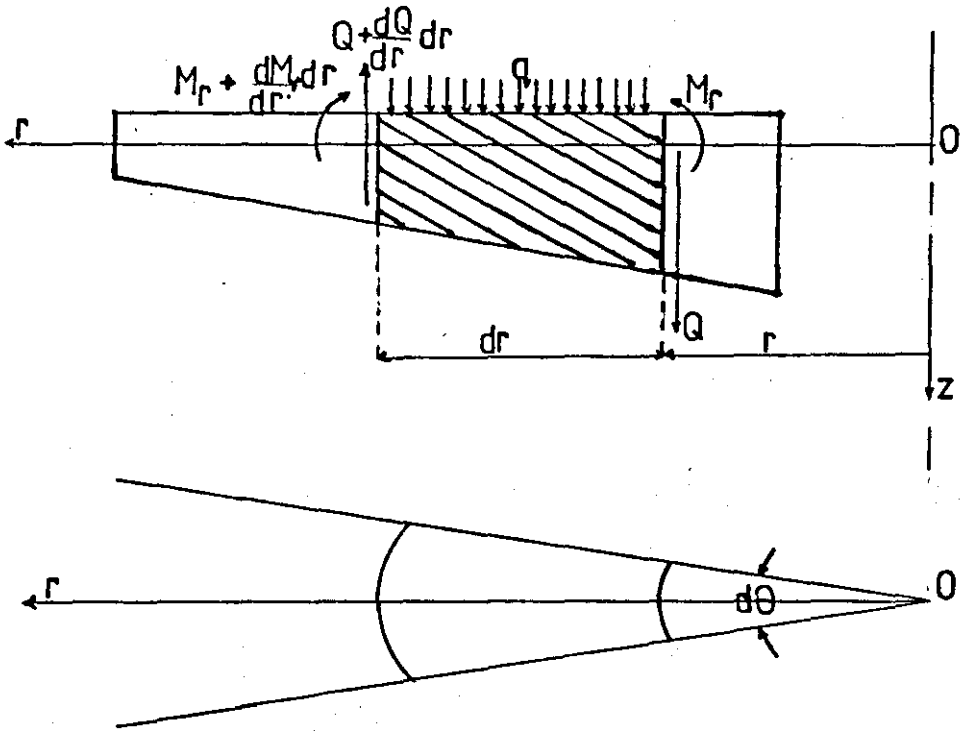

FIG. 3.2.1 EQUILIBRUM DIAGRAM OF PLATE

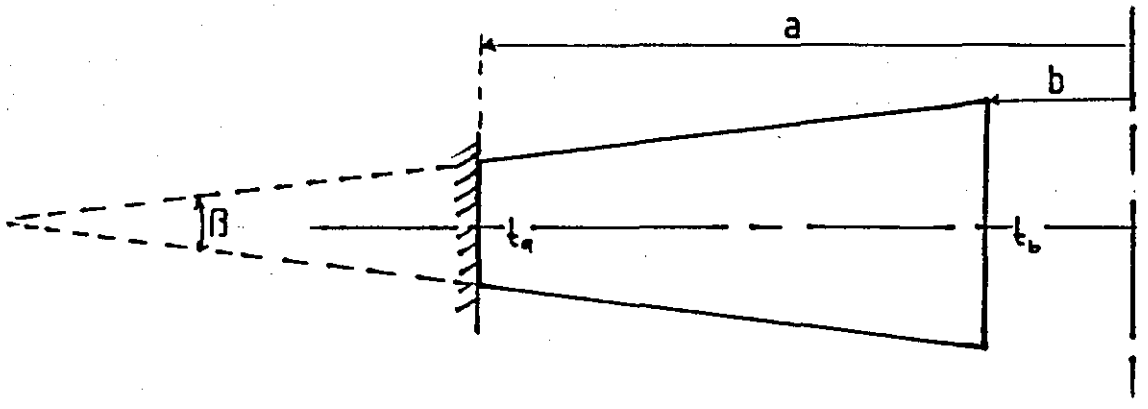

FIG.3.3.1 SYMMETRIC VARYING THICKNESS PLATE

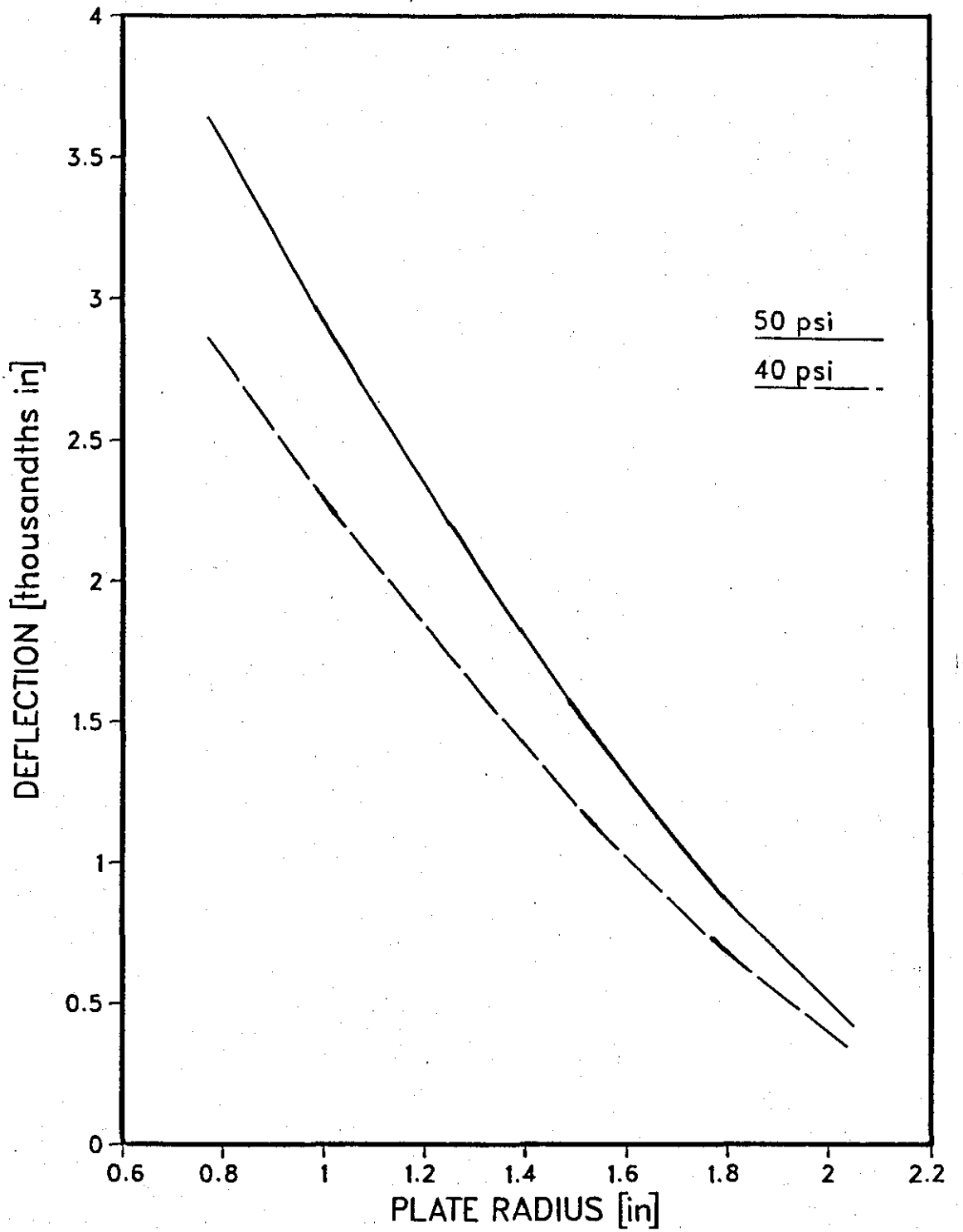

FIG. 3.4.1 VARYING THICKNESS DEFLECTION PREDICTION FOR PLATE A

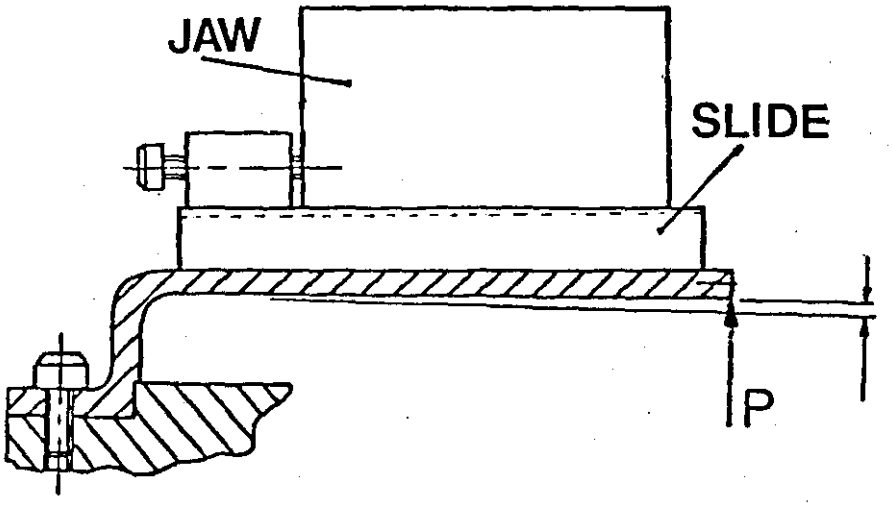

FIG.3.4.2 PLATE CARRYING JAW AND SLIDE

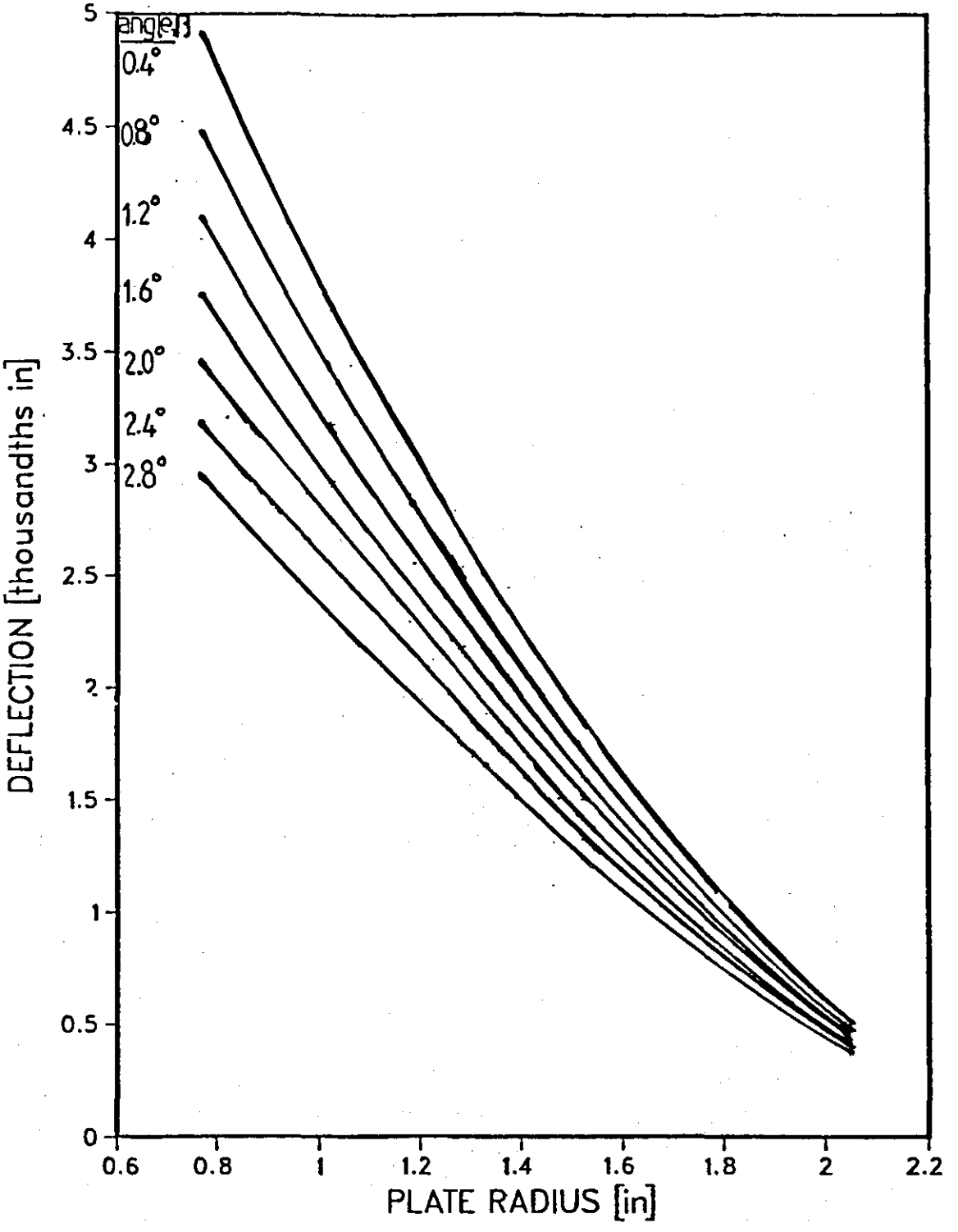

FIG.3.5.1 EFFECT OF THICKNESS VARIATION ON THE SLOPE OF PLATE DEFLECTION

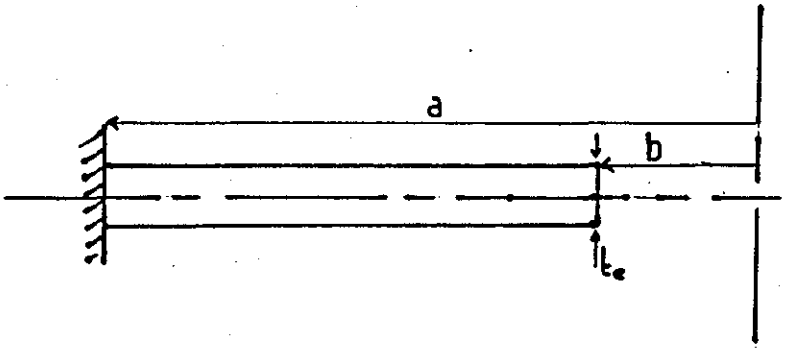

FIG.3.6.1 EQUIVALENT CONSTANT THICKNESS PLATE

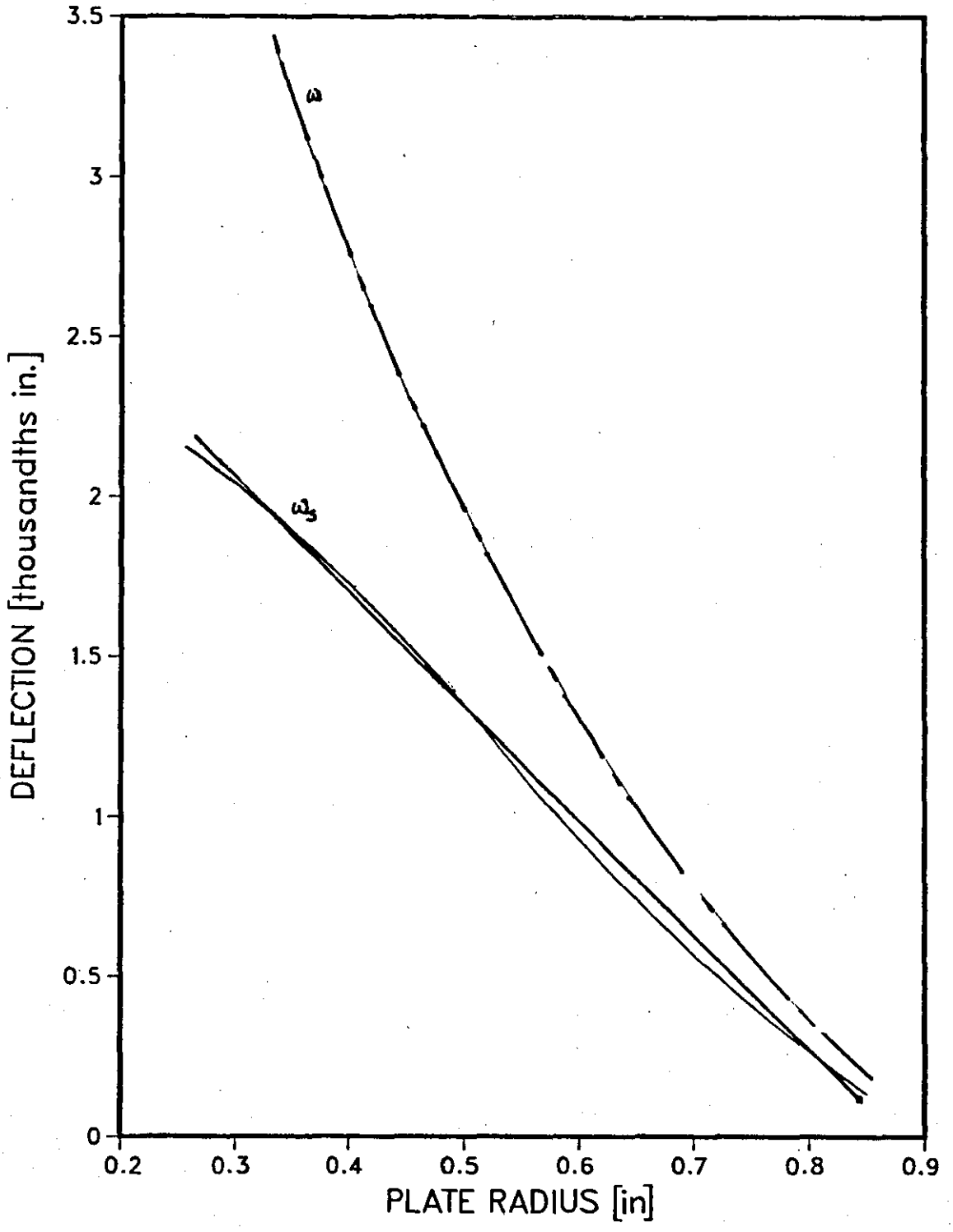

FIG. 3.7.1 CONSTANT THICKNESS PLATE DEFLECTION FOR NO JAWS AND ANNULAR STIFFENER

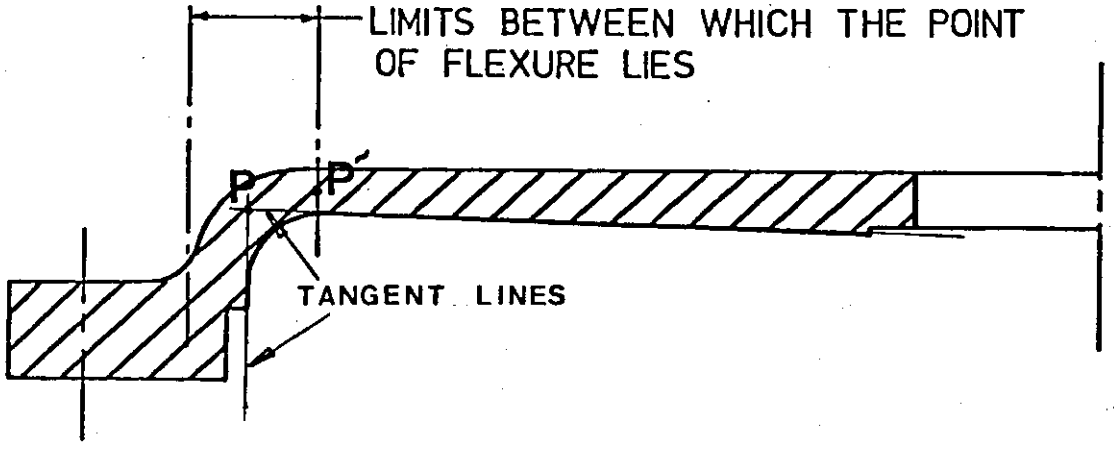

FIG.3.8.1 CROSS SECTION OF PLATE SHOWING APPROXIMATE POSITION OF FLEXING POINT

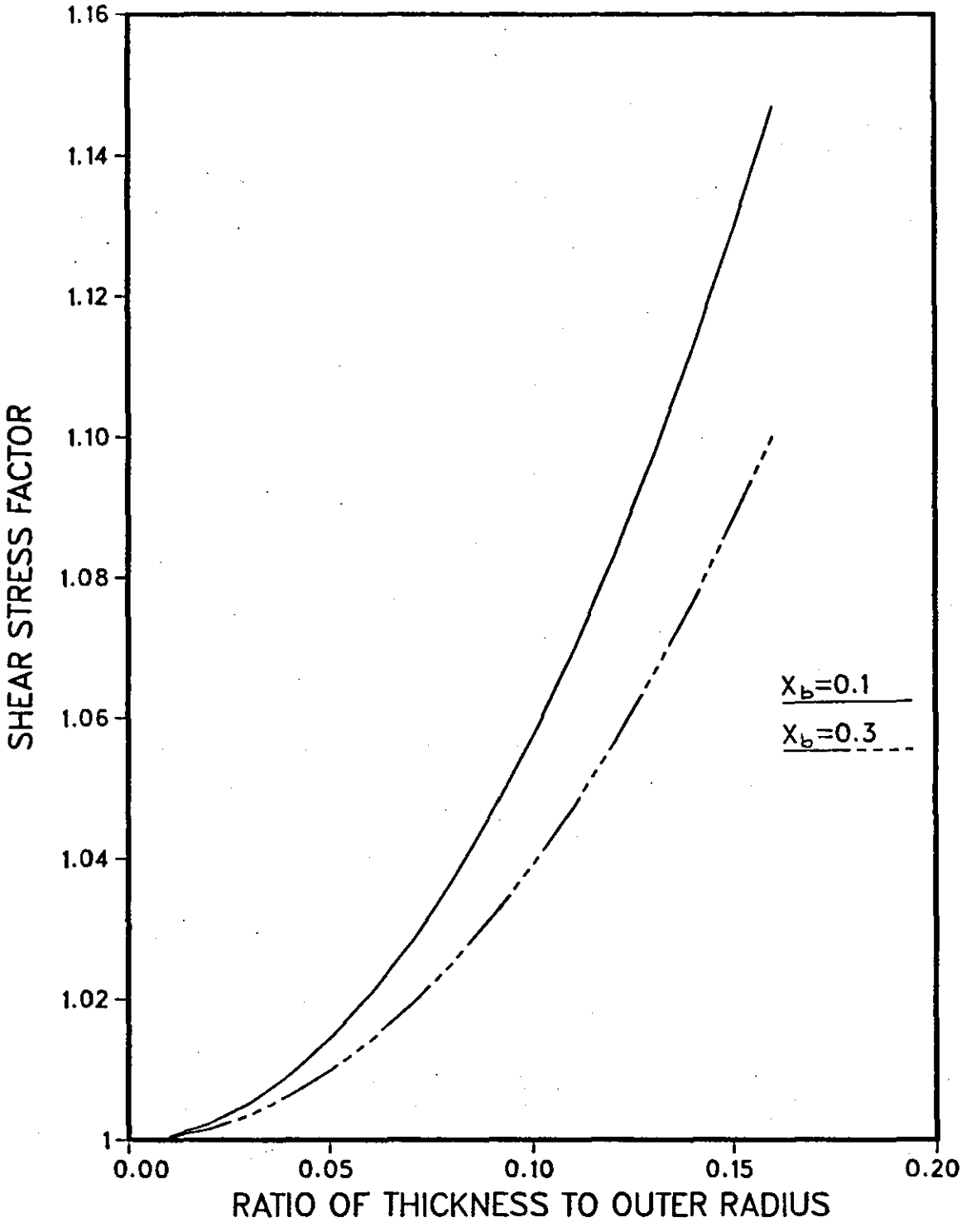

FIG. 3.9.1 SHEAR STRESS CONTRIBUTION TO MAXIMUM PLATE DEFLECTION

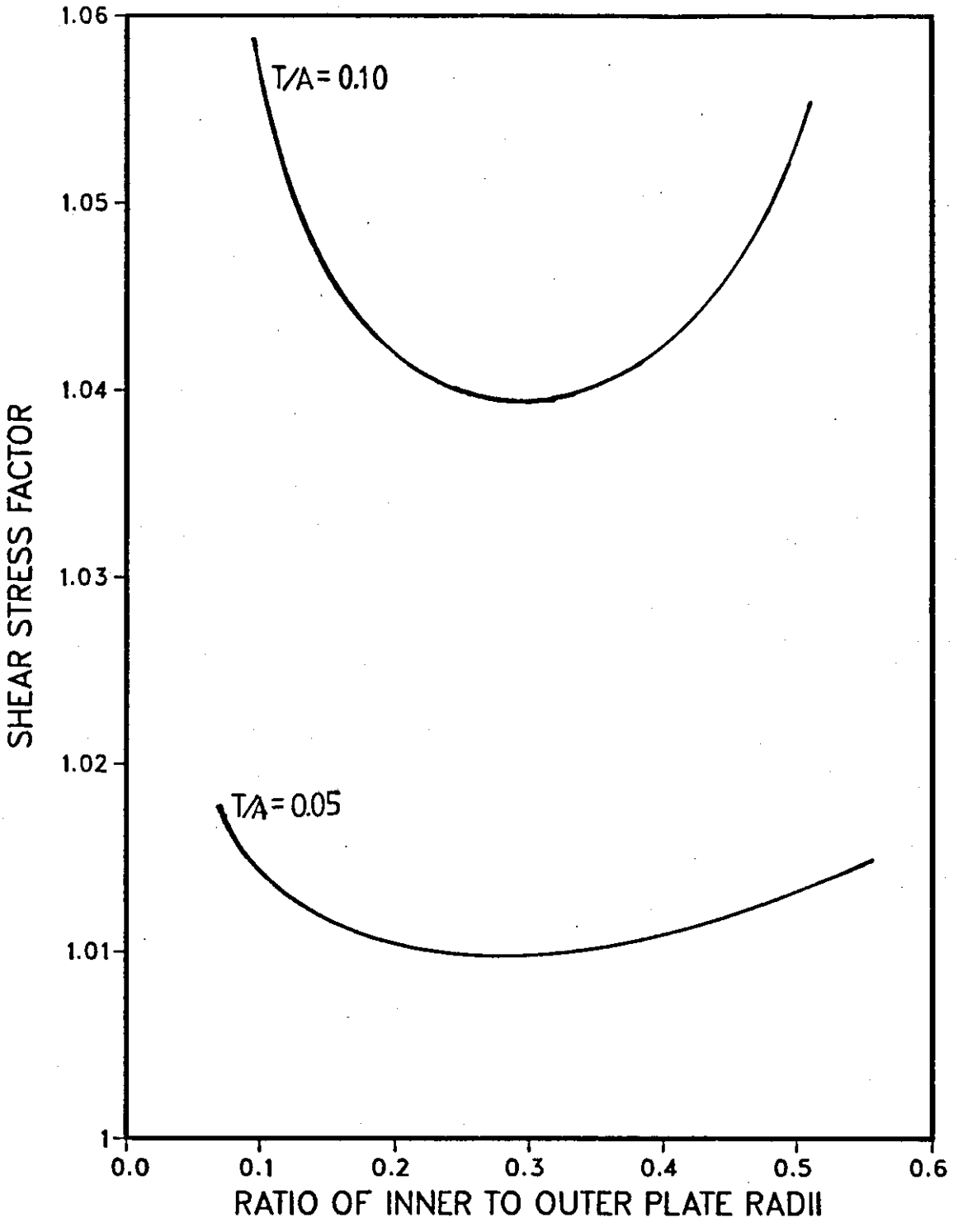

FIG. 3.9.2 SHEAR STRESS CONTRIBUTION TO PLATE DEFLECTION

CHAPTER FOUR

PLATE DEFLECTION MEASUREMENT

4.1 SCOPE OF DEFLECTION MEASUREMENT

Assumptions about the diaphragm plate thickness, the boundary conditions and the exact position of the ring thrust have been made in establishing the predicted deflection equation of the diaphragm plate of equation 3.6.8. Further assumptions of boundary conditions and deflection pattern were made to determine equation 3.7.5 for the plate deflection with any number of jaws. The purpose of this experimental measurement is to evaluate the closeness of the deflection prediction.

Measurements of deflection were taken for the symmetrical case of plate without jaws which were compared with the deflection of the plate with jaws. The measurement of deflection for plate with jaws was limited to the radial line along the jaws. This is because any couple resulting from gripping action acts along this line. It is the deflection of this line for thrust loading that is equated to its deflection by couples in order to obtain gripping force. Another reason is that the constant slope boundary condition strictly applies to the plate material under the jaws only.

The devices used in this experiment include a rig to hold and locate the chuck, a deflection measuring probe and readout system, and a pressure gauge and regulator for the air supply to the chuck cylinder (see Figure 4.1.1). The pressure gauge and regulator, and diaphragm chuck were calibrated together as an assembly using a Clockhouse proving ring for direct thrust reading. The Clockhouse proving ring was calibrated with a standard ring (see Section 4.4).

4.2 DIAPHRAGM PLATES

Two plates, A and B were used for the deflection measurements. They have the same outer and inner diameters but different thicknesses. Plate B carries only four jaws and has four locating holes that normally give the plate reduced stiffness. Plate B is made from a nickel-chrome steel and heat treated. Plate A carries three, four or six jaws without any locating holes and was manufactured from EN 3B steel (see Figures 1.2.2, 4.2.1 and 4.2.2).

The two plates have a taper of 1.85° with plate A being the thicker of the two. Steel blocks were used as stiffeners in place of the jaws. The blocks had the same length and width as the jaw slides. The specific block width, d, tested was 0.875in. Equation 3.7.5 showed that the deflection for any number of jaws varied with the width of the jaw slides. The jaws, jaw slides and cleet plates are shown in Figure 4.2.3. Details of the plates are given in Table 4.2.1.

Measurements of deflection were initially taken for Plate A without any holes for the dowels and screws. Two radial lines (A and B) were marked out on the plate and the deflections along these lines measured (see Figures 4.2.4 and 4.2.5). The deflections are given in Figure 4.2.6 as lines A1 and B1 which are essentially the same. This confirms that the deflection is symmetrical. Lines A2 and B2 of Figure 4.2.6 show the deflections after the holes were drilled with one set of holes falling on radial line B. Comparing lines A2 and B2, the loss of symmetry due to holes along radial line B can be seen to be negligible. Comparing the deflections before and after the holes were drilled, there is a reduction in the stiffness of the plate. However, the resulting increase in deflection can be neglected.

4.3 DETERMINATION OF MATERIAL PROPERTIES FOR PLATE A

Poisson's Ratio and Modulus of Elasticity, being the material properties that appear in the deflection equation, were determined experimentally for Plate A. The yield strength of the same material was also determined in order to establish a maximum allowable load on the diaphragm Plate A.

The standard test piece used is shown in Figure 4.3.1 as recommended by the British Standards Institute. The gauge length portion of the specimen was finished by filing to avoid any work-hardening of the piece.

Strain gauges were mounted on the broad side of the test piece to measure axial and transverse strains. A TECQUIPMENT STRAIN SCOPE with separate channels connected to the axial and transverse strain gauges was used as a read-out system. A Hounsfield Tensometer was used to apply different axial loads and the corresponding strains measured (Figure 4.3.2). The slope of the line obtained by plotting transverse strains against axial strains in Figure 4.3.3 is the Poisson's Ratio of the material. Poisson's Ratio, ν of Plate A was determined to be 0.298. See Appendix A.

Another test piece was mounted on a DENISON TENSION MACHINE and pulled to failure. A recorder connected to the machine produced the plot shown in Figure 4.3.4 for axial load versus elongation. The slope of the elastic zone when the axes are converted to stress and strain give the Modulus of Elasticity of the material. The yield and ultimate points are indicated on the graph. The following experimental values were obtained for Plate A:

Modulus of Elasticity, $E = 28.8 \times 10^6 \text{ LBS/IN}^2$
Yield Strength, $S_y = 36000 \text{ LBS/IN}^2$
Ultimate Strength, $S_u = 38880 \text{ LBS/IN}^2$

The standard E of 30 x 10^6 LBS/IN^2 and ν of 0.3 for steel are used in all calculations.[a]

4.4 CALIBRATION OF CLOCKHOUSE PROVING RINGS, AND PRESSURE GAUGE AND CHUCK ASSEMBLY

To determine the thrust on the diaphragm plate, accurate measurements of the air pressure and the chuck piston area are necessary. The thrust is the product of air pressure and the piston area. This method is prone to errors of pressure fluctuation and leakage. The method used in this experiment to determine thrust was to calibrate the whole assembly in terms of input air pressure as recorded by the gauge and output thrust.

Two Clockhouse Proving Rings were calibrated using a Standard Ring to give the Sensitivity charts shown in Figures 4.4.1 and 4.4.2. See Appendix B. The pressure gauge connected to each size of chucks was calibrated as shown in Figure 4.4.3. Figures 4.4.4 and 4.4.5 are the calibration charts for two sizes of chucks such that the thrust is obtained for a given input pressure read from gauge. See Appendix C.

4.5 EXPERIMENTAL PROCEDURE FOR DEFLECTION MEASUREMENT

Figure 4.5.1 is the mounted frame of a small precision drilling machine with its rotary table mounted on two slides such that movement is possible in two axes. In place of the drilling head and drive motor is a rigid device detailed in Figure 4.5.2 for holding the measuring probe. This device allows for adjusting the height of the probe in two ways. On the rotary table is mounted a fixture detailed in Figure 4.5.3 for locating the diaphragm chuck. The fixture has side windows as accesses for air supply to the chuck cylinder. This arrangement of the measuring rig was designed by Chidlow (4).

a. The use of standard values of E and ν is to apply the same values for all the plates, and to provide general tables for gripping force (Tables 5.5.1-5.5.11).

The measuring probe was a linear variable displacement transducer attached to an RDP ELECTRONICS Extensometer and Creep Monitor. Slip gauges were used to check the accuracy and precision of the measuring system. See Appendix D.

Points were marked out on radial lines on the plate surface for deflection measurements. Reference readings were taken for these points at zero pressure before loading the plate and measuring deflection for different air pressures (thrusts). The actual deflection was obtained by subtracting the readings at zero pressure from the readings at a given pressure. Errors due to flatness were eliminated in this way. Readings were taken at 50 psi (1184.02 lbs), 40 psi (929.32 lbs), and 30 psi (687.81 lbs).

Steel blocks representing jaws were mounted on the plate and corresponding deflection points marked-out. The whole process of deflection measurement was repeated for three, four and six jaws. Deflection measurements with and without jaws were compared with each other and also with theoretical predictions.

4.6 DEFLECTION RESULTS AND DISCUSSION

Figure 4.6.1 is a plot of the measured deflection for Plate A without any jaws at 30, 40 and 50 psi. The points fall very closely on a straight line and confirm the stated significant effect of the variation in thickness. This behaviour is not possible to reproduce in a constant thickness plate without manipulating the loading mode.

Another important observation is the behaviour of the plate when carrying jaws. Figures 4.6.2, 4.6.3 and 4.6.4 show the stiffening effect of the jaws. The deflection of the inner portion of the plate is reduced while the deflection of the outer portion actually increased. As the number of

jaws increases from three to six, the already increased deflection of the outer region at three jaws begins to decrease. A steady decrease in deflection continues to take place at the inner region. Figure 4.6.5 also agrees with this observation for Plate B. This observation is difficult to explain or express mathematically. This observed behaviour was instrumental in the formulation of equation 3.7.4 for the deflection of a constant thickness plate carrying any number of jaws.

Figures 4.6.6 to 4.6.8 are the measured and predicted deflections for Plate A with three, four and six jaws. Figure 4.6.9 is for Plate B with four jaws. The predicted deflections are generally higher than the measured deflections up till a point where the predicted line crosses the measured line. The prediction of the deflection within this range is acceptable. After this point, the predicted line begins to fall to much smaller values than the measured. Deflection data are given in Appendix E.

A significant discrepancy between the measured and predicted lines is the pattern of deflection. The measured deflection is approximately a straight line while the predicted pattern is mildly concave. The main reason for this discrepancy is the equivalent constant thickness plate assumption. It was stated earlier that a constant thickness plate will always have a curvilinear form of deflection.

A second reason is the behaviour of the plate with mounted jaws. The fact that the deflection of the outer region actually increases is difficult to express mathematically. In using the term $(1-x_b)(1-x)$ in equation 3.7.4, a concave pattern was introduced to the curve. This was to take account of the increase in deflection of the outer region. The third reason is the formulation of equation 3.7.4, which is based on proportioning to the number of jaws the deflections between a free plate and an annularly stiffened plate.

This again ensures that the resulting deflection remains curvilinear.

It is to be emphasized here that the discrepancy in the deflection prediction does not invalidate the deflection approach of predicting the gripping force, which is the main objective of this work. The relative behaviour of the plate under thrust loading to its behaviour under couples is the important factor in predicting gripping force.

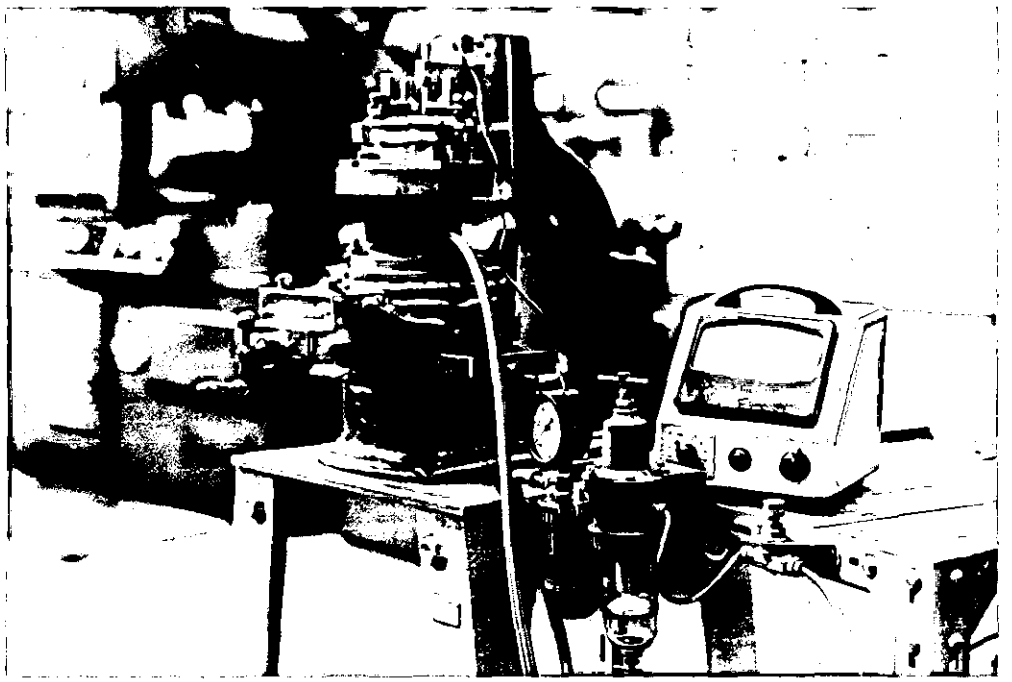

FIG.4.1.1 DEFLECTION MEASURING RIG.

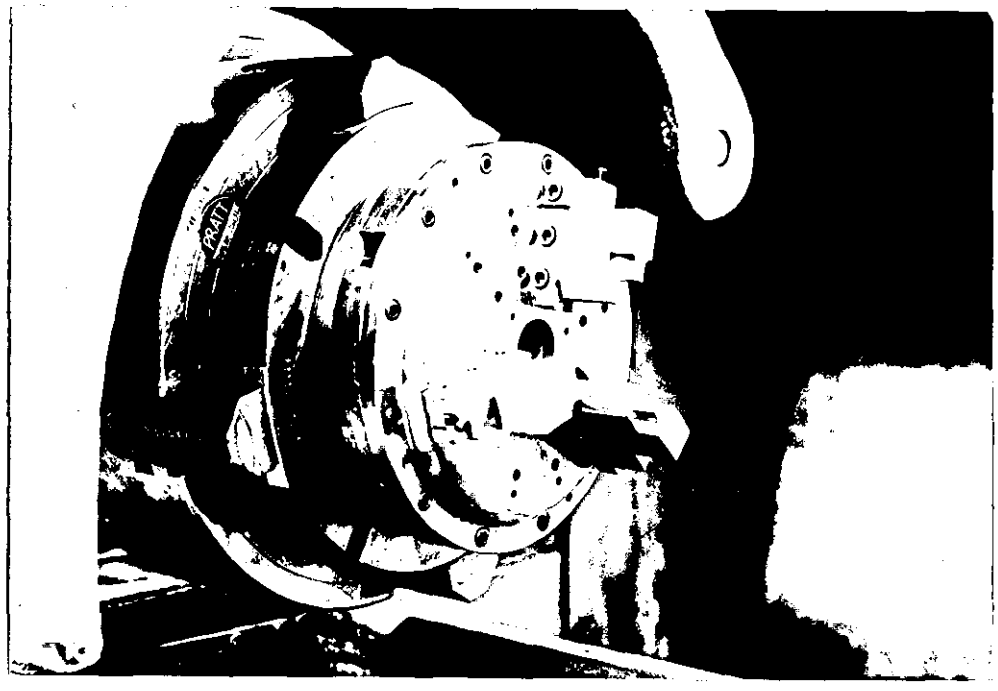

FIG.4.2.1 PLATE A WITH JAWS AND JAW SLIDES (Plate A)

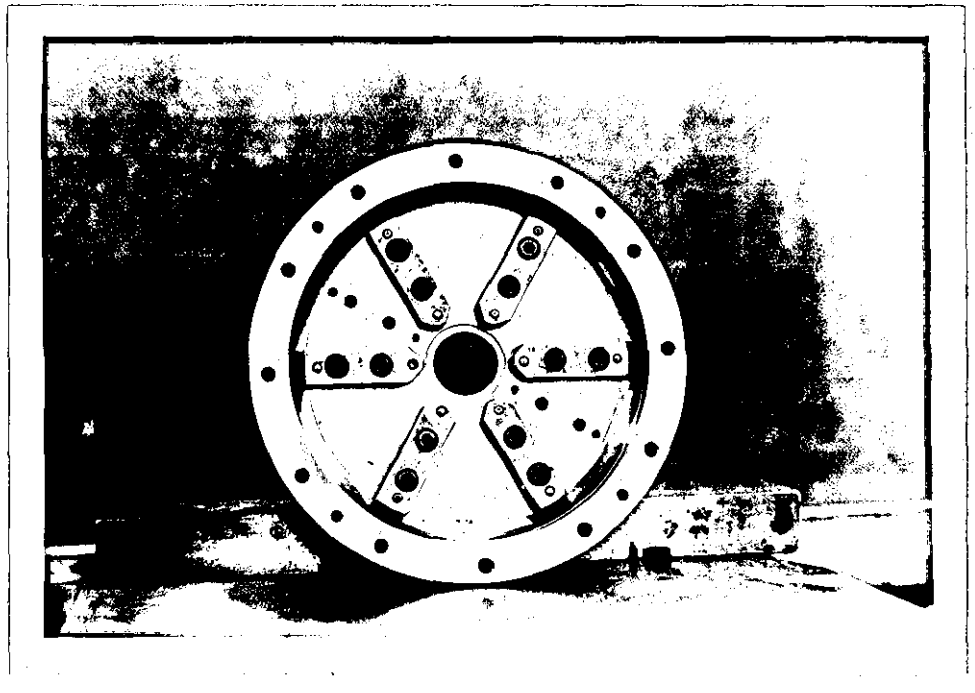

FIG. 4.2.2 PLATE A SHOWING CLEET PLATES

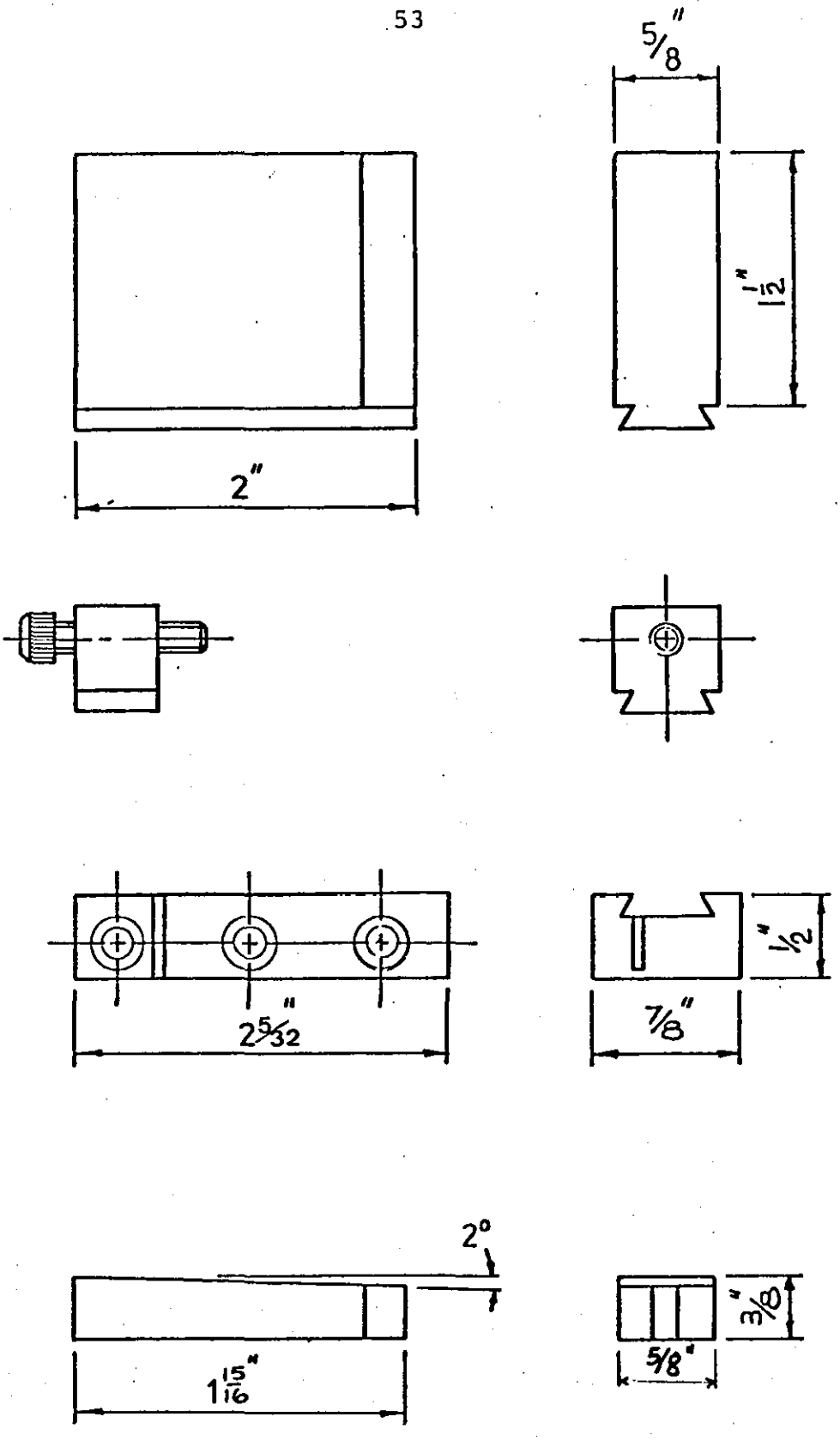

FIG.4.2.3 DETAILS OF JAW ASSEMBLY FOR DIAPHRAGM CHUCK

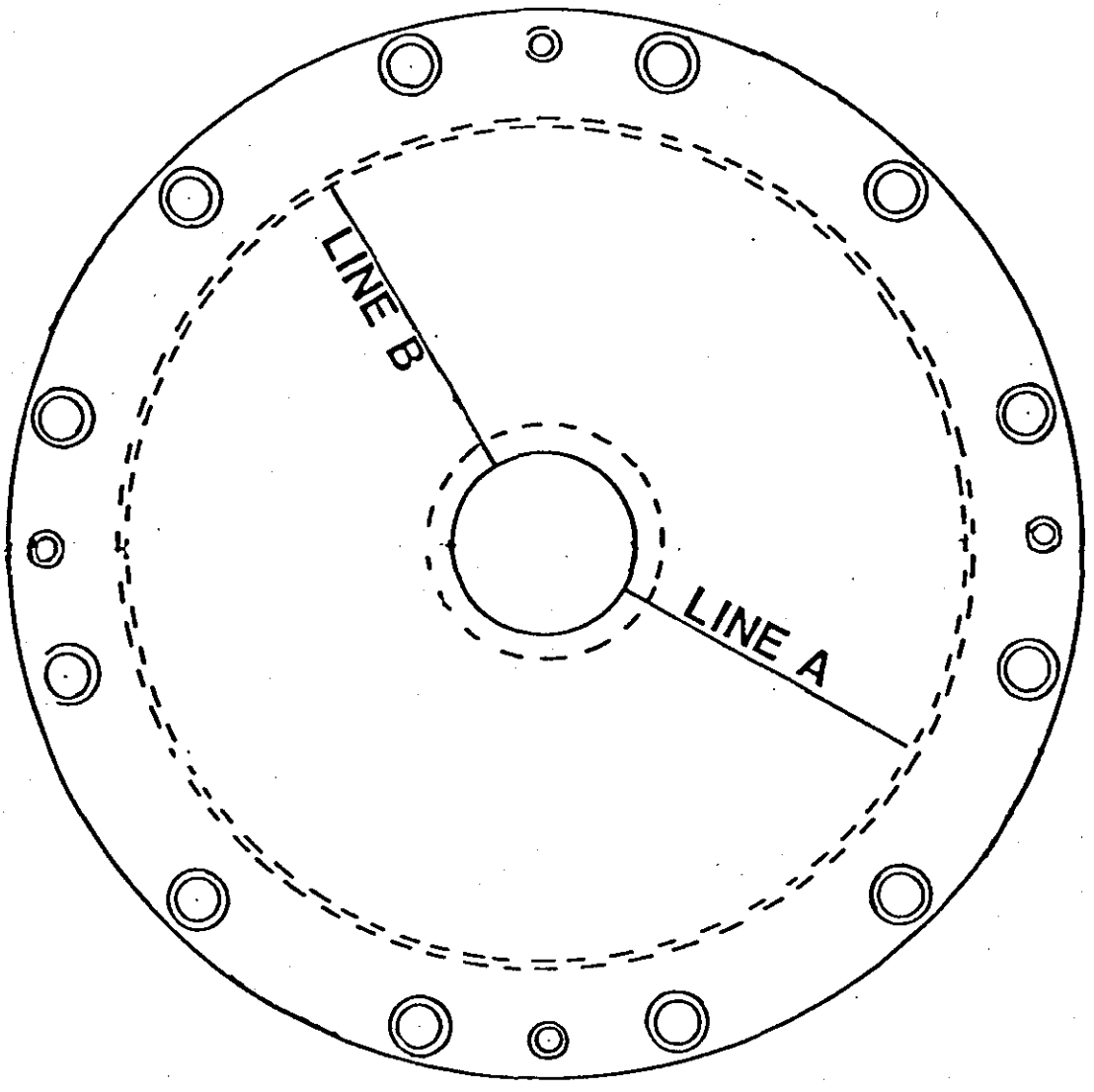

FIG. 4.2.4 PLATE A WITHOUT HOLES

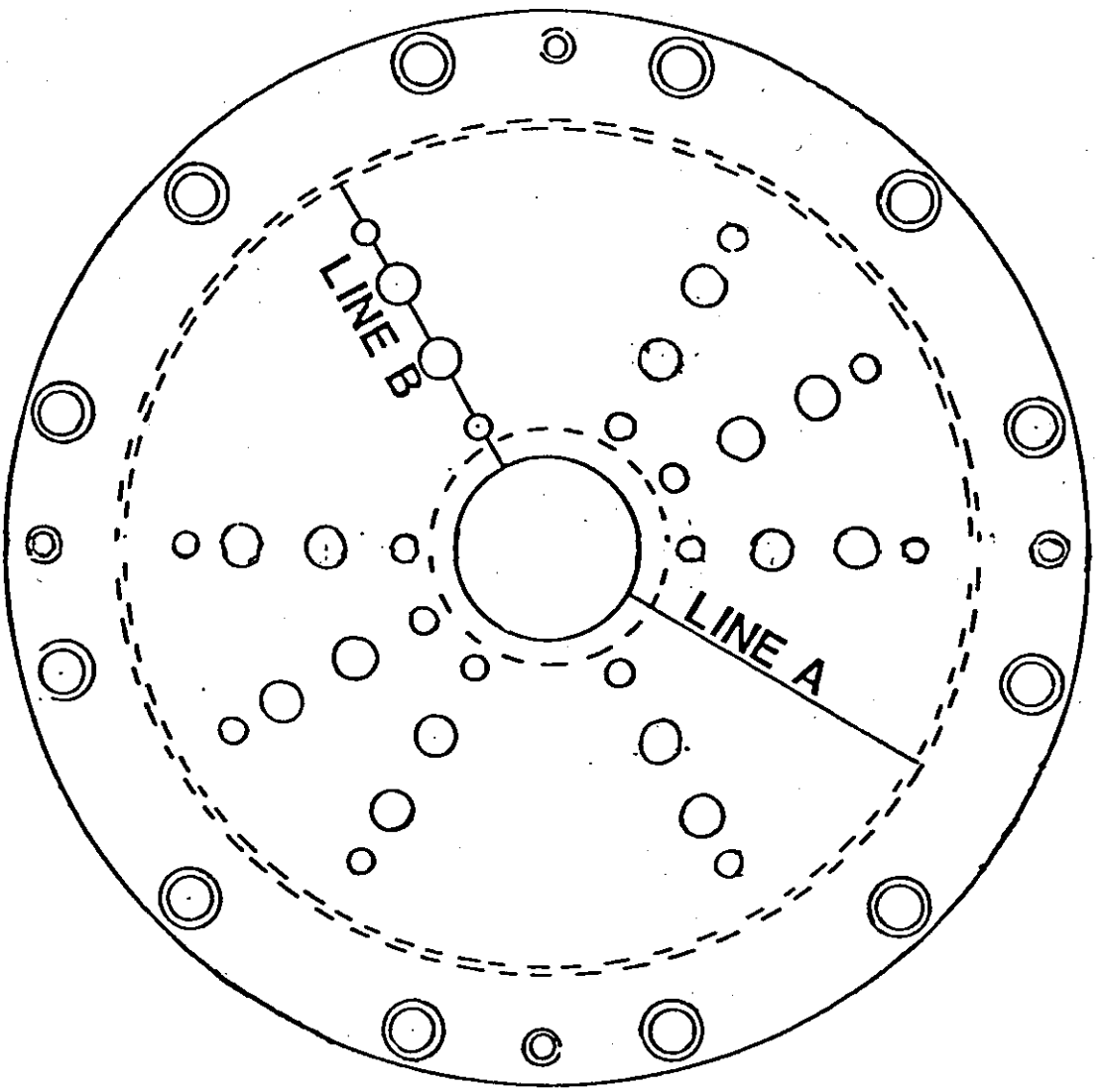

FIG. 4.2.5 PLATE A WITH HOLES

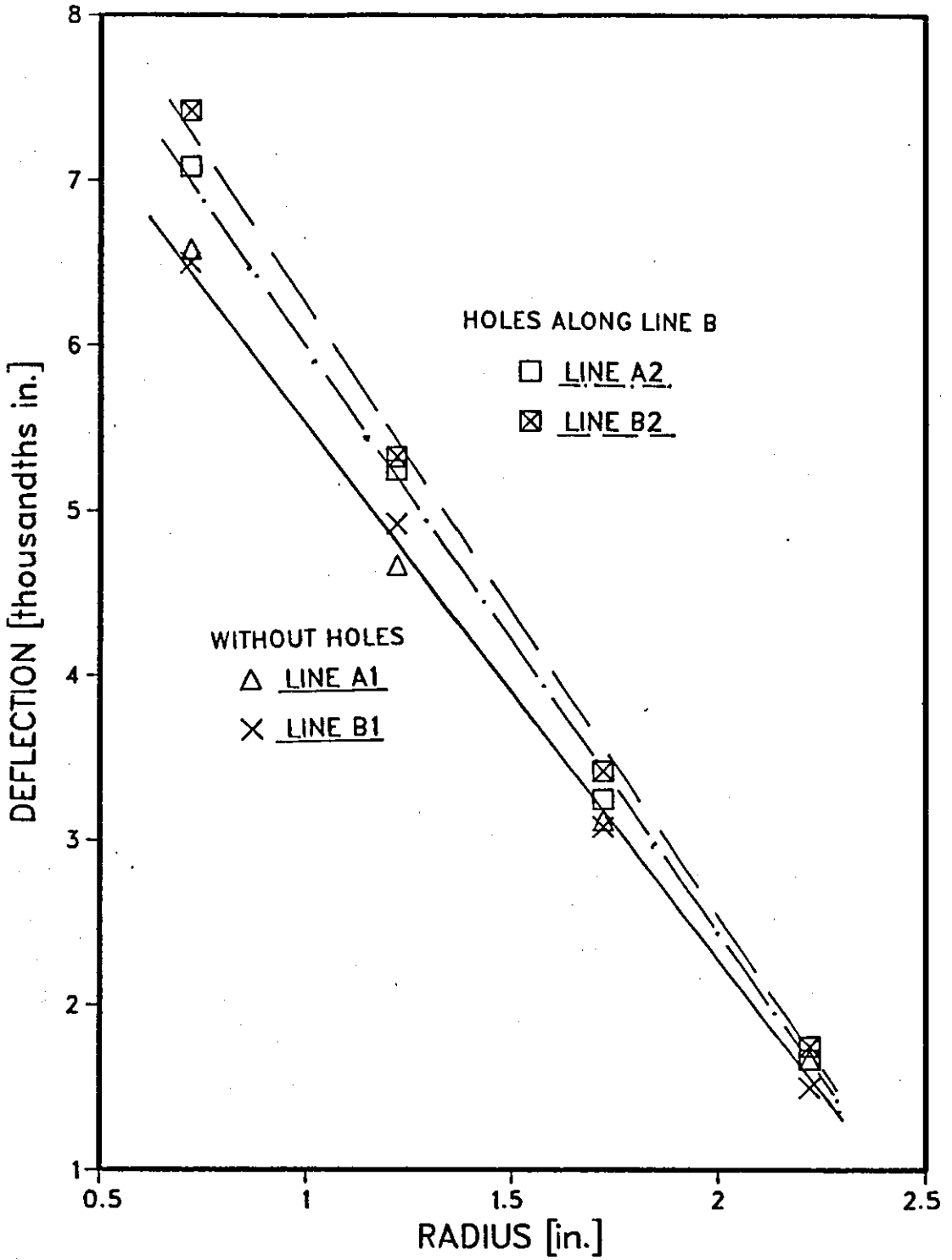

FIG. 4.2.6 DEFLECTION OF PLATE A WITH AND WITHOUT HOLES

TABLE 4.2.1. -- DIAPHRAGM PLATE DIMENSIONS

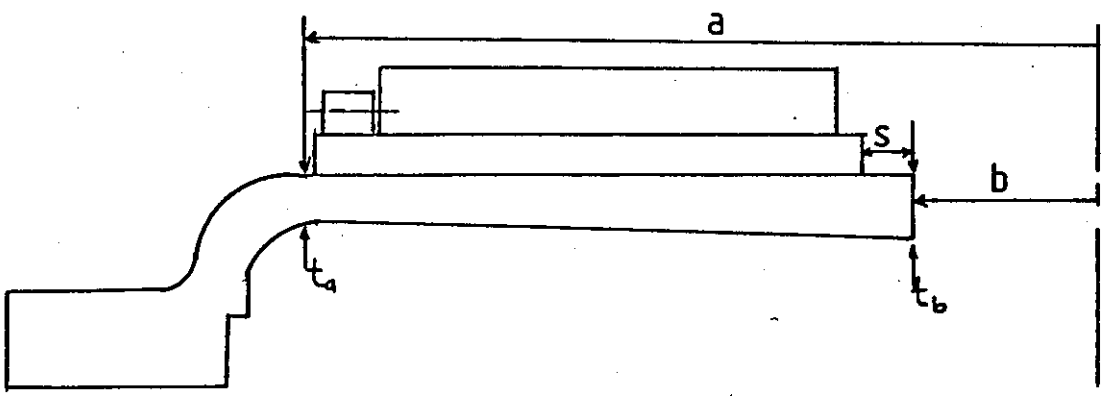

PLATE A : a = 2.5578 in. t_a = 0.208 in.
b = 0.5178 in. t_b = 0.270 in.
s = 0.20 in.

PLATE B : a = 2.5578 in. t_a = 0.168 in.
b = 0.5180 in. t_b = 0.226 in
s = 0.20 in.

PLATE C[3]: a = 2.1500 in. t_a = 0.098 in.
b = 0.4650 in. t_b = 0.152 in.
s = 0.10 in.

3. From Chidlow's (4) work, Cross-checked by this author

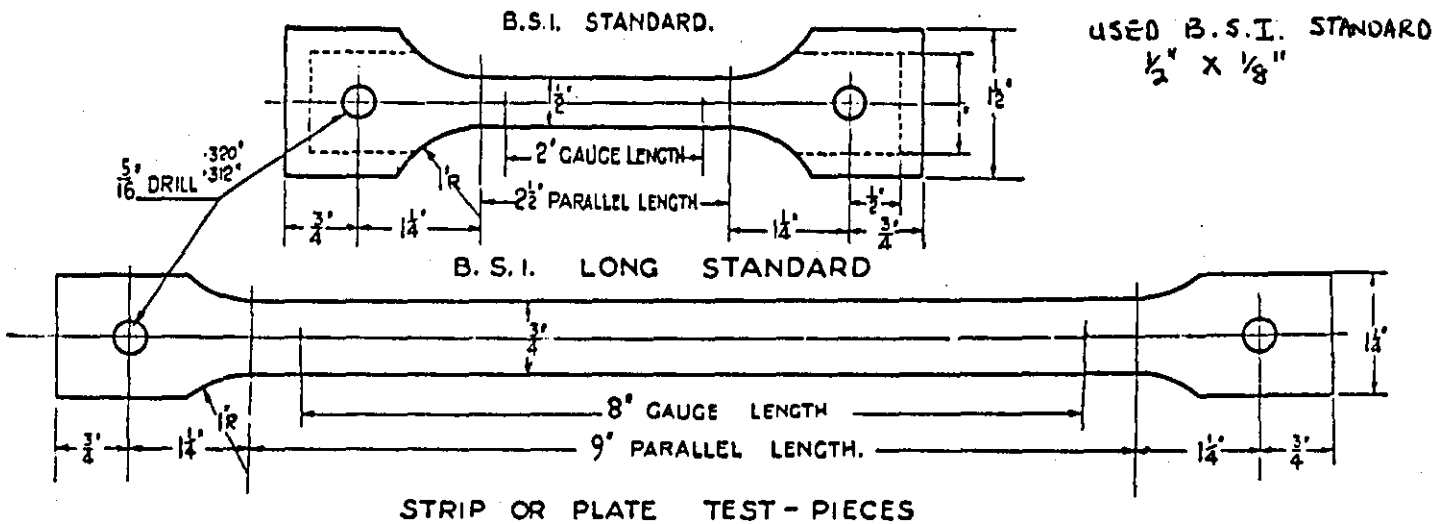

FIG. 4.3.1 TENSION TEST - PIECE

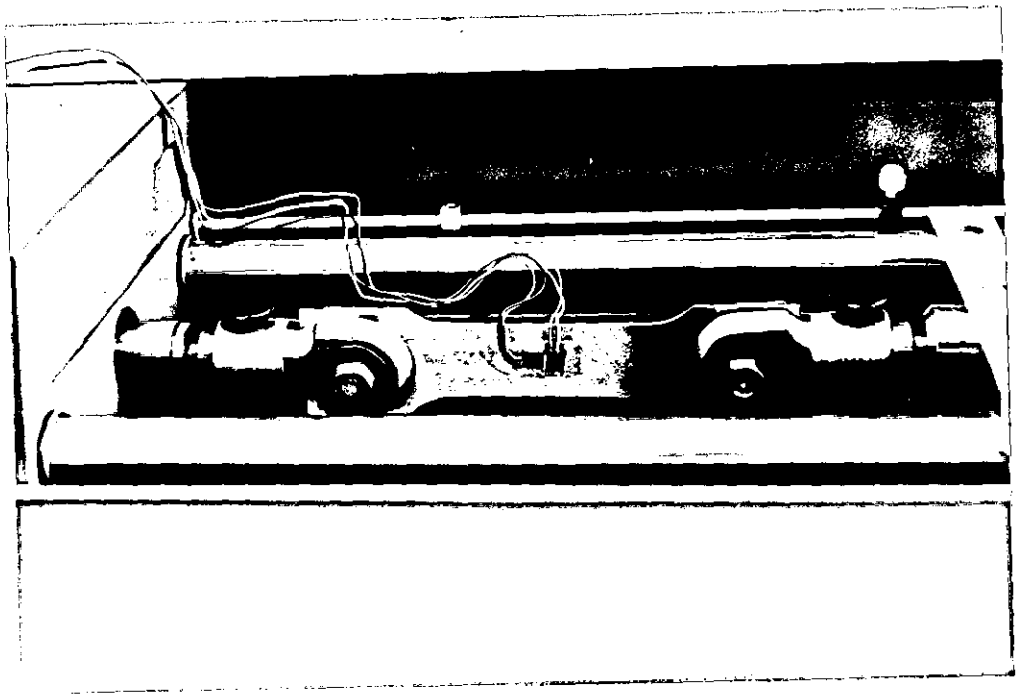

FIG. 4.3.2 TEST-PIECE IN EXTENSOMETER

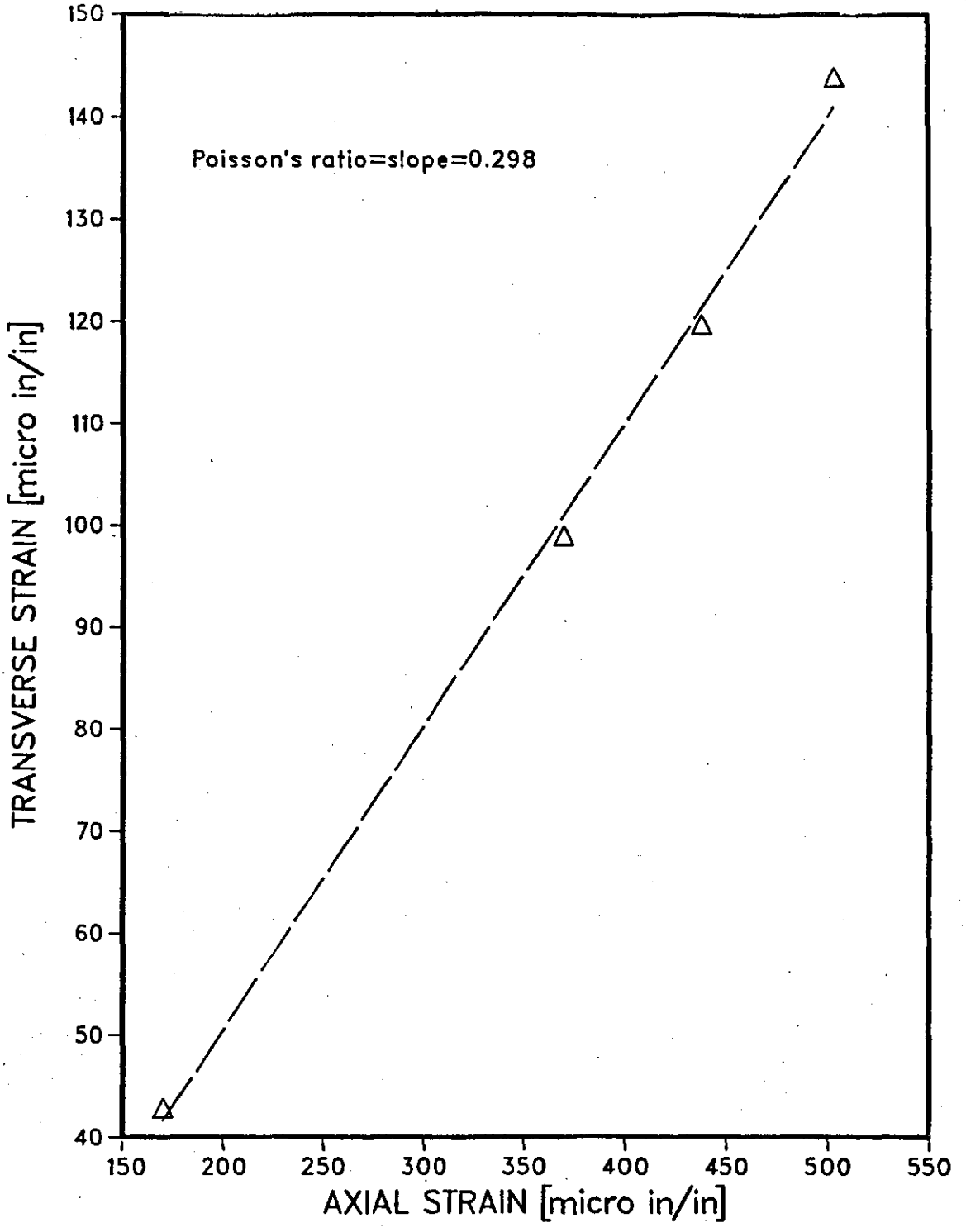

FIG. 4.3.3 POISSON'S RATIO FOR PLATE A

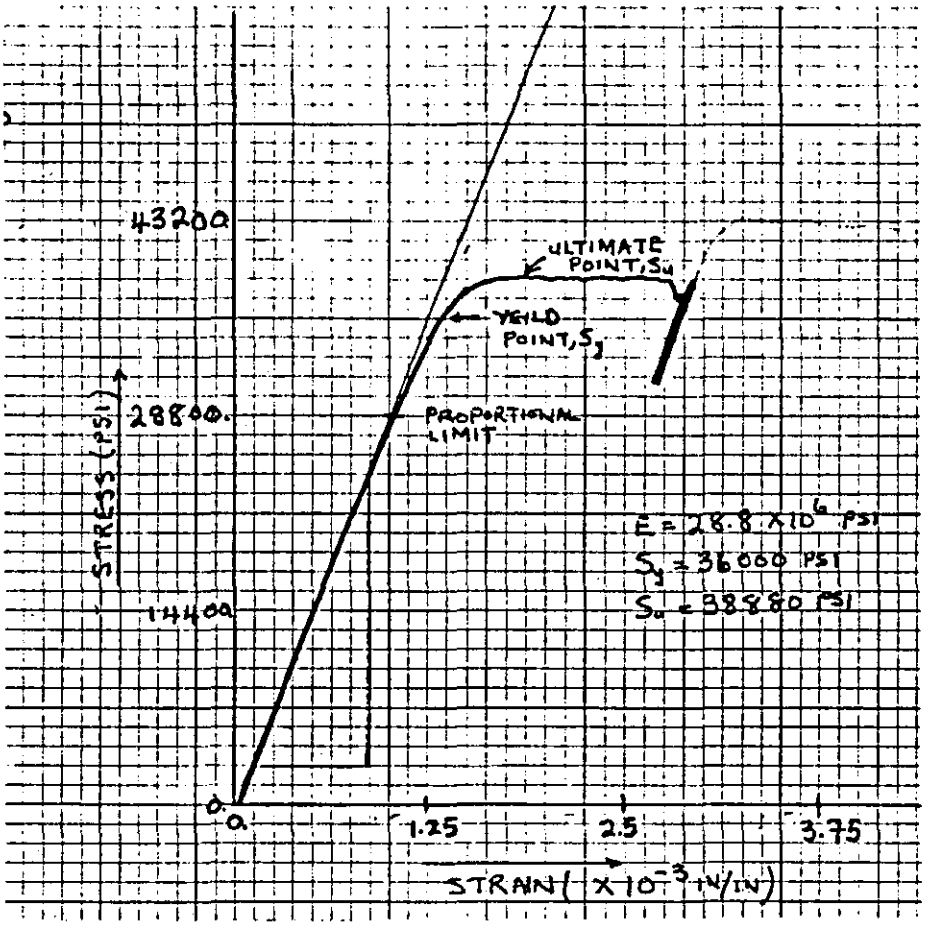

FIG. 4.3.4 MATERIAL STRESS — STRAIN CURVE

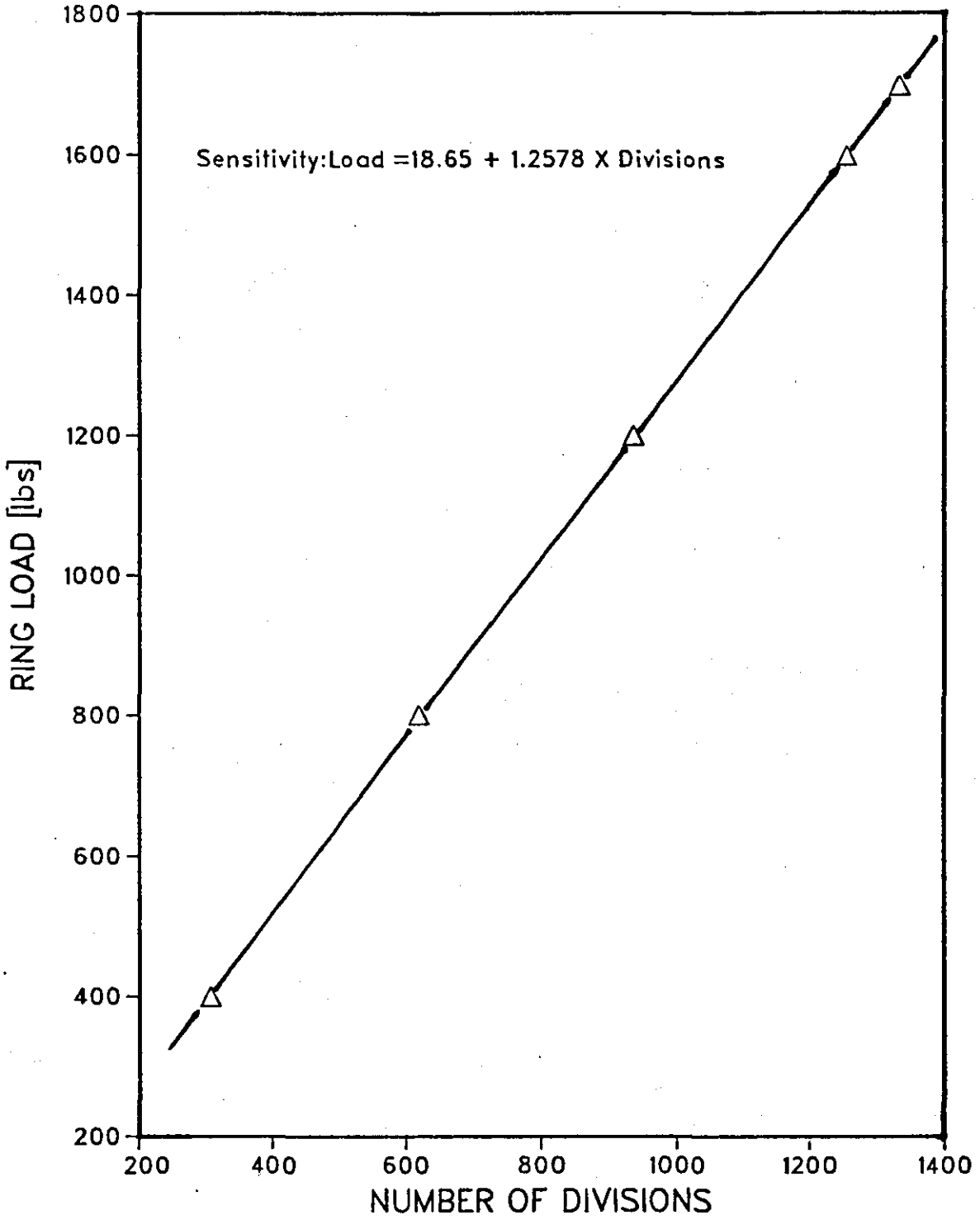

FIG.4.4.1 CALIBRATION CHART FOR 2000 LBS CLOCKHOUSE RING

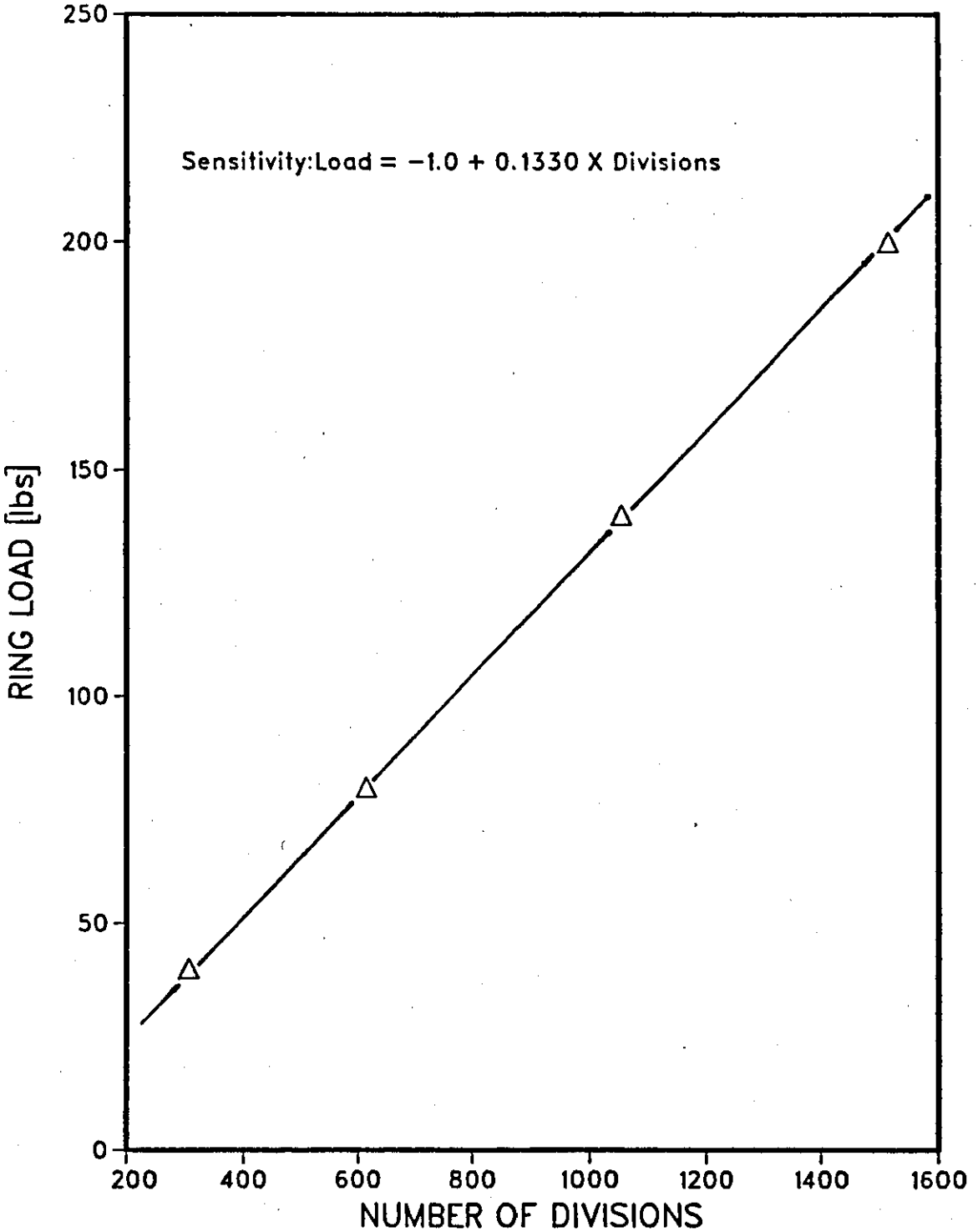

FIG.4.4.2 CALIBRATION CHART FOR 200 LBS CLOCKHOUSE RING

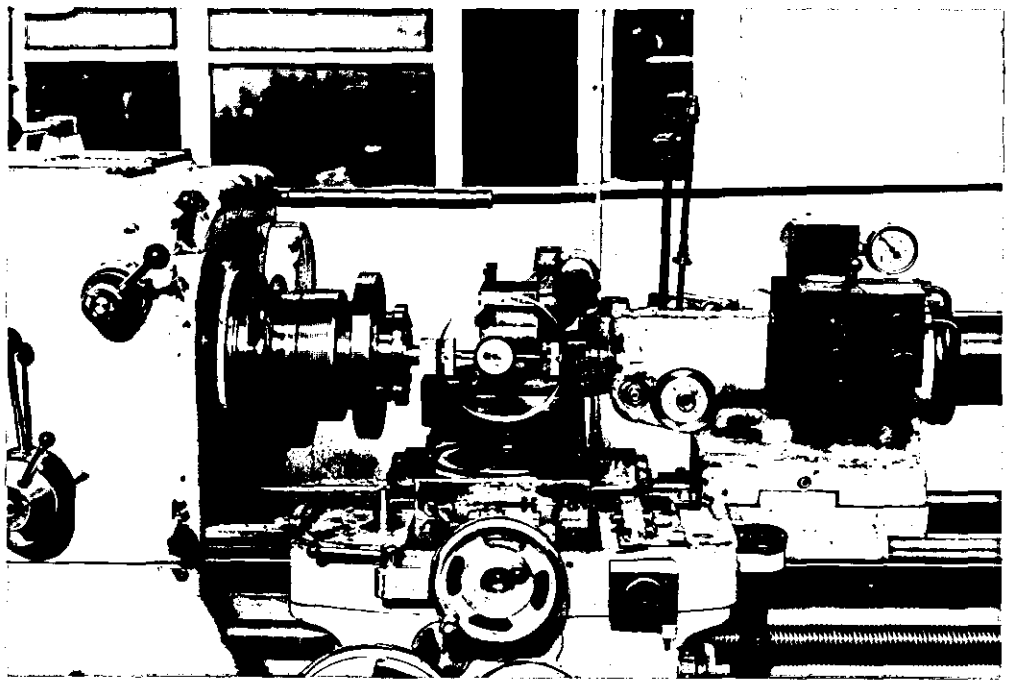

FIG.4.4 .3 CALIBRATION OF CHUCK & GAUGE ASSEMBLY

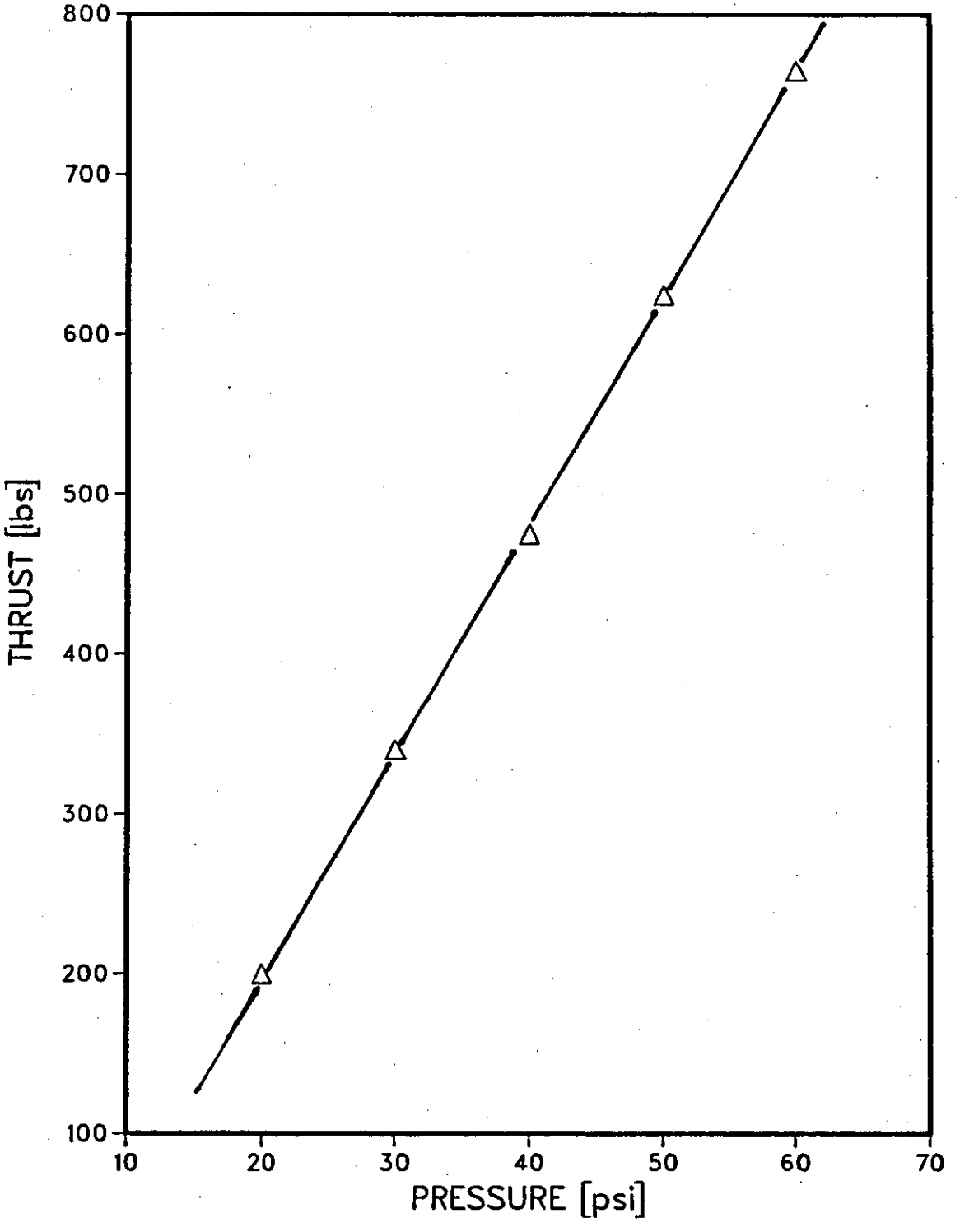

FIG. 4.4.4 CALIBRATION CHART FOR 5 1/2 IN CHUCK AND PRESSURE GAUGE ASSEMBLY

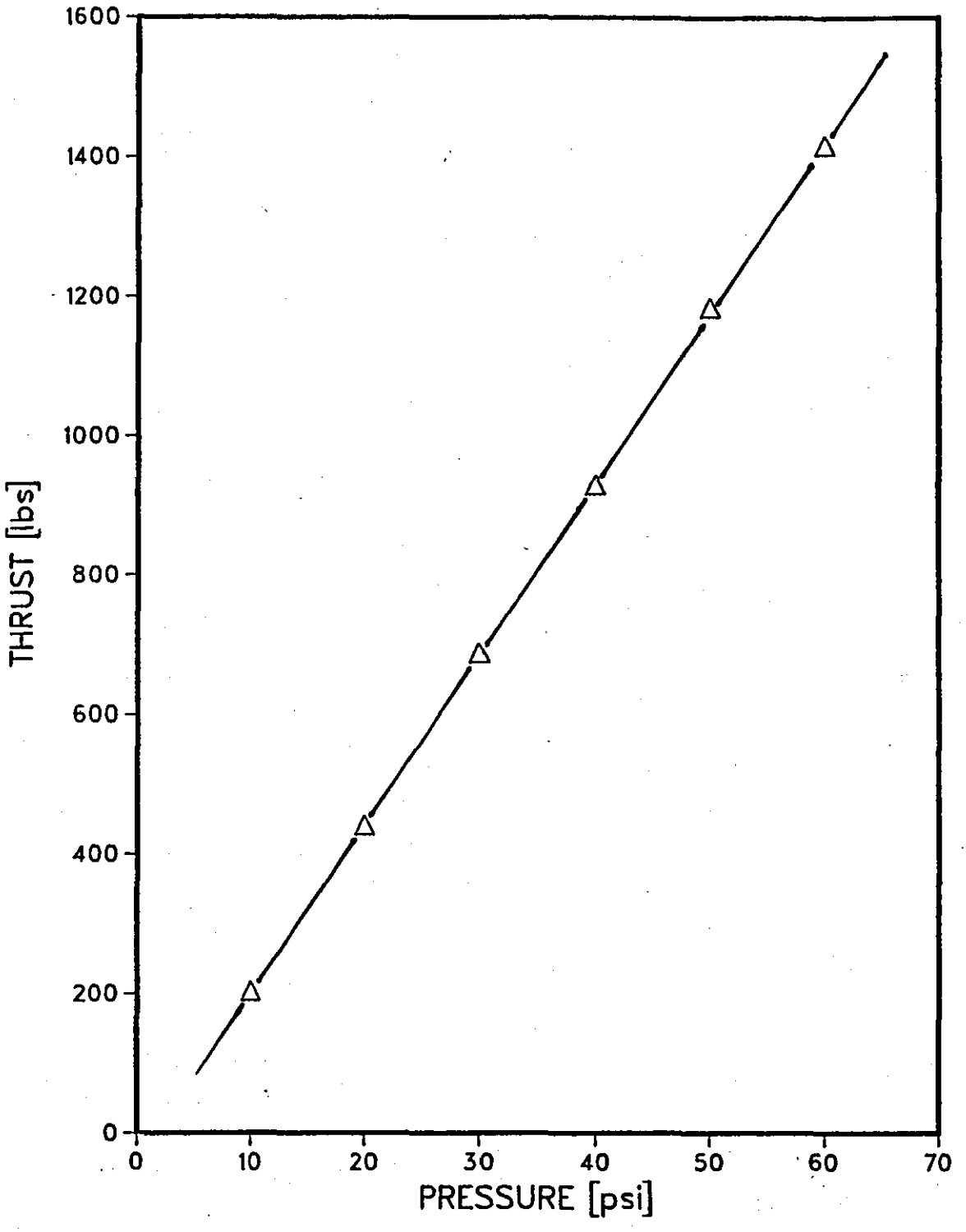

FIG.4.4.5 CALIBRATION CHART FOR 7 IN CHUCK AND PRESSURE GAUGE ASSEMBLY

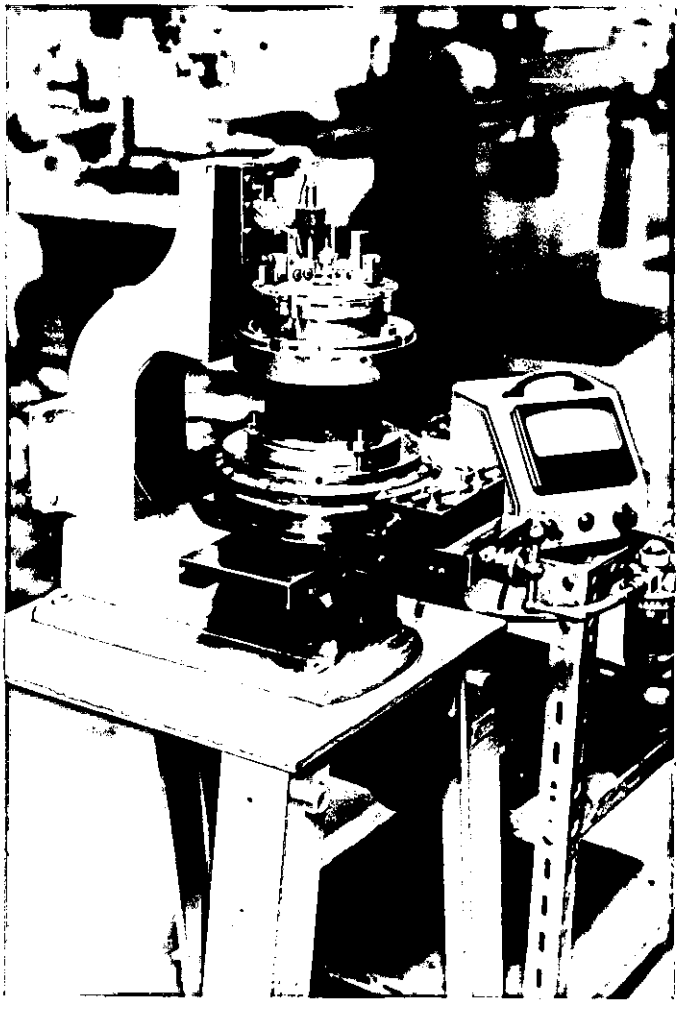

FIG. 4.5.1 DEFLECTION MEASUREMENT RIG

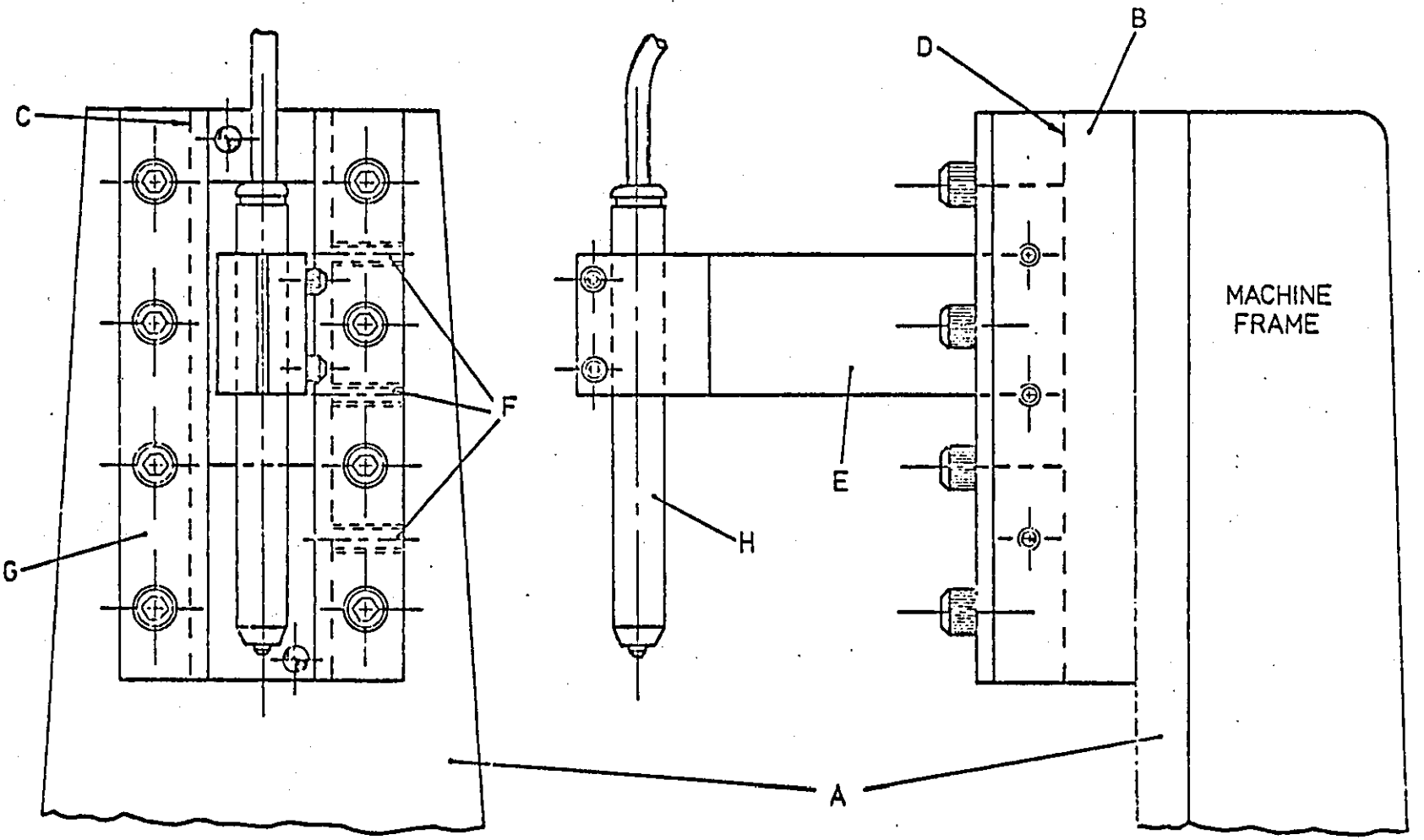

FIG. 4.5.2 DEVICE FOR HOLDING MEASUREMENT PROBE

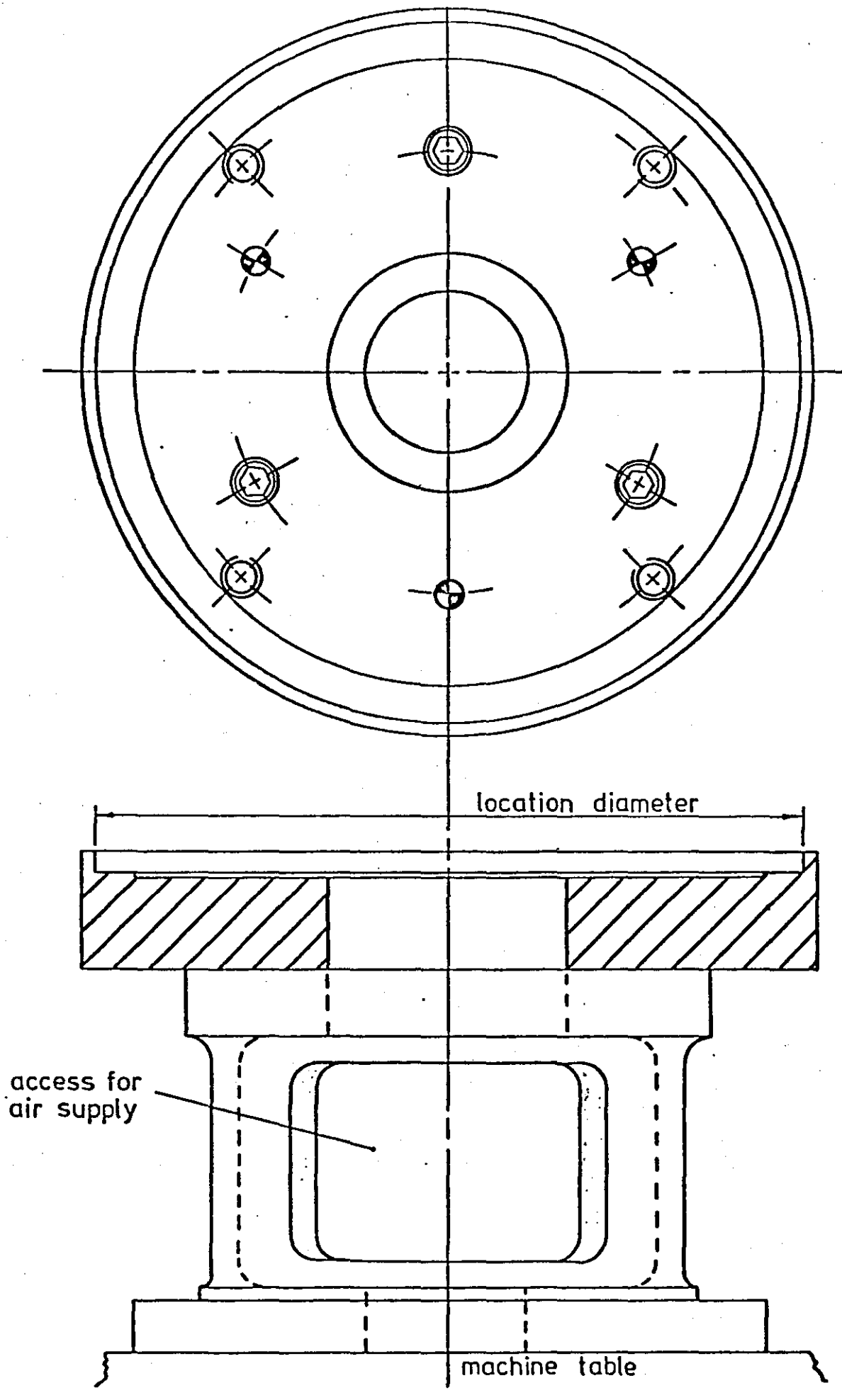

FIG. 4.5.3 FIXTURE FOR LOCATING DIAPHRAGM CHUCK DURING DEFLECTION MEASUREMENT

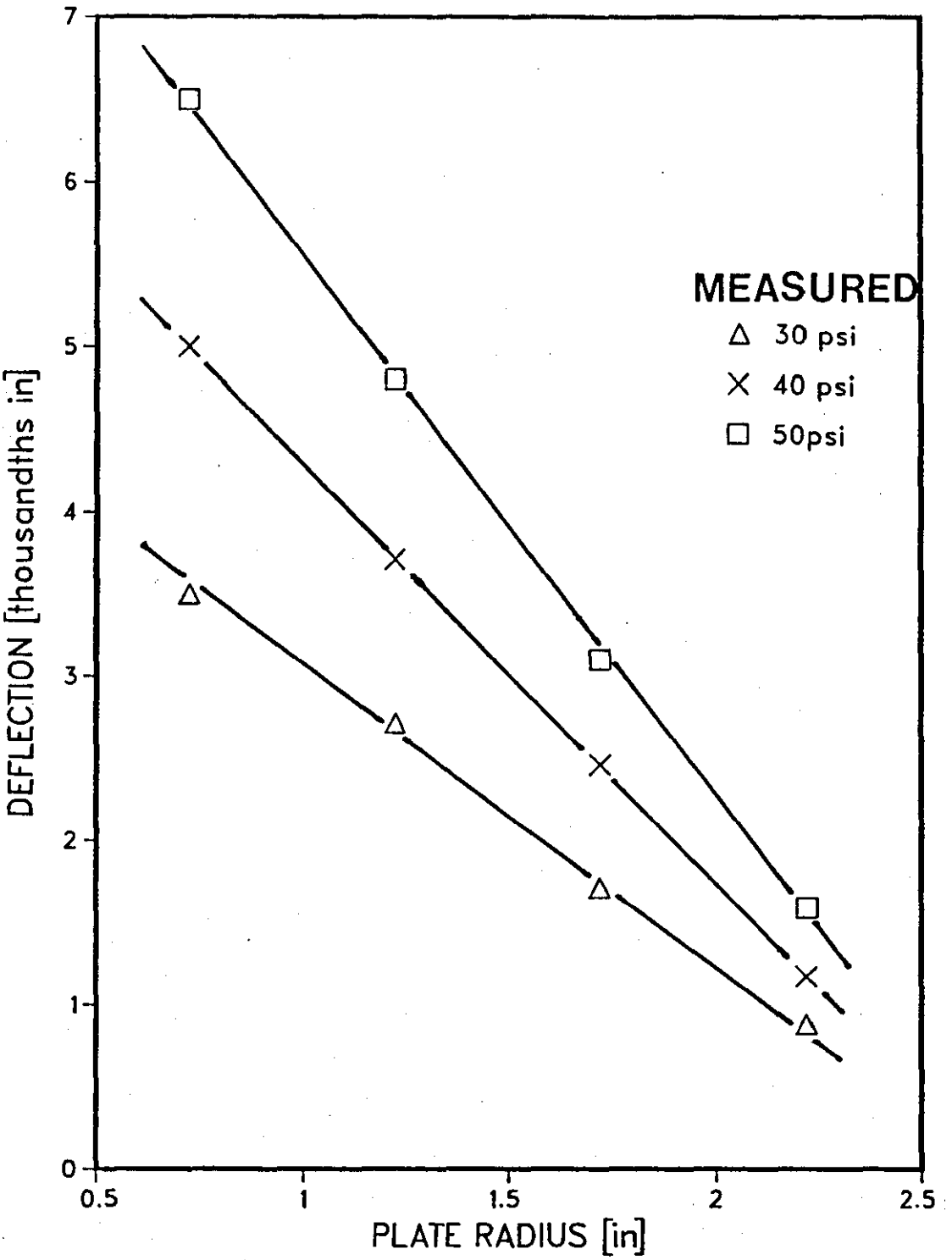

FIG. 4.6.1 PLATE DEFLECTION WITHOUT JAWS
PLATE A

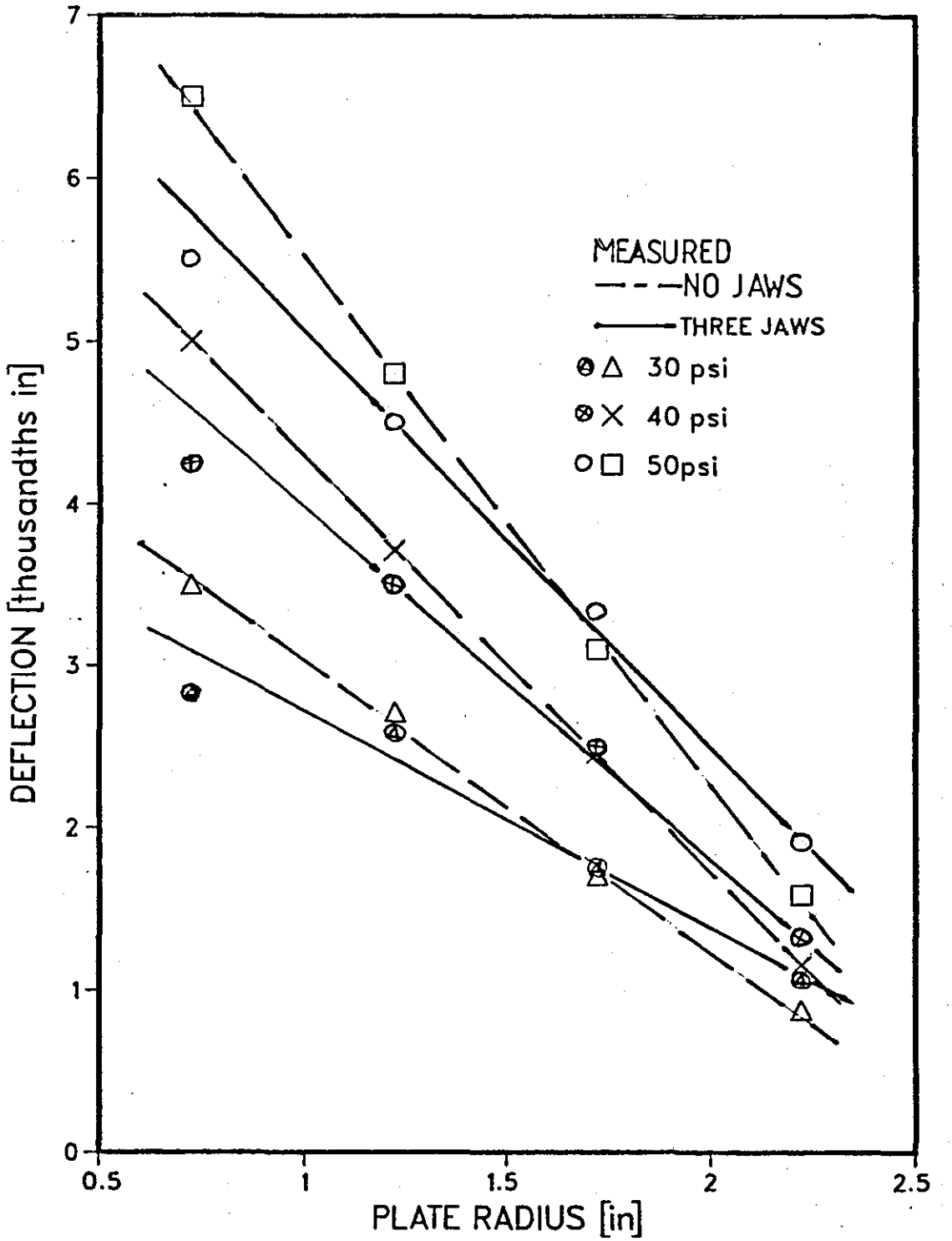

FIG.4.6.2 DEFLECTION FOR NO JAWS AND THREE JAWS;PLATE A

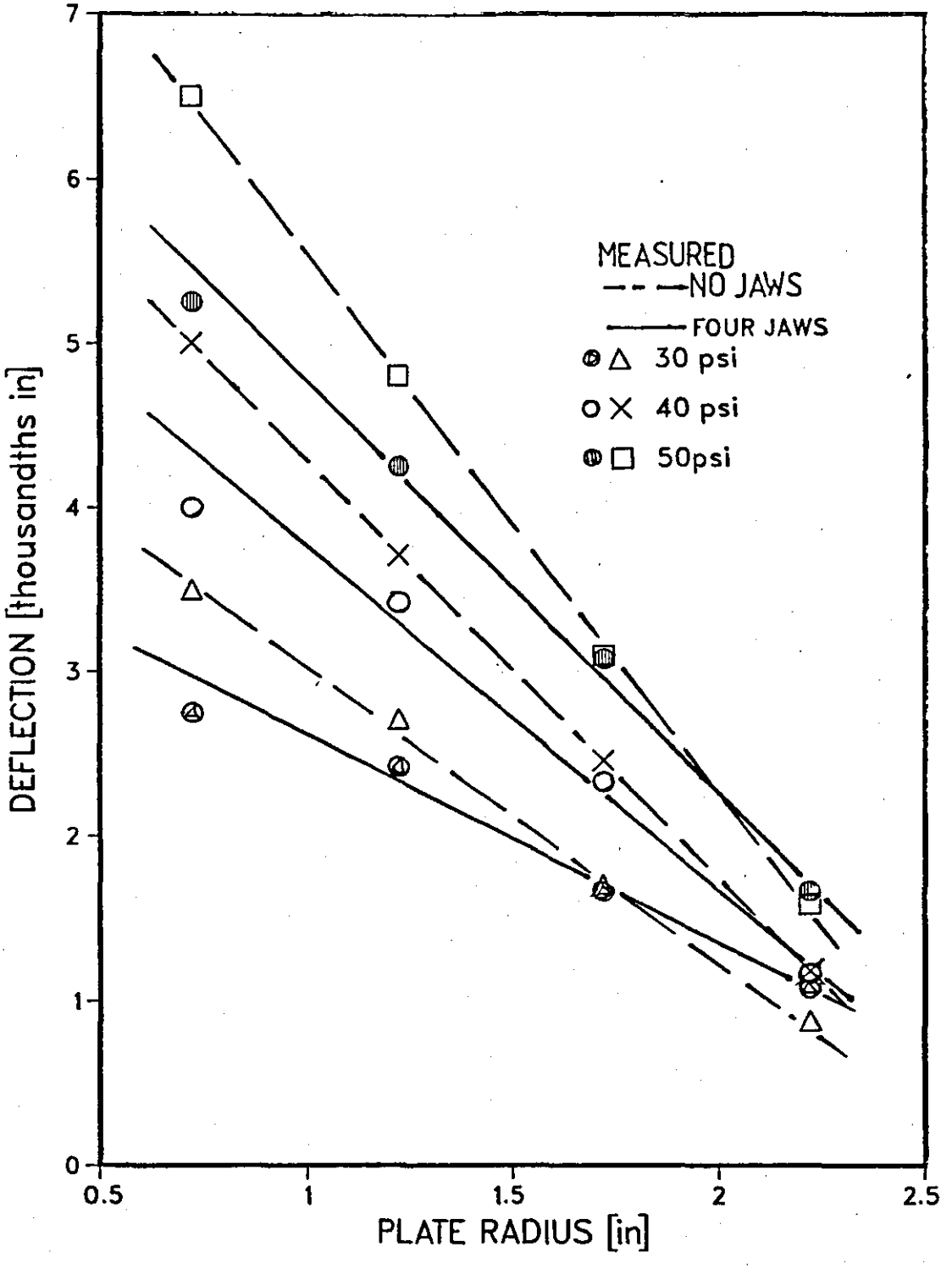

FIG. 4.6.3 DEFLECTION FOR NO JAWS AND FOUR JAWS; PLATE A

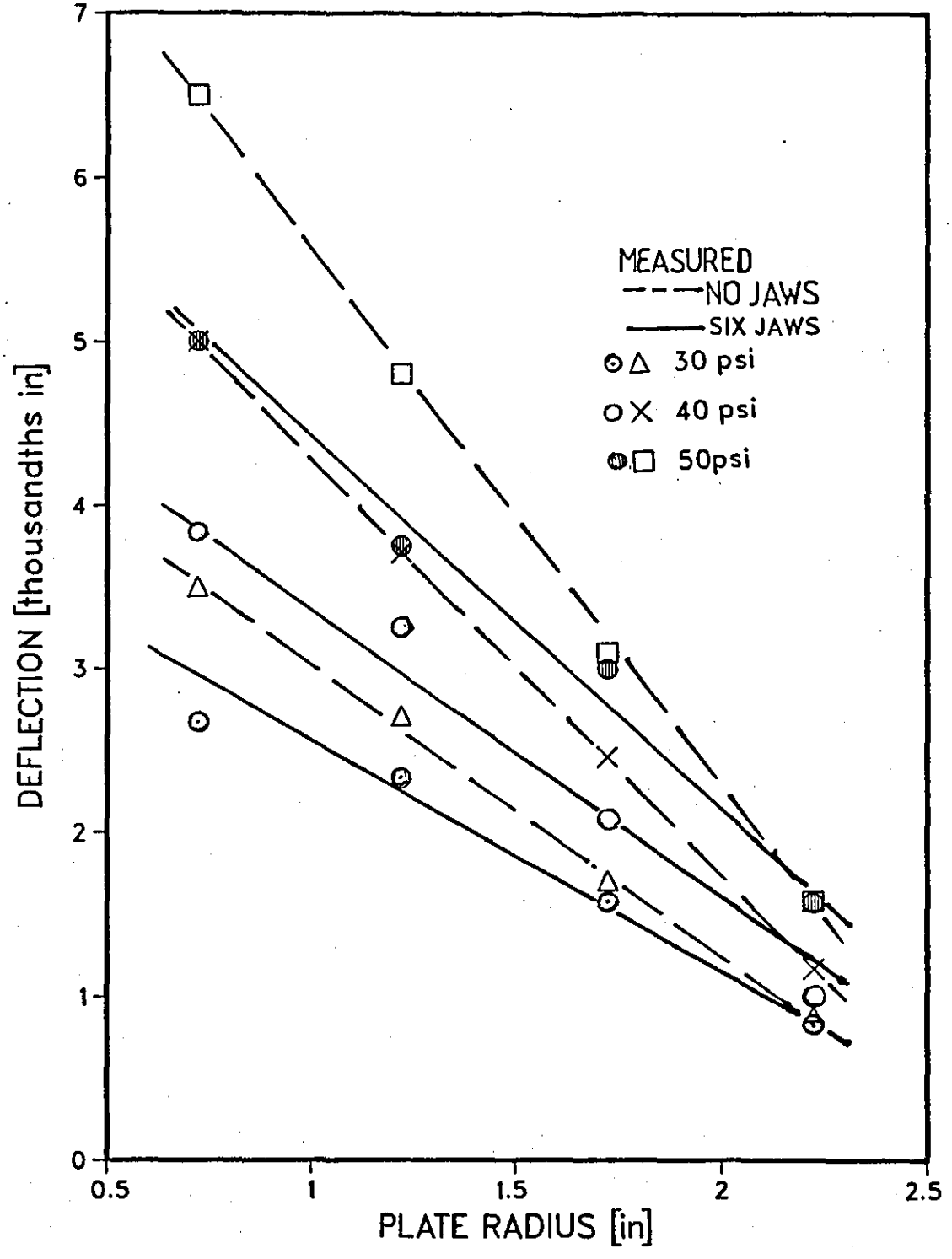

FIG. 4.6.4 DEFLECTION FOR NO JAWS AND SIX JAWS; PLATE A

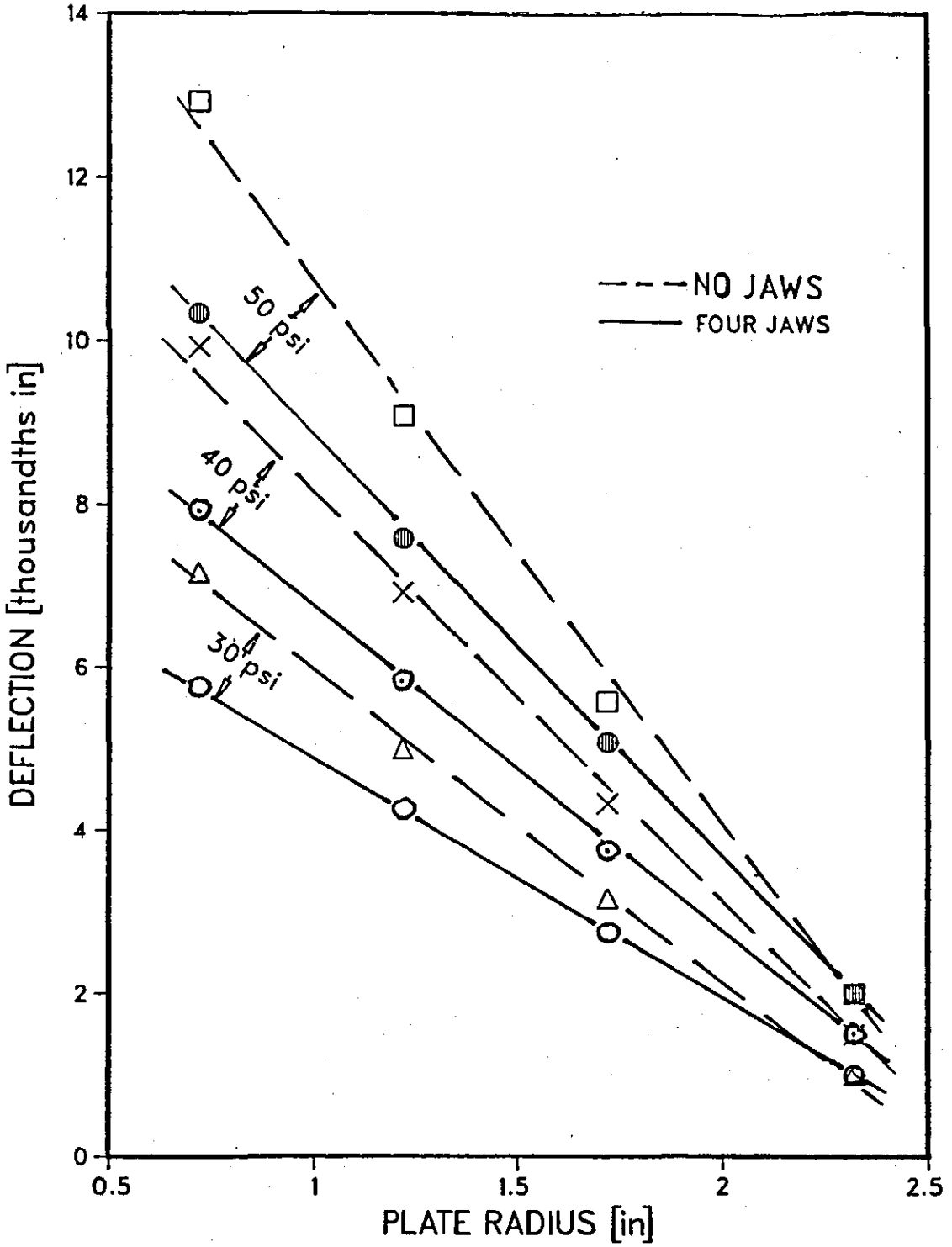

FIG.4.6.5 MEASURED DEFLECTION WITH NO JAWS AND FOUR JAWS;PLATE B

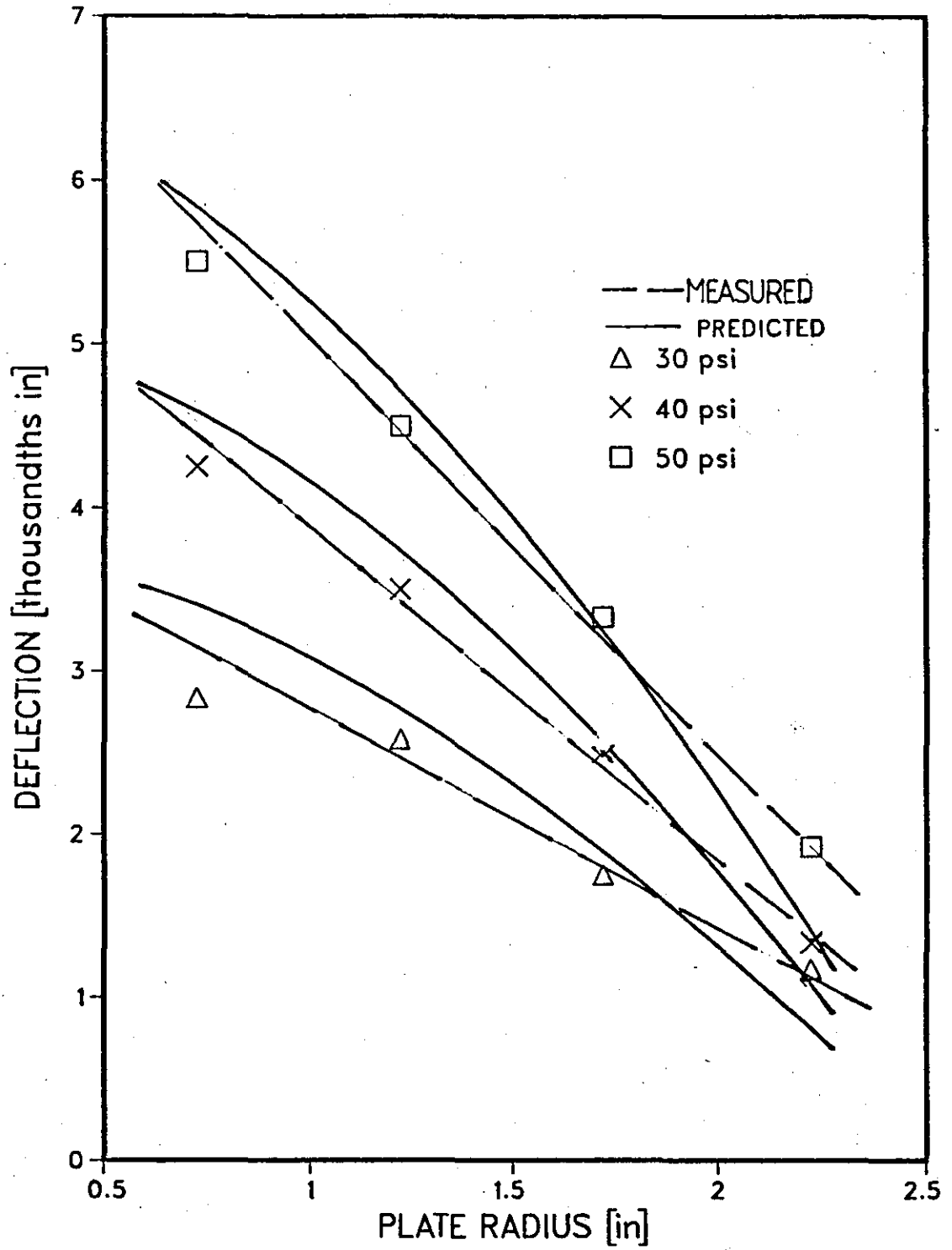

FIG. 4.6.6 MEASURED AND PREDICTED DEFLECTION FOR PLATE A;THREE JAWS

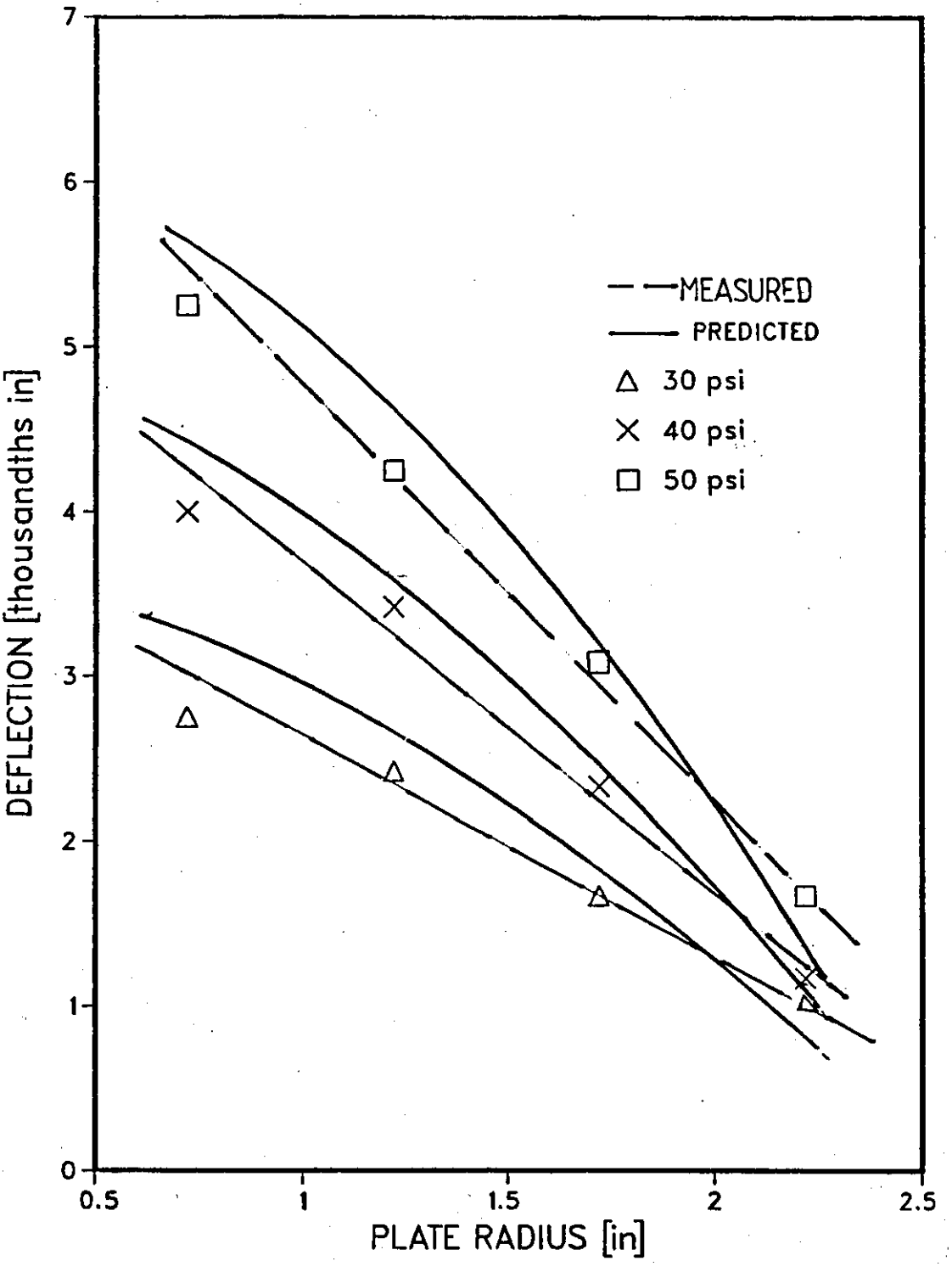

FIG.4.6.7 MEASURED AND PREDICTED DEFLECTION FOR PLATE A; FOUR JAWS

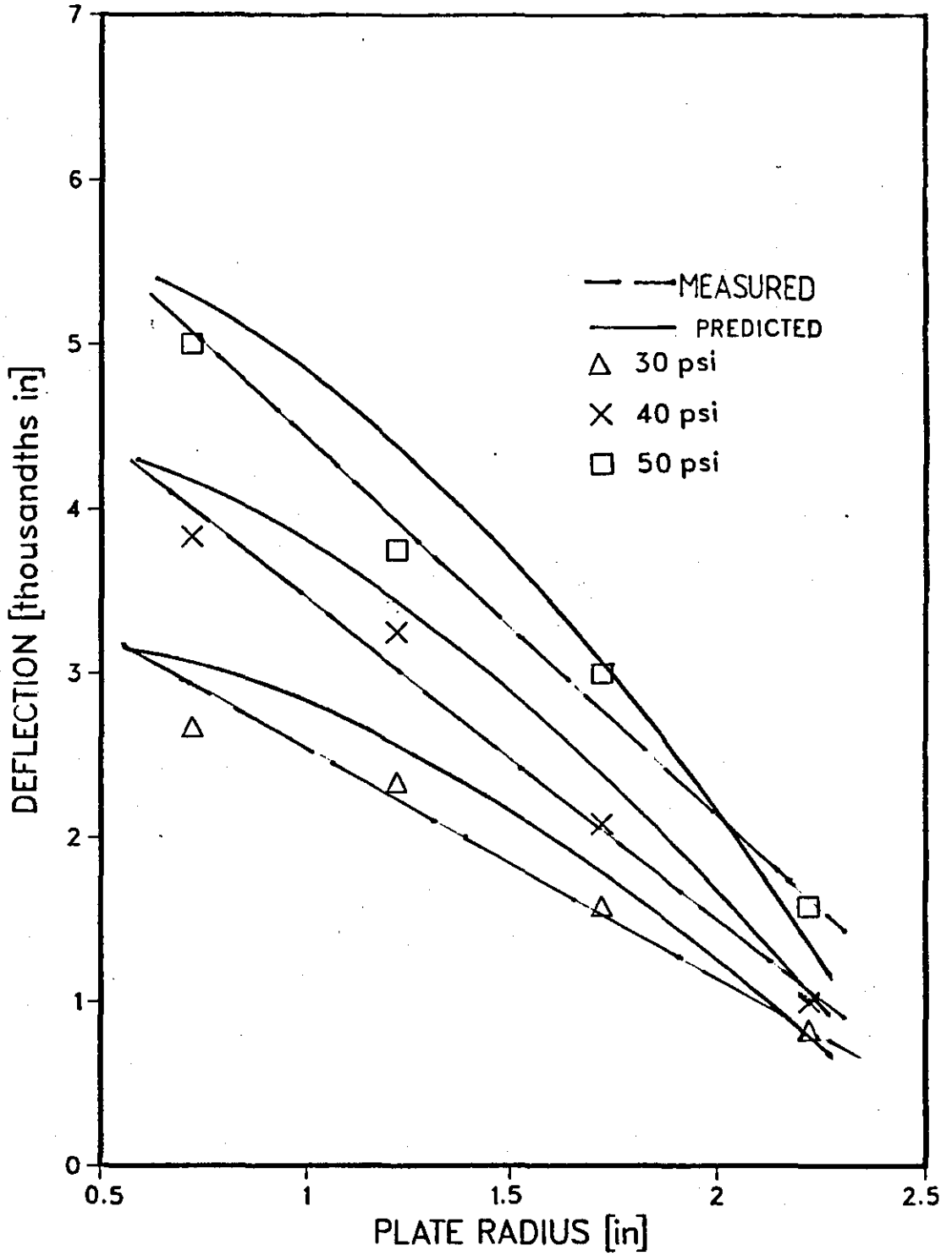

FIG.4.6.8 MEASURED AND PREDICTED DEFLECTION FOR PLATE A; SIX JAWS

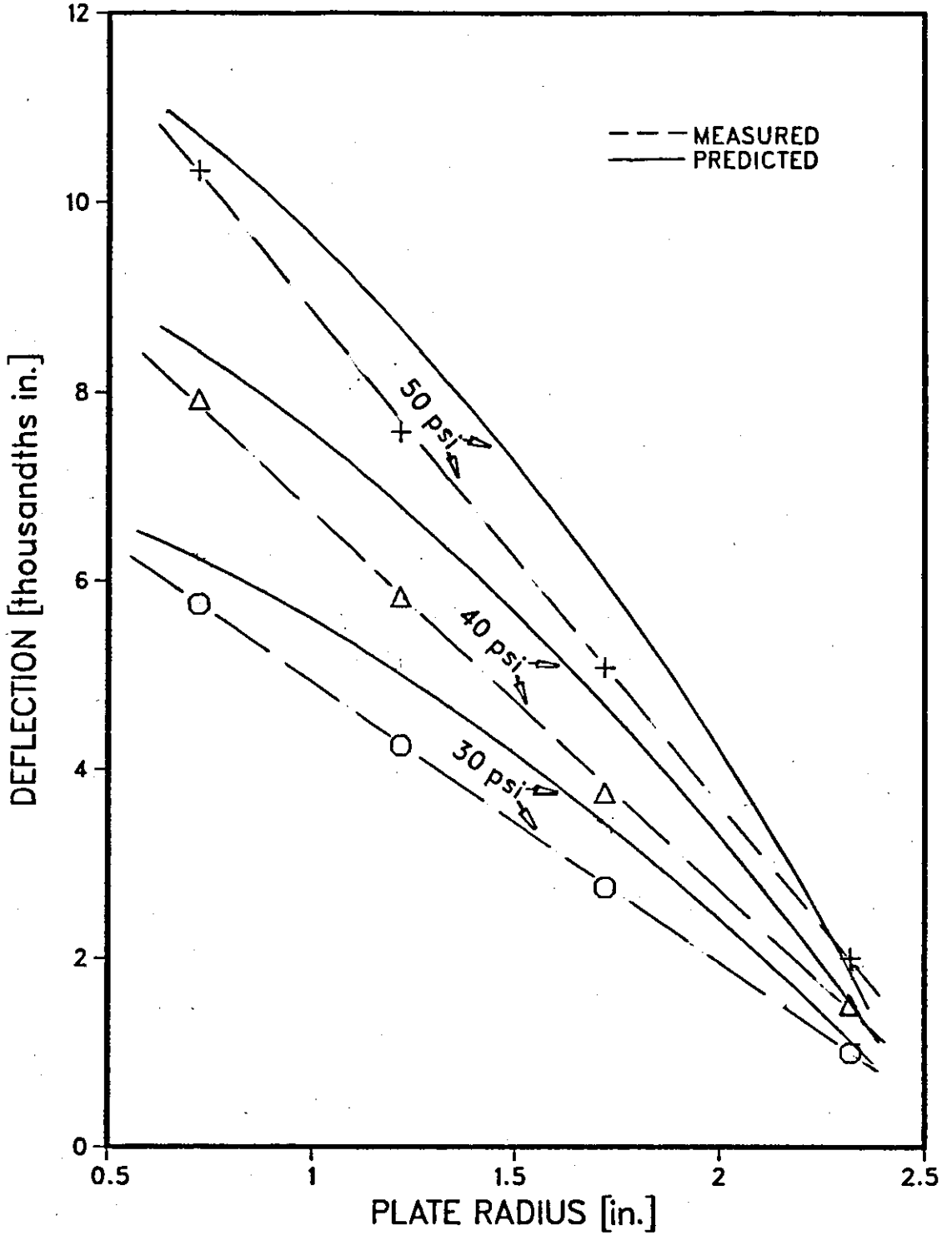

FIG.4.6.9 MEASURED AND PREDICTED DEFLECTION FOR PLATE B;FOUR JAWS

CHAPTER FIVE

THEORY OF THE GRIPPING FORCE

5.1 INTRODUCTION

The initial phase of the gripping action has been analyzed as the deflection of the diaphragm plate by a uniform ring thrust, P on the inner edge. With this thrust on, the jaws are "accurately" bored to the nominal size of the work-piece. It is evident that at this nominal bore, the work-piece cannot be positioned in the jaws without further expansion of the jaws by a further increase in thrust. On increasing the thrust to $P + \Delta P$ and inserting the work-piece, the thrust is removed and the work-piece is gripped firmly (Figure 5.1.1). This completes the gripping action and the processing of the work-piece may proceed. The work-piece is freed from the jaws by re-introducing the thrust, $P + \Delta P$. Thus the chuck is self-locating, self-centring and precise. It is obvious that the energy from ΔP is not used in the gripping action.

5.2 CONCENTRATED COUPLES

Assuming that the work-piece undergoes no diametral deformation, there is a symmetric arrangement of the reactive forces, F shown in Figure 5.2.1. These forces are considered to be concentrated at a height, h where the jaws are in contact with the work-piece. The forces produce radially distributed couples that act on the diaphragm plate as shown in Figure 5.2.2. The resulting in-plane forces, F are neglected. These couples are assumed to be holding the plate to the same deflection caused by the thrust, P.

Consequently, the final phase of this theoretical analysis of the gripping action is to determine the diaphragm

plate deflection equation under these concentrated couples. The radial distribution of each couple is one of the four forms in Figure 5.2.2. A simplified form of concentrated couples, M_o acting on the inner edge of the plate is assumed (No.1 of Figure 5.2.2); Each couple is given by

$$M_o = Fh \quad \ldots\ldots\ldots\ldots\ldots\ldots .5.2.1$$

where h is the moment arm from the face of the plate.

Considering each couple by itself, the plate response is no longer symmetrical but two-dimensional in radius, r and angular position, θ from each point couple. Using the solution of the differential equation of a varying thickness plate under concentrated couples for this problem is laborious, if not unmanagable. For a constant thickness plate, Timoshenko and Woinowsky-Krieger (7) give the homogeneous differential equation as

$$\left(\frac{\partial^2}{\partial r^2} + \frac{1}{r}\frac{\partial}{\partial r} + \frac{1}{r^2}\frac{\partial^2}{\partial \theta^2}\right)\left(\frac{\partial^2 \omega}{\partial r^2} + \frac{1}{r}\frac{\partial \omega}{\partial r} + \frac{1}{r^2}\frac{\partial^2 \omega}{\partial \theta^2}\right) = 0 \quad \ldots.5.2.2$$

where ω is the deflection at radius, r.

The solution in series form is

$$\omega = R_o + \sum_{m=i}^{\infty} R_m \operatorname{Cos} m\theta + \sum_{m=1}^{\infty} R'_m \operatorname{Sin} m\theta \quad \ldots\ldots .5.2.3$$

where $R_m = A_m r^m + B_m r^{-m} + C_m r^{m+2} + D_m r^{-m+2}$; $m>1$

$$R_o = A_o + B_o r^2 + C_o \ln r + D_o r^2 \ln r \quad \ldots .5.2.4$$

$$R_1 = A_1 r + B_1 r^3 + C_1 r^{-1} + D_1 r \ln r$$

Similar expressions are written for R'_m. Since the deflection is symmetric to the radial line running through the load point,

$$R'_m = 0 \quad \ldots\ldots\ldots\ldots\ldots\ldots .5.2.5$$

The deflection is, therefore, given by

$$\omega = R_o + \sum_{m=1}^{\infty} R_m \text{ Cos } m\theta \quad \ldots\ldots\ldots\ldots 5.2.6$$

The method of Fourier Series representation of concentrated loads used by Timoshenko and Woinowsky-Krieger is followed in this analysis.

5.3 FOURIER SERIES REPRESENTATION OF THE COUPLES

Fourier Analysis is a widely used technique in many branches of science and engineering. The idea is to represent certain physical functions that are discontinuous or piece-wise continueus with continuous functions that fairly approximate the real function. If the couples are assumed to be discontinuously distributed around the plate, the function

$$f(t) = \frac{2A\tau}{T} + \sum_{n=1}^{\infty} \frac{2A\tau}{T} \text{ Cos } \frac{2\pi nt}{T} \quad \ldots\ldots 5.3.1$$

given by Stuart (29) can be used to represent the couples. T is the period, τ is half the duration of the distribution, A for variable, t. For the couples on the diaphragm plate, the following transformation is used:

$$\begin{aligned} T &\equiv 2\pi \\ \tau &\equiv d/2 \\ A &\equiv M_o \end{aligned} \quad \ldots\ldots\ldots\ldots\ldots 5.3.2$$

where d is the circumferential width of jaw slide. By substitution, the couple, $M(\theta)$ at any circumferential point is represented as

$$M(\theta) = \frac{M_o d}{2\pi r_x} + \sum_{m=1}^{\infty} \frac{2M_o}{m\pi} \text{ Sin } \left(\frac{md}{2r_x}\right) \text{ Cos } (m\theta) \quad \ldots 5.3.3$$

where r_x is the radius of the circle around which the Fourier expansion takes place.

The first term on the right-hand side of equation 5.3.3 is an average moment acting around the plate on a circle of radius, r_x. As values of m are taken for the second term on the right-hand side, subtraction and addition from and to this average occur for varying θ. If sufficiently large values of m are used, i.e. $m \to \infty$, the function approaches the physical function of the couples.

The deflections contributed by each couple at each jaw is superposed to obtain the total deflection. Instead of deriving equation 5.3.3 for each couple, one equation can be used by exploiting symmetry and suitable movement of the coordinate, θ . It is important to emphasize that equation 5.3.3 is based on each couple at its own $\theta=0$. By this superposition method, the sum of the second term of equation 5.3.3 for all couples is zero. The total couple acting on the plate is, therefore, a uniform moment of value

$$M = \frac{NdM_o}{2\pi r_x}$$

where N is the number of jaws. This is the average resultant couple and it is used to solve the differential equation of the plate. The plate can now be treated as being loaded by a uniform and symmetric moment.

5.4 DEFLECTION EQUATION FOR SYMMETRIC MOMENT LOADING

Another way of expressing the differential equation of a circular plate loaded by uniform moments, M is

$$\frac{d}{dr}\left[\frac{1}{r}\frac{d}{dr}\left(r\frac{d\omega}{dr}\right)\right] = 0 \quad \ldots\ldots\ldots 5.4.1$$

In dimensionless form, the equation is

$$\frac{d}{dx}\left[\frac{1}{x}\frac{d}{dx}\left(x\frac{d\omega}{dx}\right)\right] = 0 \quad \ldots\ldots\ldots 5.4.2$$

where $x = r/a$, a is the outer radius of plate. By direct

integration, the deflection, ω is

$$\omega = C_1 \frac{x^2}{4} + C_2 \ell nx + C_3 \quad \ldots\ldots\ldots 5.4.3$$

Appropriate boundary conditions are used to determine the constants C_1, C_2, and C_3. The boundary conditions are

$$\omega = 0 \text{ at } x = 1$$

$$\frac{d\omega}{dx} = 0 \text{ at } x = 1 \quad \ldots\ldots\ldots 5.4.4$$

$$M_x = M \text{ at } x = x_b$$

The resulting deflection equation is

$$\omega_m = \frac{a^2 x_b^2 M(1-x^2 + 2\ell nx)}{2D\left[(1+\nu)x_b^2 + (1-\nu)\right]} \quad \ldots\ldots\ldots 5.4.5$$

where D and ν are as previously defined.

As previously stated, the jaw slides give the part of the plate under the jaws a constant slope. The condition used for this purpose was

$$\left.\frac{d\omega}{dx}\right|_{x_1} = \left.\frac{d\omega}{dx}\right|_{x_b} \quad \ldots\ldots\ldots 3.7.1$$

Applying this condition will cause the deflection equation to break down for the usual case of the jaw slides running from $x = x_b$ to the outer edge, x=1. This is as a result of the second condition of equation 5.4.4. A more appropriate and general boundary condition is

$$\frac{d^2\omega}{dx^2} = 0 \quad \text{at } x = x_1 \quad \ldots\ldots\ldots 5.4.6$$

This condition becomes clearer if x_1 is approached from the centre. For most chucks, $x_1 = 1$ and this value is used for

simplicity. It is important to note that when x_1 is significantly different from 1, a correct value is used and x_1 should remain in the equation. Therefore, the resulting deflection due to the annular stiffening is

$$\omega_{ms} = \frac{a^2 x_b^2 M\ (1-x^2-2\ell nx)}{2D\left[(1+\nu)x_b^2 - (1-\nu)\right]} \quad \ldots\ldots\ldots 5.4.7$$

The additional subscript s has been used to indicate deflection due to annular stiffening.

From ω_m and ω_{ms}, the deflection for the uniform bending moments increases with annular stiffening unlike that obtained for a plate loaded by thrust load, P. This fact may seem contradictory initially, but should be expected on closer examination. Following the form of equation 3.7.4, the deflection ω_{mN} with N symmetric jaws is

$$\omega_{mN} = \left[\omega_m + (\omega_{ms} - \omega_m)e^{\left(\frac{-Nd}{\pi(a+b)}\right)}\right]\left(\frac{1-x_b}{1-x}\right) \quad \ldots\ldots 5.4.8$$

Substituting for ω_m and ω_{ms},

$$\omega_{mN} = \frac{a^2 x_b^2 M(1-x_b)}{2D(1-x)}\left[\frac{\left[1-e^{\left(\frac{-Nd}{\pi(a+b)}\right)}\right](1-x^2+2\ell nx)}{(1+\nu)x_b^2 + (1-\nu)} + \frac{e^{\left(\frac{-Nd}{\pi(a+b)}\right)}\left[1-x^2-2\ell nx\right]}{(1+\nu)x_b^2 - (1-\nu)}\right] \ldots$$
$$\ldots\ldots 5.4.9$$

To use M as given by equation 5.3.4, the radius, r_x around which the couples are expanded must be determined. The physical constraint on the number of jaws that can fit on a chuck is

$$Nd \leq 2\pi r_x \quad \ldots\ldots\ldots\ldots\ldots\ldots\ldots 5.4.10$$

This constraint will always be satisfied if

$$r_x = \frac{a+b}{2} \quad \ldots\ldots\ldots\ldots\ldots\ldots\ldots 5.4.11$$

and prescribes the maximum number of jaws possible on a chuck.

The mechanism of deflection by a moment is based on a change in slope. The theoretically rigid jaw slides in effect transmit the moment away from $x = x_b$ to $x=1$. This is another reason for choosing $r_x = \frac{a+b}{2}$ as an average of points a and b.

Therefore,
$$M = \frac{NdM_o}{\pi(a+b)} \quad \ldots\ldots\ldots\ldots\ldots 5.4.12$$

The distributed force at the jaws, F_o produces the couple, M_o given by

$$M_o = F_o h \quad \ldots\ldots\ldots\ldots 5.4.13$$

which when substituted into equation 5.4.12 gives

$$M = \frac{NdhF_o}{\pi(a+b)} \quad \ldots\ldots\ldots\ldots 5.4.14$$

The deflection of the plate loaded by N symmetric couples with N jaws becomes

$$\omega_{mN} = \frac{a^2 x_b^2 NdhF_o\ (1-x_b)}{2\pi D(a+b)\ (1-x)}$$
$$\left\{\frac{(1-x^2+2\ell nx)\left[(1+\nu)x_b^2 - (1-\nu)\right] + 2e^{\left(\frac{-Nd}{\pi(a+b)}\right)}\left[(1-\nu)\ (1-x^2) - 2x_b^2\ (1+\nu)\ell nx\right.}{\left[(1+\nu)^2\ x_b^4 - (1-\nu)^2\right]}\right.$$
$$\ldots\ldots\ldots 5.4.15$$

5.5 GRIPPING FORCE EQUATION

Equations 3.7.5 and 5.4.15 describe the deflections, ω_N and ω_{ms} of the diaphragm plate due to ring thrust, P and concentrated couples respectively. The plate is deflected by thrust, P and held at the same deflection by gripping forces that create moment, M_o. The fundamental concept of this work is that the deflections by thrust, P and moment, M_o are equal, i.e.

$$\omega_N = \omega_{mN} \quad \ldots\ldots\ldots\ldots 5.5.1$$

Substituting for ω_N and ω_{ms} into the equation above and solving for the distributed gripping force, F_o

$$F_o \doteq \frac{(a+b)P\left[(1+\nu)^2 x_b^4 - (1-\nu)^2\right]}{8x_b^2\, Ndh} \left\{ (2C_{ss}-1)\ (1-x^2)\left[1-e^{\left(\frac{-Nd}{\pi(a+b)}\right)}\right] + 2\left[1-e^{\left(\frac{-Nd}{\pi(a+b)}\right)}\right](2C_{ss}-x^2)\ \ell nx + (x^2-1)\ (1+2C_s)e^{\left(\frac{-Nd}{\pi(a+b)}\right)} - 2e^{\left(\frac{-Nd}{\pi(a+b)}\right)}(2C_s+x^2)\ \ell nx \right\} \Big/ \left\{ (1-x^2+2\ell nx)\left[(1+\nu)x_b^2-(1-\nu)\right] + 2e^{\left(\frac{-Nd}{\pi(a+b)}\right)}\left[(1-\nu)\ (1-x^2) - 2x_b^2\ (1+\nu)\ \ell nx\right] \right\} \quad \ldots\ldots 5.5.2$$

The gripping force, F is the product of the distributed gripping force, F_o and the jaw slide width, d i.e.

$$F = F_o d \quad \ldots\ldots\ldots\ldots\ldots\ldots 5.5.3$$

Substituting for F_o,

$$F = \frac{(a+b)P}{Nh} \cdot \frac{\left[(1+\nu)^2 x_b^4 - (1-\nu)^2\right]}{8x_b^2} \left\{ (2C_{ss}-1)(1-x^2)\left[1-e^{\left(\frac{-Nd}{\pi(a+b)}\right)}\right] + 2\left[1-e^{\left(\frac{-Nd}{\pi(a+b)}\right)}\right](2C_{ss}-x^2)\ \ell nx + (x^2-1)\ (1+2C_s)e^{\left(\frac{-Nd}{\pi(a+b)}\right)} - 2e^{\left(\frac{-Nd}{\pi(a+b)}\right)}(2C_s+x^2)\ \ell nx \right\} \Big/ \left\{ (1-x^2+2\ell nx)\left[(1+\nu)x_b^2-(1-\nu)\right] + 2e^{\left(\frac{-Nd}{\pi(a+b)}\right)}\left[(1-\nu)\ (1-x^2) - 2x_b^2\ (1+\nu)\ \ell nx\right] \right\} \quad \ldots\ldots .5.5.4$$

where

$$C_s = \frac{\left[x_b^2\ (1+\nu)\,\ell nx + 1)\right]}{\left[(1-\nu)+x_b^2\ (1+\nu)\right]}$$

$$C_{ss} = \frac{x_b x_1 (x_b \ell nx_b - x_1 \ell nx_1)}{(x_1 - x_b)(1+x_b x_1)} = \frac{x_b^2\ \ell nx_b}{(1-x_b)(1+x_b)} \quad \text{for } x_1 = 1$$

a = outer radius of plate
ν = Poisson's ratio
$x_b = b/a$, b=inner radius of plate
$x = r/a$, r=workpiece radius
N = number of jaws
h = moment arm, the height of the mid-point of jaw gripping face from the plate surface.

This equation describes the gripping force of the chuck, and shows that the gripping force is independent of the plate thickness.[c] Nevertheless, it is a function of workpiece radius, outer and inner radii of diaphragm plate, number of jaws, circumferential width of jaw slide, and Poisson's ratio of material.

Referring to equation 5.5.4, the gripping force can be expressed in the form

$$F = K_r \frac{(a+b)P}{h} \quad \ldots\ldots\ldots\ldots\ldots\ldots .5.5.5$$

where K_r is tabulated as a function of the ratio of inner to outer diameters, x_b, ratio of workpiece diameter to outer diameter of plate, x, number of jaws, N and the jaw slide width, d. The variation of K_r with x is very signficant as x approaches the value of 1 i.e. as the workpiece diameter approaches the diameter of the diaphragm plate (Figure 5.5.1). K_r is undefined at the outer radius of plate but may be assumed to be zero. In practice, it is unlikely that the workpiece

c. This is an important finding. The reader may find it initially surprising, as did the author.

diameter will approach the plate diameter. The work-piece diameter is a fraction of the plate outer diameter which determines the operating range of the chuck. This operating range will be examined in conjunction with tolerance effects.

An average value of K_r may be taken over a range for the purpose of rating the chuck. The dimensionless quantity, K_r is tabulated in Tables 5.5.1 to 5.5.11 for number of jaws, N, ratio of inner to outer diameters of plate, x_b, and the ratio of work-piece diameter to outer plate diameter, x. It can be noticed that the jaw slide width, d is not varied in calculating the values for K_r. This is because d, when varied, has a very negligible effect on the gripping force. The value used for the Tables is d = 0.875 IN.

Figure 5.5.1 shows that the optimum work-piece diameter in terms of gripping force is 33% of the outer plate diameter. Figure 5.5.2 shows that the smaller the value of x_b, the higher the gripping force. There is, of course, a physical limit to which x_b can be reduced. This limit is dictated by the amount of clearance needed at the inner hole of plate. It is also in agreement with the shear stress effect condition that

$$x_b = b/a \leq 0.2$$

5.6 EFFECT OF TOLERANCE ON GRIPPING FORCE

The diaphragm chuck, being a precision work-holding device, is influenced significantly by the accuracy of the physical dimensions of the plate and work-piece. The tolerance between the component and the jaws is, in particular, very important in determining the actual gripping force. A theoretical analysis of the effects of tolerance on the gripping force has proved to be complex. Billau(5) empirically

established the influence of tolerance on gripping force. Equation 5.5.4 shows that the gripping force is inversely proportional to the moment arm, h. Thus, according to Billau, an undersize component (or oversize bore) causes gripping at a height more than for nominal size. The effect is to decrease the gripping force. On the other hand, an oversize component (or undersize jaw bore) is gripped at a height lower than for nominal size, thereby increasing the gripping force. Billau established that the gripping force acts approximately at the centre of the bottom quarter of the jaw face for oversize components; and at the centre of the top quarter of the jaw face for undersize components. This is illustrated in Figure 5.6.1. The direct contribution of this change of gripping point to the value of the moment arm, h is negligible.

The position of effective grip within the jaw face naturally depends on the angle of inclination of the diaphragm plate face. Oversize components will produce a positive increase in slope, whilst undersize components produce negative variation in the slope of the diaphragm plate face. The slope of the plate face is related directly to the deflecting thrust, P. A fractional increase or decrease in P is necessary to take-up the tolerance. The result is that the jaw grips at a higher thrust than for nominal size if the component is oversize. The effect is to increase the gripping force, since it is directly dependent on the thrust, P. The converse is also true for undersize components. Consequently, the operating air pressure should be less than the available air line pressure in order to compensate for tolerance take-up. This will also make allowance for the fractional increase in diaphragm plate deflection to slip work-piece into jaws, and for air line pressure fluctuations. It is therefore, recommended that the operating pressure should be at least 20% less than the available air line pressure.

Billau postulates that the ratio of the angles of inclination of the plate face for oversize (or undersize) components to that of nominal size is equal to the ratio of their respective gripping forces. The following example overleaf, is given by Billau to illustrate this postulation.

This approach by Billau has now been put into a general form. If ω_1 is the diaphragm plate deflection at boring, ℓ is the length of the jaw gripping face, 2δ is the tolerance and h_1 is the height of the lower edge of the jaw gripping face from the plate, the tolerance factor, R_T is given by:

$$R_T = \frac{-8\ \delta\ (a-b)}{\omega_1\left[-4(2h_1+\ell)\ \pm\ 3\ell -\ 8\omega_1\left(\frac{a-r}{a-b}\right)\right]} \quad \ldots\ldots 5.6.1$$

Since ω_1 is the deflection at radius, r, which is the radius of the work-piece, R_T can be related to the maximum deflection ω_b by assuming a constant slope deflection. This gives

$$\omega_1 = \omega_b \frac{(a-r)}{(a-b)} \quad \ldots\ldots\ldots\ldots 5.6.2$$

Substituting into equation 5.6.1

$$R_T = \frac{-8\delta\ (a-b)}{\omega_b\left(\frac{a-r}{a-b}\right)\left[-4(2h_1+\ell)\ \pm\ 3\ell - 8\omega_b\left(\frac{a-r}{a-b}\right)^2\right]} \quad \ldots 5.6.3$$

where

a = outer radius of diaphragm plate
b = inner radius of diaphragm plate
r = nominal radius of work-piece.

For the sign ±, the +ve is for oversize components and -ve is for undersize components. The effective gripping force, F_e is therefore given by

$$F_e = (1 \pm R_T)\ F \quad \ldots\ldots\ldots\ldots 5.6.4$$

where F is the gripping force for the nominal size and the ± sign is as previously defined.

ESTIMATION OF FORCE /TOLERANCE VARIATIONS (Nominal Diameter)

Chosen Conditions

Chuck: 4 Jaw 7" diameter Diaphragm

Compt.: 1.00 diameter Nominal Size

Jaws bored at 55 p.s.i.

Diaphragm Deflection at 55 p.s.i. = 16.8×10^{-3} ins.

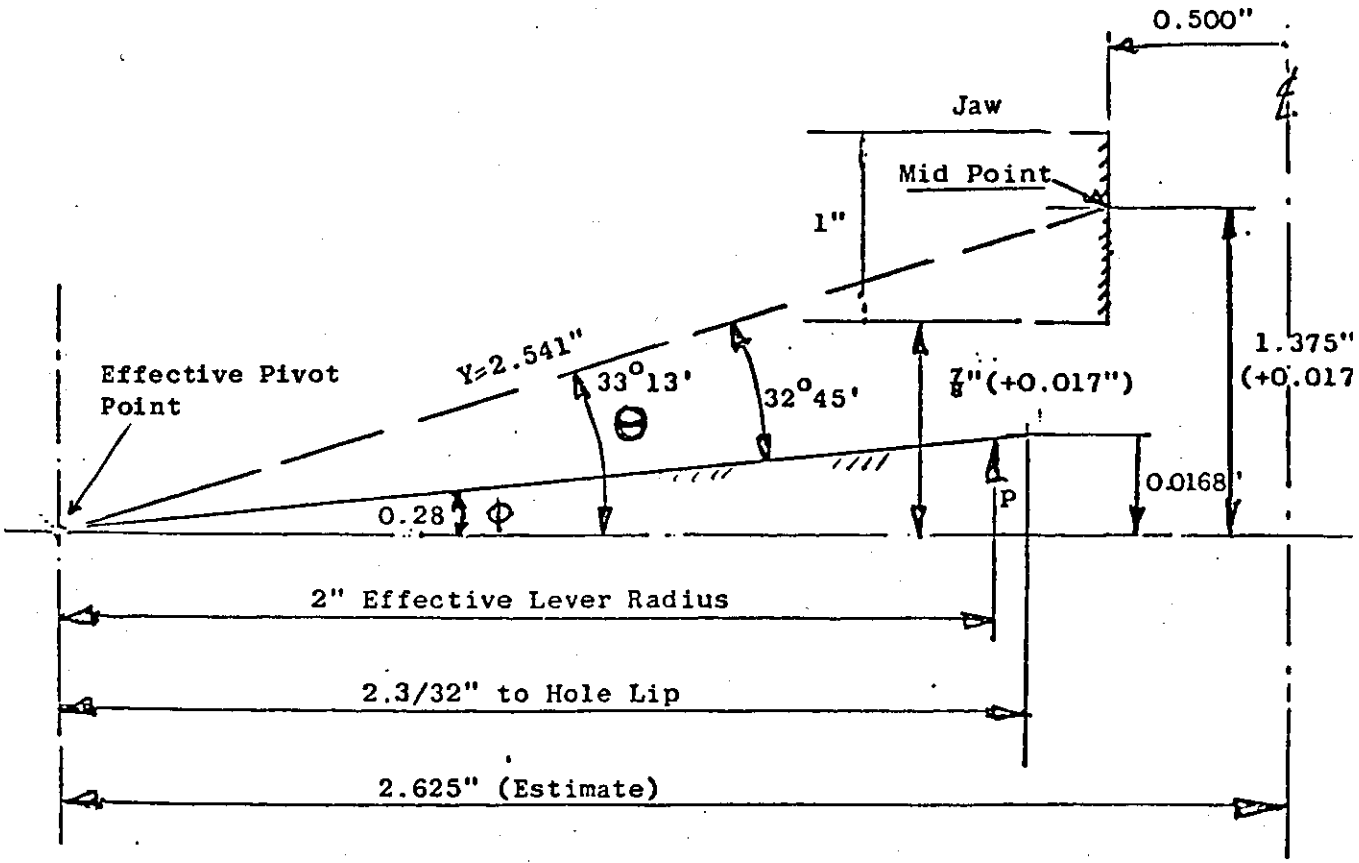

Equivalent Deflection at Point under Jaw Surface

$$\omega_1 = 0.0168 \times \frac{2.125}{2.094} = 0.017$$

$$\text{Tan } \phi = \frac{0.0168}{2.3/32} \Rightarrow \phi = \underline{0^\circ\ 28'}$$

$$\text{Tan } \theta = \frac{1.392}{2.125}$$

$$= \underline{33^\circ\ 13'}$$

$$Y = 1.392 \text{ Cosec } 33^\circ\ 13'$$

$$= \underline{2.541 \text{ ins.}}$$

To Calculate Grip for Nominal Diameter +0.005"

Effective Grip Length = Back ¼"

Point of Load from Diaphragm Face = ⅜" + ⅜" = 1"

Calculation Approximate Contact Hypotenuse (Back ¼")

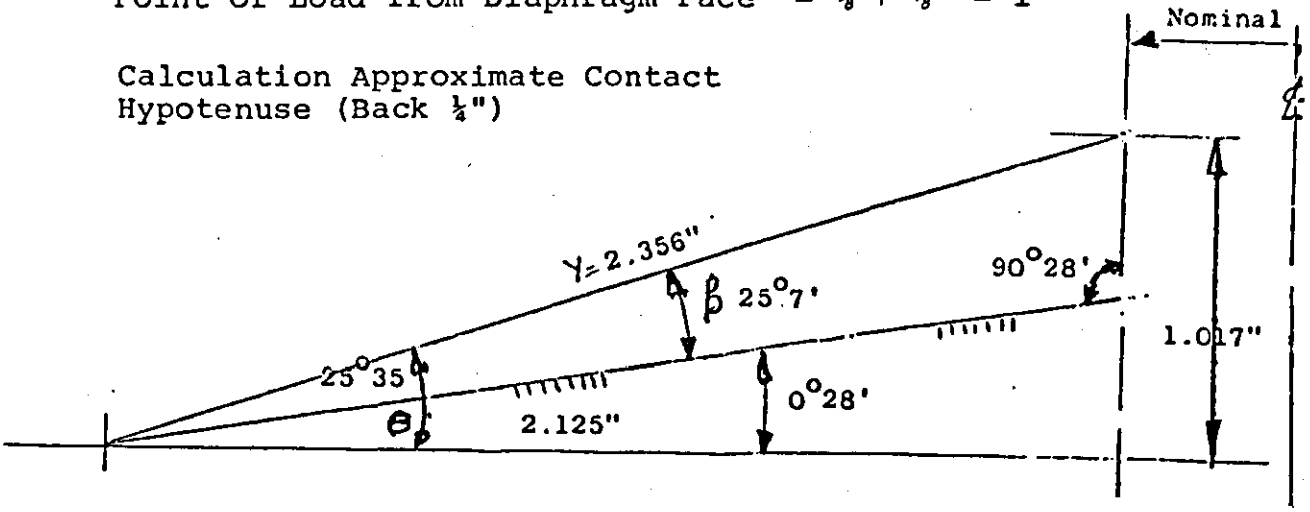

$$\text{Tan } \theta = \frac{1.017}{2.125} \Rightarrow \theta = \underline{25°\ 35'}$$

$$\therefore \beta = 25°35' - 0.28' = \underline{25°\ 7'}$$

$$Y = 1.017 \text{ Cosec } 25°\ 35' = \underline{2.356 \text{ ins.}}$$

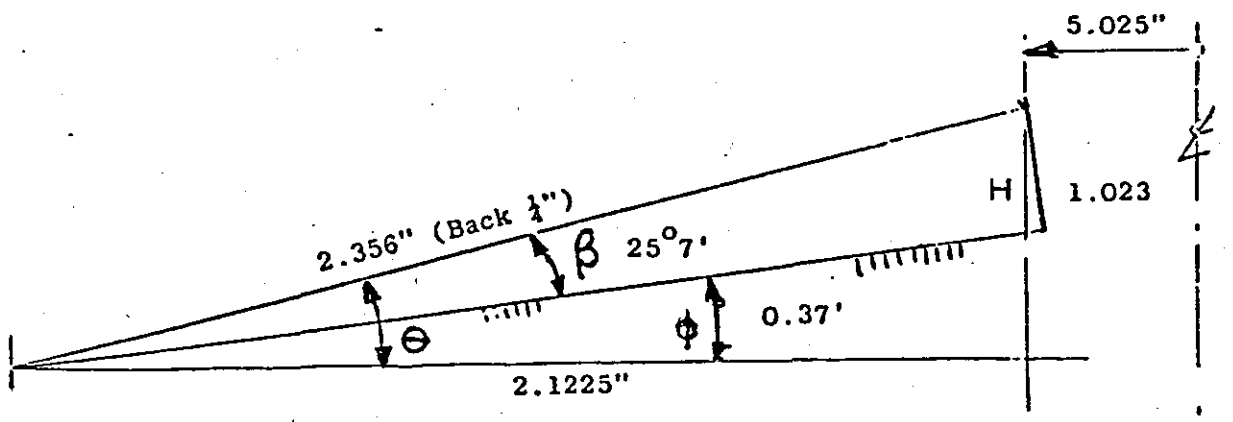

$$\text{Cos } \theta = \frac{2.1225}{2.356} \Rightarrow \theta = \underline{25°44'}$$

$$\phi = 25°44' - 25°7' = \underline{0°37'}$$

$$H = 2.356 \text{ Sin } 25°44' = \underline{1.023'}$$

Therefore the increase in the value of the gripping force will be in the ratio of the plate angle of inclination, viz .37/28 (calculated value).

To Calculate Grip for Nominal Diameter -0.005 ins.

Effective Grip Length = Front ¼"

Point of Load from Diaphragm Face = ⅜ + ⅜ = 1.75"

Calculation Approximate Contact
Hypotenuse (Front ¼")

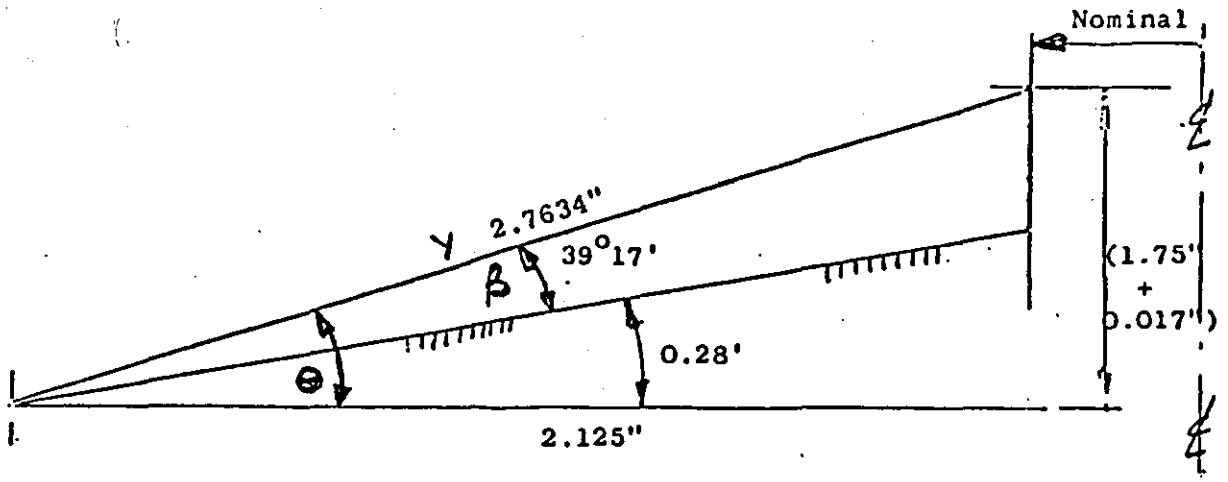

$$\text{Tan } \theta = \frac{1.767}{2.125} = 1.767 \times 8/17 \Rightarrow \Theta = \underline{39°45'}$$

$$\beta = 39°45' - 0°28' = \underline{39°17'}$$

$$Y = 1.767 \text{ Cosec } 39°45' = \underline{2.7634 \text{ ins.}}$$

The value of 2.7634 is used as the approximate dimension for the clamped position, in order to simplify the calculation procedure.

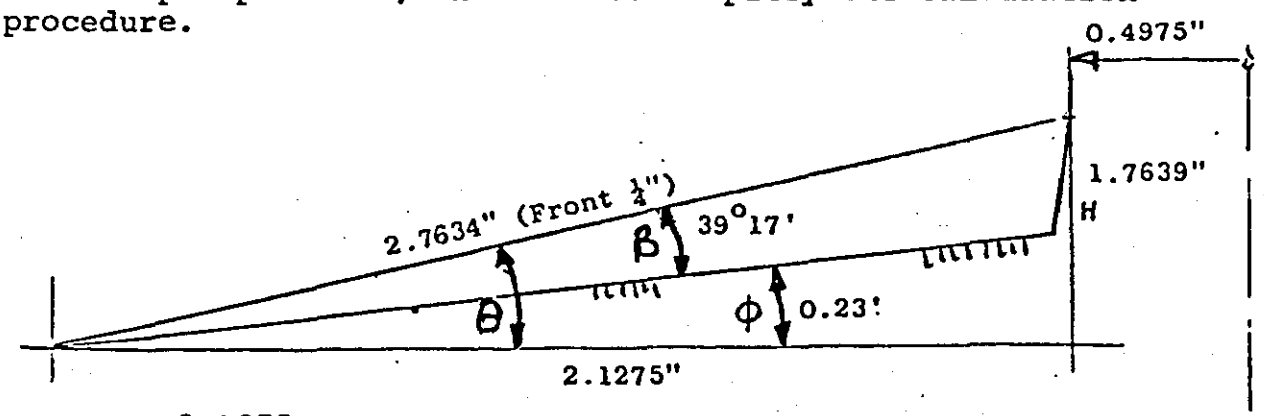

$$\text{Cos } \theta = \frac{2.1275}{2.7634} \Rightarrow \Theta = \underline{39°40'}$$

$$\phi = 39°40' - 39°17' = \underline{0°23'}$$

$$H = 2.7634 \text{ Sin } 39°40' = \underline{1.7639 \text{ ins.}}$$

Therefore the decrease in the value of the gripping force will be in the ratio of the plate angle of inclination, viz.23/28 (calculated value).

Component tolerance restricts the operating range of a diaphragm chuck. Theoretically, the chuck can be used for any work-piece diameter close but not equal to the diameter of the diaphragm. In practice, it is known that near the outer diaphragm diameter, the deflection is extremely small. The gripping force in this region is very small and is assumed to be zero at the exact outer diameter. For oversize components, the chuck will require a very large thrust in order to take-up the component tolerance. Since the deflection in this region is very small, the required thrust for tolerance take-up is bound to overstress the plate material.

A similar situation exists for undersize components. In this case the deflection reduces in order to take-up the tolerance. This is not possible because the small deflections in this region are restricted to be above zero. These deflections cannot fall below zero for that will mean reversing the direction of thrust. As a result, the component cannot be gripped. There is, therefore, a necessity to establish the operating range of the chuck.

If the higher limit of the operating range is that diameter and tolerance which do not cause the gripping force to vary by a certain proportion, equation 5.6.3 can be used to establish such a limit. The variation of gripping force, R_T due to tolerance is greater for oversize than for undersize components. To set an absolute higher limit of the chuck capacity, the +ve sign for oversize components is used in equation 5.6.3. However, the critical limit should be based on the undersize component because slipping may begin to occur when the gripping force falls below a certain proportion. Therefore, the -ve sign for undersize components is used in equation 5.6.3 to determine the higher limit of chuck capacity for safety purposes. Equation 5.6.3 is re-

arranged to give this limit in terms of maximum component diameter d_o as

$$d_o = 2a\left[1 - (q_1-q_2)\left(1-{}^{b}/_{a}\right)\right] \quad \ldots\ldots\ldots 5.6.5$$

where

$$q_1 = \left[\left\{\frac{\delta^2(a-b)^2}{4\omega_b^4 R_T^2} + \frac{1}{27}\left[\frac{4(2h_1+\ell)-3\ell}{8\omega_b}\right]^3\right\}^{\frac{1}{2}} + \frac{\delta(a-b)}{2\omega_b^2 R_T}\right]^{1/3}$$

and

$$q_2 = \left[\left\{\frac{\delta^2(a-b)^2}{4\omega_b^4 R_T^2} + \frac{1}{27}\left[\frac{4(2h_1+\ell)-3\ell}{8\omega_b}\right]^3\right\}^{\frac{1}{2}} - \frac{\delta(a-b)}{2\omega_b^2 R_T}\right]^{1/3}$$

R_T is specified by the designer, say 10%, and all the other variables are as previously defined.

It was stated earlier that gripping force is independent of the plate thickness. There is, however, an indirect effect of thickness on the gripping force through component tolerance. The plate has to have a thickness that can withstand the stresses caused by the operating pressure and the gripping action. The thinner the plate thickness gets, the more is the deflection, and consequently the more the propagation of tolerance.

Deflection also increases with the size of plate outer diameter and with decreasing plate radius (or component radius). Hence, the effects of tolerance will increase accordingly since the amount of deflection affects the tolerance which, in turn, affects the gripping force. Therefore, the tolerance requirements for a larger plate, smaller thickness, and smaller component diameter, or their combination will be tighter than all other cases if the effects of tolerance are to be minimized.

5.7 EMPIRICAL GRIPPING FORCE EQUATIONS FROM SIMILITUDE ANALYSIS

The theoretical analysis, so far, is for a diaphragm plate with linear variation in thickness as obtains in most chucks. The jaw slides of the chuck are detachable. However, there are other profiles of thickness variation, say non-linear or cases where the jaw slides are not detachable, ie. the jaw slides are corporately manufactured with the diaphragm. In these cases, any form of theoretical analysis becomes complex and almost intractable. Two methods for approaching this problem are finite element analysis and engineering similitude analysis. There are finite element packages that can be used to solve the diaphragm plate problem. This section is concerned with similitude analysis which is an empirical method.

In engineering similitude, the important parameters that influence the gripping force are arranged in dimensionless groups (pi terms). The interaction between these groups are determined experimentally to establish general empirical design equations within the ranges of pi terms tested. The design equations are general because the terms are dimensionless. This method is usually restricted to a collection of up to four pi terms.

Equation 5.5.4 shows that the significant parameters influencing gripping force, F are the thrust, P, the outer and inner radii of plate, a and b, the moment arm, h, the number of jaws, N, the work-piece radius, r and the circumferential width of the jaw slide, d. The effect of the work-piece diameter can be neglected if an average gripping force is assumed over the operating range. The effect of the jaw slide width is negligible as stated earlier and the Poisson's ratio is assumed to be constant for most steels.

Representing the gripping force function mathematically, it is reduced to

$$F = f(P, a, b, h, N) \quad \ldots\ldots\ldots 5.7.1$$

In pi terms it is

$$\frac{F}{P} = f_o\left(b/a, h/a, N\right) \quad \ldots\ldots\ldots 5.7.2$$

or

$$F/P = f_1\left[f_2(b/a), f_3(h/a), f_4(N)\right] \quad \ldots 5.7.3$$

The next step is to determine the functions f_2, f_3 and f_4 and how they combine to give the function, f_1. From equation 5.5.4, it is obvious that

$$f_3 = 1/(h/a) \quad \ldots\ldots\ldots\ldots 5.7.4$$

applies generally to all chucks and has a product relationship in f_1. Therefore,

$$f_1 = \frac{1}{(h/a)}\left[f_2\ (b/a),\ f_4(N)\right] \quad \ldots 5.7.5$$

Therefore,

$$F/P = \frac{1}{(h/a)}\left[f_2\ (b/a), f_4\ (N)\right] \quad \ldots 5.7.6$$

Murphy (30) gives the outline on how to find $f_2\ (b/a)$ and $f_4\ (N)$ empirically, and determine how they combine to give a general design equation. This general design equation is valid for the range of pi terms tested.

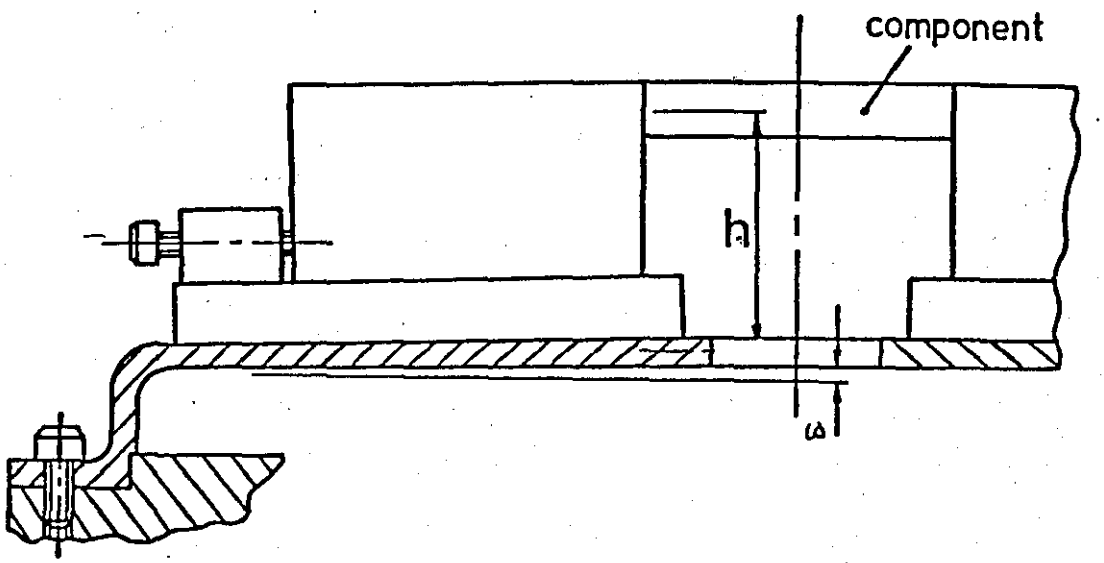

FIG.5.1.1 DEFLECTION OF PLATE WITH COMPONENT HELD IN JAWS

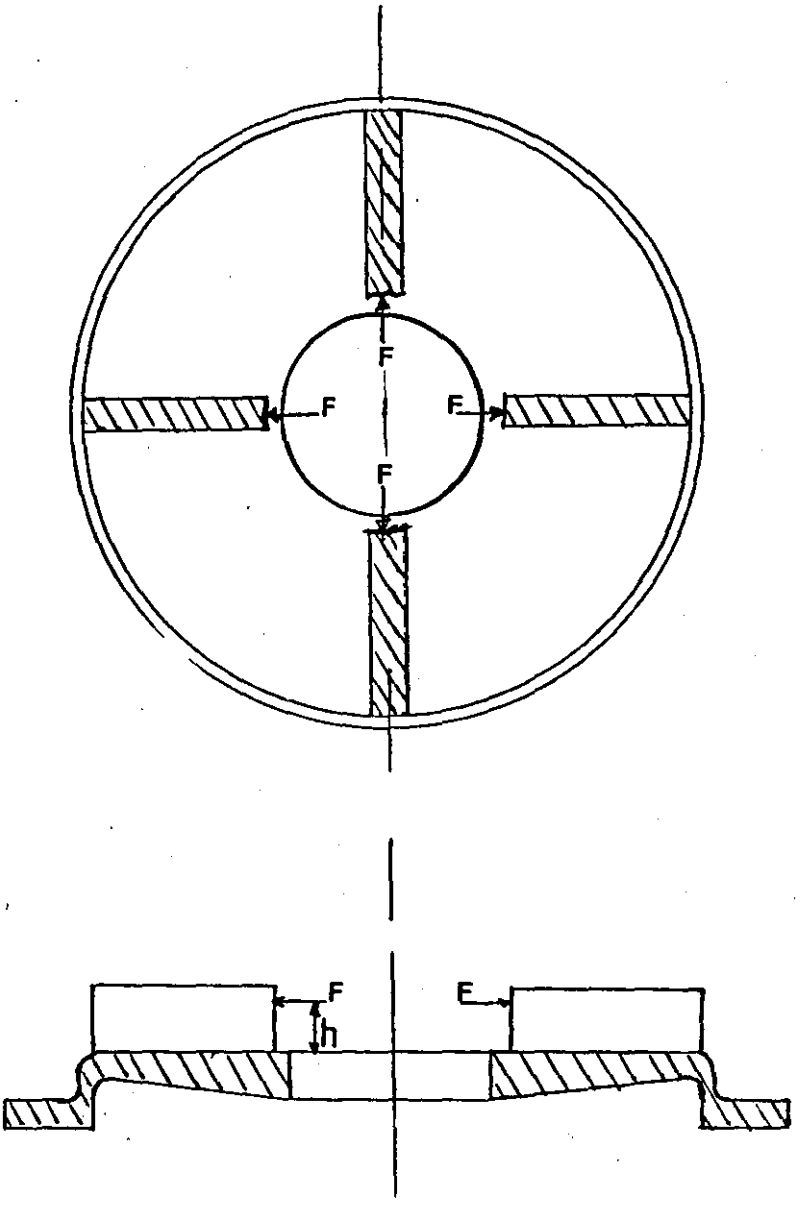

FIG.5.2.1 GRIPPING FORCES ACTING ON PLATE

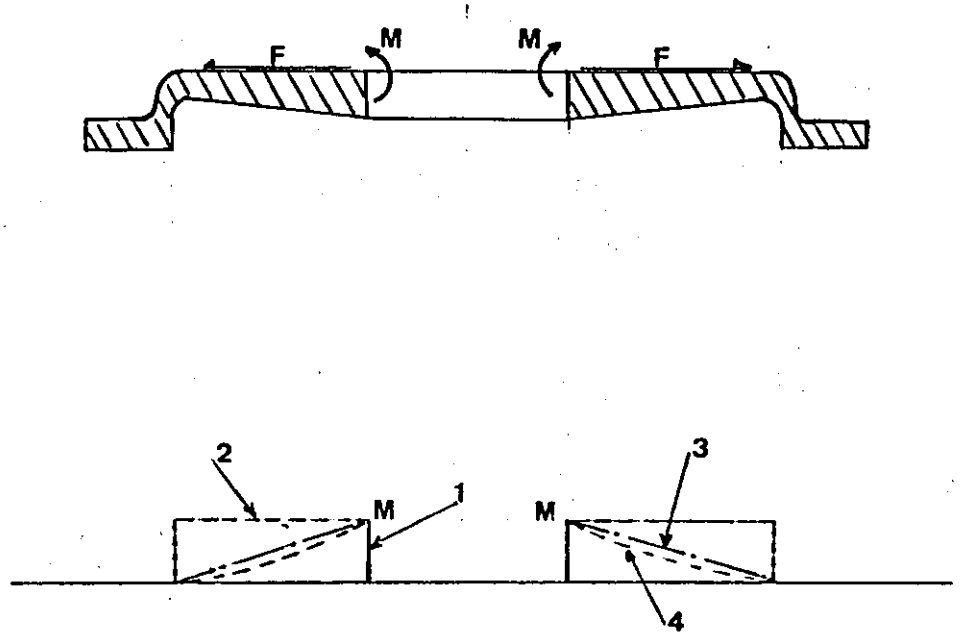

FIG. 5.2.2 COUPLES AND THEIR POSSIBLE DISTRIBUTIONS

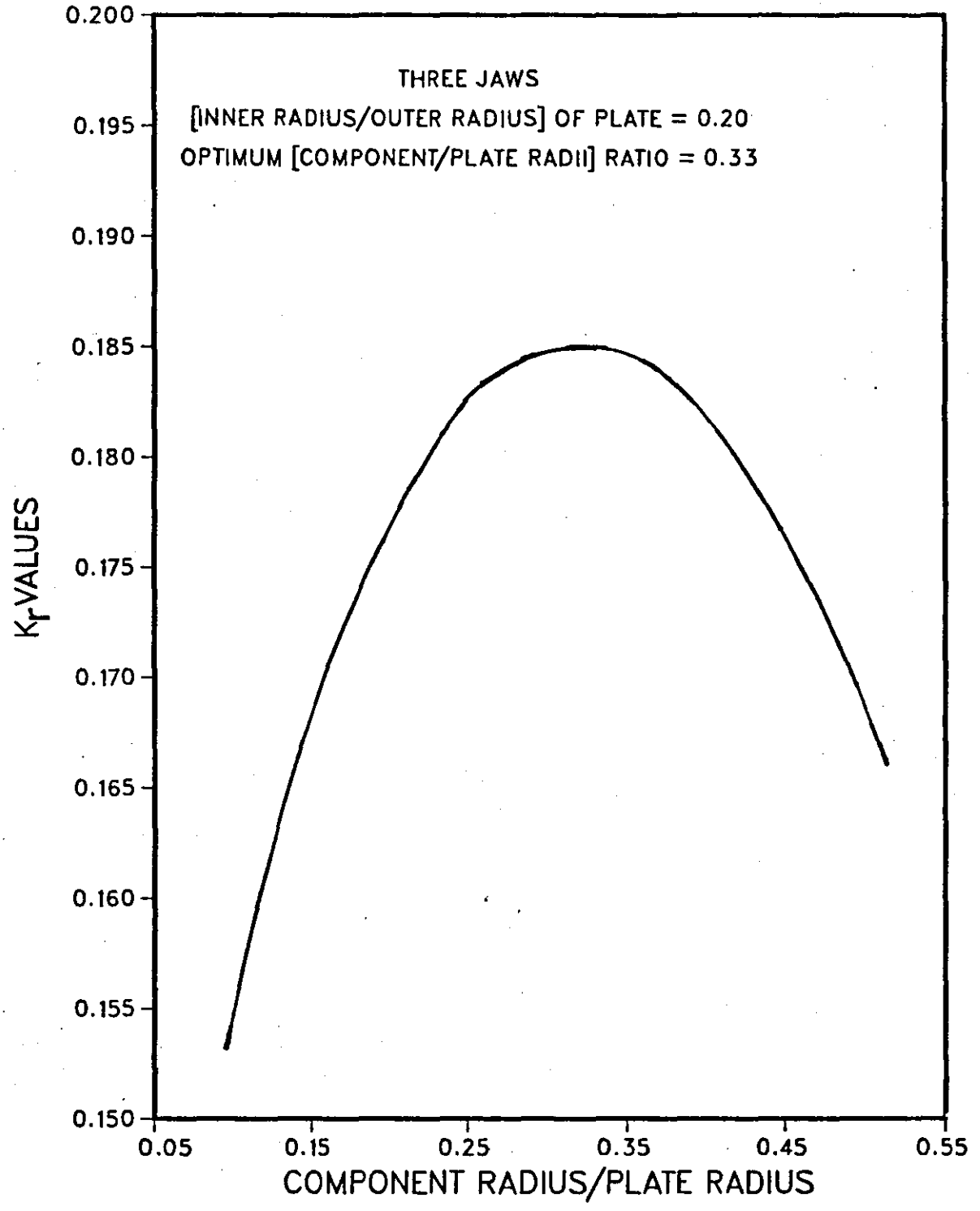

ig.5.5.1 VARIATION OF K_r WITH RATIO OF COMPONENT RADIUS TO PLATE RADIUS

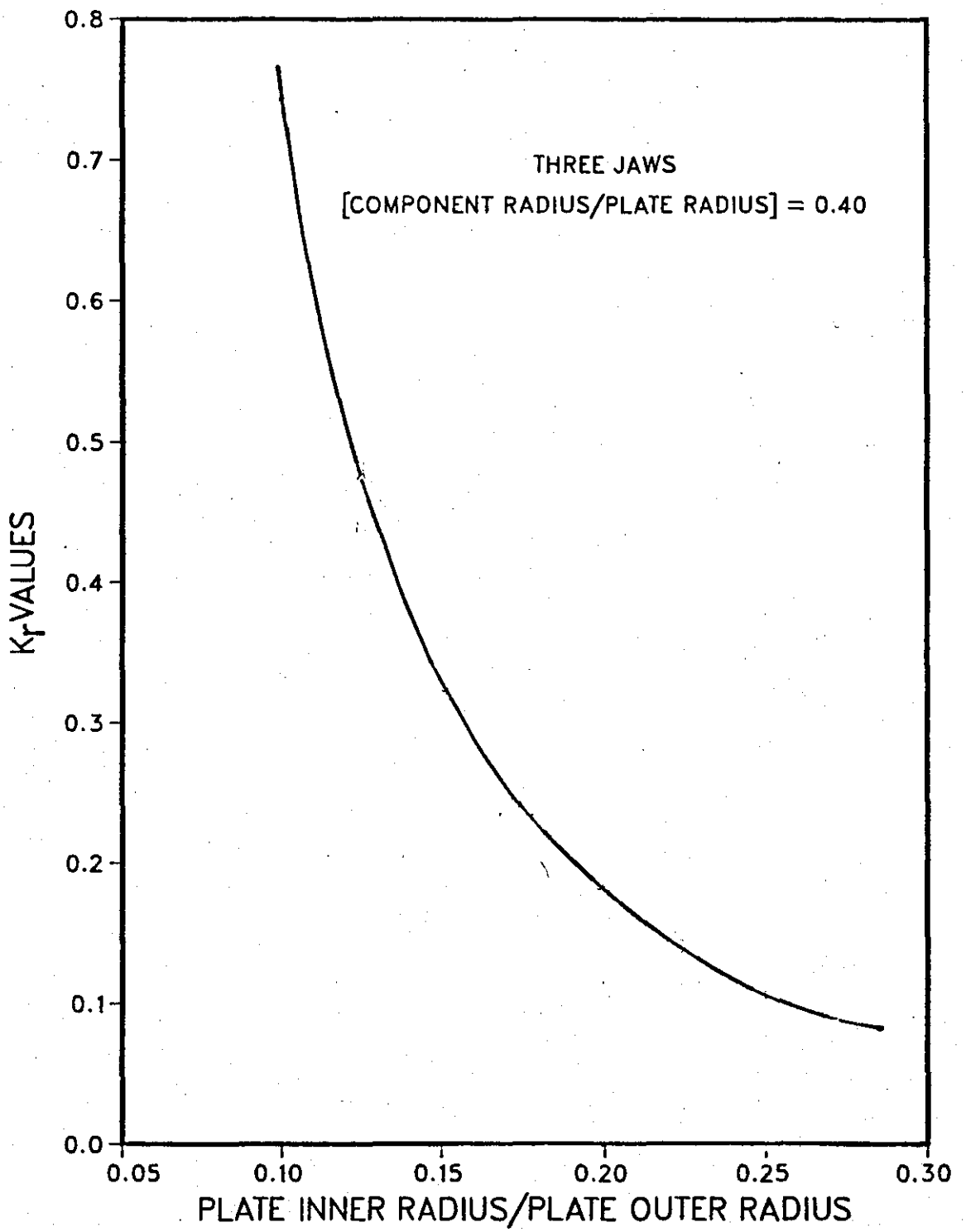

FIG.5.5.2 VARIATION OF K_r WITH RATIO OF INNER RADIUS TO OUTER RADIUS OF PLATE

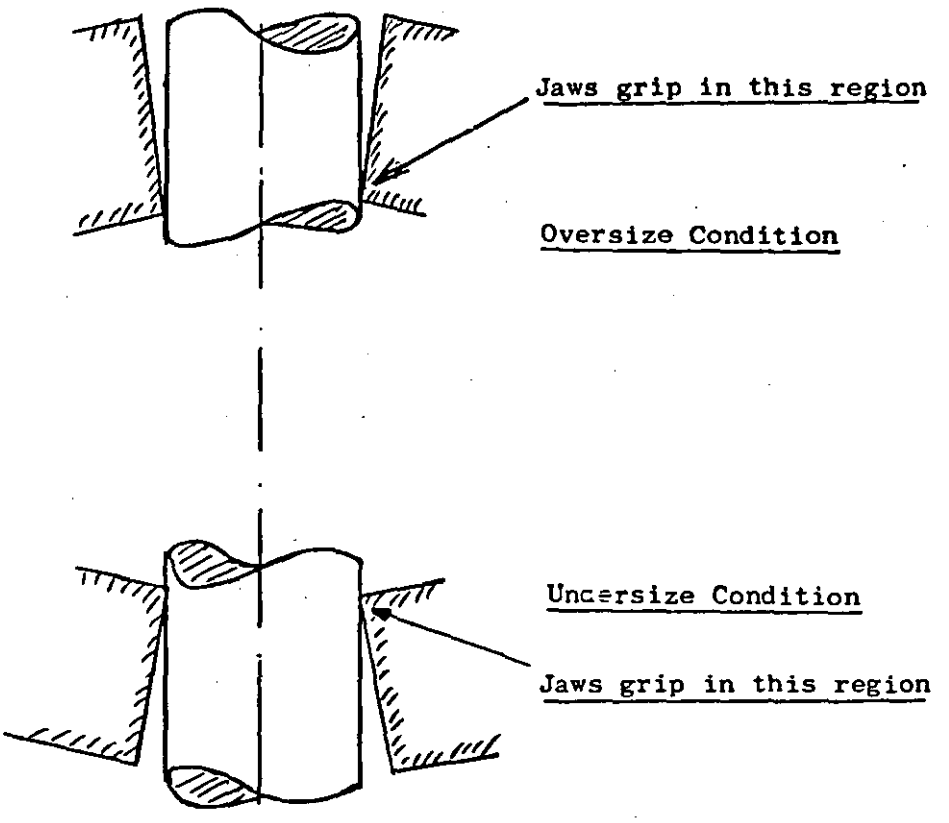

FIG. 5.6.1 Variation in Jaw Contact Points

TABLE 5.5.1.---K_r VALUES FOR TWO JAWS

JAW SLIDE WIDTH = 0.875 IN.
X= (COMPONENT DIAMETER/OUTER PLATE DIAMETER)

X	(PLATE INNER DIAMETER/PLATE OUTER DIAMETER),XB							
	0.100	0.125	0.150	0.175	0.200	0.225	0.250	0.275
.10	0.889	0.585	0.415	0.309	0.237	0.186	0.147	0.118
.15	0.973	0.637	0.450	0.333	0.255	0.199	0.158	0.126
.20	1.030	0.671	0.472	0.348	0.266	0.207	0.164	0.131
.25	1.064	0.691	0.484	0.357	0.272	0.212	0.168	0.134
.30	1.079	0.699	0.489	0.359	0.273	0.213	0.168	0.135
.35	1.078	0.697	0.486	0.357	0.271	0.211	0.167	0.133
.40	1.061	0.684	0.477	0.349	0.265	0.206	0.163	0.130
.45	1.029	0.663	0.461	0.338	0.256	0.199	0.157	0.126
.50	0.985	0.633	0.440	0.322	0.244	0.189	0.150	0.120
.55	0.928	0.596	0.414	0.302	0.229	0.178	0.140	0.112
.60	0.861	0.552	0.383	0.279	0.211	0.164	0.129	0.103
.65	0.783	0.502	0.347	0.253	0.191	0.148	0.117	0.094
.70	0.695	0.445	0.308	0.224	0.169	0.131	0.104	0.083
.75	0.598	0.383	0.265	0.193	0.145	0.113	0.089	0.071

TABLE 5.5.2.---K_f VALUES FOR THREE JAWS

JAW SLIDE WIDTH = 0.875 IN.
X= (COMPONENT DIAMETER/OUTER PLATE DIAMETER)

	(PLATE INNER DIAMETER/PLATE OUTER DIAMETER),XB							
X	0.100	0.125	0.150	0.175	0.200	0.225	0.250	0.275
.10	0.595	0.389	0.274	0.203	0.155	0.121	0.095	0.076
.15	0.658	0.428	0.300	0.221	0.168	0.131	0.104	0.082
.20	0.702	0.454	0.318	0.234	0.177	0.138	0.109	0.087
.25	0.730	0.471	0.329	0.241	0.183	0.142	0.112	0.089
.30	0.744	0.480	0.334	0.244	0.185	0.144	0.113	0.091
.35	0.747	0.481	0.334	0.244	0.185	0.143	0.113	0.090
.40	0.739	0.474	0.329	0.240	0.182	0.141	0.111	0.089
.45	0.721	0.462	0.320	0.233	0.176	0.137	0.108	0.086
.50	0.693	0.443	0.307	0.224	0.169	0.131	0.103	0.082
.55	0.656	0.419	0.290	0.211	0.159	0.123	0.097	0.077
.60	0.610	0.390	0.269	0.196	0.148	0.114	0.090	0.072
.65	0.557	0.356	0.245	0.178	0.134	0.104	0.082	0.065
.70	0.497	0.317	0.218	0.158	0.119	0.092	0.072	0.058
.75	0.429	0.273	0.188	0.137	0.103	0.079	0.062	0.050

TABLE 5.5.3.---K_f VALUES FOR FOUR JAWS

JAW SLIDE WIDTH = 0.875 IN.
X= (COMPONENT DIAMETER/OUTER PLATE DIAMETER)

	(PLATE INNER DIAMETER/PLATE OUTER DIAMETER),XB							
X	0.100	0.125	0.150	0.175	0.200	0.225	0.250	0.275
.10	0.449	0.291	0.204	0.150	0.114	0.088	0.069	0.055
.15	0.500	0.323	0.226	0.165	0.125	0.097	0.076	0.061
.20	0.537	0.346	0.241	0.176	0.133	0.103	0.081	0.065
.25	0.562	0.361	0.251	0.183	0.138	0.107	0.084	0.067
.30	0.577	0.370	0.256	0.187	0.141	0.109	0.086	0.068
.35	0.582	0.373	0.258	0.188	0.142	0.110	0.086	0.069
.40	0.579	0.370	0.256	0.186	0.140	0.108	0.085	0.068
.45	0.567	0.362	0.250	0.181	0.137	0.105	0.083	0.066
.50	0.547	0.349	0.241	0.175	0.131	0.101	0.080	0.063
.55	0.520	0.331	0.228	0.165	0.124	0.096	0.075	0.060
.60	0.487	0.310	0.213	0.154	0.116	0.089	0.070	0.056
.65	0.446	0.283	0.195	0.141	0.106	0.082	0.064	0.051
.70	0.399	0.253	0.174	0.126	0.094	0.073	0.057	0.045
.75	0.346	0.220	0.151	0.109	0.082	0.063	0.049	0.039

TABLE 5.5.4.---K_f VALUES FOR FIVE JAWS

JAW SLIDE WIDTH = 0.875 IN.
X= (COMPONENT DIAMETER/OUTER PLATE DIAMETER)

	(PLATE INNER DIAMETER/PLATE OUTER DIAMETER),XB							
X	0.100	0.125	0.150	0.175	0.200	0.225	0.250	0.275
.10	0.361	0.232	0.162	0.118	0.089	0.069	0.054	0.042
.15	0.406	0.261	0.181	0.132	0.100	0.077	0.060	0.048
.20	0.438	0.281	0.195	0.142	0.107	0.082	0.065	0.051
.25	0.462	0.295	0.204	0.148	0.112	0.086	0.068	0.054
.30	0.476	0.304	0.210	0.152	0.115	0.089	0.069	0.055
.35	0.483	0.308	0.212	0.154	0.116	0.089	0.070	0.056
.40	0.482	0.307	0.211	0.153	0.115	0.089	0.070	0.055
.45	0.475	0.302	0.208	0.150	0.113	0.087	0.068	0.054
.50	0.461	0.293	0.201	0.145	0.109	0.084	0.066	0.052
.55	0.440	0.279	0.192	0.138	0.104	0.080	0.063	0.050
.60	0.413	0.262	0.179	0.130	0.097	0.075	0.058	0.046
.65	0.380	0.241	0.165	0.119	0.089	0.068	0.054	0.042
.70	0.342	0.216	0.148	0.107	0.080	0.061	0.048	0.038
.75	0.298	0.188	0.129	0.093	0.069	0.053	0.041	0.033

TABLE 5.5.5.---K_f VALUES FOR SIX JAWS

JAW SLIDE WIDTH = 0.875 IN.
X= (COMPONENT DIAMETER/OUTER PLATE DIAMETER)

	(PLATE INNER DIAMETER/PLATE OUTER DIAMETER),XB							
X	0.100	0.125	0.150	0.175	0.200	0.225	0.250	0.275
.10	0.302	0.193	0.134	0.097	0.073	0.056	0.044	0.034
.15	0.342	0.219	0.151	0.110	0.082	0.063	0.049	0.039
.20	0.372	0.238	0.164	0.119	0.089	0.069	0.054	0.042
.25	0.394	0.251	0.173	0.125	0.094	0.072	0.057	0.045
.30	0.409	0.260	0.179	0.129	0.097	0.075	0.058	0.046
.35	0.417	0.265	0.182	0.132	0.099	0.076	0.059	0.047
.40	0.418	0.265	0.182	0.132	0.099	0.076	0.059	0.047
.45	0.414	0.262	0.180	0.130	0.097	0.075	0.058	0.046
.50	0.403	0.255	0.175	0.126	0.094	0.072	0.057	0.045
.55	0.387	0.245	0.167	0.121	0.090	0.069	0.054	0.043
.60	0.365	0.231	0.157	0.113	0.085	0.065	0.051	0.040
.65	0.338	0.213	0.145	0.105	0.078	0.060	0.047	0.037
.70	0.305	0.192	0.131	0.094	0.070	0.054	0.042	0.033
.75	0.267	0.168	0.114	0.082	0.061	0.047	0.036	0.029

TABLE 5.5.6.---K_f VALUES FOR SEVEN JAWS

JAW SLIDE WIDTH = 0.875 IN.
X= (COMPONENT DIAMETER/OUTER PLATE DIAMETER)

	(PLATE INNER DIAMETER/PLATE OUTER DIAMETER),XB							
X	0.100	0.125	0.150	0.175	0.200	0.225	0.250	0.275
.10	0.260	0.165	0.114	0.082	0.061	0.047	0.036	0.028
.15	0.297	0.189	0.130	0.094	0.070	0.054	0.042	0.033
.20	0.325	0.206	0.142	0.102	0.077	0.059	0.046	0.036
.25	0.346	0.220	0.151	0.109	0.081	0.062	0.049	0.038
.30	0.361	0.229	0.157	0.113	0.085	0.065	0.051	0.040
.35	0.370	0.234	0.160	0.115	0.086	0.066	0.052	0.041
.40	0.373	0.236	0.161	0.116	0.087	0.067	0.052	0.041
.45	0.370	0.234	0.160	0.115	0.086	0.066	0.051	0.041
.50	0.363	0.229	0.156	0.112	0.084	0.064	0.050	0.040
.55	0.350	0.220	0.150	0.108	0.080	0.062	0.048	0.038
.60	0.331	0.209	0.142	0.102	0.076	0.058	0.045	0.036
.65	0.308	0.193	0.132	0.094	0.070	0.054	0.042	0.033
.70	0.279	0.175	0.119	0.085	0.063	0.048	0.038	0.030
.75	0.245	0.154	0.104	0.075	0.055	0.042	0.033	0.026

TABLE 5.5.7.---K_r VALUES FOR EIGHT JAWS

JAW SLIDE WIDTH = 0.875 IN.
X= (COMPONENT DIAMETER/OUTER PLATE DIAMETER)

	(PLATE INNER DIAMETER/PLATE OUTER DIAMETER),XB							
X	0.100	0.125	0.150	0.175	0.200	0.225	0.250	0.275
.10	0.228	0.144	0.099	0.071	0.053	0.040	0.031	0.024
.15	0.263	0.166	0.114	0.082	0.061	0.046	0.036	0.028
.20	0.289	0.183	0.125	0.090	0.067	0.051	0.040	0.031
.25	0.310	0.196	0.134	0.096	0.072	0.055	0.043	0.034
.30	0.325	0.205	0.140	0.101	0.075	0.057	0.045	0.035
.35	0.334	0.211	0.144	0.103	0.077	0.059	0.046	0.036
.40	0.338	0.213	0.145	0.105	0.078	0.060	0.046	0.037
.45	0.338	0.213	0.145	0.104	0.078	0.059	0.046	0.036
.50	0.332	0.209	0.142	0.102	0.076	0.058	0.045	0.036
.55	0.322	0.202	0.137	0.099	0.073	0.056	0.044	0.034
.60	0.306	0.192	0.131	0.093	0.069	0.053	0.041	0.033
.65	0.286	0.179	0.122	0.087	0.065	0.049	0.038	0.030
.70	0.260	0.163	0.110	0.079	0.059	0.045	0.035	0.027
.75	0.230	0.144	0.097	0.069	0.051	0.039	0.030	0.024

TABLE 5.5.8.---K_f VALUES FOR NINE JAWS

JAW SLIDE WIDTH = 0.875 IN.
X= (COMPONENT DIAMETER/OUTER PLATE DIAMETER)

	(PLATE INNER DIAMETER/PLATE OUTER DIAMETER),XB							
X	0.100	0.125	0.150	0.175	0.200	0.225	0.250	0.275
.10	0.204	0.128	0.087	0.062	0.046	0.035	0.027	0.020
.15	0.236	0.149	0.101	0.072	0.054	0.041	0.031	0.024
.20	0.261	0.165	0.112	0.080	0.060	0.045	0.035	0.028
.25	0.281	0.177	0.121	0.087	0.064	0.049	0.038	0.030
.30	0.296	0.186	0.127	0.091	0.068	0.052	0.040	0.032
.35	0.306	0.193	0.131	0.094	0.070	0.053	0.042	0.033
.40	0.312	0.196	0.133	0.096	0.071	0.054	0.042	0.033
.45	0.312	0.196	0.133	0.096	0.071	0.054	0.042	0.033
.50	0.309	0.194	0.132	0.094	0.070	0.053	0.041	0.033
.55	0.300	0.188	0.128	0.091	0.068	0.052	0.040	0.032
.60	0.287	0.180	0.122	0.087	0.065	0.049	0.038	0.030
.65	0.269	0.168	0.114	0.081	0.060	0.046	0.036	0.028
.70	0.246	0.154	0.104	0.074	0.055	0.042	0.032	0.025
.75	0.219	0.136	0.092	0.066	0.048	0.037	0.028	0.022

TABLE 5.5.9.---K_p VALUES FOR TEN JAWS

JAW SLIDE WIDTH = 0.875 IN.
X= (COMPONENT DIAMETER/OUTER PLATE DIAMETER)

	(PLATE INNER DIAMETER/PLATE OUTER DIAMETER),XB							
X	0.100	0.125	0.150	0.175	0.200	0.225	0.250	0.275
.10	0.184	0.115	0.078	0.055	0.041	0.030	0.023	0.018
.15	0.214	0.134	0.091	0.065	0.048	0.036	0.028	0.022
.20	0.239	0.150	0.102	0.073	0.054	0.041	0.031	0.025
.25	0.258	0.162	0.110	0.079	0.058	0.044	0.034	0.027
.30	0.273	0.171	0.116	0.083	0.062	0.047	0.036	0.029
.35	0.284	0.178	0.121	0.086	0.064	0.049	0.038	0.030
.40	0.290	0.182	0.123	0.088	0.066	0.050	0.039	0.030
.45	0.292	0.183	0.124	0.089	0.066	0.050	0.039	0.031
.50	0.290	0.182	0.123	0.088	0.065	0.050	0.038	0.030
.55	0.283	0.177	0.120	0.086	0.063	0.048	0.037	0.029
.60	0.272	0.170	0.115	0.082	0.061	0.046	0.036	0.028
.65	0.256	0.160	0.108	0.077	0.057	0.043	0.033	0.026
.70	0.236	0.147	0.099	0.070	0.052	0.039	0.031	0.024
.75	0.210	0.131	0.088	0.063	0.046	0.035	0.027	0.021

TABLE 5.5.10.---K_r VALUES FOR ELEVEN JAWS

JAW SLIDE WIDTH = 0.875 IN.
X= (COMPONENT DIAMETER/OUTER PLATE DIAMETER)

	(PLATE INNER DIAMETER/PLATE OUTER DIAMETER),XB							
X	0.100	0.125	0.150	0.175	0.200	0.225	0.250	0.275
.10	0.168	0.104	0.070	0.050	0.036	0.027	0.020	0.016
.15	0.197	0.123	0.083	0.059	0.043	0.033	0.025	0.019
.20	0.220	0.138	0.093	0.066	0.049	0.037	0.028	0.022
.25	0.239	0.150	0.101	0.072	0.053	0.041	0.031	0.024
.30	0.254	0.159	0.108	0.077	0.057	0.043	0.033	0.026
.35	0.265	0.166	0.112	0.080	0.059	0.045	0.035	0.027
.40	0.272	0.170	0.115	0.082	0.061	0.046	0.036	0.028
.45	0.275	0.172	0.117	0.083	0.062	0.047	0.036	0.029
.50	0.274	0.172	0.116	0.083	0.061	0.047	0.036	0.028
.55	0.269	0.168	0.114	0.081	0.060	0.045	0.035	0.028
.60	0.260	0.162	0.109	0.078	0.058	0.044	0.034	0.027
.65	0.246	0.153	0.103	0.073	0.054	0.041	0.032	0.025
.70	0.228	0.142	0.095	0.068	0.050	0.038	0.029	0.023
.75	0.204	0.127	0.085	0.060	0.044	0.034	0.026	0.020

TABLE 5.5.11.---K_f VALUES FOR TWELVE JAWS

JAW SLIDE WIDTH = 0.875 IN.
X= (COMPONENT DIAMETER/OUTER PLATE DIAMETER)

	(PLATE INNER DIAMETER/PLATE OUTER DIAMETER),XB							
X	0.100	0.125	0.150	0.175	0.200	0.225	0.250	0.275
.10	0.154	0.096	0.064	0.045	0.033	0.024	0.018	0.014
.15	0.182	0.113	0.076	0.054	0.039	0.030	0.023	0.017
.20	0.205	0.128	0.086	0.061	0.045	0.034	0.026	0.020
.25	0.223	0.139	0.094	0.067	0.049	0.037	0.029	0.022
.30	0.238	0.149	0.101	0.072	0.053	0.040	0.031	0.024
.35	0.249	0.156	0.105	0.075	0.055	0.042	0.033	0.026
.40	0.257	0.161	0.109	0.077	0.057	0.043	0.034	0.026
.45	0.261	0.163	0.110	0.078	0.058	0.044	0.034	0.027
.50	0.261	0.163	0.110	0.078	0.058	0.044	0.034	0.027
.55	0.258	0.161	0.108	0.077	0.057	0.043	0.033	0.026
.60	0.250	0.156	0.105	0.074	0.055	0.042	0.032	0.025
.65	0.238	0.148	0.099	0.071	0.052	0.039	0.030	0.024
.70	0.221	0.137	0.092	0.065	0.048	0.036	0.028	0.022
.75	0.199	0.123	0.083	0.059	0.043	0.032	0.025	0.020

CHAPTER SIX

MEASUREMENT OF GRIPPING FORCE

6.1 SCOPE OF EXPERIMENT

An expression for the prediction of the gripping force of a diaphragm chuck with any number of jaws is given in equation 5.5.4. The important parameters that affect gripping force are the thrust load, number of jaws, ratio of inner to outer diameters of the diaphragm plate, ratio of work-piece to diaphragm plate diameters, Poisson's ratio of plate material, the moment arm, and the circumferential width of the jaw slide. The purpose of this experimental measurement is to evaluate how close the gripping force can be predicted with equation 5.5.4. This research is not concerned with the dynamic characteristics of the chuck. The measurements are, therefore, taken under static conditions and in the normal operating position on a lathe machine shown in Figure 6.1.1. Strain gauges mounted on rings as in Figure 6.1.2 were used as primary measuring devices (i.e. ring force transducers) for the gripping force. The design, manufacture, calibration and use of the ring force transducers are discussed in following sections.

6.2 DESIGN AND MANUFACTURE OF RING FORCE TRANSDUCERS

In designing the ring force transducers, Chidlow (4) assumed that the gripping forces constituted a system of point forces acting on the ring. This approach, while it does not make the calibration incorrect, deviates from the actual load condition and obscures the behaviour of the ring under load. It is also only applicable to the jaw width used in the calibration. There is no way of accurately relating that calibration to any other jaw width except to repeat the calibration

process for that specific jaw width. The ring is actually loaded with forces distributed over the faces of the jaws. When this fact is taken into account, the theoretical bending moment along the ring becomes different from that given by Chidlow. The design of the ring provides for the choice of rings that are sensitive enough to the range of experimental loads and at the same time able to withstand the loads without permanent set. Design of rings with distributed loads is developed from the case of point loads.

Chidlow (4) and Prickett (6) designed fixtures that were used to calibrate the rings loaded by three forces. Difficulties exist in designing calibration fixtures for load systems exceeding three forces. The force application mechanism has to move simultaneously and contact the ring at a central location. Since more than three contact points are involved, some of the points are rendered ineffective or do not apply equal forces because the movement of the operating mechanism ceases when two or three points make contact with the ring before the rest. This renders the remaining contact faces redundant. In addition, fixtures will have to be designed for as many times as there are number of jaws. To eliminate these problems, the ring loaded by three forces is used as a basis for calibration; and all other force systems are related to this basic three-force system. Excluding the two-force system which has a lot of centring problems, the three-force system stresses the ring most. Designing a ring that withstands stresses due to a three-force system ensures that the ring can withstand stresses caused by any force system greater than three without a significant loss of strain sensitivity. The analysis of the strain in the ring follows the outline used by Pippard and Baker (31).

If a ring is loaded as shown in Figure 6.2.1, it is a redundant system. Redundant in the sense that the ring carries

loads without collapsing if it is cut at any section. Thus, it is an indeterminate system. At ε equal to such a value as to create a symmetric loading, the radial shear stress at a section along a line of symmetry is zero. On other sections the radial shear stresses are negligible. The following assumptions are made:

1. Negligible radial shear stresses.
2. Strain energy of a curved bar is approximately the same as for a straight bar.
3. Effects of the thickness of the ring on the forces and moments are negligible.

The resultant actions necessary to restore the original conditions if the ring is cut at section A are the moment M_o, and the tangential force H_o shown in Figure 6.2.1. Shear force at A is zero due to symmetry. Let α be the angle of a point $\underline{X}$ from the section A. The bending moment at α is

$$M = M_o - H_o R\,(1-\cos\alpha) - PR \sin(\alpha-\varepsilon) \quad \ldots\ldots 6.2.1$$

The boundary conditions at A are that ϕ' and δ', the angular and linear displacements are zero. From energy methods these conditions are represented as

$$\phi'_A = \frac{\partial U}{\partial M_o} = \frac{2}{EI'}\int_o^{\pi} M \frac{\partial M}{\partial M_o}\, ds = 0$$

$$\delta'_A = \frac{\partial U}{\partial H_o} = \frac{2}{EI'}\int_o^{\pi} M \frac{\partial M}{\partial H_o}\, ds = 0 \quad \ldots\ldots 6.2.2$$

where U is the total strain energy, s is a circumferential distance, E is the Modulus of Elasticity, and I' is the area moment of inertia. Substituting for M in equation 6.2.2, integrating and solving for H_o and M_o give

$$H_o = \frac{-P}{\pi}\left(\pi - \frac{\pi\varepsilon}{180}\right) \sin\varepsilon$$

$$M_o = \frac{PR}{\pi}\left[1 + \cos\varepsilon - \pi\left(1 - \frac{\varepsilon}{180}\right) \sin\varepsilon\right] \quad \ldots 6.2.3$$

which are substituted back into equation 6.2.1 to give M. H_o and M_o are really the maximum tangential force and moment respectively in the ring. The last term on the right-hand side of equation 6.2.1 is the moment contribution due to point load, P. Suppose P is replaced by a distributed load p as in Figure 6.2.2; the moment due to this load is determined as follows:

$$dM = -pR^2 \text{ Sin } (\alpha-\varepsilon)\, d\varepsilon \qquad \ldots\ldots 6.2.4$$

$$M = -pR^2 \int_{\varepsilon-\psi}^{\varepsilon+\psi} (\text{Sin } (\alpha-\varepsilon)\, d\psi \qquad \ldots\ldots 6.2.5$$

Integrating,

$$M = -pR^2 \left[\text{Cos } (\alpha-\varepsilon)\right]_{\varepsilon-\psi}^{\varepsilon+\psi} \qquad \ldots\ldots 6.2.6$$

By trignometric manipulation,

$$M = -2pR^2 \text{ Sin}\psi \text{ Sin } (\alpha-\varepsilon) \qquad \ldots\ldots 6.2.7$$

where ψ is the half-angle subtending the distributed load. This shows that the point force P is replaced by $2pR^2$ Sinψ for a distributed load.

Roark(32) gives the maximum bending moment in a ring under any number of equally spaced radial point forces as

$$M_o = \frac{PR}{2} \left(\frac{1}{\text{Sin } \varepsilon} - \frac{1}{\varepsilon}\right) \qquad \ldots\ldots 6.2.8$$

In terms of number of forces (or jaws), N,

$$M_o = \frac{PR}{2} \left[\frac{1}{\text{Sin}(\frac{180}{N})} - \frac{N}{\pi}\right] \qquad \ldots\ldots 6.2.9$$

Therefore, for a distributed load 2p

$$M_o = pR^2 \text{ Sin } \psi \left[\frac{1}{\text{Sin}(\frac{180}{N})} - \frac{N}{\pi}\right] \qquad \ldots\ldots 6.2.10$$

For the geometry of ring shown in Figure 6.2.3, the outer and inner strains in the ring according to Hall et al (33) are respectively

$$\xi_o = \frac{M_o h_o}{AEer_i} \quad \ldots\ldots\ldots\ldots 6.2.11$$

$$\xi_i = \frac{M_o h_i}{AEer_i}$$

The total strain produced by summing the two strains is

$$\xi_T = \frac{M_o h'}{AEer_i} \quad \ldots\ldots\ldots\ldots 6.2.12$$

Substituting for M_o,

$$\xi_T = \frac{p R^2 h' \sin\psi}{AEer_i} \left[\frac{1}{\sin(\frac{180}{N})} - \frac{N}{\pi} \right] \ldots 6.2.13$$

Noting that the distributed load is the gripping force divided by the jaw face area; and that Sin ψ is related to the jaw face width and mean radius of ring, a single calibration for a given jaw face can be used for estimating the load on any other jaw face. The gripping force remains the same irrespective of the jaw face dimensions, but the distributed force changes. From equation 6.2.10 the ratio of the moment M_o^N due to N jaws (N > 3) to the moment M_o^3 due to three jaws is determined. This is also the ratio of the resulting strains. For the four and six jaws

$$\frac{M_o^4}{M_o^3} = \frac{\xi_T^4}{\xi_T^3} = 0.7051$$

$$\ldots\ldots\ldots 6.2.14$$

$$\frac{M_o^6}{M_o^3} = \frac{\xi_T^6}{\xi_T^3} = 0.4519$$

From this equation 6.2.14 it is obvious that the gripping force is not strictly proportional to the inverse of the direct ratio of the number of jaws, ie. the gripping force for six jaws is not exactly half of the gripping force for three jaws. For all practical purposes, the gripping force ratio is equal to the inverse of the numerical ratio of the number of jaws.

A total of eight rings was manufactured. Five were made from mild steel (EN3B) with a radial thickness of 10mm[e]. This thickness ensured minimum deviation from roundness under load since the theory of ring force transducers assumes that the ring maintains a round shape. The other three rings were made from EN8 steel with a radial thickness of 5mm for better strength and sensitivity.

A dividing head was used to mark-out the positions of the strain gauges and the jaws on the ring such that the gauges were always positioned mid-way between jaws for any number of jaws. A pair of TML gauges were mounted on the ring (inside and outside) at the marked-out positions and connected in a half-bridge circuit to provide adequate compensation and sensitivity.

6.3 CALIBRATION OF THE RING FORCE TRANSDUCERS

The fixture in Figures 6.3.1 and 6.3.2 used for the calibration of the strain rings was designed and manufactured by Prickett(6). This fixture consists of a rigid circular frame carrying a rigid guide ring. Plungers radially run through the guide side holes that are set 120° apart. The inner end of each plunger is a square head that has a stepped back face which flushes with the inner face of the guide ring for locating purposes. The heads of the plungers are machined to duplicate the shape and dimensions of the chuck jaws. Each set of three plungers is located and clamped to the

e. Pahlitzsch (2) was the first chuck investigator to use 10 mm thick rings. Subsequent researchers have followed this practice.

inner face of the guide ring; and bored-out to the nominal diameters of the strain rings. Very thin sheets are placed behind the locating heads of the plungers prior to boring such that, on removal, there is enough clearance to allow for the placement of the strain ring for calibration.

At the centre of the guide ring and through the base frame is a vertical plunger pushing down on three bell crank levers set at corresponding angular positions to the horizontal plungers. When a force is applied downwards through the vertical plunger, the levers in turn push the outer end of the horizontal plungers and force them radially into the strain ring placed concentrically within the guide ring. Thus, the strain ring is loaded by three equally spaced forces. The ratio of the horizontal plunger force to the vertical force was established by Prickett to be 0.371 for the fixture.

The strain ring is placed into the calibration fixture ready for calibration after the horizontal plungers are released. The plungers are then aligned to the marks on the ring for three jaws; making sure that the gauges are mid-way between the plungers. Vertical forces are applied using a large vertical milling machine. A TECQUIPMENT STRAIN SCOPE is used as a strain read-out system. See Figures 6.3.3 and 6.3.4.

The bridge is balanced and read before and after loading. The strain output is recorded against the applied load and increments of the applied load. The applied load is converted to plunger force or gripping force by the factor 0.371. In order to eliminate the error due to deviation from symmetry, the loading process is repeated after rotating the strain ring to place the gauges between the other pairs of plungers in the

set. The guide ring is then rotated to bring the outer end of each plunger in turn against each bell crank lever, and the loading process is repeated. This is to minimize the overall effects of dimensional and frictional variations in the lever-guide arrangement. The readings are averaged to give the calibration charts of Figures 6.3.5 to 6.3.12 for the force transducers. Calibration data are given in Appendix F.

The calibrations are used directly for the three-jaw chuck. If

$$\frac{\xi^N}{\xi^3} = K_N \qquad \ldots\ldots\ldots\ldots\ldots\ldots 6.3.1$$

for the total strains, K_N = 0.7051 and 0.4519 respectively for four and six jaws, N being four or six. To use the calibration charts for four and six jaws, the measured strain for N jaws is divided by K_N to obtain an equivalent strain in terms of three jaws. The equivalent gripping force is read off the charts for the equivalent strain. This equivalent gripping force is then multiplied by K_N to give the gripping force for N number of jaws. This is in fact a quasi-experimental method. It follows, therefore, that if F is the gripping force, then

$$\frac{F^N}{F^3} = K_N \qquad \ldots\ldots\ldots\ldots\ldots\ldots 6.3.2$$

An examination of equation 6.2.13 shows that the strain in a ring for a given load increases with the mean radius of the ring. In other words, the slope of the calibration chart increases with decreasing mean radius. Comparing the slopes of the charts for those rings with radial thickness of 10mm, there is agreement with equation 6.2.13 for 60mm to 90mm outer diameter rings. The slopes decrease for 55mm and 50mm rings

contrary to equation 6.2.13. For the rings with 5mm radial thickness, the slope for the 50mm ring is expectedly greater than for 60mm and 90mm rings. The 90mm ring has a higher slope than the 60mm ring contrary to equation 6.2.13. These deviations may be explainable in terms of localized stresses, but indicate some inadequacies in the use of strain rings for gripping force measurements.

Localized stress effects at the jaws influence the strain gauges as the distance between the gauges and the jaws decreases. That is, localized stress effects are more in rings of small diameters. On the other hand, the smaller rings tend to be stiffer at the jaws because the ring behaves like three different curved beams supported at the jaws. This is due to a high jaw face width to ring radius ratio. The effects of localized stresses and the face width/radius ratio are in conflict with each other. It is therefore suggested that large rings are more suitable than small rings for the measurement of gripping force.

6.4 EXPERIMENTAL PROCEDURE

To evaluate the generality of equation 5.5.4, measurements are taken for three, four and six jaws, and for different thrusts. Two different chuck sizes are tested to measure the effect of the ratio of inner to outer diameters of the diaphragm plate on the gripping force. And two 7 in. diameter plates are also tested to determine the direct influence of thickness on the gripping force. One of the 7 in. plates, Plate A, carries three, four or six jaws, and has no locating holes. See Figures 6.4.1, 6.4.2 and 6.4.3. This Plate A is additionally used to measure how gripping force changes with the number of jaws. The second 7 in. plate, Plate B is less thick and carries four jaws only. Plate B has four locating holes as well. The smaller 5½ in. chuck,Plate C carries a plate with three locating holes and suited for three

4. From Chidlow's(4) Measurements. Cross-checked by this author.

jaws only (Figure 6.4.4). Details of the plates have been given in Table 4.2.1.

The number of parametric effects measured are limited by the cost of the tests. This author accepts Chidlow's(4) analysis that the gripping force is inversely proportional to the first power of the moment arm. Thus, the moment arm is kept constant at 1.6551 in. throughout the experiment. It was stated earlier that the width of the jaw slide affects the gripping force negligibly. Hence, the width is kept constant at 0.875 in.

The jaws are modified by machining to the circumferential face width of ¼ in. to avoid crushing the strain gauges on the smaller rings (Figure 6.4.5). Boring of the jaws to the nominal diameter of the ring at a given thrust is within ± 0.001 in tolerance. The thrusts at which readings are taken are 1417.22 LBS, 1184.02 LBS, 929.32 LBS. and 687.81 LBS. for the 7 in. chuck. For the 5½ in. chuck, the thrusts are 200 LBS, 340 LBS, 475 LBS, 625 LBS and 765 LBS. The bores are checked with a tri-bore micrometer and a depth gauge is used to check that the bore has a depth equal to the width of the ring. The depth gauge is also used to measure the distance between the step supporting the ring and the plate surface. This way, the moment arm can be obtained. The air line pressure is kept constant during boring by taking small cuts at a time. It is to be emphasized here that the precision required of a diaphragm chuck makes it necessary that the tolerance between bore and ring diameter remains tight. The taking of small cuts during boring reduces the small changes in bore dimensions due to the elasticity of the air-plate system.

Increasing the line pressure slightly allows the ring to be slipped into the jaws. The jaws are lined to the marked-

out lines on the ring for the given number of jaws such that the gauges are mid-way between the jaws. The bridge is balanced and read from the TECQUIPMENT before loading. Gripping action takes place when the air pressure is relieved. The bridge is again balanced and read. The difference between the two readings is the total amount of maximum strain in the ring from the gauges. The actual strain can be obtained from the equation

$$\text{Actual Strain} = \frac{2 \times \text{Nominal Strain}}{\text{Strain Gauge Factor}} \quad \ldots . 6.4.1$$

where the Nominal strain is the reading from the bridge. The gripping force is read from the calibration charts of the ring. Three readings are taken for each space between jaws and averaged

The procedure is repeated for each ring transducer and for each level of thrust. The gripping force for the six-jaw case is measured for one set of readings only from the 90mm ring. This is because the circumferential lengths between jaws for the other rings are too small to allow for the positioning of the gauges between jaws without crushing. Figure 6.4.6 is a further illustration of the experimental process.

6.5 RESULTS AND DISCUSSION

The observed values of gripping forces are given in Appendix G for the deflecting thrusts and ring transducer diameters. In discussing the experimental results, these data are used to illustrate the comparison between predicted and experimental gripping forces. The predicted gripping forces are obtained from equation 5.5.4. Further illustrations are made of the effects of plate thickness and diameters, number of jaws, and workpiece diameter on the gripping force.

Plates A, B and C have different thicknesses; with A and B having the same inner and outer diameters, and C being of different diameters.

6.5.1 GRIPPING FORCE AND DEFLECTING THRUST

A direct comparison between experimental and theoretical gripping force is made in Figures 6.5.1 to 6.5.11 for given deflecting thrusts and workpiece diameters. There is close agreement between the predicted and measured values. The closeness of the prediction is evaluated in terms of the percentage deviation from the experimental results for the absolute values of the data points and the slopes of the graphs. The slopes of the graphs compare the trend of the relationship between gripping force and thrust. The quantitative data points measure the accuracy of the prediction of individual points.

For the three-jaw case of Plate A, Figures 6.5.1 to 6.5.5 show that the slopes of the gripping force - thrust relationship are within 9% of measured slope. The absolute values of the predicted gripping force are within 10% of the measured values except for the second lowest point for the 70mm ring and the lowest point for the 50mm ring where the predicted is within 12% of measured. The errors are reduced if the predicted values are considered relative to the regression line points. Some predicted values are as close as 0.6% of the measured values. There is no general pattern as to whether the measured force is higher or lower than the predicted values. This result is different from what was obtained in Chidlow's(4) work where predicted forces were consistently lower than measured. A major reason for this difference is that the couples were expanded around the geometric average radius of the plate r = (a+b)/2. Chidlow expanded the couples around the inner edge (r=b).

A similar pattern of behaviour is observed for the same plate with four jaws. The plots are shown in Figures 6.5.6 to 6.5.10. The error for the 55mm ring is the highest at 27% for the slope. The second highest error in slope occurs for the 70mm ring at 14%. The other predicted slopes are within 9% of the experimental. Considering the absolute values, the highest errors occur at the lowest two points for the 50mm ring at 14% and 15%. All the other errors are within 10% of the experimental values. Again, the prediction is improved when compared with the regression points of the experimental results.

Measurement data of the gripping force for six jaws are limited to one set of readings from the 90mm ring (Figure 6.5.11). This is due to the fact that the diameters of the transducer rings have to be large enough to carry strain gauges between the jaws without the gauges being crushed. The predicted gripping force in this case is within 4% of the measured values. The closeness of all the predicted values is significant.

6.5.2 GRIPPING FORCE AND PLATE THICKNESS

Plate B carries four jaws only and has the same geometric dimensions as Plate A except for the thickness. The thickness of Plate B is 18% less than that of Plate A. For Plate B, the gripping force data were collected for the 50mm and 70mm rings. For both rings, the slopes are within 6% of the measured values (Figures 6.5.12 and 6.5.13). Comparing the slopes of the measured gripping forces of Plates A and B for the effect of thickness, it is shown in Figures 6.5.14 and 6.5.15 that the slopes are within 8% of each other. Plate B has a higher gripping force slope. The measured points for Plate B are higher than for Plate A by as much as 28% at the lowest point for the 50mm ring, and as little as 0.7% for the lowest point for the 70mm ring.

The large difference in the gripping forces for the 50mm ring is attributable to the effects of tolerance that are higher for thinner plates and smaller workpiece diameters. Therefore, there does not seem to be any contradiction to Chidlow's(4) conclusion on the effects of plate thickness. His conclusion is in agreement with equation 5.5.4 and the experimental results that the direct effect of thickness on gripping force is not significant.

6.5.3 GRIPPING FORCE AND RATIO OF INSIDE TO OUTSIDE DIAMETERS

Equation 5.5.4 shows that gripping force varies with the ratio of the inner diameter to the outer diameter of a plate. The outer and inner diameters have a directly linear effect on gripping force. Plates A and C have outer diameters of 2.5578in. and 2.15in., and inner diameters of 0.5178in. and 0.465in. respectively.

Figures 6.5.16 and 6.5.17 show the gripping force for Plate C (three jaws) with the 50mm and 60mm rings. For both rings, the predicted gripping force is less than the experimental, but the slopes are within 4% of the experimental with the predicted being higher. The difference between the measured and predicted is due to the effect of shear which increases the deflection by the ring thrust, and the effect of bending beyond the assumed outer radius of the plate. The location error of the outer radius for a smaller plate is higher than for a large plate. The smaller thickness also causes some bending beyond the theoretical location of the outer radius.

In comparison with Plate A, there is a significant reduction in the gripping force for Plate C due to a lower sum of outer and inner diameters. The predicted change in the gripping force due to a change in the outer and inner diameters is primarily confirmed by the different slopes for

Plates A and C in Figures 6.5.18 and 6.5.19. The other reason for the higher gripping force for Plate A is that ratio of the inner to outer diameters is smaller for Plate A than for Plate C.

6.5.4 GRIPPING FORCE AND NUMBER OF JAWS

The effect of the number of jaws on the gripping force per jaw is shown in Figure 6.5.20. The slopes of the gripping force per jaw plots decrease as the number of jaws increases. The rate of decrease in slope also decreases as the number of jaws increases. This fact suggests that there is a limiting number of jaws above which there is no significant change in the gripping force per jaw. If a minimum change of 10% is specified, then the limiting number of jaws is ten. This is obtained from Tables 5.5.9 and 5.5.10 where the change in gripping force per jaw is less than 10% going from ten jaws to eleven jaws as indicated by the K_r values.

6.5.5 GRIPPING FORCE AND WORKPIECE DIAMETER

Figure 6.5.21 shows the effect of workpiece diameter on measured and predicted gripping force. The graphs are obtained from the slopes of the gripping force-thrust plots for the various ring diameters. The slopes indicate the gripping force per jaw to thrust ratio. This method is used to illustrate clearly the effects of workpiece diameter. It is evident that both the predictions and the measurements agree that gripping force is significantly affected by workpiece diameter. This observation is in disagreement with Chidlow's(4) conclusion that workpiece diameter does not affect gripping force. Measurements from Chidlow's work are used to plot Figure 6.5.22 which shows gripping force-thrust ratio against workpiece diameter for Plate C at a moment arm, h of 32mm. Examination of the points agrees with the decreasing trend of gripping force with workpiece diameter. Chidlow would have reached this conclusion had he analysed his data from the perspective of gripping force-thrust ratio.

6.5.6 GRIPPING FORCE RATIOS BETWEEN ANY NUMBER OF JAWS

In calibrating the ring force transducers, the constants of equation 6.2.14 related the gripping force per jaw for three jaws to the gripping force per jaw of four and six jaws. Consequently, the experimental gripping forces will obey similar built-in proportions. These proportions are, however, to be evaluated in comparison with their predicted values. The predicted ratios are on the average

$$\frac{F_O^4}{F_O^3} = 0.77$$

$$\frac{F_O^6}{F_O^3} = 0.44$$

and these values are within 10% and 3% respectively of the first and second ratios of equation 6.2.14.

Again these ratios show that gripping force per jaw is not strictly in direct inverse proportion to the numerical ratio of the number of jaws, i.e. the gripping force per jaw for four jaws is not exactly 75% of the gripping force per jaw for three jaws. For all practical purposes, however, the numerical ratio of the number of jaws is a close approximation of the inverse of gripping force per jaw ratios. As a result, the gripping force per jaw for any number of jaws can be estimated without using equation 5.5.4 or 5.5.5 if the gripping force per jaw for one set of jaws is known.

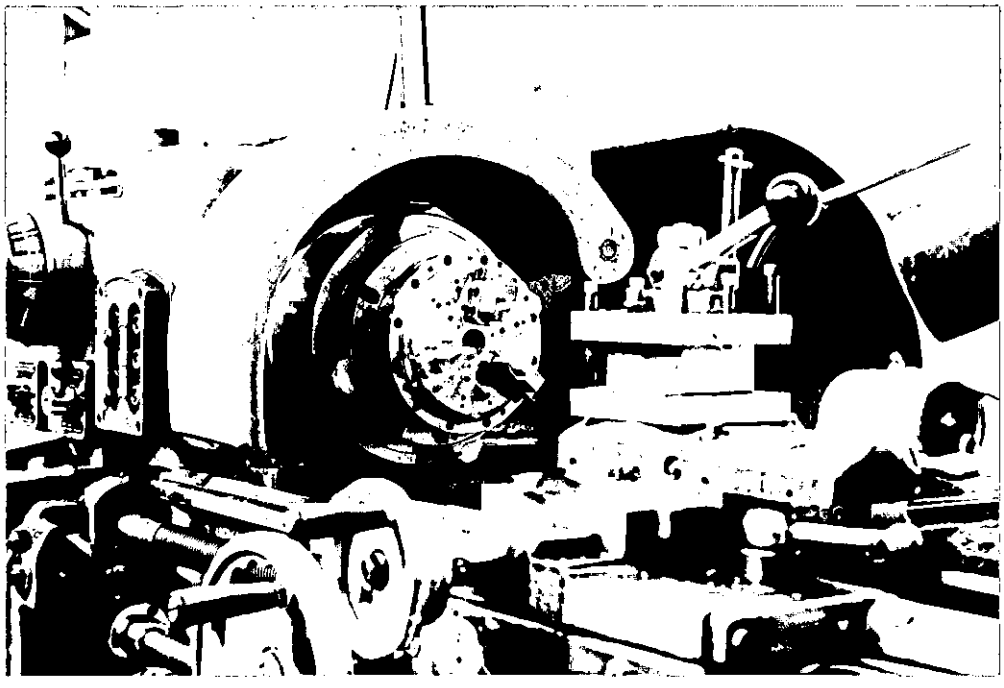

FIG.6.1.1 DIAPHRAGM CHUCK IN NORMAL OPERATING POSITION

FIG.6.1.2 STRAIN RING

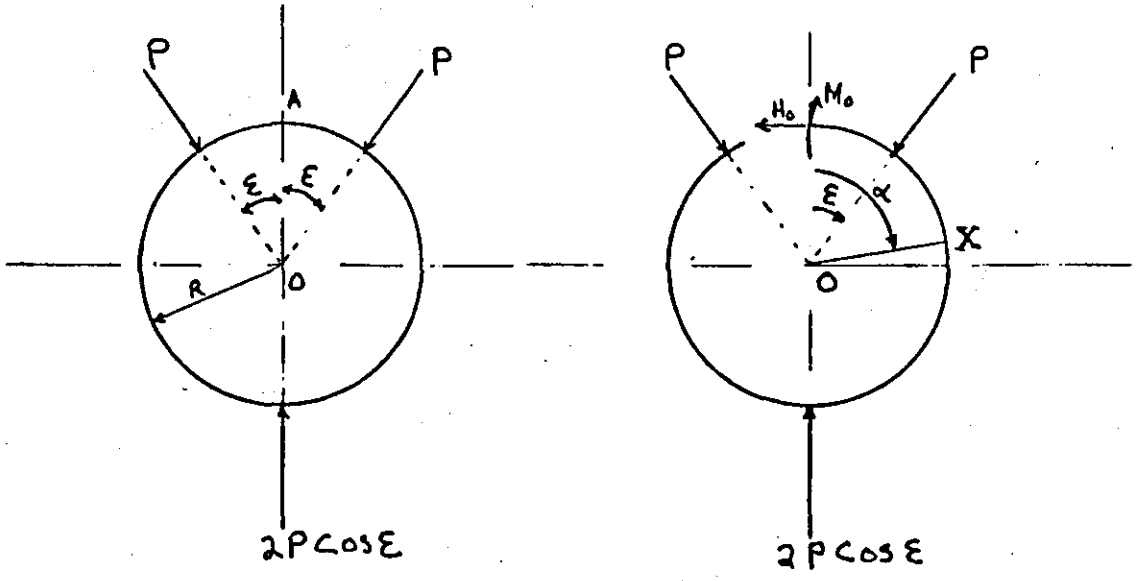

FIG.6.2.1 RING WITH POINT LOADS

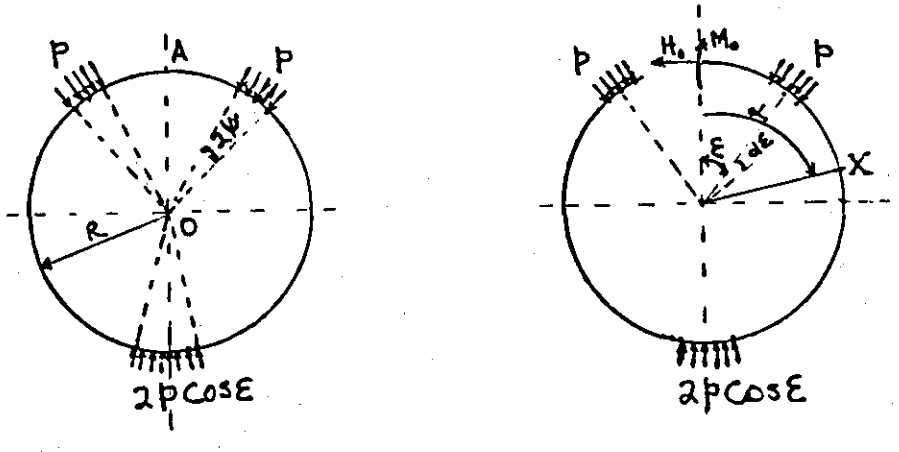

FIG.6.2.2 RING WITH DISTRIBUTED LOADS

h_i is the distance from the noutral axis inside fibre ($h_i = r_n - r_i$)

r_i is the radius of curvature of the inside fibre.

M is the bending moment with respect to the centroidal axis

A' is the area of the section $A' = h' \times b$

e is the distance from the centre of gravity axis to the neutral axis $e = R - r_n$

r_n is the radius of curvature of the neutral axis $r_n = \frac{h'}{\log_e r_o/r_i}$

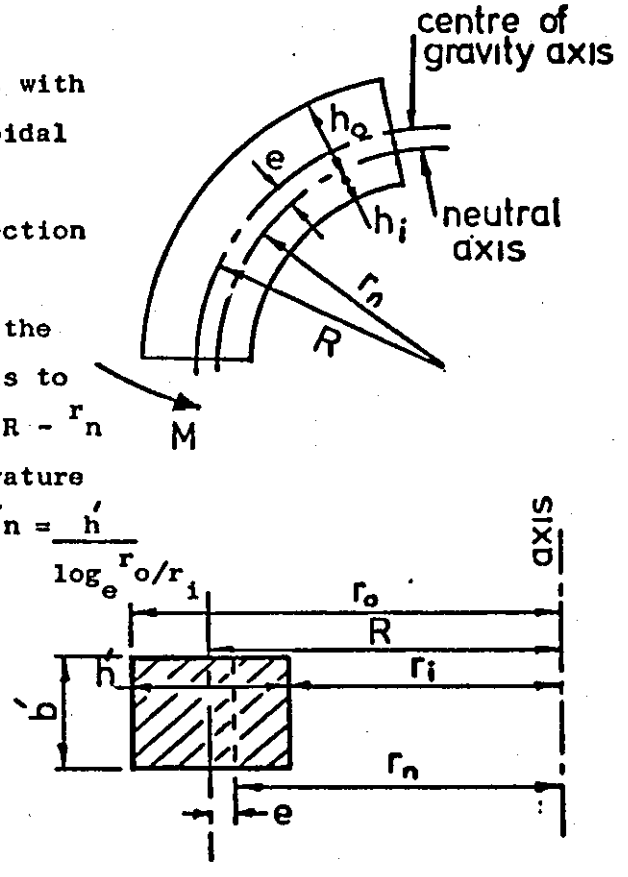

FIG.6.2.3 RING GEOMETRY

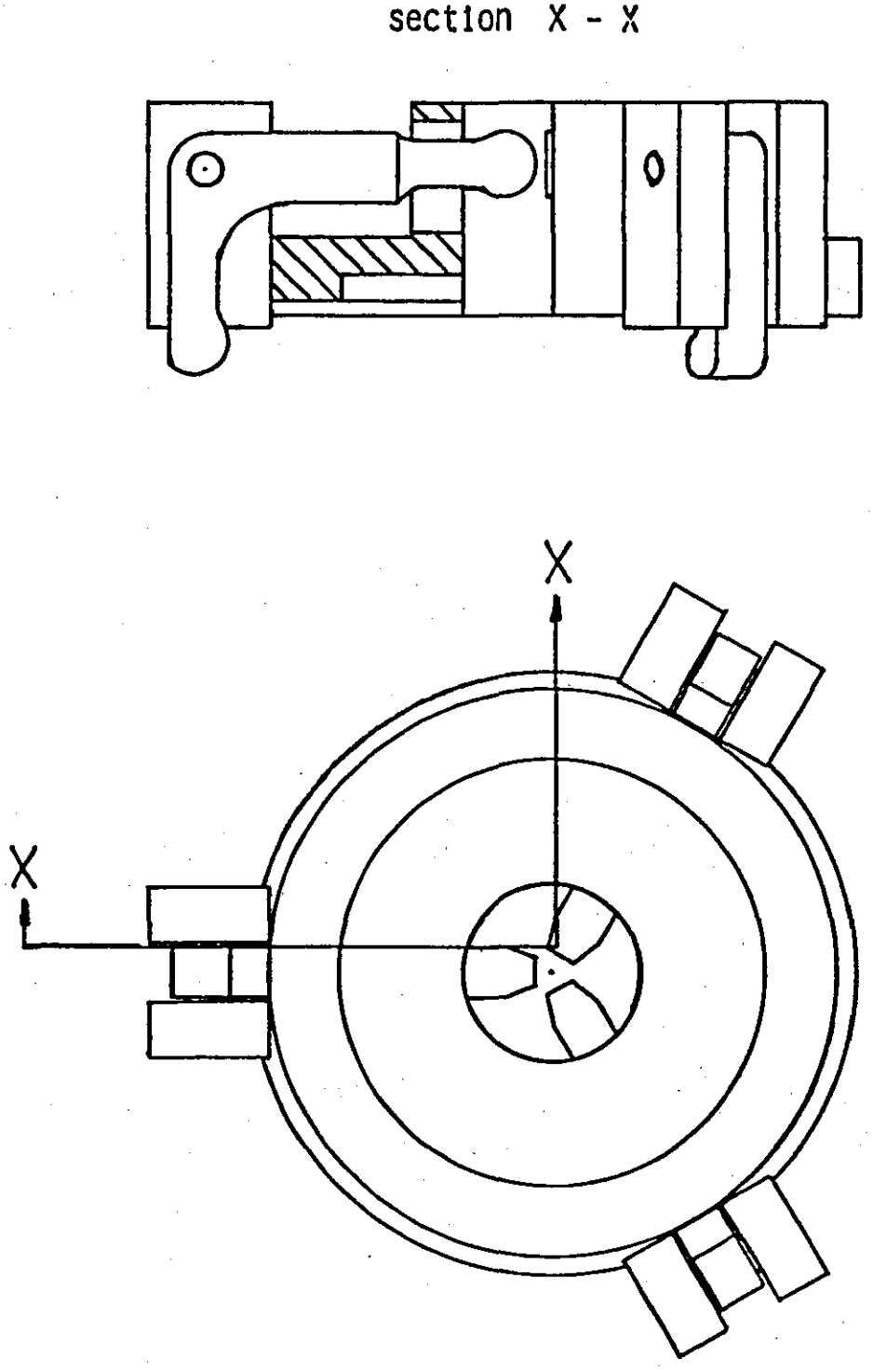

FIG.6.3.1 CALIBRATION FIXTURE FOR STRAIN RINGS

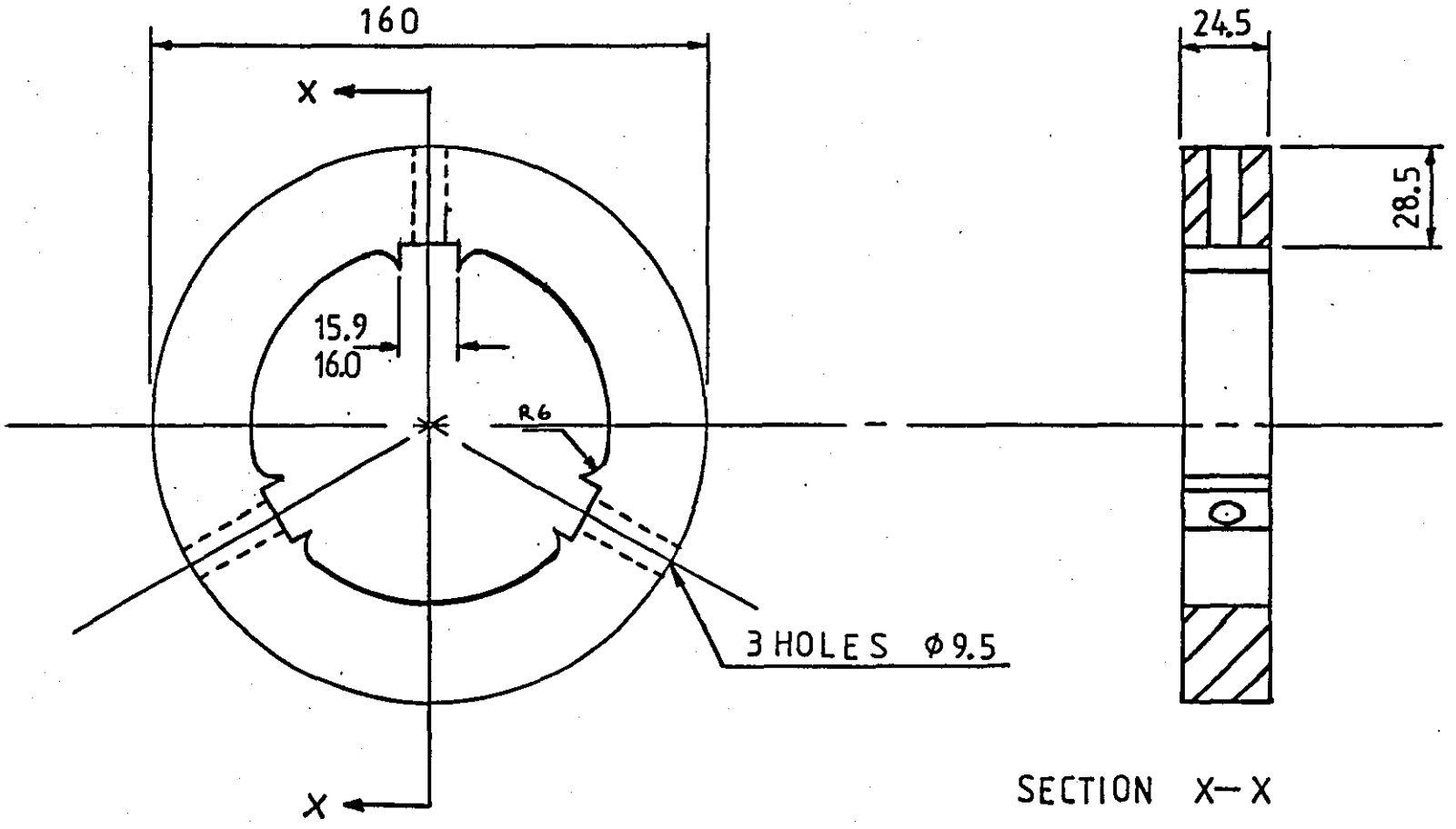

FIG.6.3.2 PLUNGER GUIDE

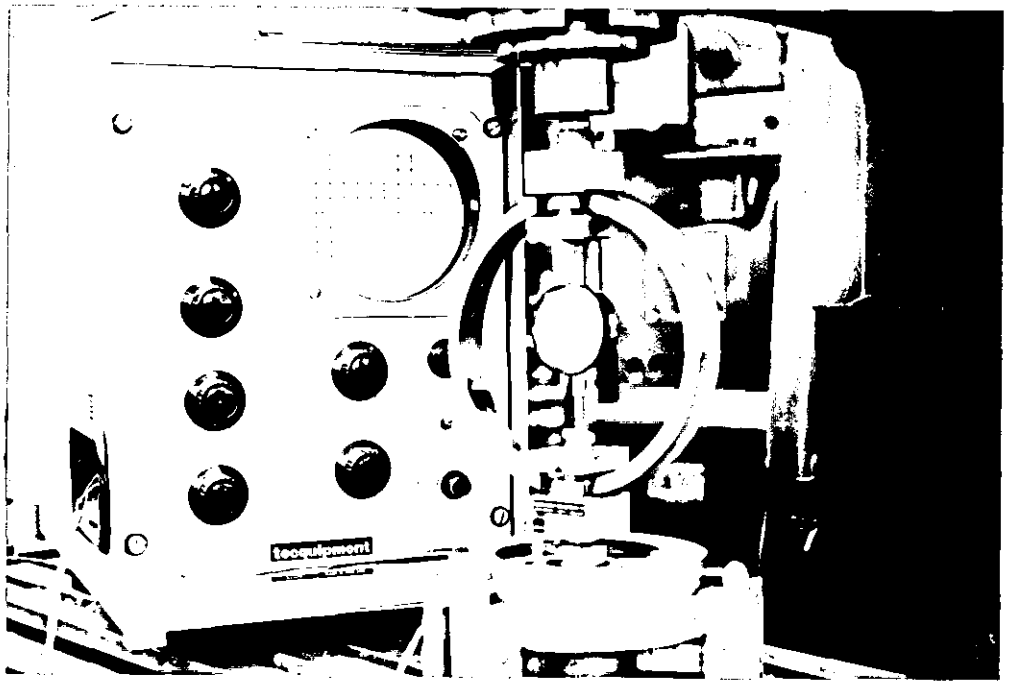

FIG.6.3.3 STRAIN SCOPE AND CALIBRATION FIXTURE

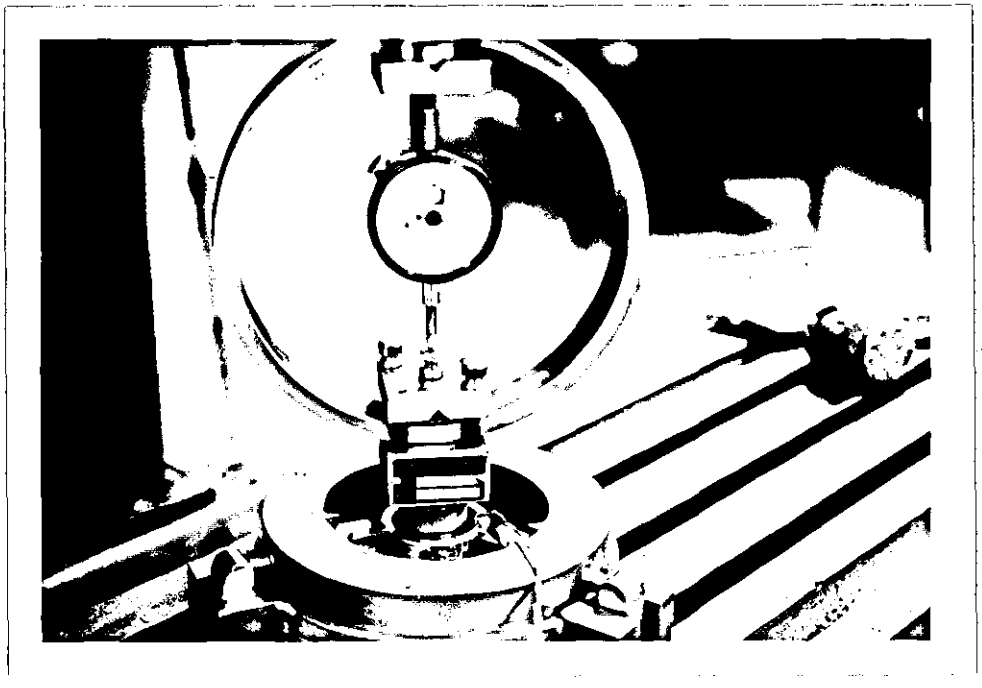

FIG.6.3.4 RING IN CALIBRATION FIXTURE

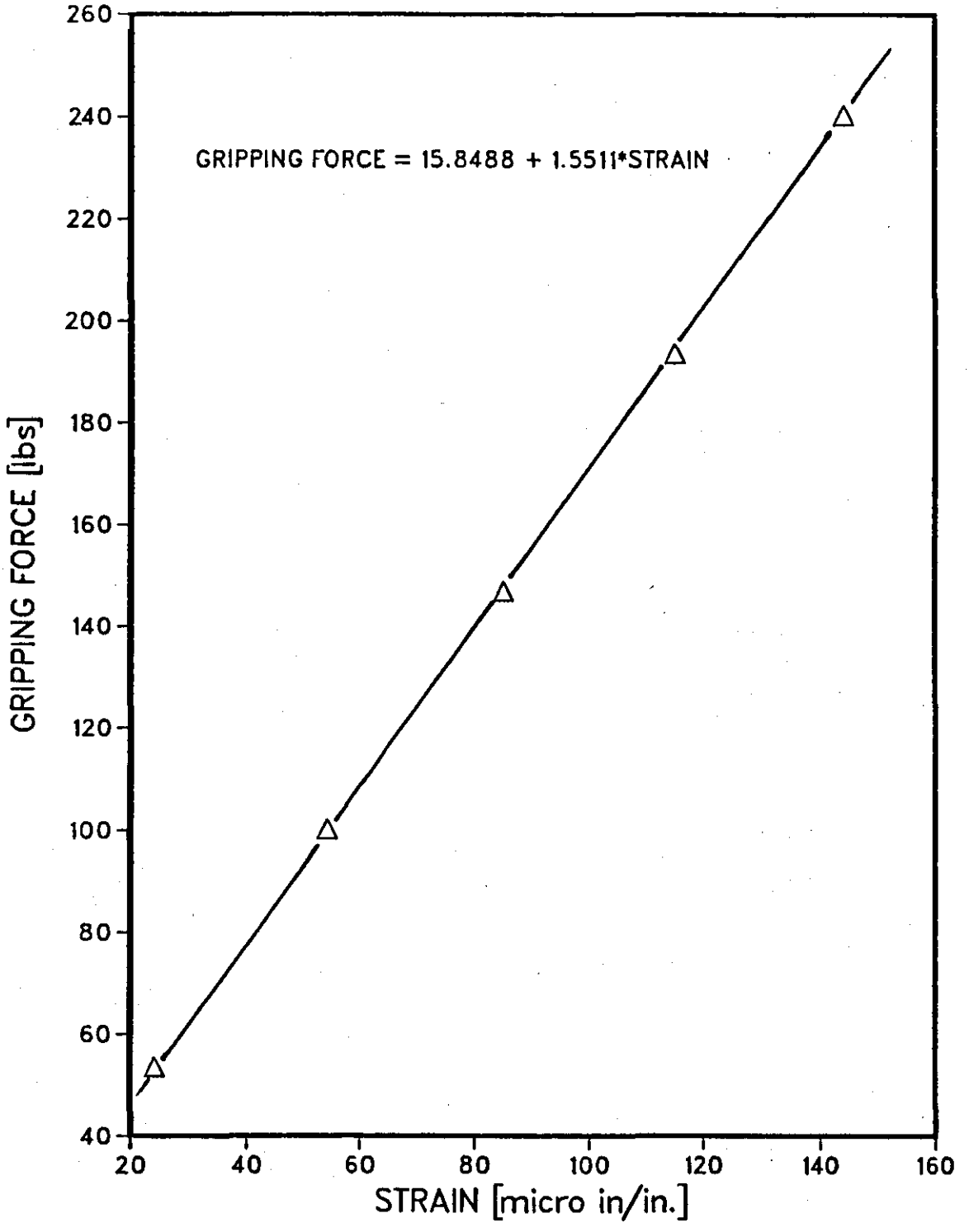

FIG.6.3.5 CALIBRATION CHART FOR 50 MM RING [10 MM WIDE]

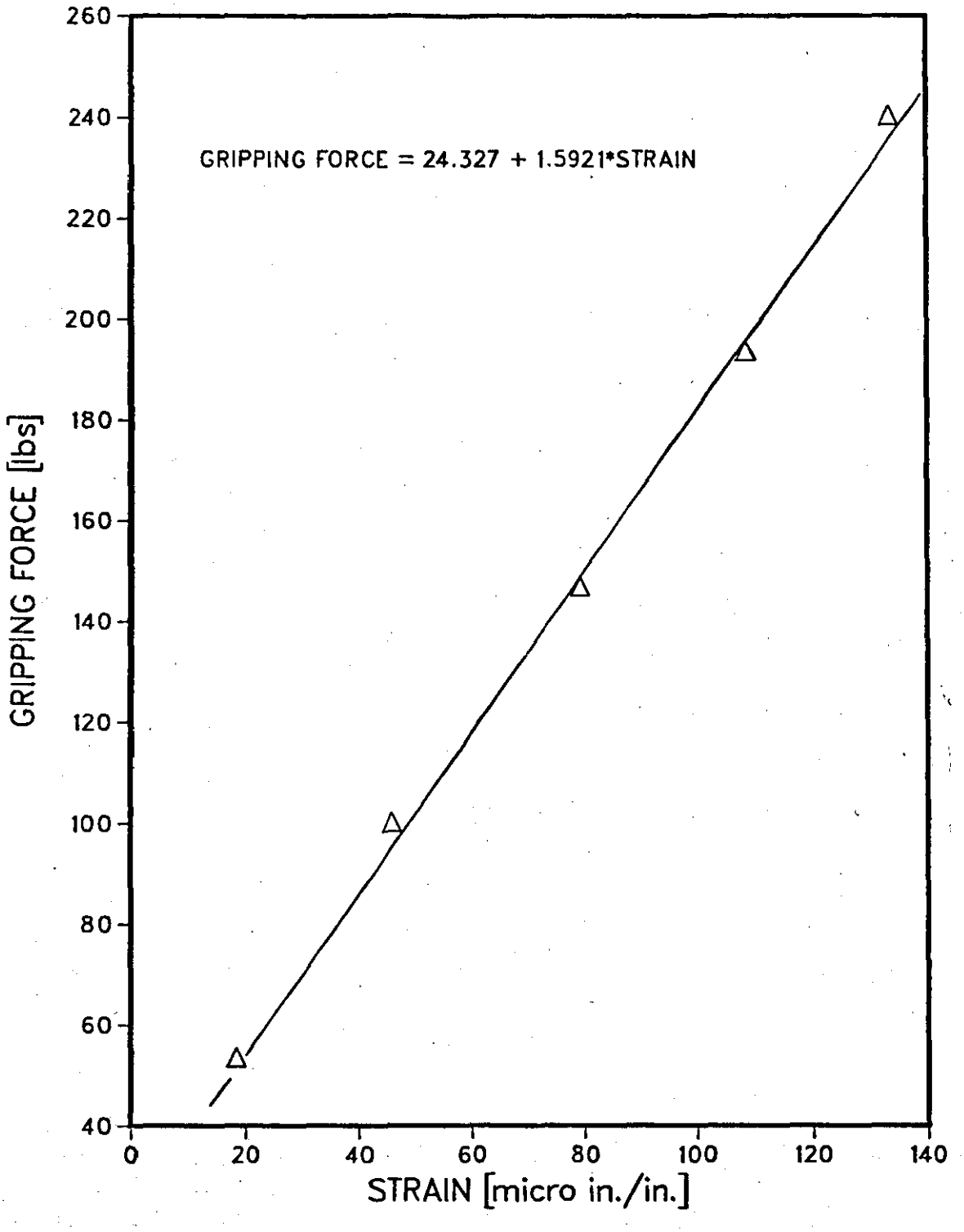

FIG.6.3.6 CALIBRATION CHART FOR 55 MM RING [10 MM WIDE]

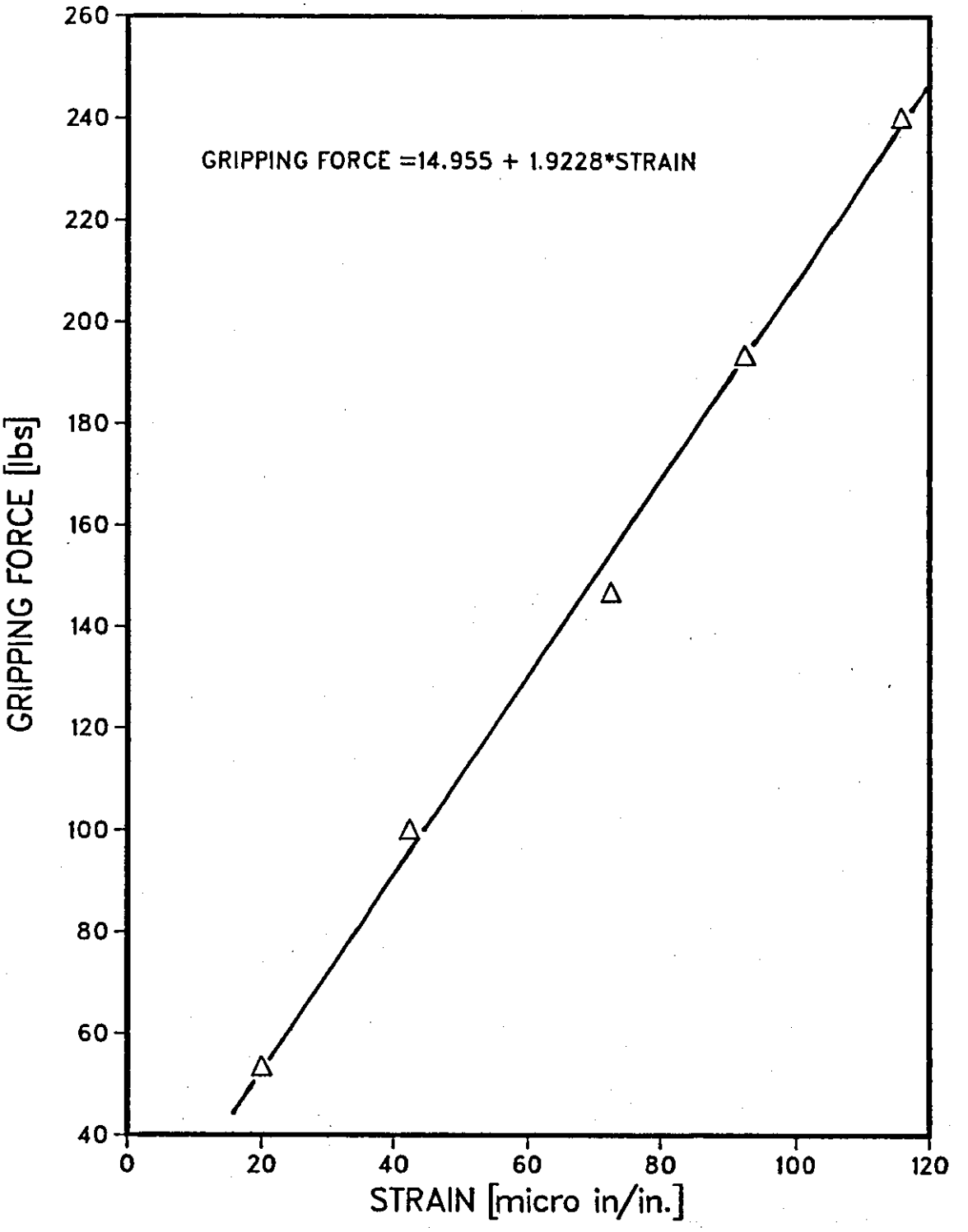

FIG.6.3.7 CALIBRATION CHART FOR 60 MM RING [10 MM WIDE]

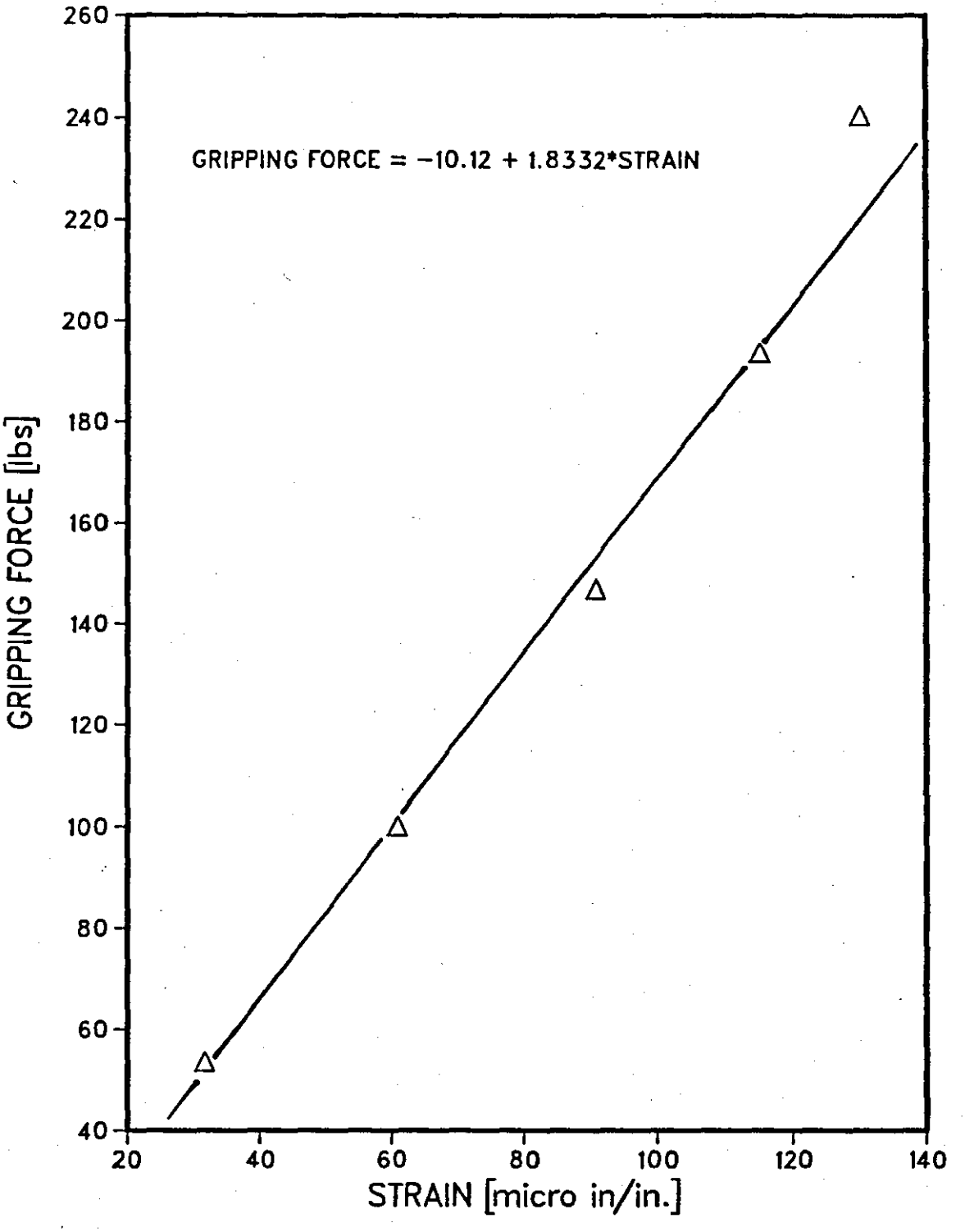

FIG. 6.3.8 CALIBRATION CHART FOR 65 MM RING [10 MM WIDE]

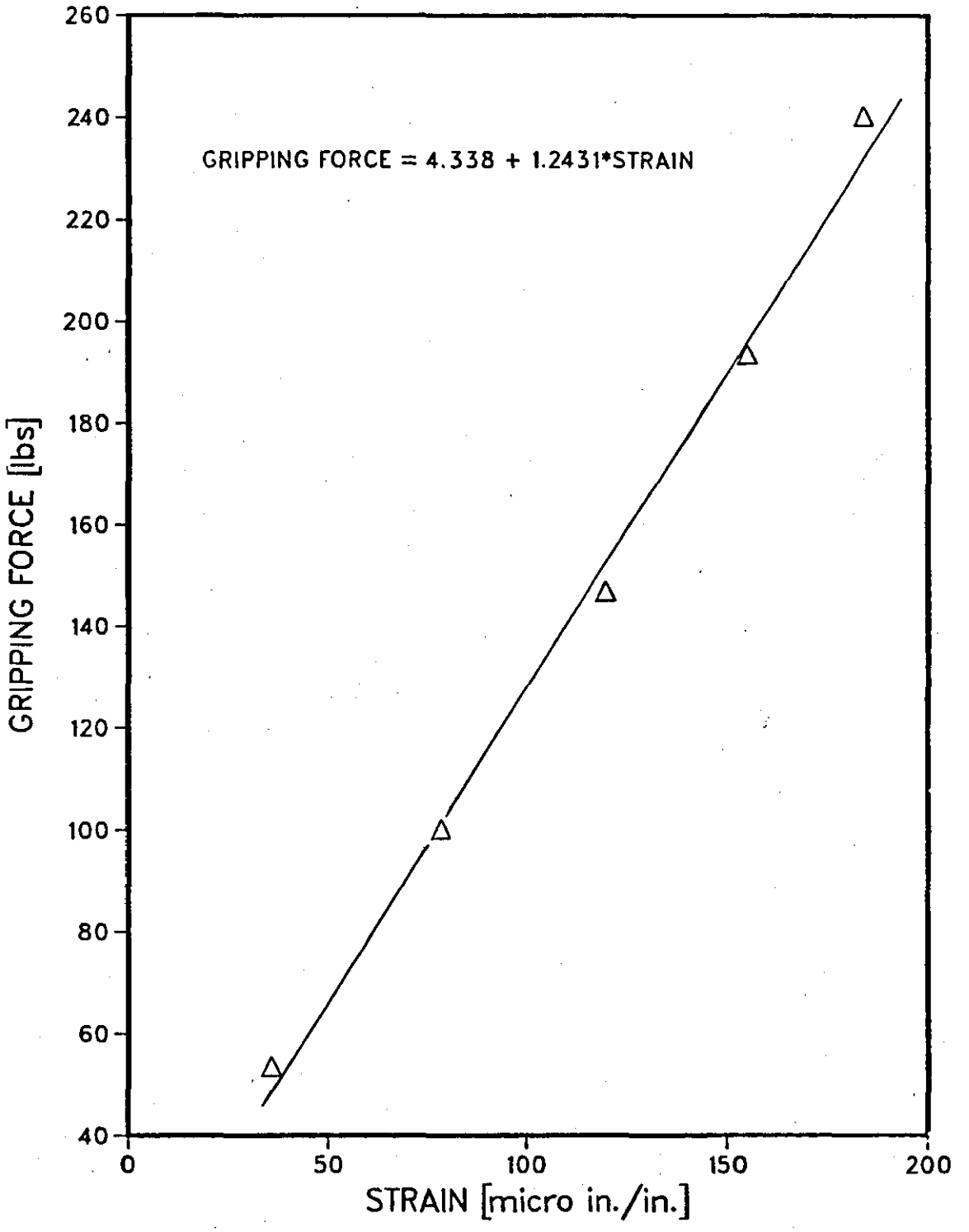

FIG.6.3.9 CALIBRATION CHART FOR 70 MM RING [10 MM WIDE]

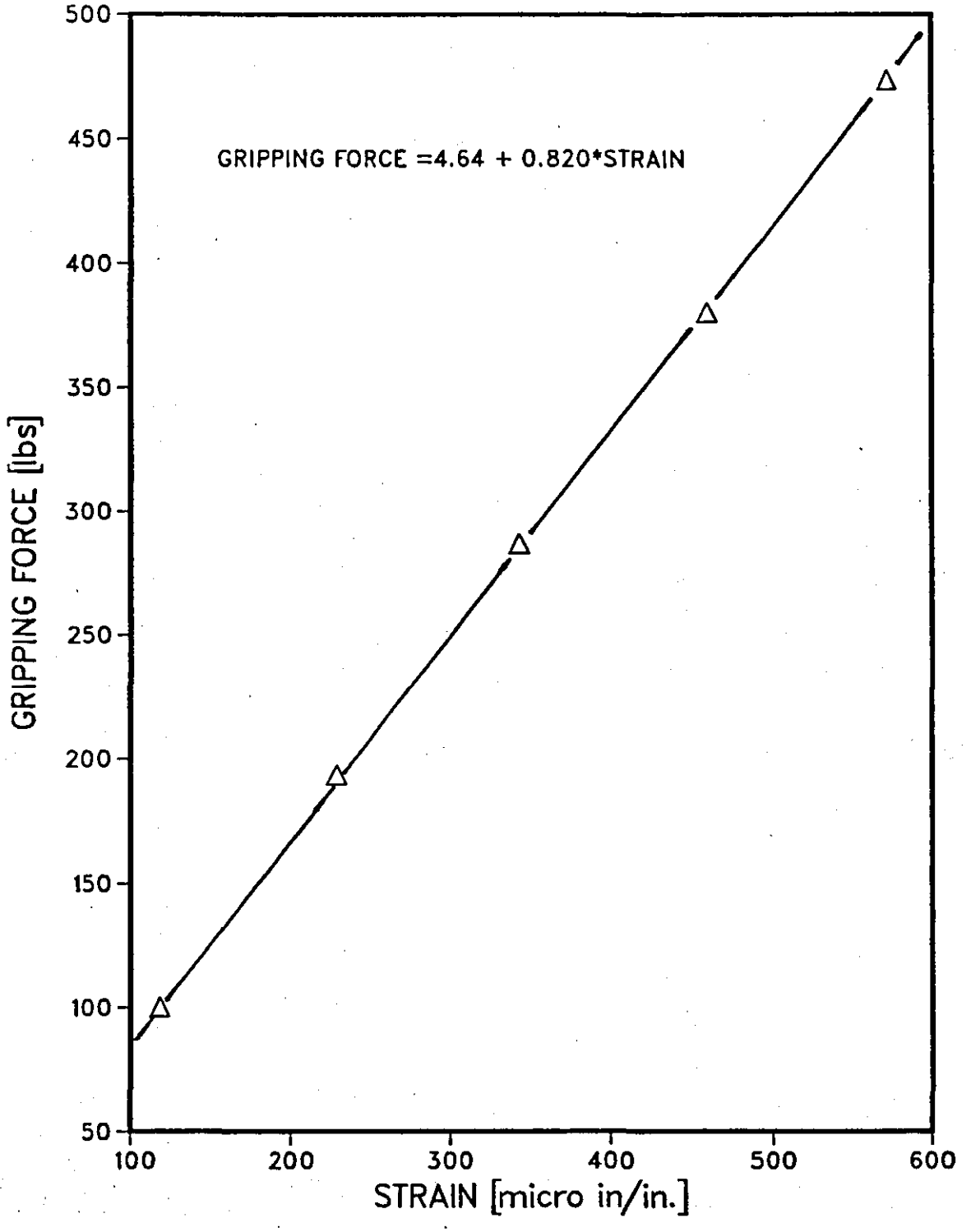

FIG.6.3.10 CALIBRATION CHART FOR 50 MM RING [5 MM WIDE]

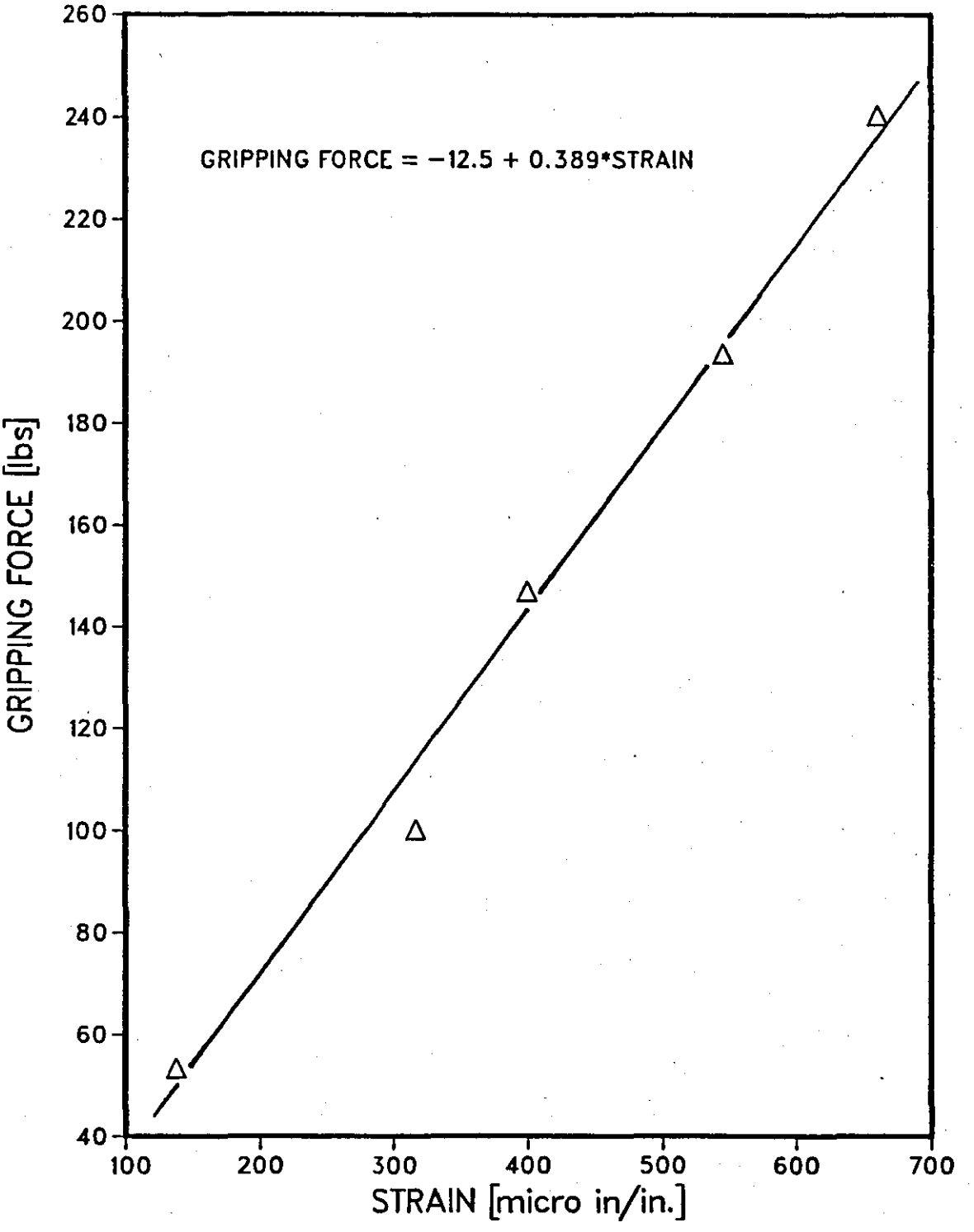

FIG.6.3.11 CALIBRATION CHART FOR 60 MM RING [5 MM WIDE]

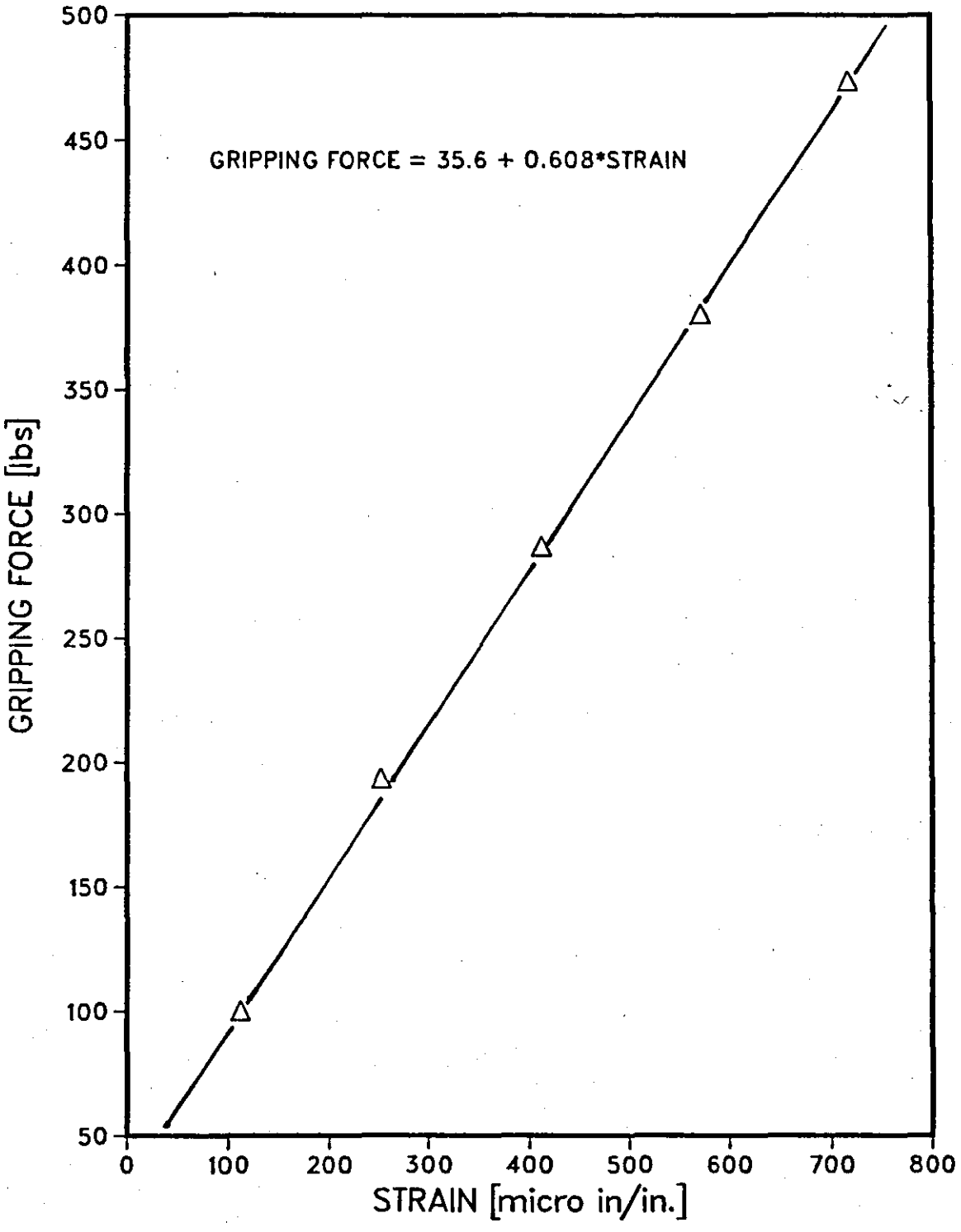

FIG.6.3.12 CALIBRATION CHART FOR 90 MM RING [5 MM WIDE]

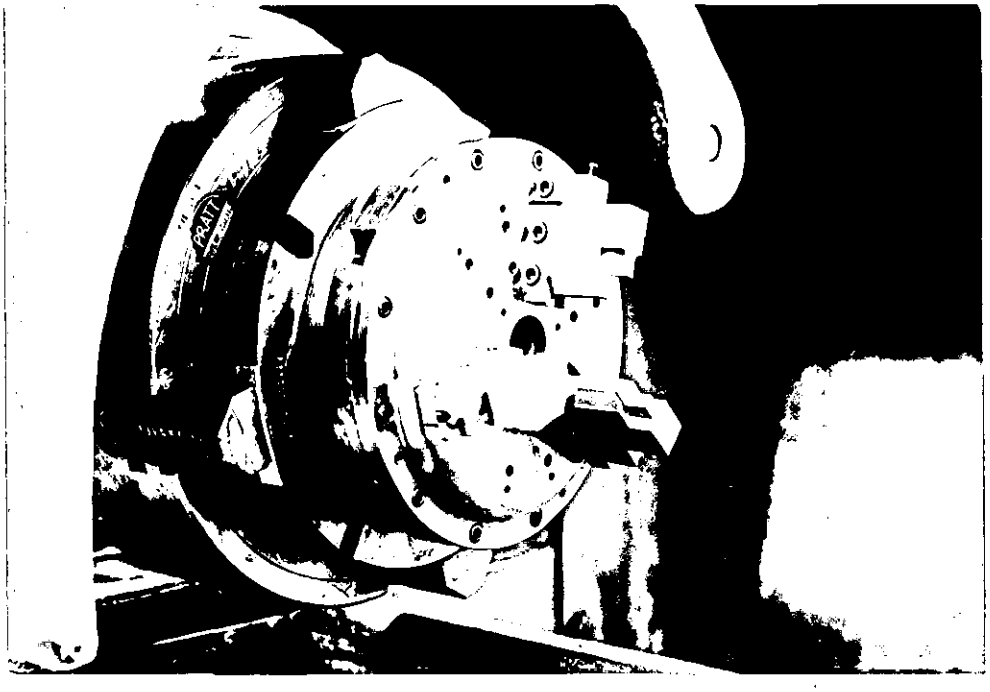

FIG. 6.4.1 PLATE A WITH THREE JAWS

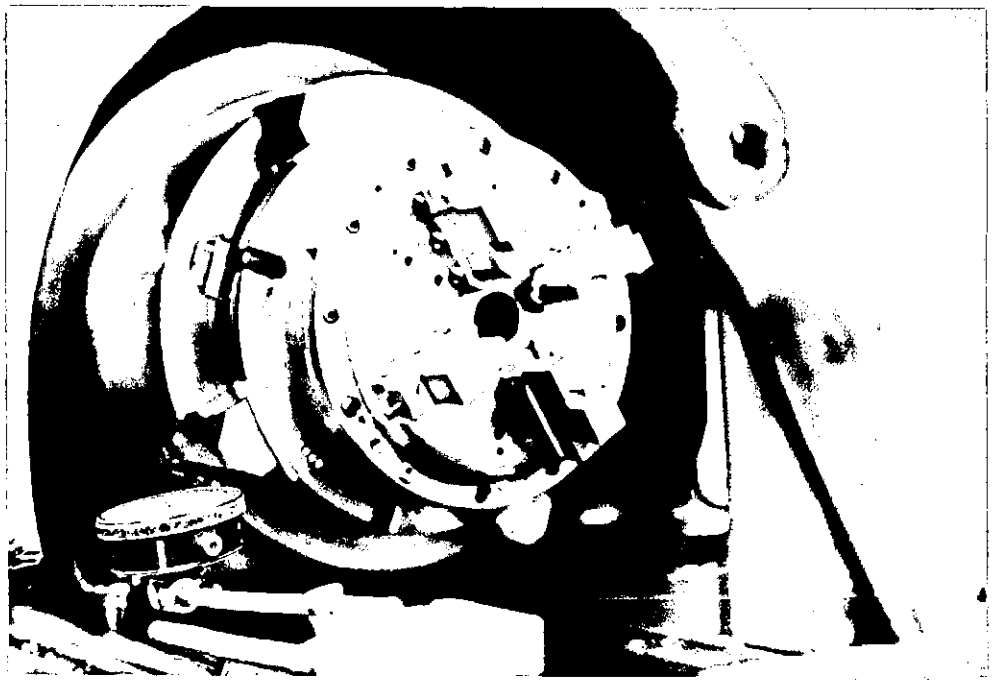

FIG.6.4.2 PLATE A WITH FOUR JAWS

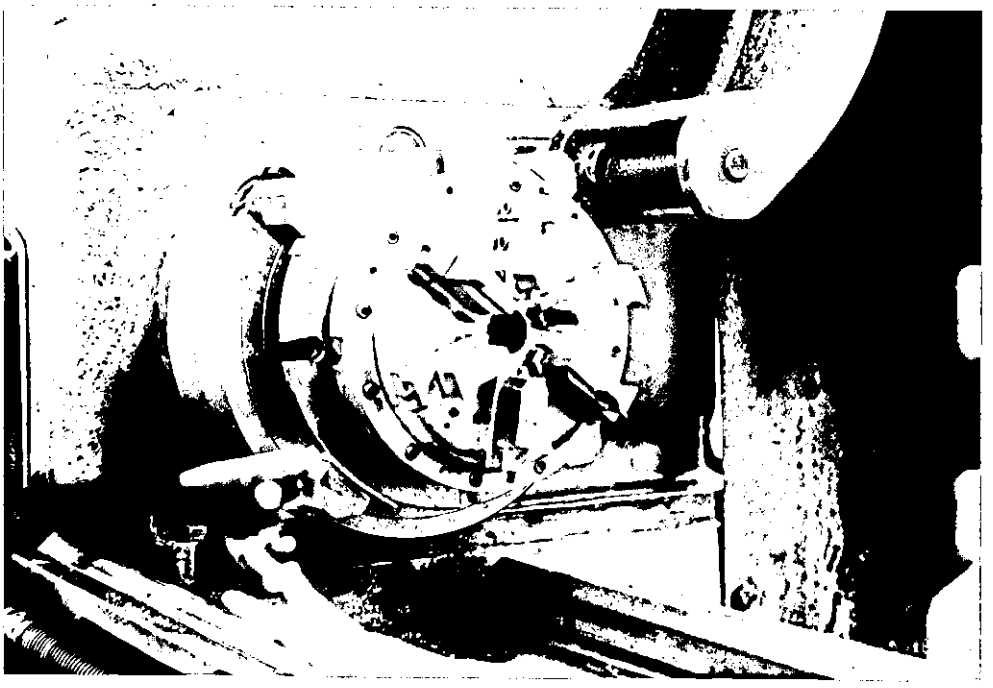

FIG.6.4.3 PLATE A WITH SIX JAWS

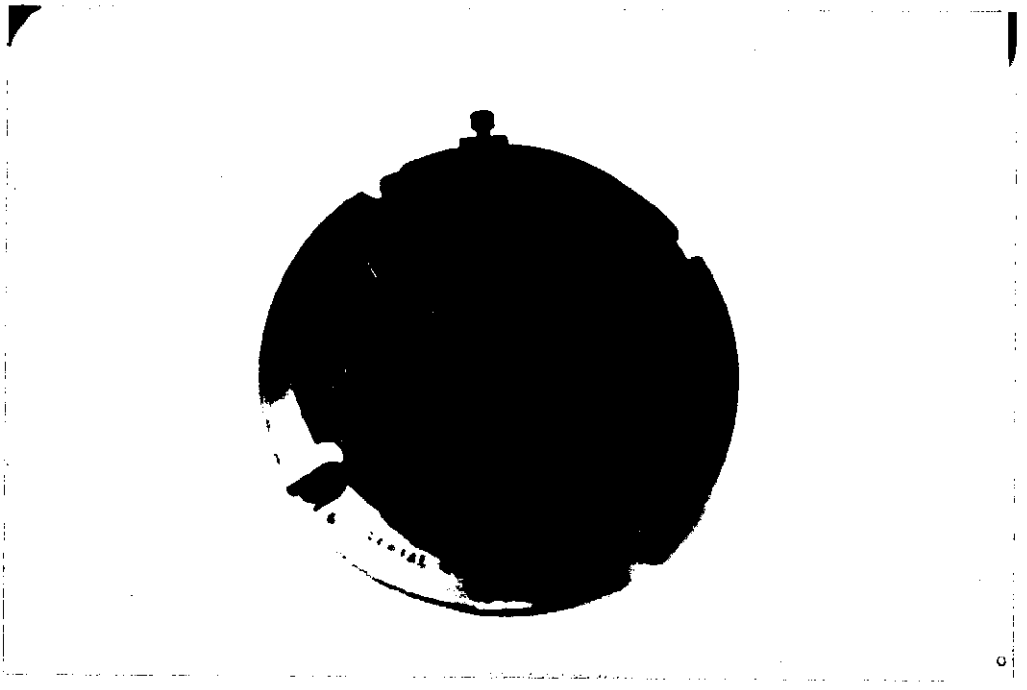

FIG.6.4.4 PLATE C WITH THREE JAWS

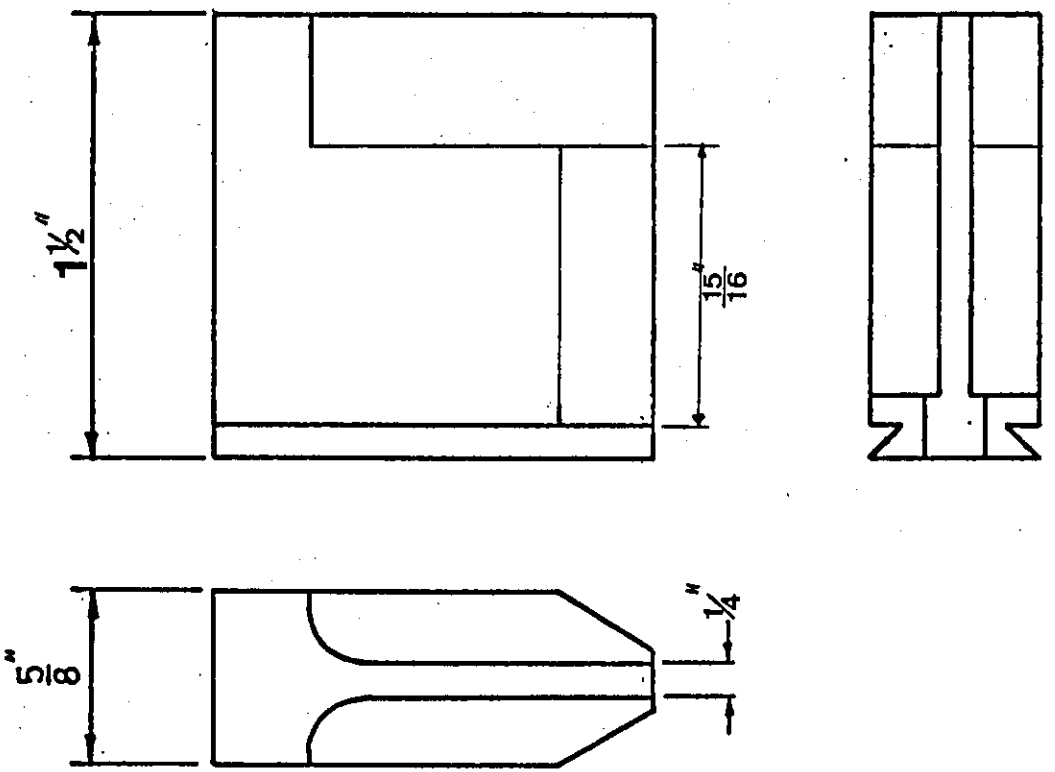

FIG. 6.4.5 THE MODIFIED JAWS

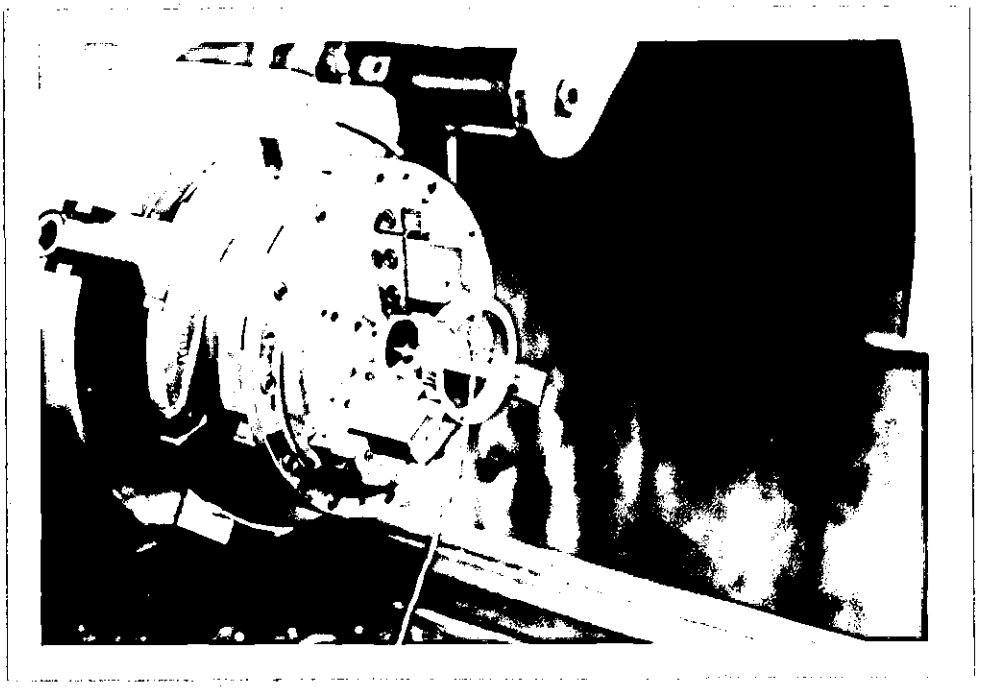

FIG. 6.4.6 PLATE A WITH THREE JAWS GRIPPING RING TRANSDUCER

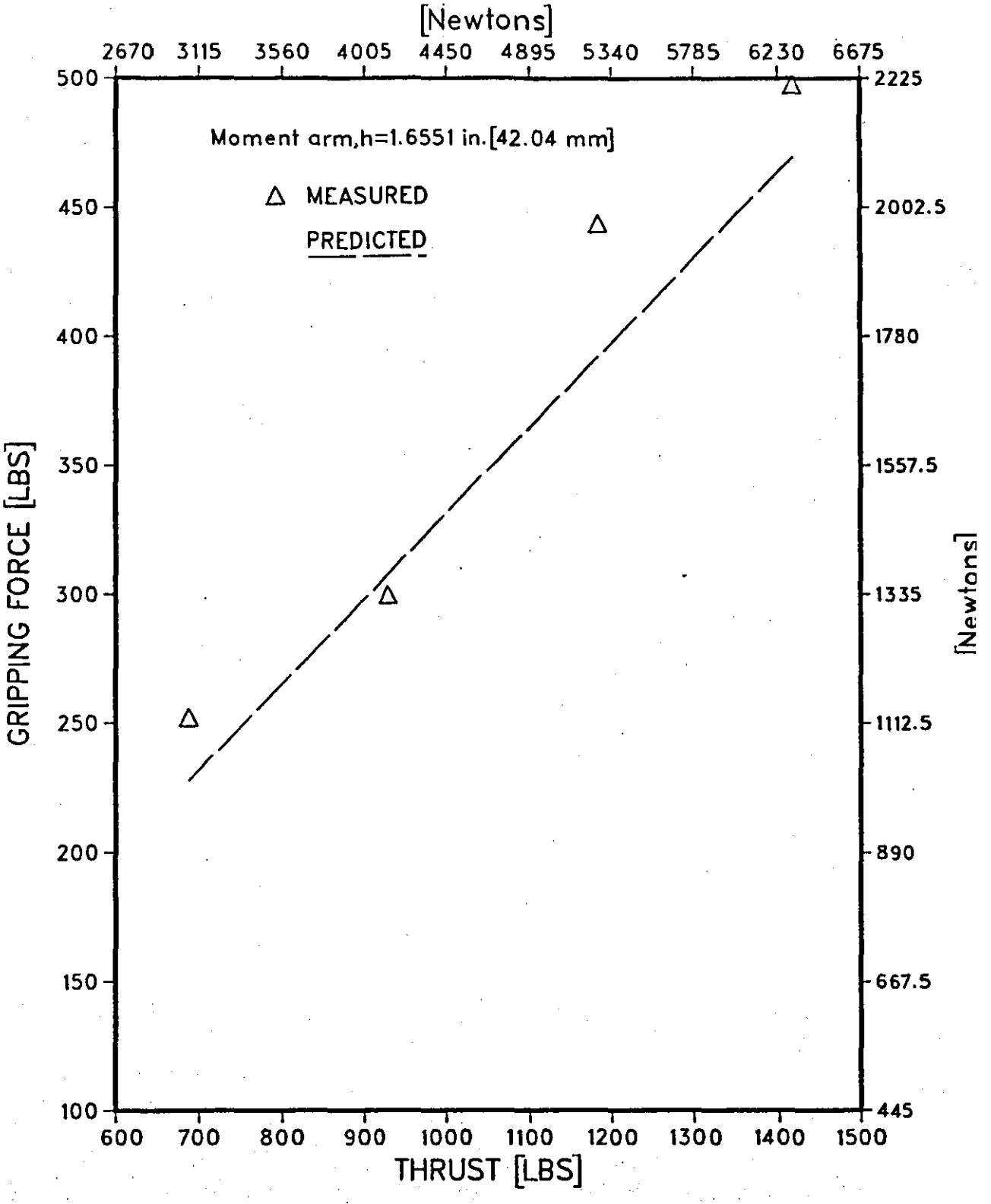

FIG.6.5.1 GRIPPING FORCE FOR 50 MM RING PLATE A,THREE JAWS

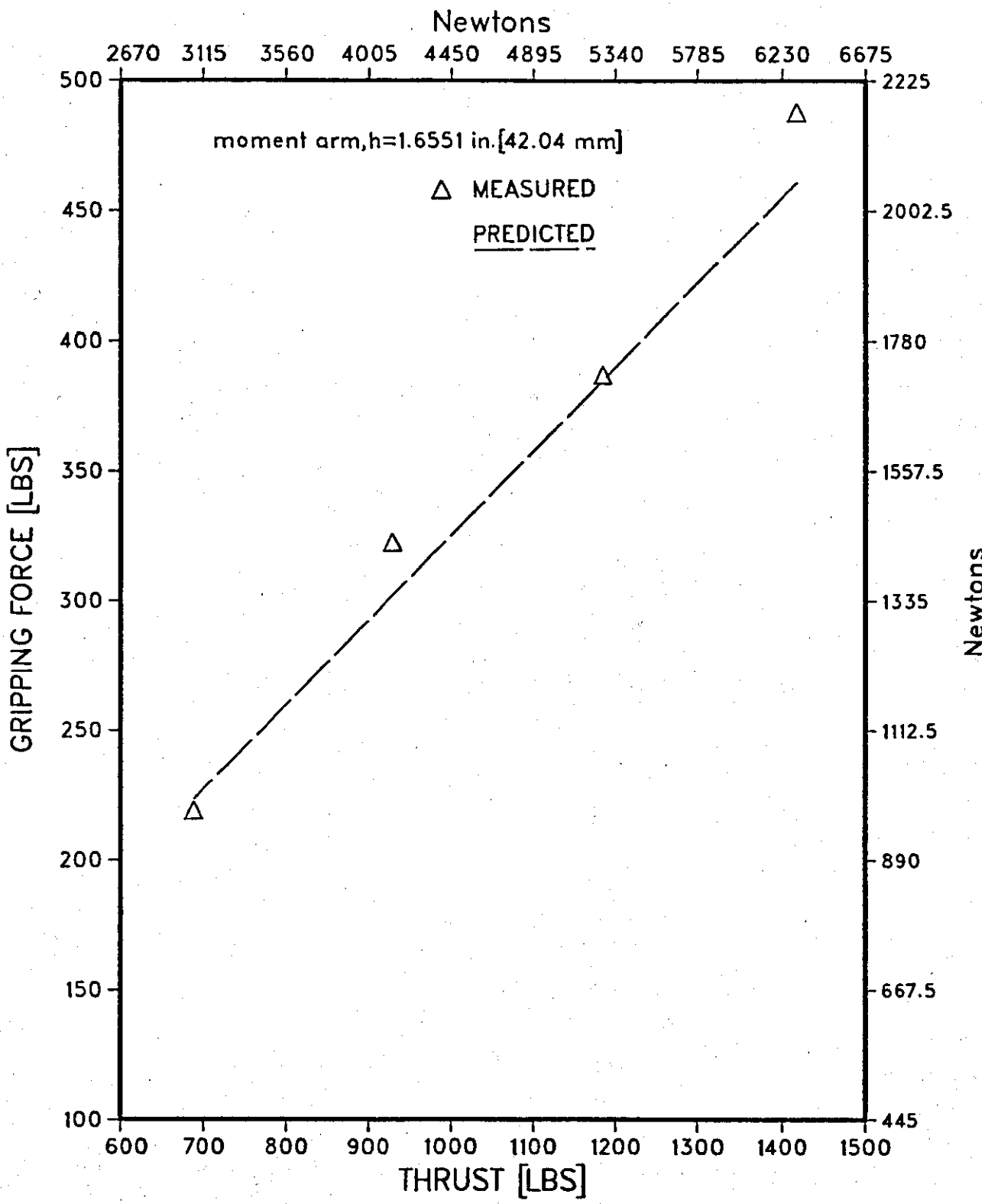

FIG.6.5.2 GRIPPING FORCE FOR 55 MM RING PLATE A,THREE JAWS

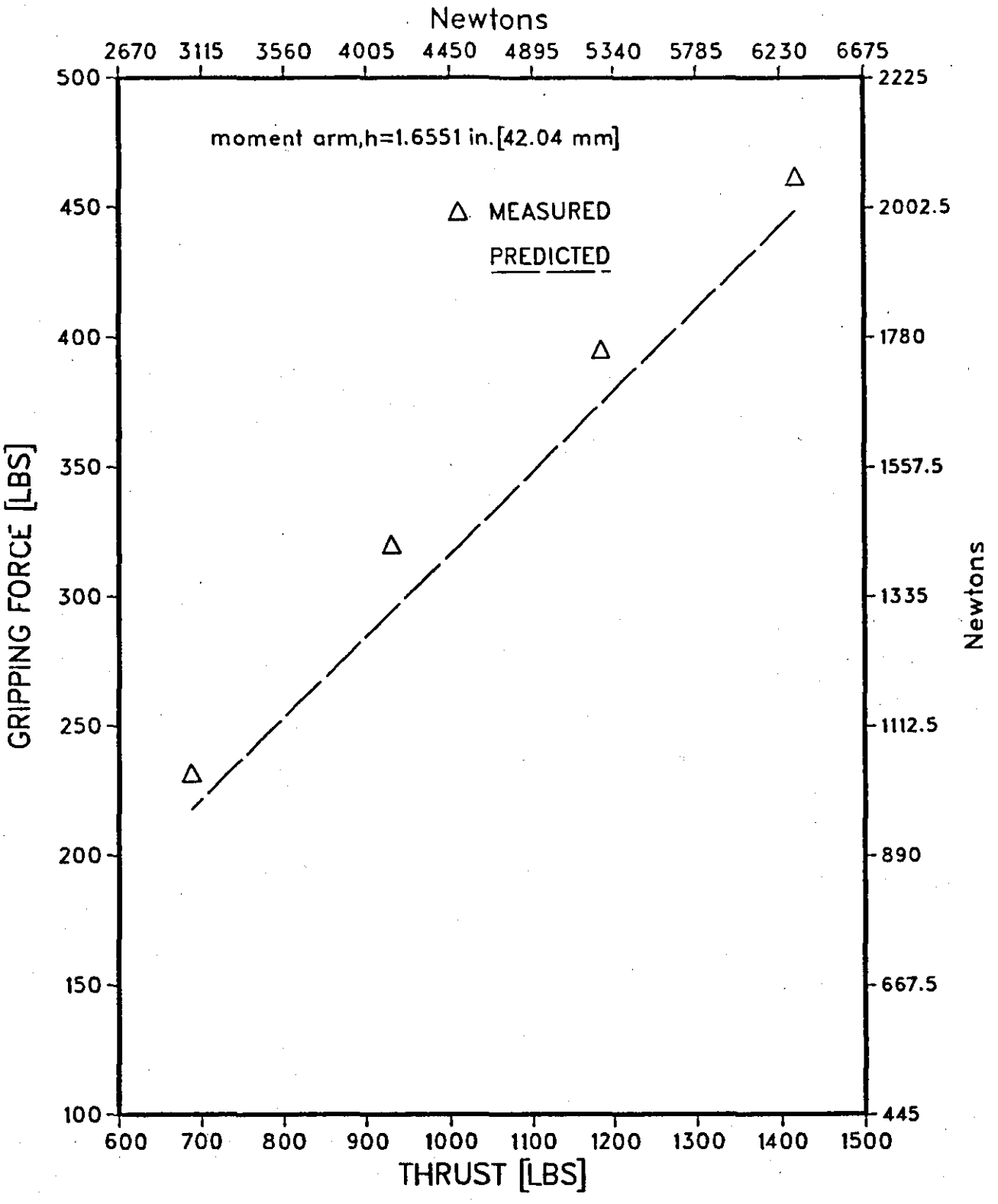

FIG.6.5.3 GRIPPING FORCE FOR 60 MM RING PLATE A,THREE JAWS

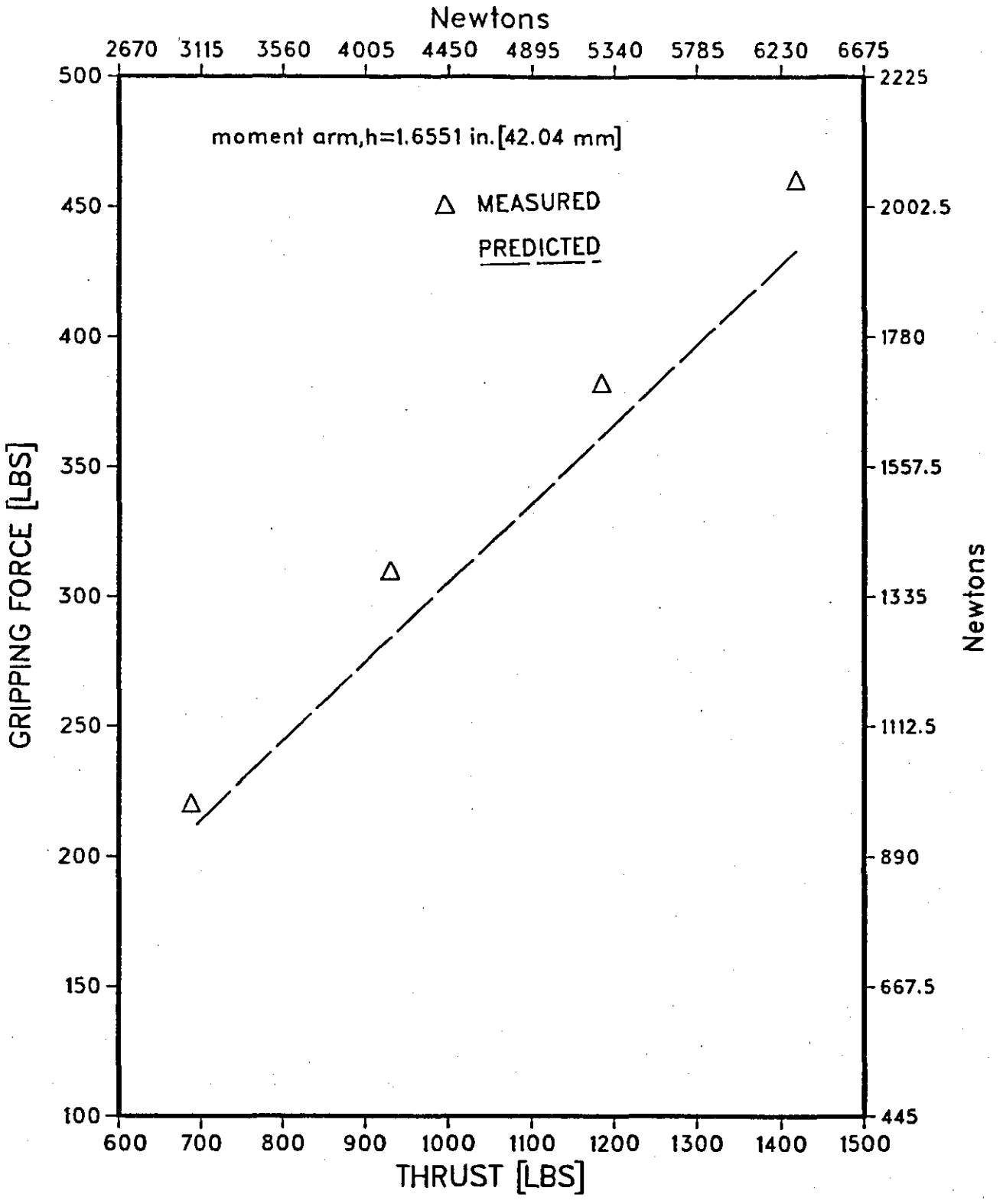

FIG.6.5.4 GRIPPING FORCE FOR 65 MM RING PLATE A,THREE JAWS

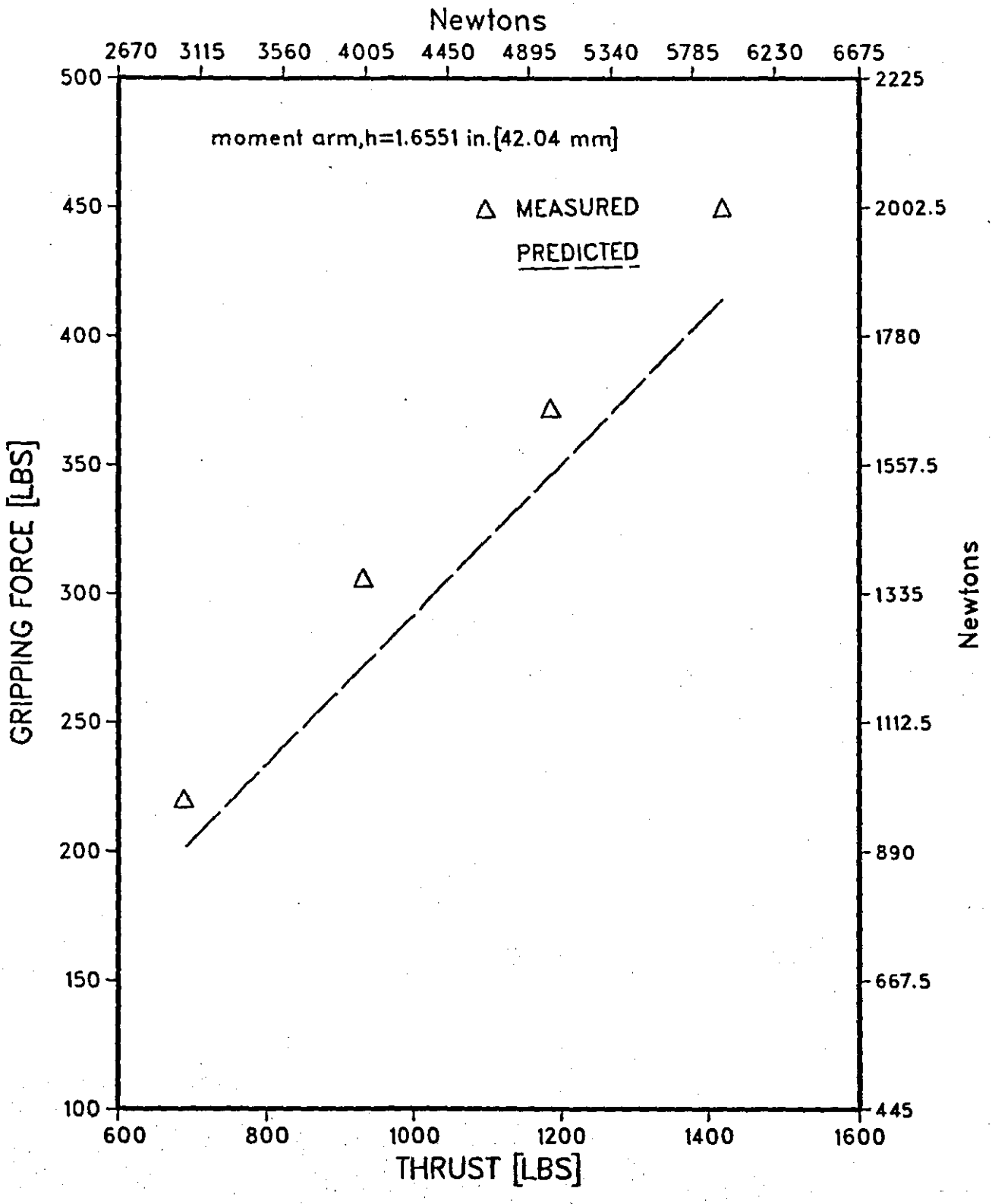

FIG.6.5.5 GRIPPING FORCE FOR 70 MM RING PLATE A,THREE JAWS

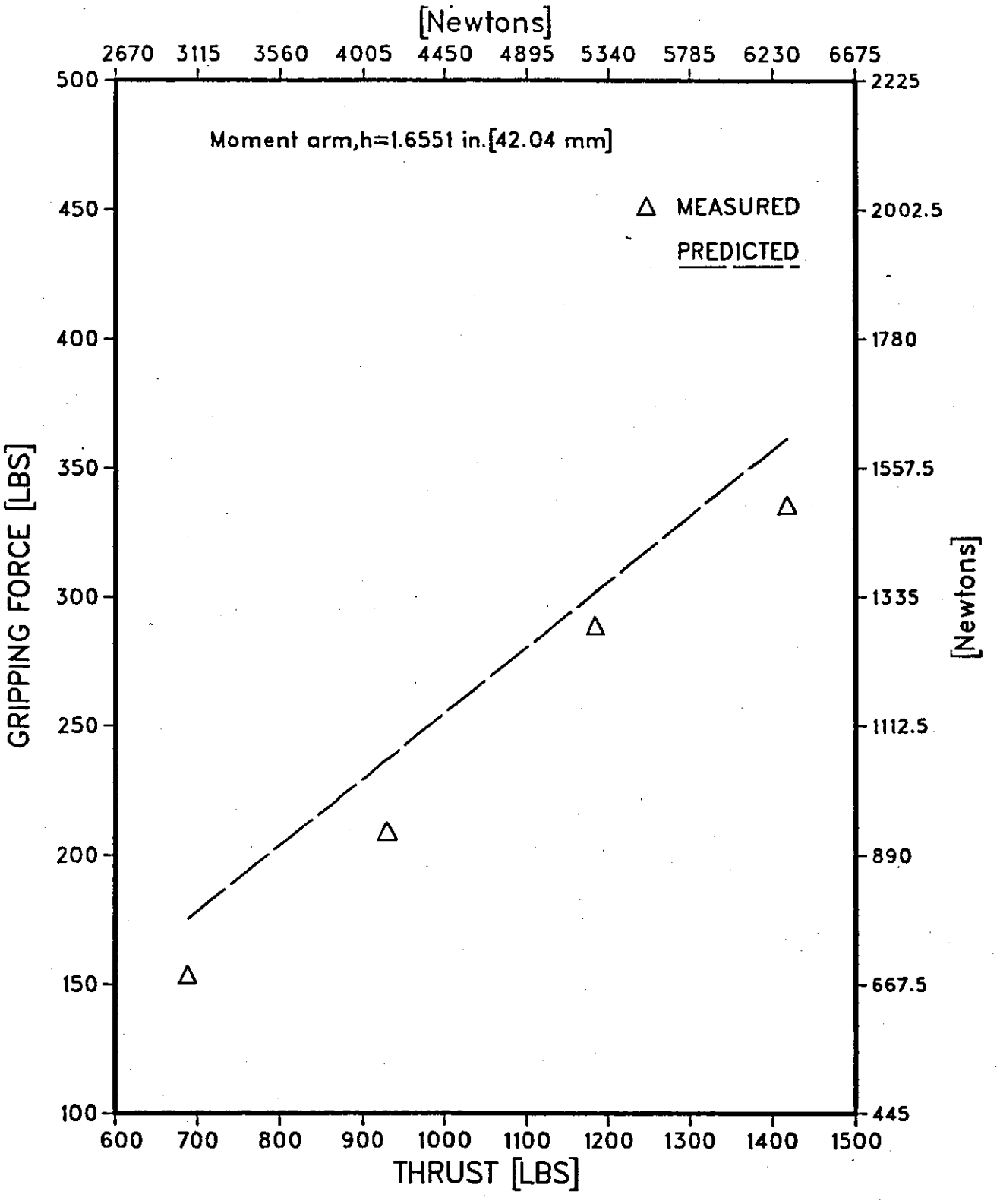

FIG.6.5.6 GRIPPING FORCE FOR 50 MM RING PLATE A,FOUR JAWS

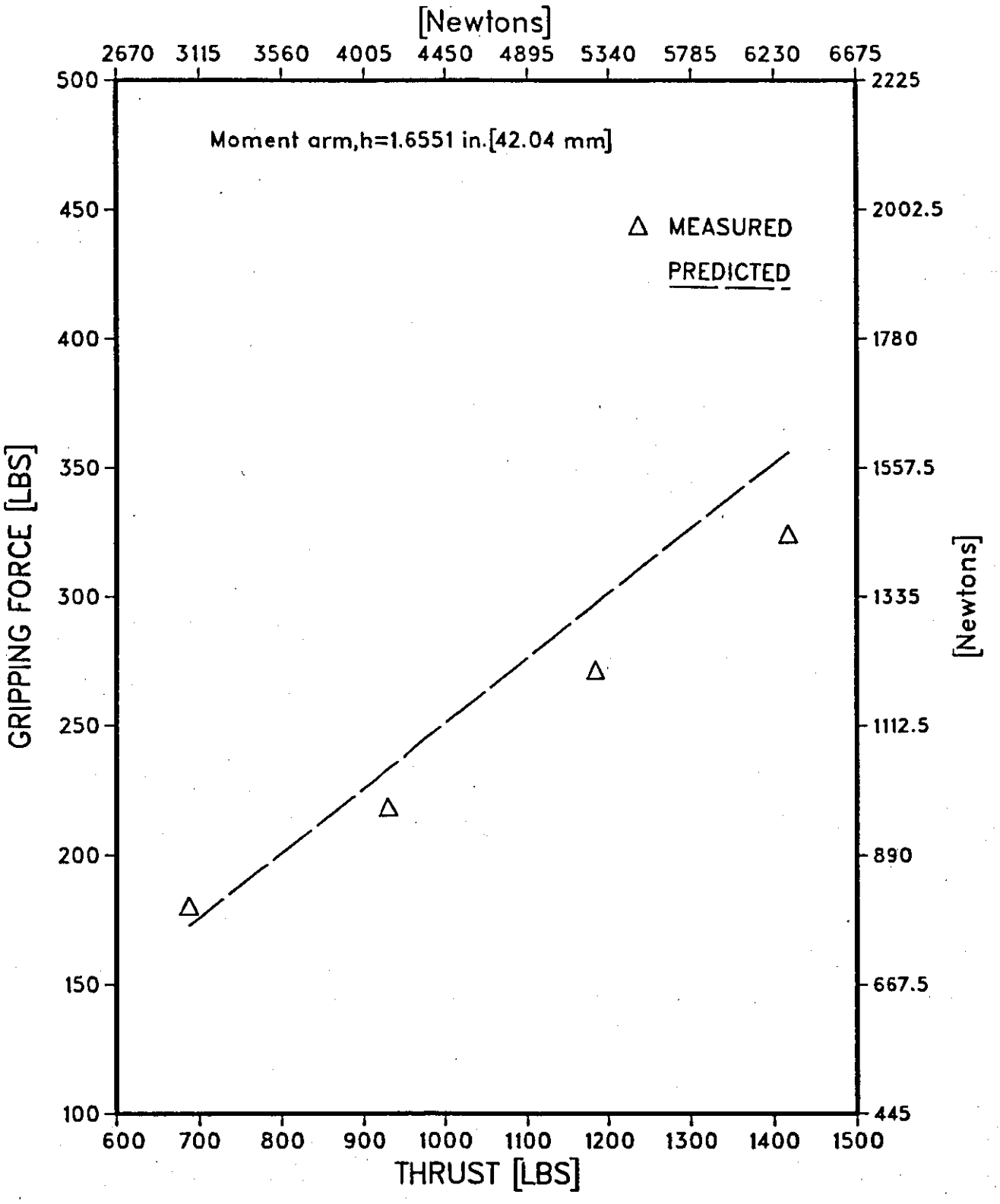

FIG.6.5.7 GRIPPING FORCE FOR 55 MM RING PLATE A,FOUR JAWS

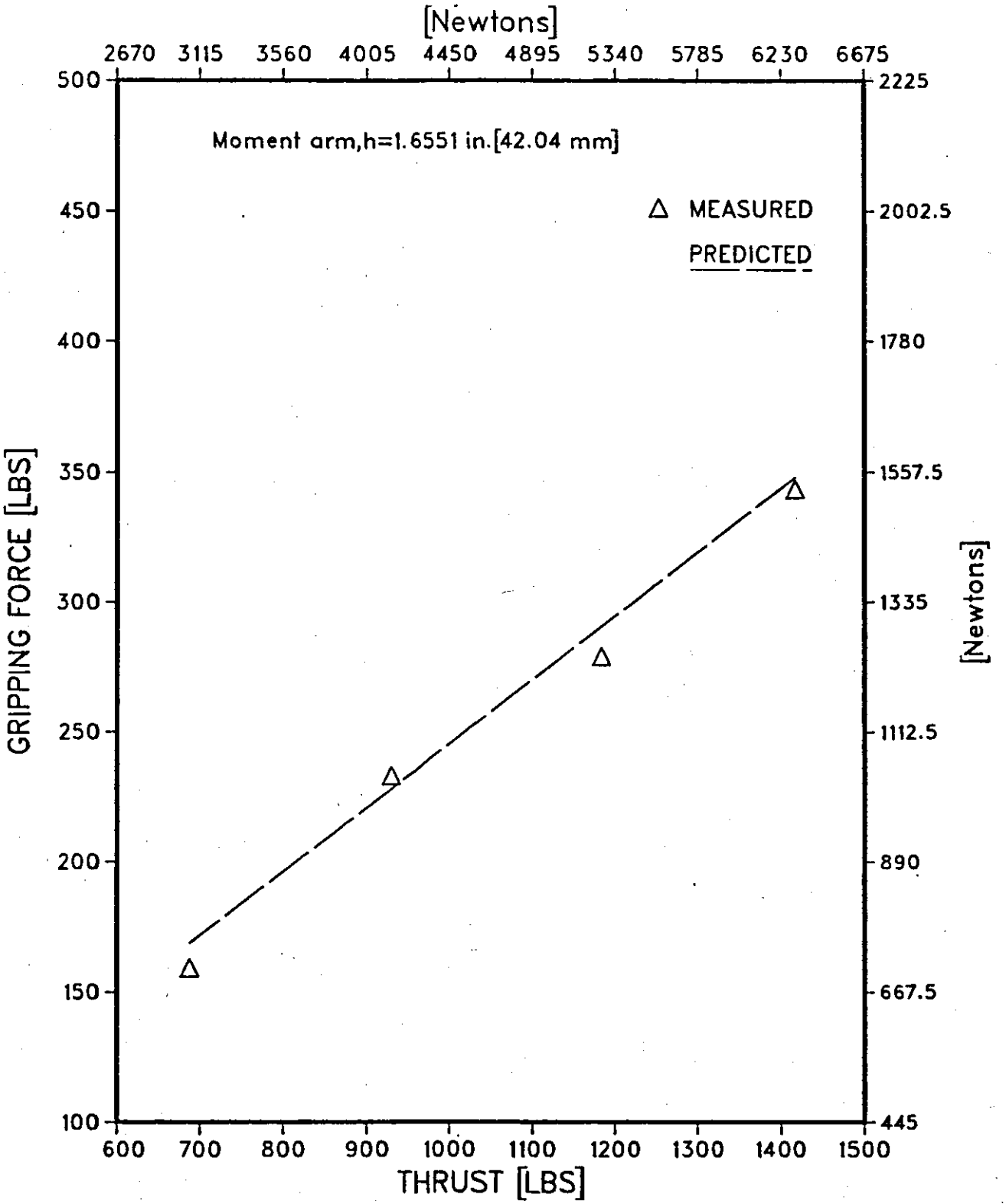

FIG.6.5.8 GRIPPING FORCE FOR 60 MM RING PLATE A,FOUR JAWS

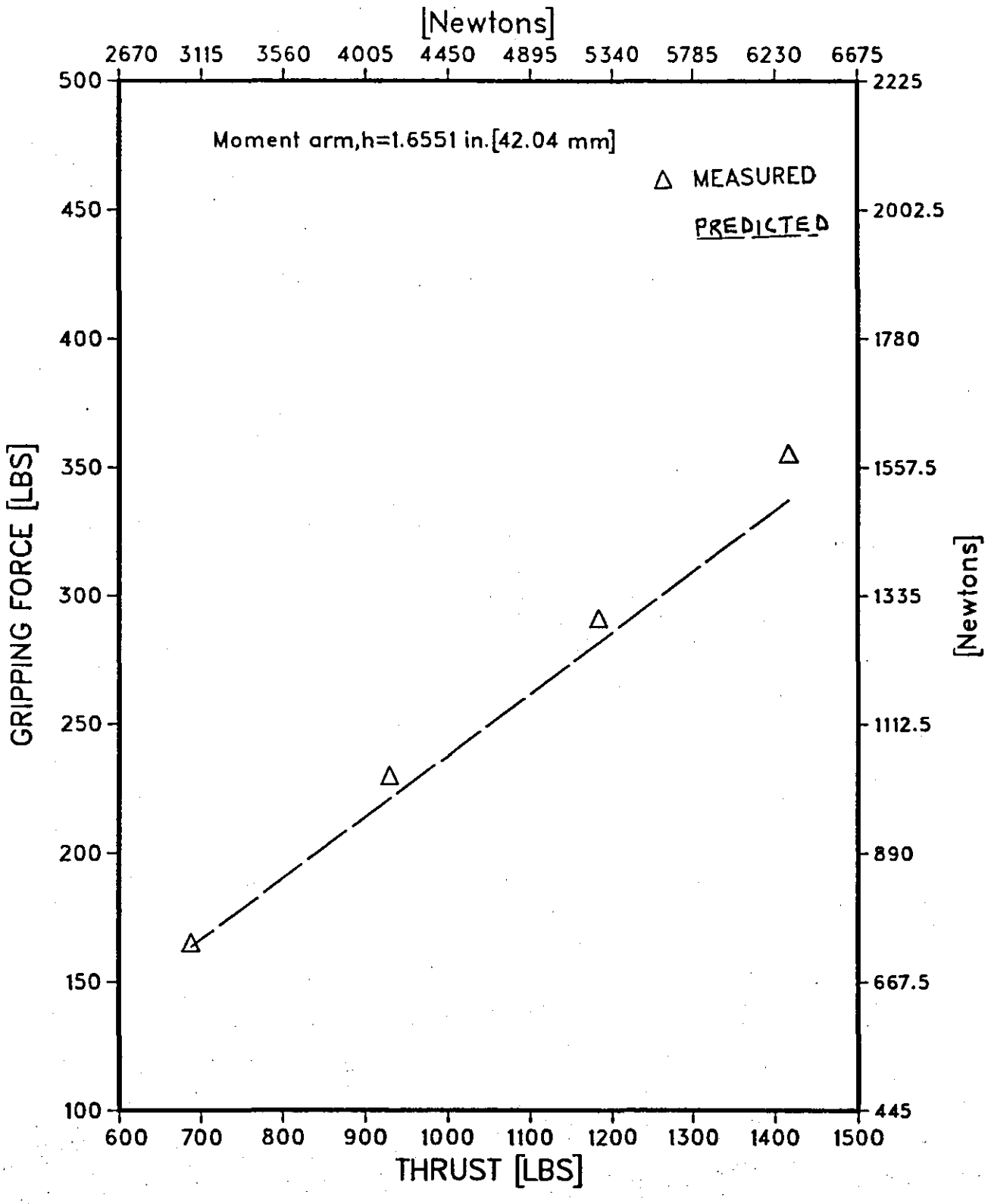

FIG.6.5.9 GRIPPING FORCE FOR 65 MM RING PLATE A,FOUR JAWS

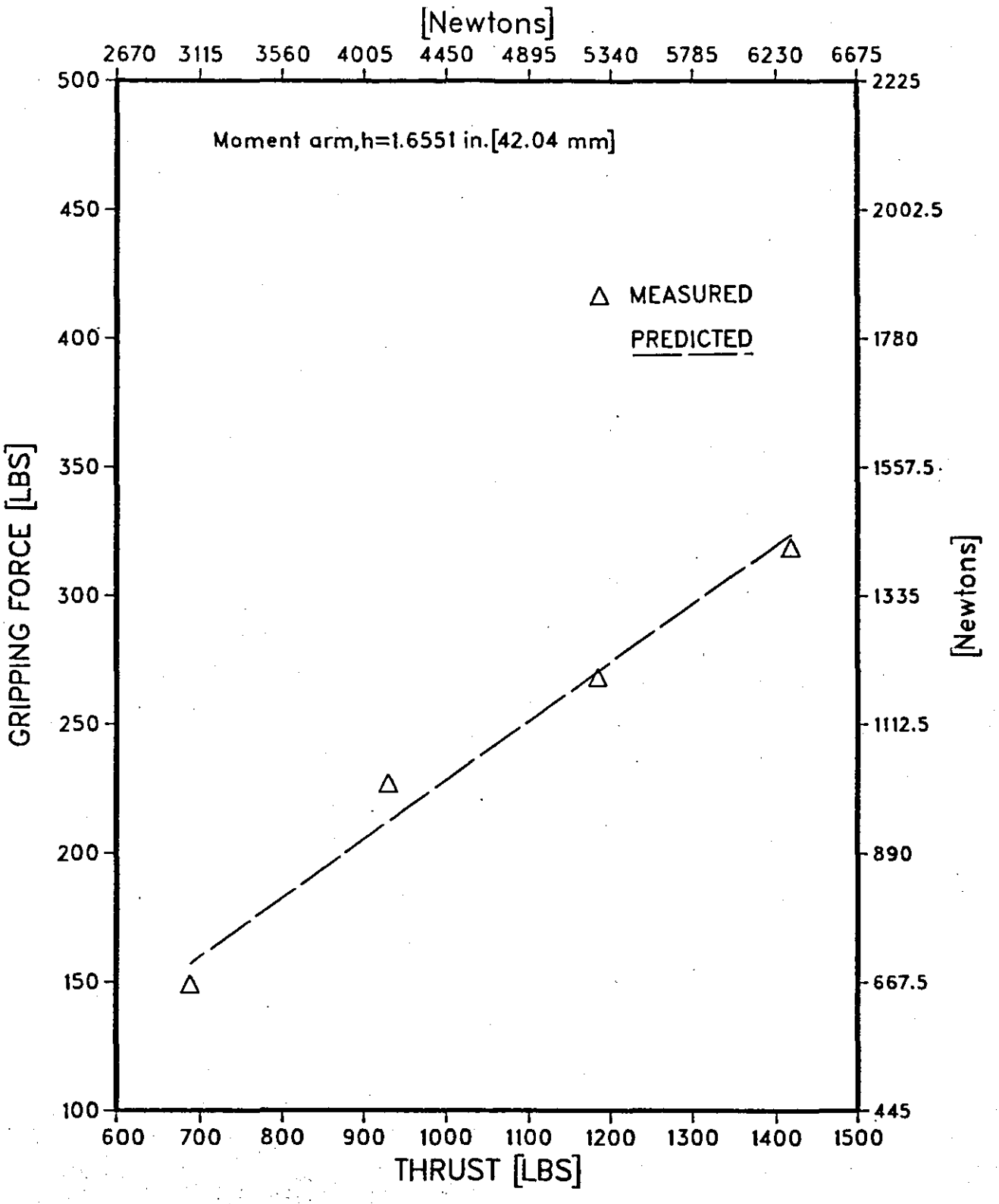

FIG.6.5.10 GRIPPING FORCE FOR 70 MM RING PLATE A,FOUR JAWS

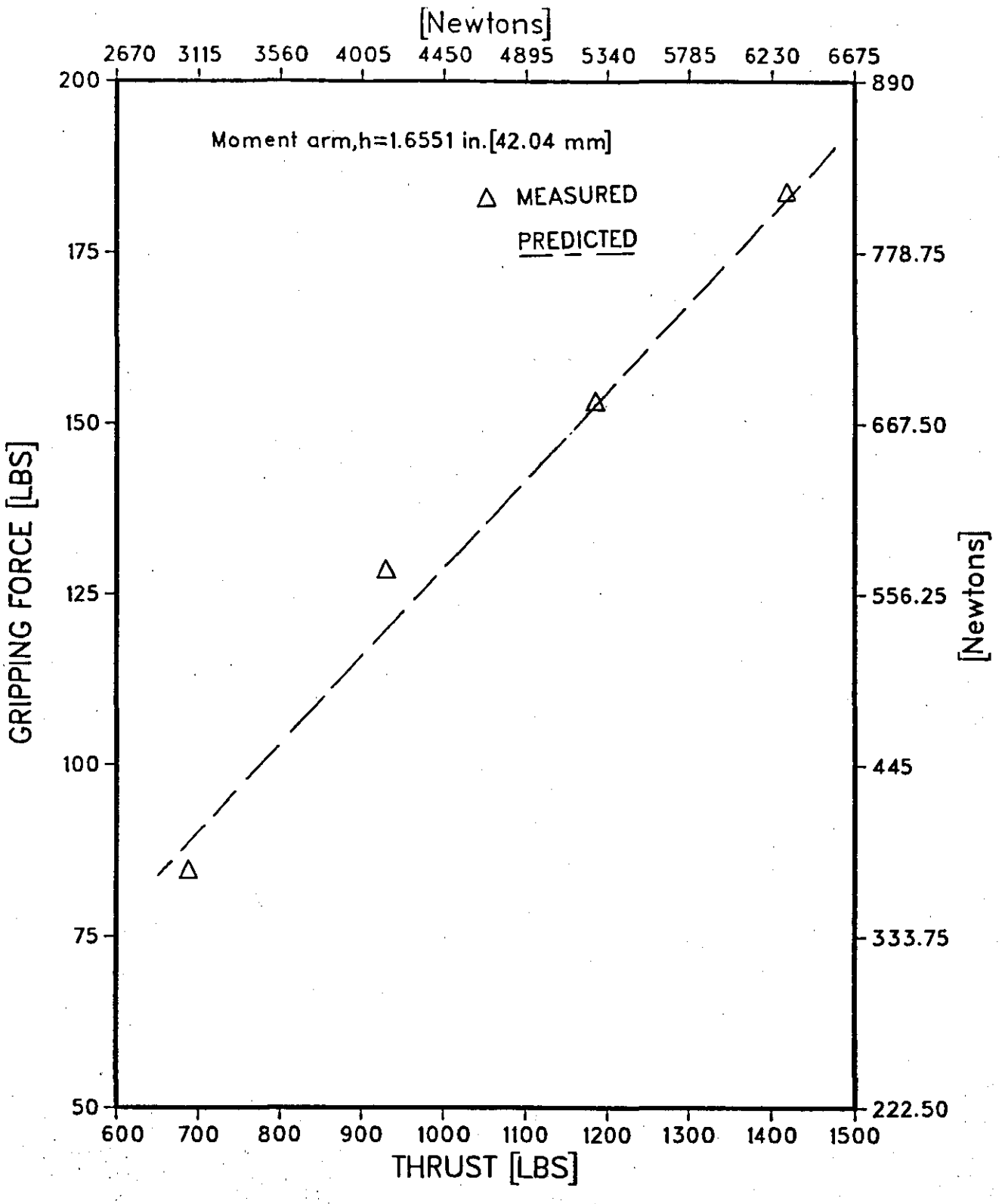

FIG.6.5.11 GRIPPING FORCE FOR 90 MM RING PLATE A,SIX JAWS

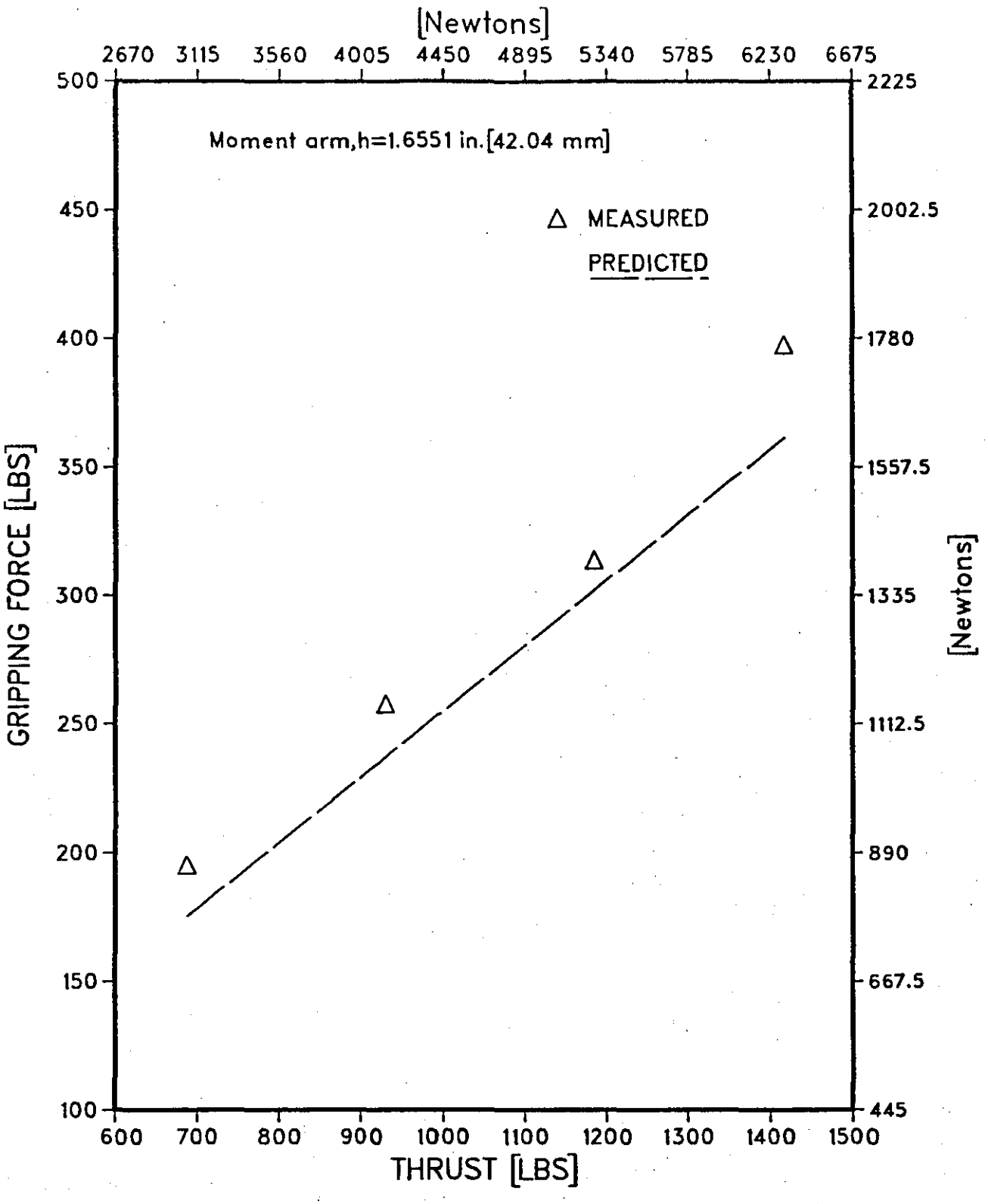

FIG.6.5.12 GRIPPING FORCE FOR 50 MM RING PLATE B,FOUR JAWS

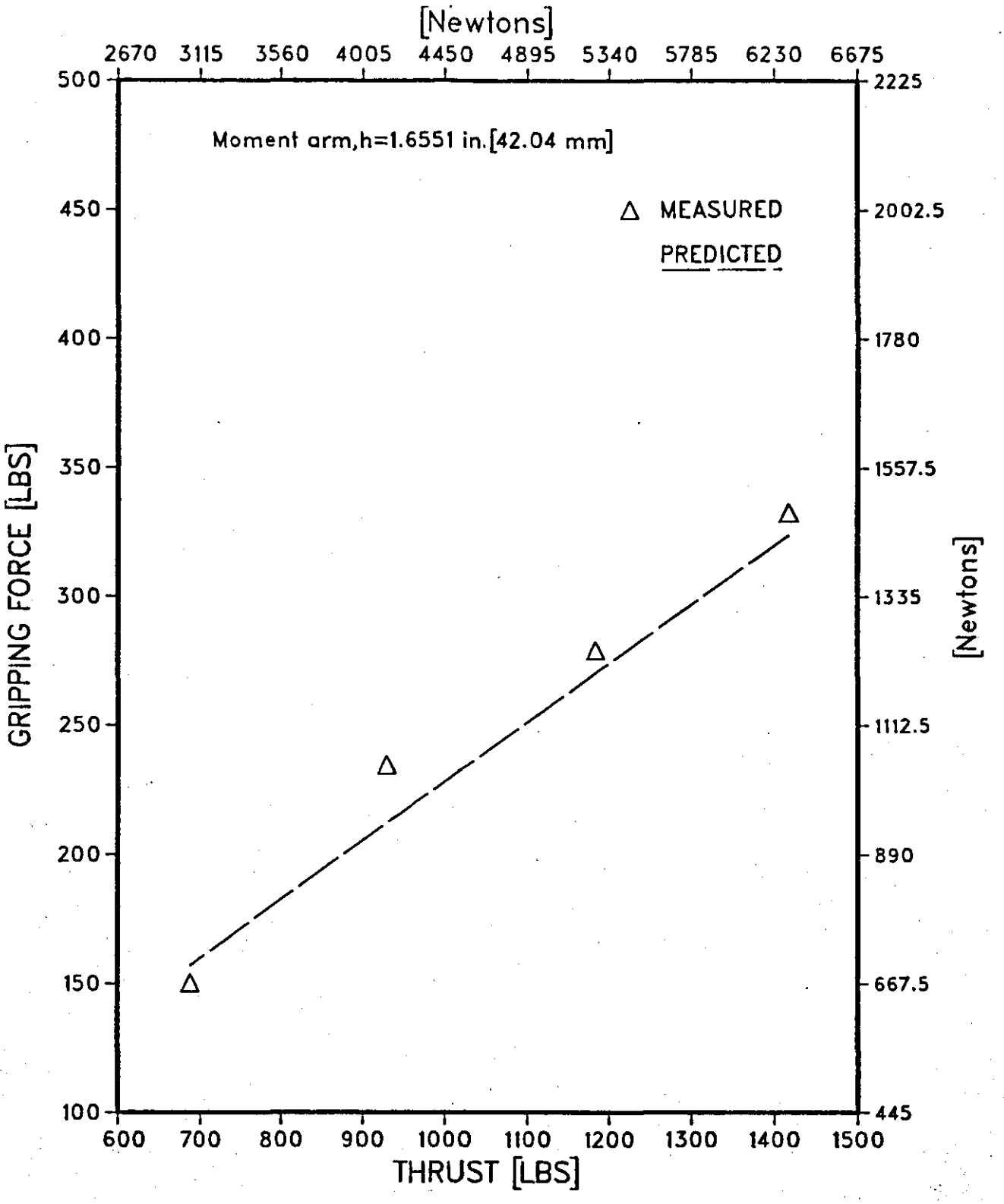

FIG.6.5.13 GRIPPING FORCE FOR 70 MM RING PLATE B,FOUR JAWS

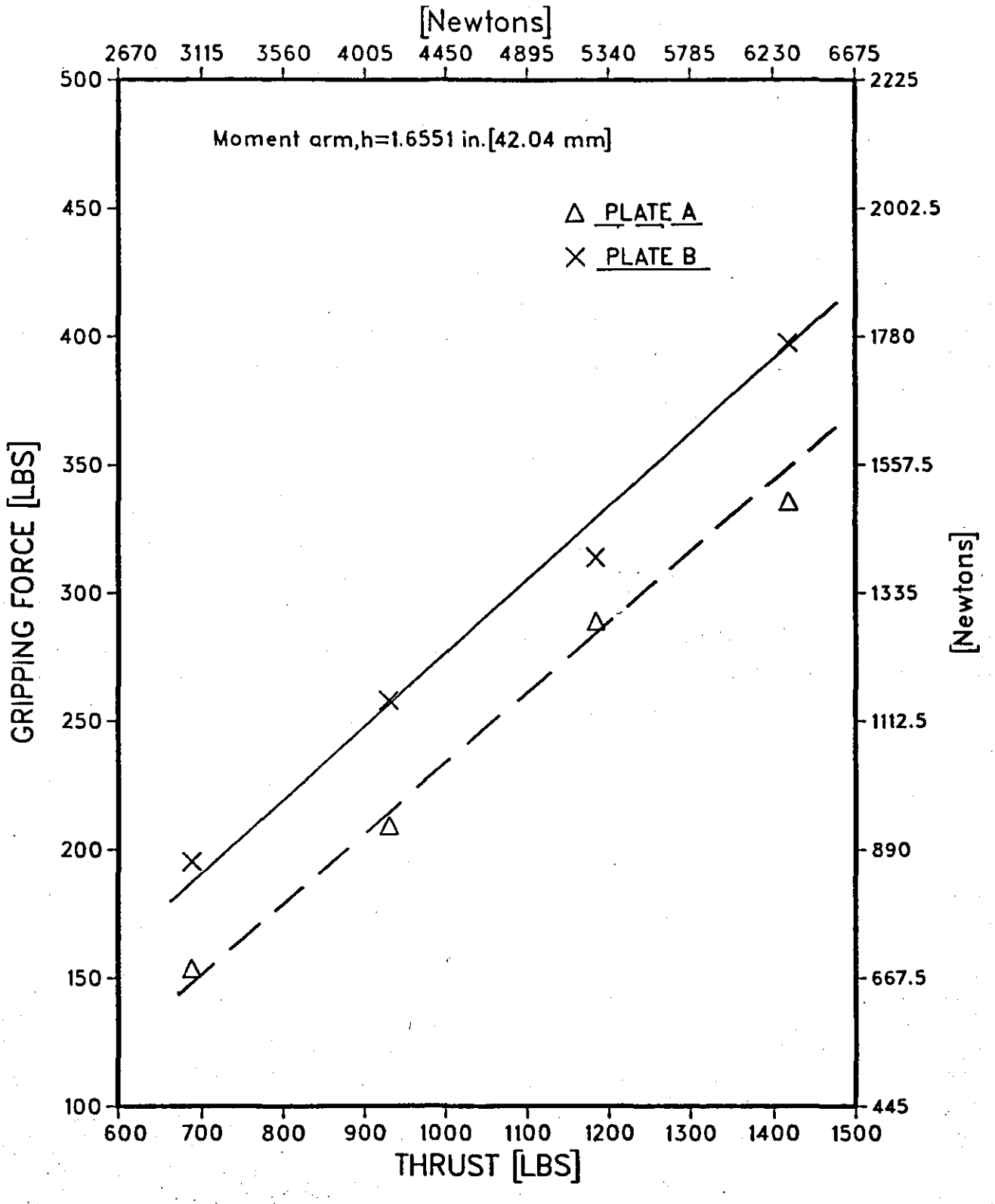

FIG.6.5.14 MEASURED GRIPPING FORCE FOR PLATES A AND B,50 MM RING

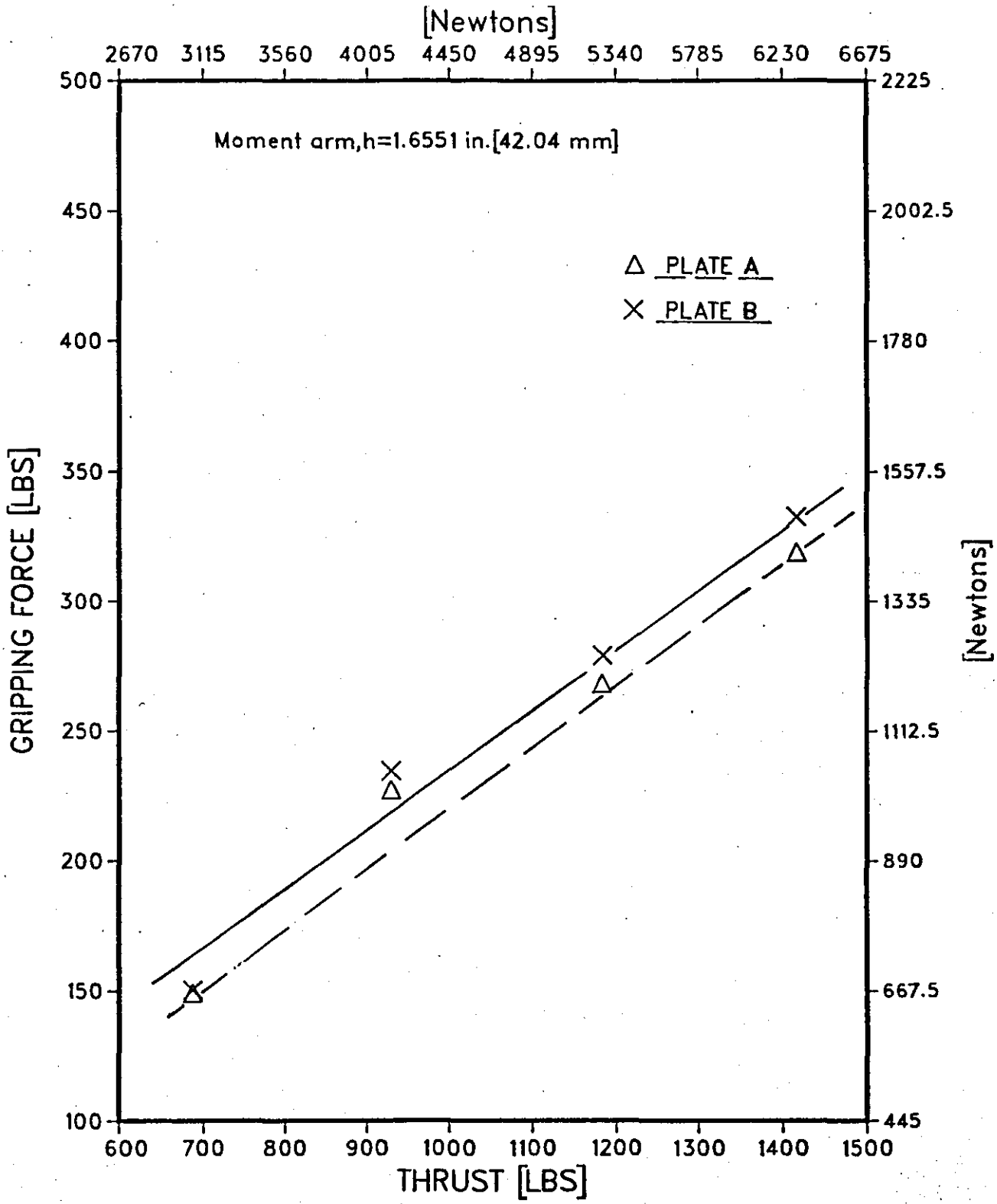

FIG.6.5.15 MEASURED GRIPPING FORCE FOR PLATES A AND B, 70 MM RING

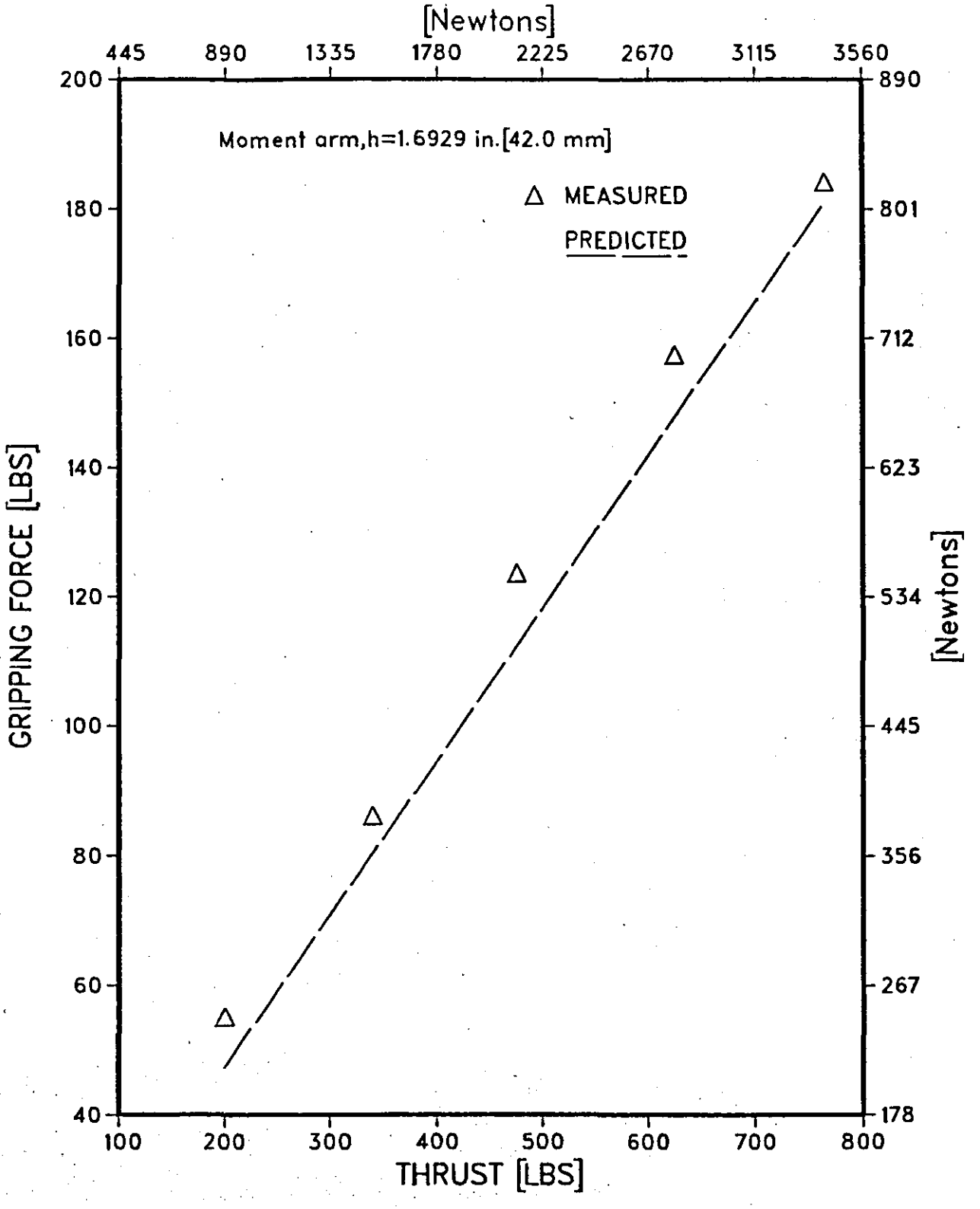

FIG.6.5.16 GRIPPING FORCE FOR 50 MM RING PLATE C,THREE JAWS

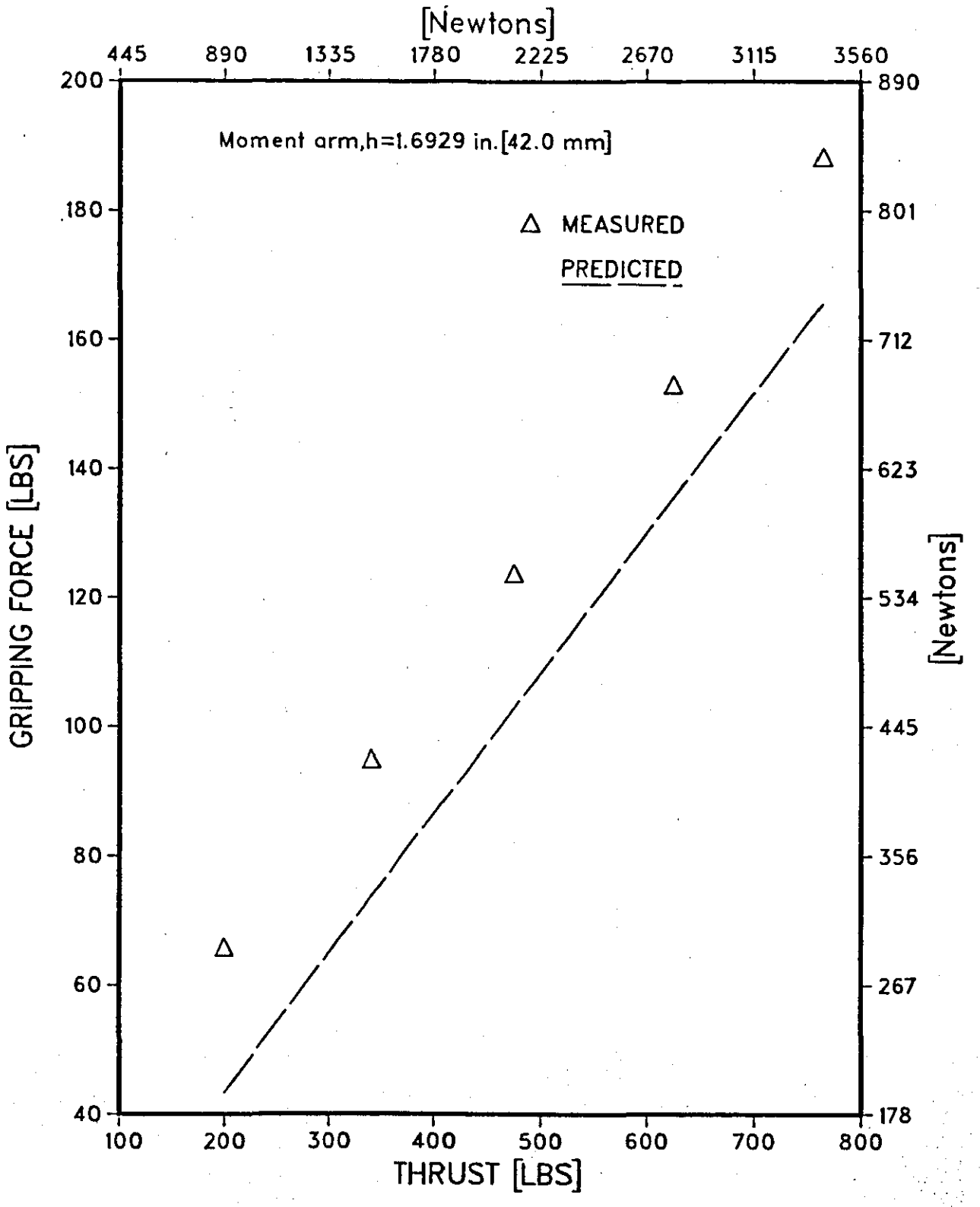

FIG.6.5.17 GRIPPING FORCE FOR 60 MM RING PLATE C,THREE JAWS

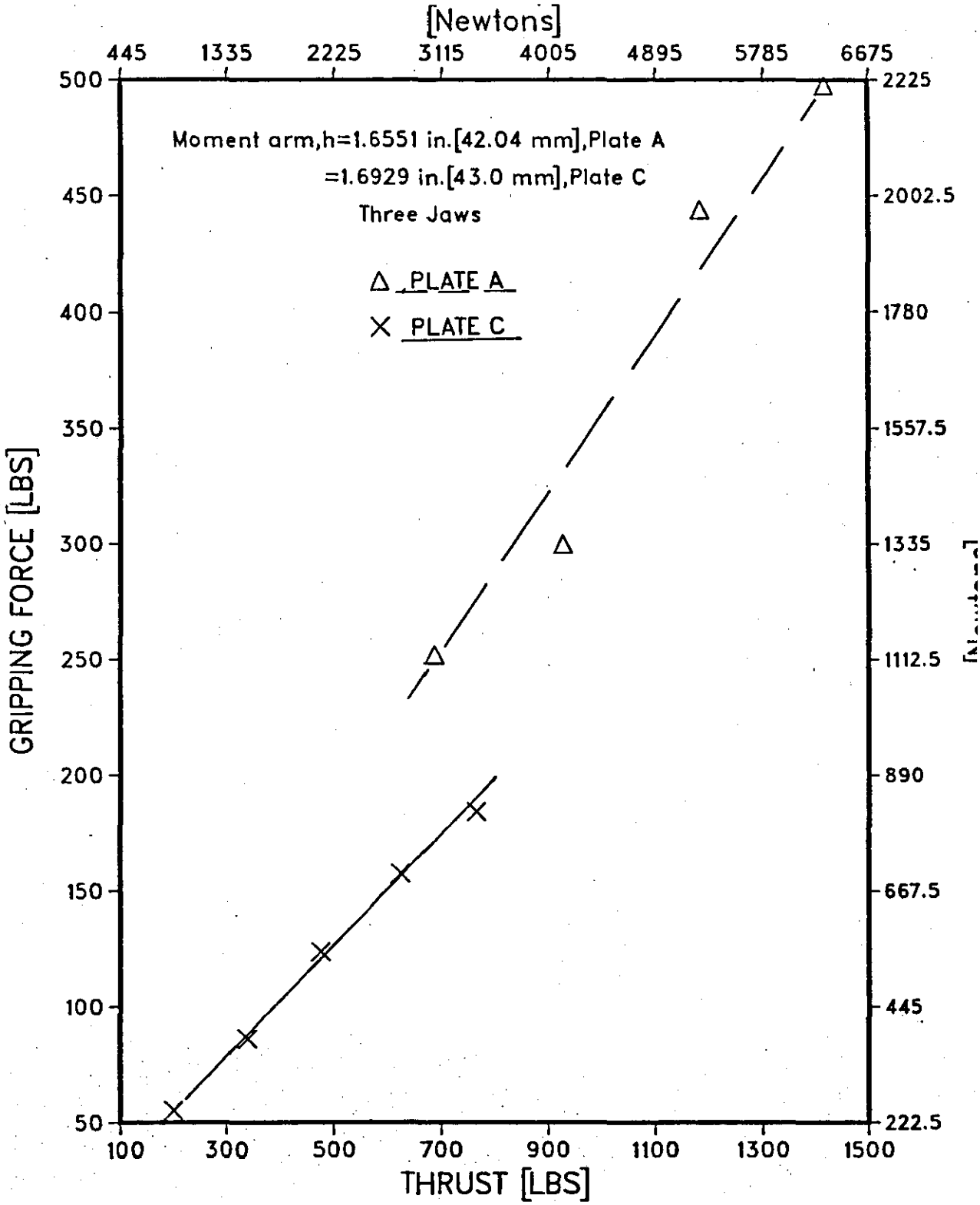

FIG.6.5.18 MEASURED GRIPPING FORCE FOR PLATES A AND C,50 MM RING

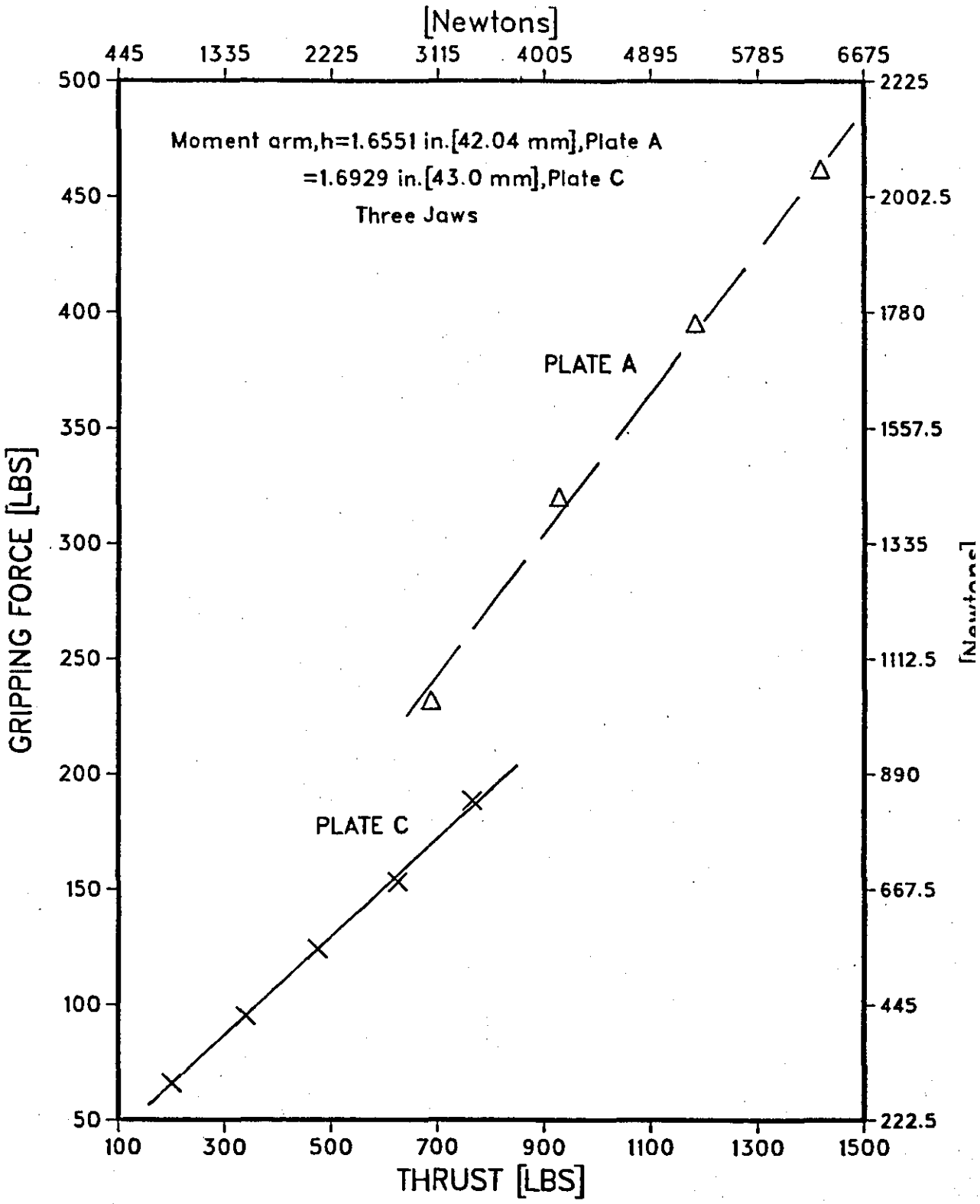

FIG.6.5.19 MEASURED GRIPPING FORCE FOR PLATES A AND C,60 MM RING

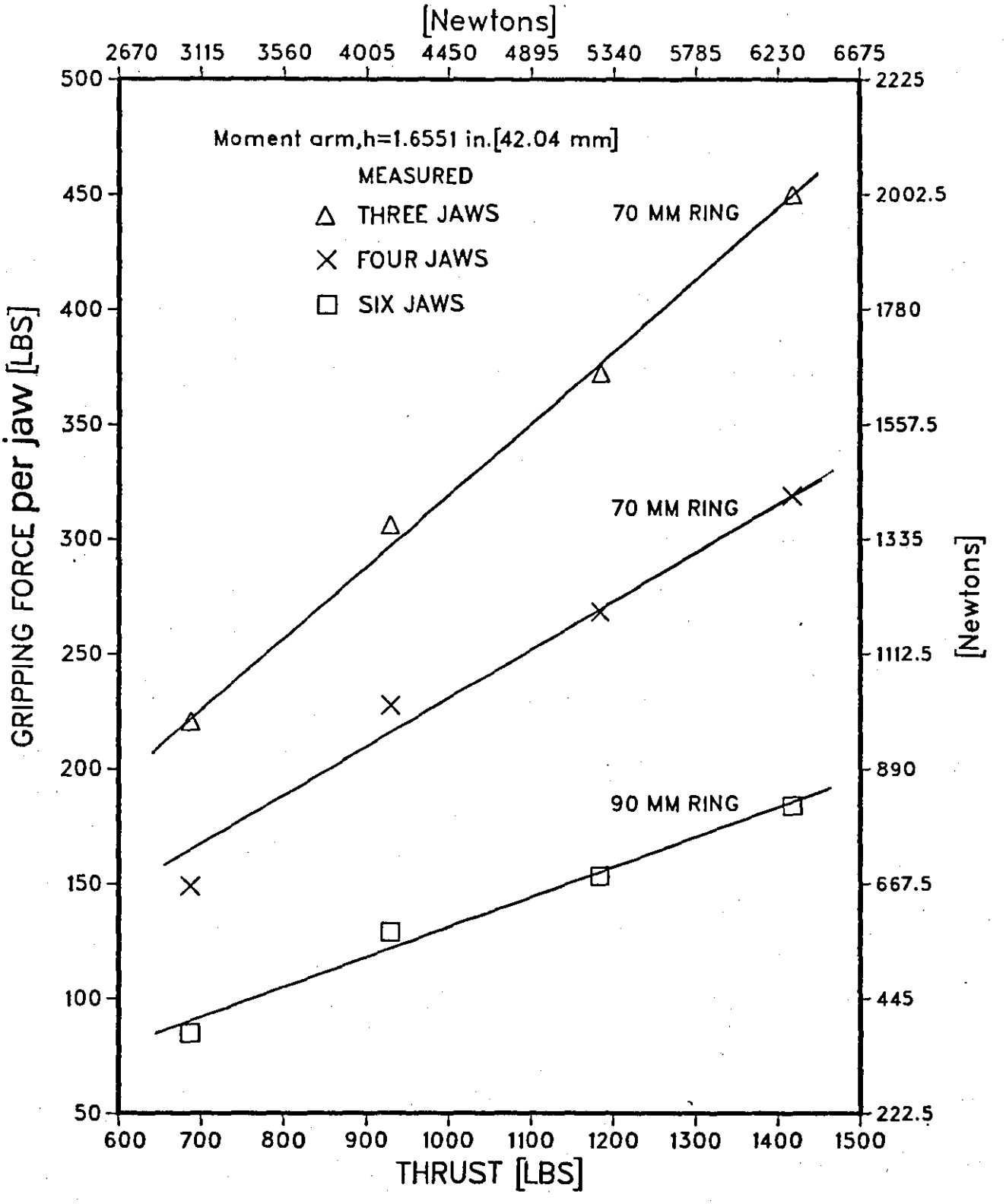

FIG.6.5.20 EFFECT OF NUMBER OF JAWS ON GRIPPING FORCE,PLATE A

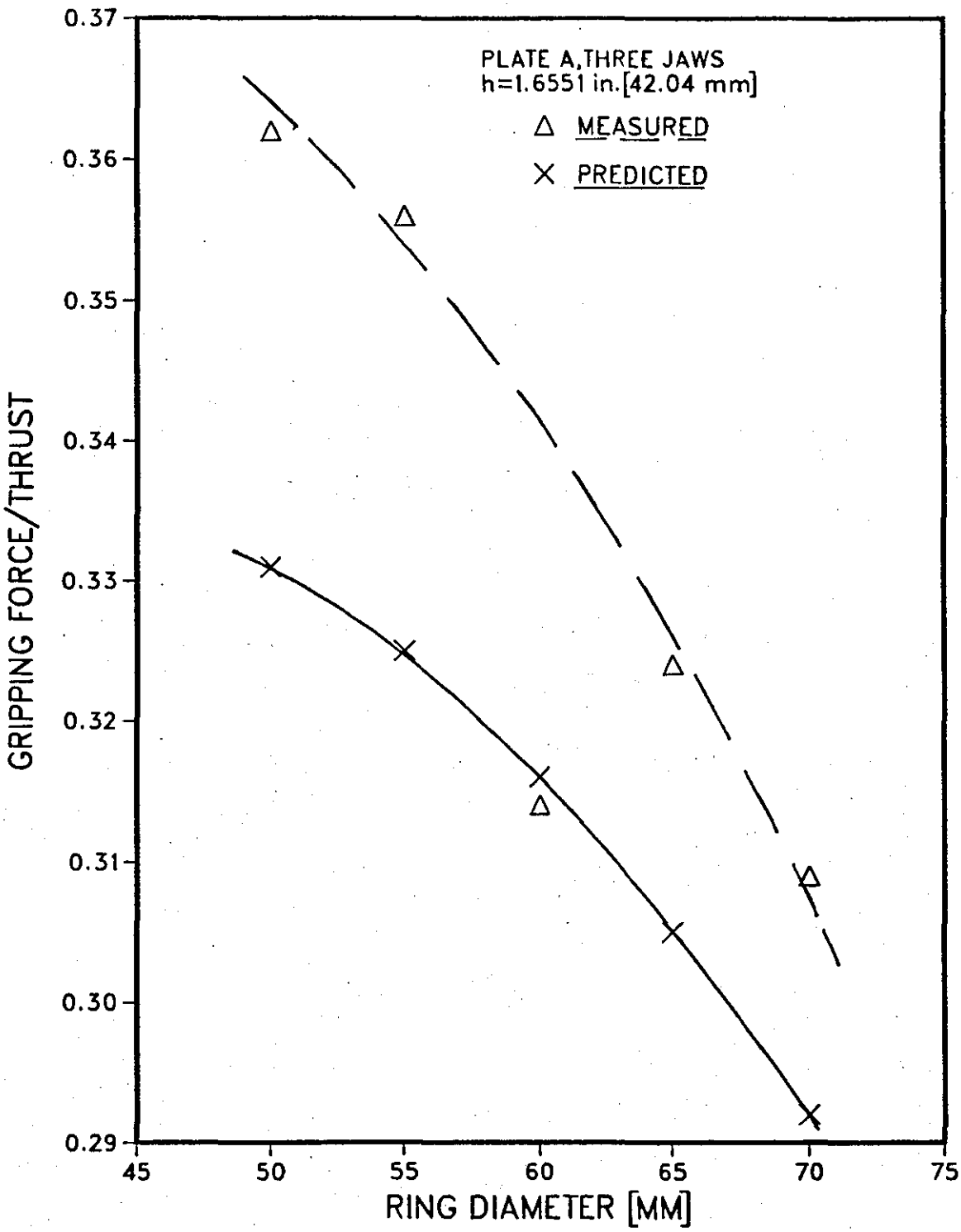

FIG.6.5.21 GRIPPING FORCE/THRUST RATIO VERSUS RING DIAMETER

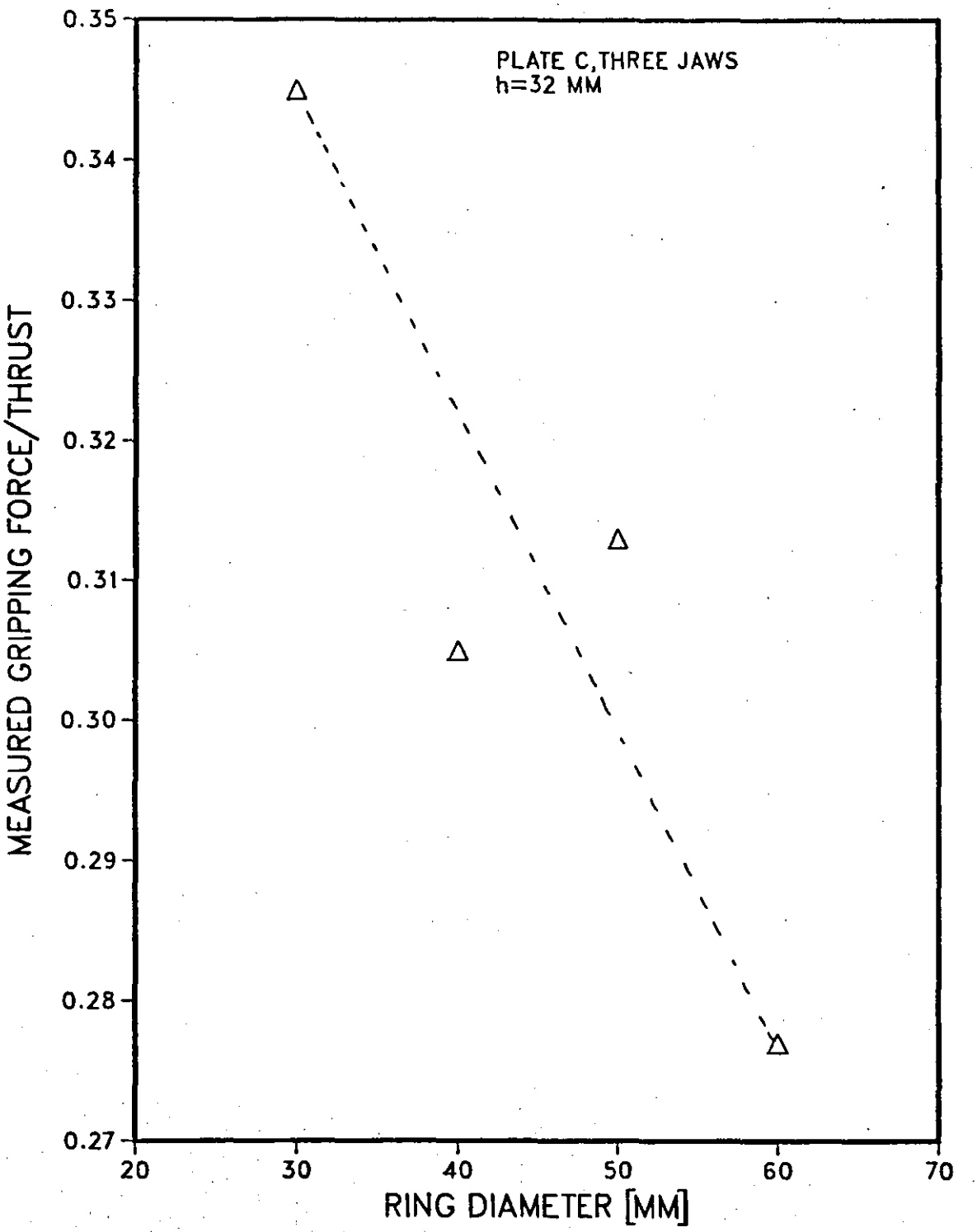

FIG.6.5.22 CHIDLOW'S GRIPPING FORCE/THRUST RATIO VERSUS RING DIAMETER

CHAPTER SEVEN

DIAPHRAGM CHUCK DESIGN METHODOLOGY

The theoretical analysis of diaphragm chucks having been established, is used for providing a format for the step-by-step design of the diaphragm chuck. The purpose is to provide such a methodology that allows the designer to proceed from gripping force requirements and constraints to the decisions on the pertinent physical dimensions of the diaphragm chuck. The design parameters are categorized into three groups - functional requirements, design constraints and design decisions.

7.1 FUNCTIONAL REQUIREMENTS

The functional requirements are those parameters that the designer pre-specifies for the performance of the diaphragm chuck. These performance parameters include the gripping force and workpiece diameter which are derived from the cutting forces required to process the material.

From the gripping force requirement, decision is made on the number of jaws that can grip the workpiece while protecting the material surface from indentation. The designer may pre-specify the size of the diaphragm chuck which is represented by the outer diameter of the diaphragm plate. On the other hand, the chuck size may be classified as a design constraint if it is limited to a given space.

7.2 DESIGN CONSTRAINTS

Design constraints include the parameters or operating conditions over which the designer has no choice or control. The main design constraint is the available air line pressure

or as the case may be, maximum available thrust. The allowable diameter of the inner hole may be restrictive, in which case, it is classified as a constraint. The operating space may constrain the outer diaphragm plate diameter to a particular maximum. Cutting tool space and arrangement may also constrain both the inner hole diameter and the moment arm, h to particular values. It can therefore be noticed that the parameters that are grouped under the functional requirements and design constraints vary according to the design problem. The same variation applies to the parameters under design decisions.

7.3 DESIGN DECISION

Design decisions are made on all other performance parameters not grouped into the functional requirements or design constraints. These parameters include minimum diaphragm plate thickness, diaphragm plate taper angle and material, input thrust, and piston and cylinder sizes. Parameters such as circumferential width of jaw slides, jaw slide thickness and radial length and jaw face area have not been analysed theoretically in this research. The designer has to use judgement and experience here.

7.4 DESIGN METHODOLOGY

A. List of Functional Requirements:

1. Total Gripping Force
2. Number of jaws
3. Gripping Force per jaw, $F = \frac{\text{Total Gripping Force}}{\text{Number of Jaws}}$

The choice of total gripping force is based on the cutting forces involved in the manufacturing

process. The number of jaws depends on the surface texture and resilience of the workpiece. The jaw gripping face area and the number of jaws are used to prevent surface indentation and deformation of the workpiece.

B. List of Design Constraints:

1. Maximum Available Air Line Pressure or Maximum Available Thrust.

2. Operating Air Pressure (Thrust) = 60% of Maximum Available Pressure (Thrust).

This specification is to allow for fluctuations, tolerance take-up and other variations. The thrust applied to the diaphragm plate is equal to or less than this value. To accommodate a range of workpiece diameters, the thrust is made as high as possible. This may mean that the diaphragm chuck cannot perform optimally in terms of the gripping force for some workpieces.

C. Design Decisions:

1. Taper Angle, $\beta = 2°$.

This choice of taper angle is made from an optimal range of $1.6°$ to $2.4°$. Any choice of taper angle within this range is acceptable.

2. Outer Diaphragm Plate Radius, a

$$\text{Outer radius, } a = \frac{\text{Workpiece radius, } r}{0.33}$$

This is based on the optimal operation of the chuck in terms of gripping force (See Section 5.5).

The resulting diaphragm plate outer radius may be too small or too large for operating purposes. In such a case, a convenient outer radius is used, but the diaphragm chuck will not be operating optimally.

3. Inner Diaphragm Plate Radius,b

Inner radius, $b \leq 0.2 \times$ (outer radius, a).

This is again in terms of optimum gripping force.

A larger outer radius, a,may result in a large inner radius, b,if the factor 0.2 is used. For such a case, a factor less than 0.2 is chosen to make the inner radius, b smaller. The smaller the size of the inner hole, the larger the gripping force (See Section 5.5).

Conversely, the smaller the size of the inner hole, the smaller the input thrust required to produce the specified gripping force per jaw. Similarly, a factor higher than 0.2 may be used if the inner radius, b is required to be larger. This will, of course, give a smaller gripping force.

4. Input Thrust, P

Tables 5.5.1 to 5.5.11 are used to determine K_r

Input Thrust, $P = \frac{Fh}{K_r(a+b)}$

Since gripping force varies with moment arm, h, the designer makes a suitable choice of h; and the input thrust, P is calculated.

5. Diaphragm Plate Material

The material is generally Nickel-Chrome Steel. For steel, Poisson's ratio, $\nu = 0.3$ has been used to prepare Tables 5.5.1 to 5.5.11. If a

material other than steel is used, the Poisson's ratio should be used to generate similar tables from equation 5.5.4.

The designer also obtains the yield strength of the material.

6. Minimum Diaphragm Plate Thickness, t_a

$$t_a = \left[\frac{S_f\, P_m(1-2C_s)}{\pi\, S_y}\right]^{\frac{1}{2}}$$

where $$C_s = \frac{x_b^2\left[(1+\nu)\,\ell n\, x_b + 1\right]}{\left[(1-\nu) + x_b^2(1+\nu)\right]}$$

S_f = Factor of safety

P_m = Maximum Operating Thrust

S_y = Yield Strength of Diaphragm Plate Material

ν = Poisson's Ratio of Diaphragm Plate Material

$x_b = b/a$

This is the thickness at the outer edge of the diaphragm plate.

The designer chooses the values for factor of safety and maximum operating thrust. If the difference between maximum operating thrust and input thrust is large, a rather large diaphragm plate thickness may result. In such cases, the input thrust, P or a value between the input thrust and the maximum operating thrust may be used in calculating t_a.

7. Diaphragm Plate Inner Edge Thickness, t_b

$$t_b = t_a + (a-b)\ \text{Tan}\ \beta$$

8. Piston Area

$$\text{Piston Area} = \frac{\text{Maximum Operating Thrust, } P_m}{\text{Operating Air Pressure}}$$

or

$$\frac{s_f P}{\text{Operating Air Pressure}}$$

The designer makes this choice.

9. Cylinder

The piston stroke is governed by the maximum allowable diaphragm plate deflection which is related to the operating thrust and factor of safety. A built-in stop in the piston-cylinder arrangement ensures that the diaphragm plate is not over-stressed. The maximum allowable deflection is given by

$$\omega_{max} = \frac{a^2(1-\nu^2)\ S_y}{2t_a E(1-2C_s)s_f}\left[(1-x_b^2)(1+2C_s) + 2(2C_s+x_b^2)\ell n x_b\right]$$

where E is the Modulus of Elasticity of the diaphragm plate material, and all other parameters are as previously defined. It is to be noted that in the choice of factor of safety, s_f, it should be kept in mind that the smallest thickness, t_a, has been used as the limiting case.

CHAPTER EIGHT

CONCLUSIONS AND RECOMMENDATIONS FOR FURTHER WORK

8.1 CONCLUSIONS

The theoretical and experimental results have been discussed in Chapters Four and Six of this work following the research objectives stated in Chapter One. From these discussions, it is concluded that the gripping force of a diaphragm chuck can be closely predicted using the equivalent constant thickness method for the analysis of the diaphragm plate. Furthermore, it is concluded that a designer of diaphragm chucks can decide on the amount of force required to grip a workpiece on a diaphragm chuck, and proceed methodically to design the required diaphragm chuck. The methodology and design data for designing a diaphragm chuck *a priori* are provided.

In the course of this research, optimum design specifications of the diaphragm chuck, and conclusions based on the theoretical and experimental analyses of the diaphragm chuck have emerged. The following specifications and conclusions arise:

1. The optimum range of the taper angle for the thickness of the diaphragm plate is between 1.6° and 2.4°. Within this range of taper, the deflection of the diaphragm plate is closest to a straight line without the introduction of high shear stresses and warping (See Section 3.5).
2. The equivalent constant thickness method is adequate for the prediction of the diaphragm plate deflections, and the gripping force of the diaphragm chuck. This method gives a different deflection pattern from the

actual pattern for the diaphragm plate. Therefore, the method is not suitable for predicting the stress distributions in the diaphragm plate (See Sections 3.6 and 4.6).

3. The method given for the location of the outer diameter of the diaphragm plate is suitable for all practical applications of the diaphragm chuck. The intersection point of the tangents at the ends of the radiused support of the diaphragm plate locates the outer diameter. For large plates, the outer diameter is located approximately at the inner end of the radiused support (See Section 3.8).

4. The ratio of the inner radius, b to the outer radius, a of the diaphragm plate is specified to be

$$b/_a \leq 0.2$$

based on the maximum shear stress contribution to gripping force. This ratio allows for higher contributions of any shear effects to the gripping force. The gripping force increases as the ratio $b/_a$ decreases (See Section 3.9).

5. The method of equating the deflection of the diaphragm plate with uniform thrust to its deflection with symmetric couples closely predicts the actual gripping force of the diaphragm chuck. The gripping force equation is simplified to the form

$$F = \frac{K_r(a+b)P}{h}$$

where F is the gripping force, a and b are the respective outer and inner radii of the diaphragm plate, P is the applied thrust load, h is the moment arm of the point of gripping, and K_r is a non-dimensional factor obtained from given tables (See Section 5.5).

6. The optimum workpiece diameter in terms of maximum gripping force is 33% of the outer diameter of the diaphragm plate. The gripping force changes with changing workpiece diameter (See Sections 5.5 and 6.5,5).

7. The tolerance effects on the gripping force are quantifiable. An equation is given to predict the change in gripping force due to workpiece - jaw bore tolerance. In addition, an equation for establishing the higher limit of the operating capacity of a diaphragm chuck is provided for the designer (See Section 5.6).

8. The gripping force is directly proportional to the thrust load applied to the diaphragm plate (See Section 6.5.1).

9. The thickness of the diaphragm plate has no direct effect on the gripping force. The indirect effect of thickness on gripping force is through the tolerance contributions. The diaphragm plate thickness must, of course, be of such a value as to withstand the stresses imposed by the whole gripping action (See Section 6.5.2).

10. The circumferential width of the jaw slide does not significantly affect the gripping force.

11. The gripping force per jaw for any number of jaws can be estimated if the gripping force per jaw for one set of jaws is known. The numerical ratio of the number of jaws is a close approximation of the inverse of their gripping force per jaw ratios. That is to say, the gripping force per jaw for four jaws is three-quarters of the gripping force per jaw for three jaws (See Section 6.5.6).

12. It is recomnended that the maximum operating air pressure should be at least 15 psi less than the

available line air pressure. This makes allowance for further deflection of the diaphragm plate to slip the workpiece into the jaws. It also allows for tolerance take-ups and line fluctuations

8.2 RECOMMENDATIONS FOR FURTHER WORK

During the course of this research, a number of interesting and important topics have been found to deserve closer investigation. Further studies and experimental work on these topics will extend the knowledge of diaphragm chucks and prove worthwhile for their design. It is therefore recommended that further work be carried on the following topics:

1. Determination of the effects of the radial length of the jaw slides on the deflections and gripping force of a diaphragm chuck. It is necessary to extend this work to determining the minimum thickness of the jaw slide that will impose a constant slope deflection on the diaphragm plate.
2. Experimental verification of the diaphragm plate behaviour as the taper angle is varied. This could be extended to include further measurements of gripping force for more number of jaws. A plot of the gripping forces for as many number of jaws as possible establishes the assymptotic minimum gripping force per jaw for a diaphragm chuck.
3. An investigation into the concept of annular stiffening of the diaphragm plate. Further investigation could include the methods for loading a diaphragm plate with couples and the deflection under such couples.
4. Experimental verification of the effects of the workpiece - jaw bore tolerance and the ratio of inner to outer radii of the diaphragm plate on gripping force is important.

5. An alternative method for the Analysis of Diaphragm Chucks is the Finite Element Method. This method could be used to analyze the deflections, forces and stresses that occur in a diaphragm plate. It could be extended to the diaphragm plate with non-detachable (or incorporated) jaw slides, the effects of the diaphragm plate taper angle, and the determination of the minimum height of the jaw slides.

REFERENCES

1. Astrop, A.W. "The Erickson Diaphragm Chuck and some Applications". Machinery 102 (1963) : 763-766.

2. Pahlitzsch, G. "Measurement of Gripping Capacity of Hand-operated Three-jaw Chucks". Micro Technic 13(1) (1959) : 16-19.

3. Robertson, J.S. "Investigation of the Factors which Influence the Design of Diaphragm Chucks". M.Sc. Thesis, University of Nottingham, 1966.

4. Chidlow, J. "An Investigation to Facilitate Prediction of the Gripping Force of a Diaphragm Chuck". M.Sc. Thesis, Loughborough University of Technology, 1976.

5. Billau, D.J. "The Design of Diaphragm Chucks". Project Report,Centre for Industrial Studies, Loughborough University of Technology, 1976.

6. Prickett, P.J. "An Investigation into the Effects of Centrifugal Forces on the Gripping Force of a Diaphragm Chuck". Masters Thesis, Loughborough University of Technology, 1984.

7. Timoshenko, S.P., and S.Woinowsky-Krieger. Theory of Plates and Shells. 2nd ed. New York: McGraw-Hill, 1970.

8. Vinson, J.R. Structural Mechanics : The Behaviour of Plates and Shells. New York : John Wiley, 1974.

9. Jaeger, L.G. Elementary Theory of Elastic Plates. Oxford : Pergamon, 1964.

10. Ugural, A.C. Stresses in Plates and Shells. New York: McGraw-Hill, 1981.

11. Szilard, R. Theory and Analysis of Plates. New Jersey: Prentice-Hall, 1974.

12. Mansfield, E.H. The Bending and Stretching of Plates. Oxford : Pergamon, 1964.

13. Wahl, A.M., and G.Lobo. "Stresses and Deflections in Flat Circular Plates with Central Holes". Trans. A.S.M.E. 52 (Part 1) (1930), Paper APM-52-3 : 29-43.

14. Lord, H.W., and S.S.Yousef. "Elastic Bending of Circular Plates of Variable Thickness : An Analytical and Experimental Study". International Journal of Mechanical Sciences 12(1970) : 417-434.

15. Conway, H.D. "Axially Symmetrical Plates with Linearly Varying Thickness". Journal of Applied Mechanics, Trans. A.S.M.E. 73 (1951) : 140-142.

16. Conway, H.D. "The Ribbed Circular Plate". Journal of Applied Mechanics 30(1963) " 464-466.

17. Simitses, G.J. "Optimal vs The Stiffened Circular Plate". AIAA Journal 11(10) (1973) : 1409-1412.

18. Lekhnitskii, S.G. Anisotropic Plates. Translated from the 2nd Russian Ed. by S.W.Tsai and T.Cheron. New York : Gordon and Breach, 1968.

19. Harvey, J., and J.P.Duncan. "The Rigidity of Rib-Reinforced Cover Plates". Proc. I. Mech.E. (London) 177(5) (1963) : 115-121,

20. Blake, A. Practical Stress Analysis in Engineering Design. New York : Marcell Dekker, 1982.

21. Yu, Y., "Bending of Isotropic Thin Plates by Concentrated Edge Couples and Forces". Journal of Applied Mechanics 21(1954): 129-139.

22. Amon, R., and O.E.Widera. "Problem of the Annular Plate, Simply Supported and Loaded with an Eccentric Concentrated Force". AIAA Journal 8(5) (1970) : 961-963.

23. Amon, R., and O.E.Widera. "Clamped Annular Plate under a Concentrated Force". AIAA Journal 7(1) (1969) : 151-153.

24. Dhaliwal, R.S. "Bending of a Circular Plate with a Central Hole by Concentrated Edge Forces and Couples". Applied Scientific Research. Sec.A. 9(6) (1960) : 411-423.

25. Bussali, W.A. "Bending of a Singularly Loaded Thin Circular Annulus with Free Boundaries". J. of Mechanics and Physics of Solids 8(2) (1960) : 123-140.

26. Symonds, P.S. "Concentrated-Force Problems in Plane Strain, Plane Stress, and Transverse Bending of Plates". Journal of Applied Mechanics 13(3) (1946) : A183-A197.

27. Lukasiewicz, S. Local Loads in Plates and Shells. The Netherlands : Sijthoff and Noordhoff, 1979.

28. Conway, H.D. "Non-Axial Bending of Ring Plates of Varying Thickness". Journal of Applied Mechanics, Trans. A.S.M.E. 25 (1958) : 386-388.

29. Stuart, R.D. An Introduction to Fourier Analysis. London: Methuen and Co., 1961.

30. Murphy, G. Similitude in Engineering. New York : The Ronald Press Co., 1950.

31. Pippard, A.J.S., and J.Baker. The Analysis of Engineering Structures. 4th Ed. London: Edward Arnold, 1968.

32. Roark, R.J., and W.C.Young. Formulas for Stress and Strain. 5th Ed. Tokyo : McGraw-Hill Kogakusha, 1975.

33. Hall, A.S., A.R.Holowenko, and H.G.Laughlin. Theory and Problems of Machine Design. New York : McGraw-Hill, 1961.

APPENDIX A

DETERMINATION OF POISSON'S RATIO FOR PLATE A MATERIAL

DETERMINATION OF POISSON'S RATIO FOR PLATE A MATERIAL

LOAD (KN)	AXIAL STRAIN ($\times 10^{-6}$ IN/IN)	TRANSVERSE STRAIN ($\times 10^{-6}$ IN/IN)
0.5	200, 140, 170	52.5, 33, 43
1.5	385, 357.5, 365	109, 87.5, 100.5
2.0	450, 422.5, 440.5	130, 110, 119
2.5	515, 495, 500.5	157.5, 130, 144

REGRESSION LINE → TRANSVERSE STRAIN = -9.08 + 0.298 AXIAL STRAIN

SLOPE = POISSON'S RATIO = 0.298

APPENDIX B

CALIBRATION DATA FOR CLOCKHOUSE PROVING RINGS

CALIBRATION OF CLOCKHOUSE PROVING RINGS

2000 LB. RING

RING NUMBER 1762 WITH DIAL GAUGE NUMBER 17622

LOAD (LBS)	GAUGE READING
0.0	0.0, 0.0
400.0	305.0, 306.0
800.0	618.0, 620.0
1200.0	937.0, 937.0
1600.0	1258.0, 1258.0
1700.0	1338.0, 1338.0

200 LB. RING

RING NUMBER 1527 WITH DIAL GAUGE NUMBER 74462

LOAD (LBS)	GAUGE READING
0.0	0.0, 0.0
40.0	301.0, 312.0
80.0	614.0, 615.0
140.0	1053.0, 1054.0
200.0	1514.0, 1513.0

APPENDIX C

CALIBRATION DATA FOR PRESSURE GAUGE AND 7 IN. DIAMETER CHUCK

CALIBRATION OF PRESSURE GAUGE AND CHUCK CYLINDER USED 2000 LB CLOCKHOUSE PROVING RING

7 IN. CHUCK

SERIAL NUMBER ST. 744

PISTON AREA = 24.72 SQ.IN.

PRESSURE (PSI)	DIAL GAUGE READING	THRUST (LBS)
10.0	145.0, 147.0, 148.0, 148.5	203.68
20.0	336.0, 338.0, 336.0, 335.0	441.66
30.0	531.0, 534.0, 531.0, 532.0	687.81
40.0	725.0, 722.0, 725.0, 724.0	929.32
50.0	928.0, 926.0, 927.0, 925.0	1184.02
60.0	1110.0, 1113.5, 1110.0, 1114.0	1417.22

APPENDIX D

ACCURACY CHECK DATA FOR DEFLECTION PROBE UNIT

ACCURACY CHECK DATA FOR RDP ELECTRONICS' EXTENSOMETER AND CREEP MONITOR UNIT TYPE D8 (6/DF/IN/16) WITH LVDT TYPE D5/100A (SER.NO. RDP 254)

RANGE 100 (0.10 IN.)			RANGE 30 (0.03 IN.)		
SLIP GAUGE HEIGHT (IN.)	PROBE UNIT READING (IN.)		SLIP GAUGE HEIGHT (IN.)	PROBE UNIT READING (IN.)	
	Up	Down		Up	Down
0.200	0.000	0.000	0.200	0.0000	0.0000
0.210	0.010	0.010	0.2010	0.0010	0.0010
0.215	0.015	0.015	0.2020	0.0020	0.0020
0.220	0.020	0.020	0.2030	0.0030	0.0030
0.230	0.030	0.030	0.2040	0.0040	0.0040
0.240	0.040	0.040	0.2050	0.0050	0.0050
0.250	0.050	0.050	0.2060	0.0060	0.0060
0.260	0.060	0.060	0.2070	0.0070	0.0070
0.270	0.070	0.070	0.2080	0.0080	0.0080
0.280	0.080	0.080	0.2090	0.0090	0.0090
0.290	0.090	0.090	0.2100	0.0100	0.0100
0.300	0.100	0.100	0.2200	0.0200	0.0200

APPENDIX E

PLATE DEFLECTION DATA

PLATE A
NO JAWS
WITHOUT HOLES
RADIAL LINE A

DEFLECTIONS ($\times 10^{-3}$ IN.)

PRESSURE (PSI)	RADIUS (IN.)			
	0.72	1.22	1.72	2.22
20.0	2.25	1.5	1.0	0.5
	2.25	1.75	1.0	0.5
	2.25	1.75	1.25	0.5
30.0	3.75	2.5	1.5	1.0
	3.5	2.75	1.75	1.0
	3.5	2.75	1.75	0.75
40.0	5.0	3.5	2.25	1.25
	5.0	3.75	2.5	1.25
	5.0	3.75	2.5	1.25
50.0	6.75	4.5	3.0	1.5
	6.5	4.75	3.25	1.75
	6.5	4.75	3.25	1.75
60.0	8.0	5.75	3.5	1.75
	8.0	5.75	4.0	2.0
	8.0	6.0	4.0	2.0

PLATE A
NO JAWS
WITHOUT HOLES
RADIAL LINE B

DEFLECTIONS ($\times 10^{-3}$ IN.)

PRESSURE (PSI)	RADIUS (IN.) 0.72	1.22	1.72	2.22
20.0	2.25	1.5	1.0	0.5
	2.25	1.75	1.0	0.5
	2.25	1.75	1.25	0.5
30.0	3.75	2.75	1.5	1.0
	3.5	2.75	2.0	0.75
	3.5	2.75	1.75	0.75
40.0	5.0	3.75	2.5	1.25
	5.0	3.75	2.5	1.0
	5.25	3.75	2.5	1.0
50.0	6.75	5.0	3.0	1.5
	6.25	5.0	3.0	1.5
	6.5	4.75	3.25	1.5
60.0	8.0	6.0	3.75	1.75
	7.75	6.0	3.75	1.75
	8.0	6.0	3.75	1.75

PLATE A

NO JAWS

WITH SYMMETRIC HOLES

RADIAL LINE A

DEFLECTIONS ($\times 10^{-3}$ IN.)

PRESSURE (PSI)	RADIUS (IN.) 0.72	1.22	1.72	2.22
20.0	2.75	2.0	1.0	0.25
	2.50	2.0	1.0	0.25
	2.50	1.75	1.0	0.50
30.0	4.25	3.0	2.0	0.75
	4.0	3.0	1.75	1.0
	4.0	3.0	2.0	1.0
40.0	5.75	4.25	2.5	1.0
	5.5	4.0	2.5	1.0
	5.5	3.75	2.25	1.25
50.0	7.25	5.5	3.25	1.5
	7.0	5.25	3.25	1.75
	7.0	5.0	3.25	1.75

PLATE A
NO JAWS
WITH SYMMETRIC HOLES
RADIAL LINE B
(HOLES FALL ON RADIAL LINE B)

DEFLECTIONS ($\times 10^{-3}$ IN.)

PRESSURE (PSI)	RADIUS (IN.) 0.72	1.22	1.72	2.22
20.0	2.5	2.0	1.0	0.5
	2.5	2.0	1.0	0.75
	2.75	2.0	1.25	1.0
30.0	4.25	3.0	2.0	0.75
	3.75	3.0	2.0	1.0
	4.25	3.0	2.0	1.25
40.0	5.5	4.25	2.5	1.25
	5.25	4.25	2.75	1.75
	5.5	4.25	2.75	1.5
50.0	7.25	5.5	3.25	1.5
	7.5	5.25	3.5	2.0
	7.5	5.25	3.5	1.75

PLATE A

THREE JAWS

DEFLECTIONS ($\times 10^{-3}$ IN.)

PRESSURE (PSI)	RADIUS (IN.)			
	0.72	1.22	1.72	2.22
20.0	1.5	1.5	1.0	0.5
	1.75	1.5	1.0	0.5
	2.0	1.5	1.0	0.5
30.0	2.5	2.5	1.5	1.0
	3.0	2.5	1.75	1.0
	3.0	2.75	2.0	1.5
40.0	4.0	3.5	2.75	1.25
	4.25	3.25	2.25	1.25
	4.5	3.75	2.5	1.5
50.0	5.5	4.5	3.25	1.75
	5.5	4.5	3.25	2.0
	5.5	4.5	3.5	2.0
60.0	7.0	5.5	4.25	2.25
	6.5	5.5	3.75	2.25
	6.75	5.5	4.25	2.25

PLATE A

FOUR JAWS

DEFLECTION (x 10^{-3} IN.)

PRESSURE (PSI)	RADIUS (IN.) 0.72	1.22	1.72	2.22
20.0	1.50	1.25	1.0	0.25
	1.5	1.25	1.0	0.5
	1.5	1.25	1.0	0.25
30.0	2.75	2.25	1.75	1.0
	2.75	2.5	1.75	1.25
	2.75	2.5	1.5	1.0
40.0	4.0	3.25	2.25	1.5
	4.0	3.5	2.5	2.0
	4.0	3.5	2.25	1.0
50.0	5.25	4.5	3.0	1.75
	5.25	4.25	3.25	1.5
	5.25	4.0	3.0	1.75
60.0	6.25	5.5	4.0	2.0
	6.25	5.25	3.75	2.0
	6.25	5.50	3.75	1.75

PLATE A

SIX JAWS

DEFLECTION (x 10^{-3} IN.)

PRESSURE (PSI)	RADIUS (IN.) 0.72	1.22	1.72	2.22
20.0	1.5	1.5	1.0	0.0
	1.5	1.25	.75	0.25
	1.25	1.0	.75	0.25
30.0	2.75	2.5	1.5	1.0
	2.75	2.25	1.75	0.75
	2.5	2.25	1.5	0.75
40.0	4.0	3.25	2.0	1.0
	4.0	3.25	2.25	1.0
	3.5	3.25	2.0	1.0
50.0	5.0	4.0	3.0	1.50
	5.0	3.25	3.0	1.75
	5.0	3.75	3.0	1.5
60.0	5.5	5.25	3.5	1.75
	6.25	5.25	3.5	2.0
	6.0	5.25	3.5	1.5

PLATE B

NO JAWS

DEFLECTIONS ($\times 10^{-3}$ IN.)

PRESSURE (PSI)	RADIUS (IN.) 0.72	1.22	1.72	2.32
20.0	4.25	3.25	1.75	0.5
	4.25	3.25	2.0	0.5
	4.5	3.0	2.0	0.5
30.0	7.0	5.0	3.0	1.0
	7.25	5.0	3.25	1.0
	7.25	5.0	3.25	1.0
40.0	10.0	7.0	4.5	1.5
	9.75	7.0	4.25	1.5
	10.0	6.75	4.25	1.5
50.0	13.0	9.25	5.5	2.0
	12.75	9.0	5.75	2.0
	13.0	9.0	5.5	2.0

PLATE B

FOUR JAWS

DEFLECTIONS ($\times 10^{-3}$ IN.)

PRESSURE (PSI)	RADIUS (IN.) 0.72	1.22	1.72	2.32
20.0	3.5	2.50	1.5	0.5
	3.5	2.5	1.5	0.5
	3.5	2.5	1.5	0.5
30.0	5.75	4.25	2.75	1.0
	5.75	4.25	2.75	1.0
	5.75	4.25	2.75	1.0
40.0	8.0	6.00	3.75	1.5
	8.0	5.75	3.75	1.5
	7.75	5.75	3.75	1.5
50.0	10.5	7.75	5.25	2.0
	10.25	7.5	5.0	2.0
	10.25	7.5	5.0	2.0

APPENDIX F

TRANSDUCER RINGS CALIBRATION DATA

RING CALIBRATION DATA

50 MM (10 MM WIDE) RING

CLOCKHOUSE READING	VERTICAL FORCE (LBS)	PLUNGER FORCE (LBS)	TOTAL STRAIN ($\times 10^{-6}$ IN/IN)
100.0	144.44	53.59	22.5, 25.0, 25.0
200.0	270.22	100.25	50.0, 55.0, 57.5
300.0	396.0	146.92	82.5, 87.5, 85.0
400.0	521.78	193.58	112.5, 117.5, 115.0
500.0	647.56	240.25	142.5, 145.0, 145.0

55 MM (10 MM WIDE) RING

CLOCKHOUSE READING	VERTICAL FORCE (LBS)	PLUNGER FORCE (LBS)	TOTAL STRAIN ($\times 10^{-6}$ IN/IN)
100.0	144.44	53.59	20.0, 17.5, 17.5
200.0	270.22	100.25	50.0, 45.0, 42.5
300.0	396.0	146.92	80.0, 80.0, 77.5
400.0	521.78	193.58	110.0, 107.5, 107.5
500.0	647.56	240.25	135.0, 132.5, 132.5

60 MM (10 MM WIDE) RING

CLOCKHOUSE READING	VERTICAL FORCE (LBS)	PLUNGER FORCE (LBS)	TOTAL STRAIN ($\times 10^{-6}$ IN/IN)
100.0	144.44	53.59	20.0, 22.5, 17.5
200.0	270.22	100.25	45.0, 42.5, 40.0
300.0	396.0	146.92	75.0, 70.0, 72.5
400.0	521.78	193.58	95.0, 90.0, 92.5
500.0	647.56	240.25	115.0, 117.5, 115.0

65 MM (10 MM WIDE) RING

CLOCKHOUSE READING	VERTICAL FORCE (LBS)	PLUNGER FORCE (LBS)	TOTAL STRAIN ($\times 10^{-6}$ IN/IN)
100.0	144.44	53.39	30.0, 30.0, 35.0
200.0	270.22	100.25	60.0, 60.0, 62.5
300.0	396.0	146.92	92.5, 87.5, 92.5
400.0	521.78	193.58	115.0, 115.0, 115.0
500.0	647.56	240.25	127.5, 135.0, 127.5

70 MM (10 MM WIDE) RING

CLOCKHOUSE READING	VERTICAL FORCE (LBS)	PLUNGER FORCE (LBS	TOTAL STRAIN ($\times 10^{-6}$ IN/IN)
100.0	144.44	53.59	37.5, 37.5, 32.5
200.0	270.22	100.25	80.0, 80.0, 75.0
300.0	396.0	146.92	120.0, 122.5, 117.5
400.0	521.78	193.58	155.0, 157.5, 152.5
500.0	647.56	240.25	182.5, 187.5, 182.5

50 MM (5 MM WIDE) RING

CLOCKHOUSE READING	VERTICAL FORCE (LBS)	PLUNGER FORCE (LBS)	TOTAL STRAIN ($\times 10^{-6}$ IN/IN)
200.0	270.2	100.2	120.0, 115.0, 120.0
400.0	521.8	193.6	230.0, 225.0, 230.0
600.0	773.3	286.9	345.0, 340.0, 345.0
800.0	1024.9	380.2	460.0, 455.0, 460.0
1000.0	1276.5	473.6	570.0, 570.0, 575.0

60 MM (5 MM WIDE) RING

CLOCKHOUSE READING	VERTICAL FORCE (LBS)	PLUNGER FORCE (LBS)	TOTAL STRAIN ($\times 10^{-6}$ IN/IN)
100.0	144.4	53.39	140.0, 135.0, 140.0
200.0	270.22	100.25	320.0, 312.5, 317.5
300.0	396.0	146.92	405.0, 395.0, 400.0
400.0	521.78	193.58	552.5, 537.5, 547.5
500.0	647.56	240.25	662.5, 655, 662.5

90 MM (5 MM WIDE) RING

CLOCKHOUSE READING	VERTICAL FORCE (LBS)	PLUNGER FORCE (LBS)	TOTAL STRAIN ($\times 10^{-6}$ IN/IN)
200.0	270.2	100.2	115.0, 110.0, 110.0
400.0	521.8	193.6	250.0, 250.0, 255.0
600.0	773.3	286.9	415.0, 410.0, 410.0
800.0	1024.9	380.2	570.0, 570.0, 575.0
1000.0	1276.5	473.6	720.0, 715.0, 720.0

APPENDIX G

GRIPPING FORCE MEASUREMENTS

GRIPPING FORCE MEASUREMENTS

PLATE A

MOMENT ARM, h=1.6551 IN.(42.04mm)

THREE JAWS

RING DIAMETER (MM)	GAUGE PRESSURE (PSI)	STRAIN READINGS (MICRO IN./IN.)	GRIPPING FORCE (LBS)
50.0	*30.0	305.0, 295.0, 305.0, 300.0, 300.0, 300.0, 305.0, 305.0, 300.0	252.0
	*40.0	360.0, 355.0, 370.0, 350.0, 340.0, 345.0, 370.0, 380.0, 370.0,	299.8
	50.0	277.5, 277.5, 275.0, 275.0, 275.0, 275.0, 275.0, 277.5, 275.0	443.9
	60.0	305.0, 305.0, 305.0, 312.5, 312.5, 310.0, 315.0, 312.5, 317.5	497.63
55.0	30.0	115.0, 115.0, 115.0, 125.0, 125.0, 122.5, 127.5, 127.5, 127.5	219.11
	40.0	185.0, 185.0, 185.0, 190.0, 190.0, 190.0, 185, 187.5, 187.5	322.5
	50.0	225.0, 225.0, 230.0, 235.0, 235.0, 235.0, 222.5, 220.0, 222.5	386.98
	60.0	297.5, 292.5, 300.0, 297.5, 300.0, 295.0, 280.0, 280.0, 285.0	487.82

* 5mm WIDE RINGS WERE USED

60.0	*30.0	625.0, 625.0, 630.0, 625.0, 620.0, 630.0, 630.0, 635.0, 630.0	231.7
	*40.0	860.0, 855.0, 865.0, 855.0, 855.0, 855.0, 855.0, 850.0, 850.0, 850.0	320.1
	50.0	200.0, 205.0, 200.0, 195.0, 195.0, 195.0, 195.0, 200.0, 195.0	395.3
	60.0	230.0, 235.0, 235.0, 235.0, 237.5, 230.0, 230.0, 232.5, 227.5	462.0
65.0	30.0	120.0, 115.0, 130.0, 125.0, 125.0, 125.0, 132.5, 127.5, 132.5	220.4
	40.0	175.0, 175.0, 177.5, 175.0, 172.5, 172.5, 175.0, 175.0, 175.0	310.0
	50.0	215.0, 215.0, 217.5, 217.5, 215.0, 215.0, 212.5, 210.0, 210.0	382.5
	60.0	252.5, 252.5, 252.5, 257.5, 257.5, 257.5, 260.0, 260.0, 260.0	460.3
70.0	30.0	172.5, 172.5, 175.0, 170.0, 170.0, 172.5, 177.5, 175.0, 175.0	220.4
	40.0	240.0, 245.0, 235.0, 250.0, 245.0, 240.0, 255.0, 235.0, 240.0	306.1
	50.0	297.5, 297.5, 295.0, 295.0, 295.0, 295.0, 297.0, 292.5, 300.0	372.3
	60.0	352.5, 350.0, 347.5, 355.0, 355.0, 355.0, 370.0, 370.0, 372.5	450.0

FOUR JAWS

RING DIAMETER (MM)	GAUGE PRESSURE (PSI)	STRAIN READINGS (MICRO IN./IN)	GRIPPING FORCE (LBS)
50.0	30.0	95.0, 92.5, 92.5, 90.0, 92.5, 92.5, 90.0, 90.0, 90.0, 92.5, 92.5, 92.5	153.6
	40.0	127.5,127.5,125.0,130.0, 130.0,130.0,127.5,127.5, 127.5,127.5,125, 127.5	209.3
	50.0	180.0,185.0,180.0,175.0, 175.0,175.0,177.5,177.5, 177.5,182.5,182.5,182.5	288.96
	60.0	215.0,215.0,215.0,210.0, 210.0,210.0,205.0,207.5, 207.5,205.0,205.0,205.0	335.6
55.0	30.0	102.5,102.5,102.5,102.5, 102.5,105.0,102.5,102.5, 102.5,102.5,100.0,125.5	180.5
	40.0	125.0,125.0,127.5,127.5, 127.5,127.5,127.5,127.5, 127.5,125.0,125.0,127.5	218.7
	50.0	157.5,157.5,157.5,160.0, 155.0,165.0,165.0,157.0, 152.5,157.5,170.0,162.5,	271.6
	60.0	190.0,192.5,190.0,190.0, 190.0,190.0,200.0,195.0, 195.0,195.0,192.5,195.0	324.3
60.0	*30.0	425.0,430.0,430.0,425.0, 435.0,435.0,435.0,435.0, 435.0,430.0,435.0,435.0	159.3
	*40.0	620.0,620.0,620.0,625.0, 620.0,625.0,630.0,630.0, 625.0,620.0,615.0,615.0	233.2

* 5 mm WIDE RINGS WERE USED

	50.0	142.5,142.5,142.5,132.5, 132.5,137.5,137.5,137.5, 140.0,142.5,145.0,145.0	278.93
	60.0	170.0,165.0,165.0,170.0, 172.5,172.5,172.5,172.5, 177.5,180.0,180.0,180.0	343.3
65.0	30.0	95.0, 95.0, 100.0,100.0, 100.0,95.0, 90.0, 90.0, 90.0, 92.5, 90.0, 90.0	165.2
	40.0	127.5,127.5,127.5,130.0, 130.0,130.0,127.5,127.5, 127.5,132.5,132.5,132.5	230.1
	50.0	170.0,162.5,165.0,160.0, 160.0,160.0,157.0,157.0, 157.0,170.0,170.0,162.5	291.1
	60.0	205.0,202.5,200.0,205.0, 202.5,207.5,205.0,180.0, 190.0,195.0,190.0,190.0	355.3
70.0	30.0	120.0,122.5,120.0,115.0, 115.0,117.5,117.5,117.5, 117.5,115.0,117.5,115.0	149.1
	40.0	190.0,190.0,195.0,180.0, 175.0,175.0,180.0,185.0, 185.0,170.0,170.0,170.0	227.3
	50.0	220.0,210.0,220.0,205.0, 210.0,205.0,217.5,220.0, 220.0,210.0,210.0,212.5	268.3
	60.0	247.5,247.5,250.0,252.5, 245.0,240.0,250.0,250.0, 260.0,265.0,265.0,275.0	318.8

SIX JAWS

RING DIAMETER (MM)	GAUGE PRESSURE (PSI)	STRAIN READINGS (MICRO IN./IN)	GRIPPING FORCE (LBS.)
90.0	30.0	115.0,110.0,105.0,120.0, 130.0,130.0,130.0,120.0, 120.0,120.0,115.0,115.0, 105.0,105.0,105.0,100.0, 100.0, 90.0	84.9
	40.0	180.0,185.0,170.0,190.0, 190.0,185.0,205.0,200.0, 205.0,180.0,175.0,170.0, 185.0,185.0,185.0,185.0, 180.0,180.0	128.8
	50.0	200.0,215.0,215.0,225.0, 225.0,225.0,235.0,230.0, 230.0,225.0,220.0,215.0, 230.0,230.0,230.0,235.0, 240.0,240.0	153.4
	60.0	285.0,290.0,290.0,295.0, 295.0,295.0,260.0,260.0, 255.0,285.0,285.0,285.0, 280.0,285.0,290.0,245.0, 245.0,245.0	183.96

PLATE B

MOMENT ARM, h=1.6551 IN.(42.04mm)

FOUR JAWS

RING DIAMETER (MM)	GAUGE PRESSURE (PSI)	STRAIN READINGS (MICRO $IN./_{IN.}$)	GRIPPING FORCE (LBS)
50.0	30.0	235.0,235.0,235.0,230.0, 230.0,235.0,230.0,235.0, 230.0,240.0,240.0,235.0	195.3
	40.0	335.0,335.0,335.0,335.0, 335.0,335.0,330.0,340.0, 335.0,240.0,235.0,235.0	257.8
	50.0	385.0,380.0,375.0,400.0, 410.0,400.0,400.0,400.0, 400.0,330.0,335.0,330.0	313.8
	60.0	520.0,520.0,520.0,520.0, 525.0,525.0,425.0,425.0, 425.0,455.0,455.0,455.0	397.5
70.0	30.0	110.0,110.0,110.0,117.5, 117.5,117.5,130.0,122.5, 122.5,120.0,122.5,122.5	150.2
	40.0	190.0,185.0,190.0,180.0, 180.0,180.0,170.0,165.0, 165.0,210.0,210.0,210.0	234.6
	50.0	225.0,225.0,225.0,215.0, 215.0,215.0,215.0,210.0, 215.0,235.0,235.0,235.0	279.1
	60.0	285.0,285.0,285.0,265.0, 265.0,265.0,265.0,265.0, 265.0,245.0,245.0,245.0	332.5